Casper Hügel

Flexibility services by a community microgrid

TU Delft

SPECTRAL

Flexibility services by a community microgrid

Quantifying the value of flexibility services by a community microgrid in the context of the Dutch electricity sector using Schoonschip as case study

by

Casper Hügel

in partial fulfilment of the requirements for the degree of

Master of Science
in Sustainable Energy Technology

at the Delft University of Technology,
to be defended publicly on 5 July 2018.

Supervisor:	Prof. dr. ir. J.A. La Poutré	
Thesis committee:	Prof.dr. P. Palensky,	TU Delft
	ir. T. Woudstra,	TU Delft
	P. Gladek,	Spectral

TU Delft
Delft University of Technology

SPECTRAL

Preface

Before you lies the dissertation ‘’Flexibility services by a community microgrid”. It has been written to fulfil the graduation requirements of the master Sustainable energy technology at Delft University of Technology. I was engaged in researching and writing this dissertation throughout 2017 and part of 2018.

The project is inspired by a research proposal that was originally submitted by Spectral. A company involved in smart energy solutions. At that time, I was struggling to find a suitable graduation project. Not that there were little projects available, but because I wanted to combine multiple disciplines in my research. Eventually, the proposal by Spectral contained exactly the right ingredients for this purpose. And although the multidisciplinary aspect has been challenging, I have also learned a great deal, which will come in very useful in my further career as an energy consultant.

With the thesis now complete, I would like to take the opportunity to thank my supervisor Prof La Poutré. His attention to detail has very much sharpened my own abilities in that realm. Although at times I was fickle, Prof La Poutré would remain calm and always willing to give feedback when needed. Also, I would like to thank ir. Woudstra for his time and willingness to help me finish this research. I also thank Philip Gladek (CEO Spectral) for our short but intense and fruitful sessions. Throughout the process, you inspired me to think of new possibilities and create valuable insights.

Next, I would like to thank my parents for their continuous and unconditional support throughout the process. You have been so kind and patient, especially in times that you have helped me deal with difficult situations. Also, I would like to thank my girlfriend Liset Vliegen, for her energy, kind words, and support.

At the university, I thank my dear friends, Wessel de Jong, Veikko Schepel, Irma Stegmann, Rik van der Vossen, Sebas Joosten, Bas Gradussen, Max Capelle and Eva Nieuwenhuis for their feedback.

Casper Hügel

Delft, July 21, 2018

Content

Abstract

The volatile production of renewable energy sources is often considered a key issue in future sustainable energy systems. Drawing on microgrid research, we argue that the potential synergy between microgrid energy management and provision of flexibility services to the wider grid could be further explored. In addition, the trade-off between cost minimisation and energy autarky of a community microgrid has not yet been fully investigated. This study therefore investigates the role of community microgrids in managing the volatility of renewable energy production in the wider grid, while also considering local optimisation trade-offs. The goal of this study is threefold: (1) identifying possibilities for market interactions, (2) developing simulation models and optimization/decision software, and (3) conducting exploratory experiments.

To illustrate our ideas, the community microgrid of Schoonschip was used as a case study. This Schoonschip microgrid contains 30 floating houseboats, that are equipped with the following energy resources: PV panels, batteries, modulating heat pumps, thermal collectors, buffer tanks, underfloor heating systems and electrical boilers. The resources are centrally controlled by an energy management system and the Schoonschip microgrid is connected via an interconnection of 160kVA. Simulation models were created for simulating the energy resources and heat demand of the houses. Optimization/decision software was developed and used for microgrid energy management and control of flexibility services.

This thesis provides insights into (1) potential market interactions between a community microgrid and the Dutch electricity wholesale market, (2) the trade-off between maximisation of the forecasted solar self-consumption and minimisation of electricity costs, and (3) the potential value and the problems associated with the provision of grid stability services. This study has resulted in a simulation model and decision software, which can also be used and further extended for additional experimental studies into microgrids and flexibility services.

List of figures

List of tables

Chapter 1

Introduction

As is generally known, society needs to decarbonise its economy in order to prevent (drastic) climate change. Amongst others, this has given rise to the uptake of various types of renewable energy sources (RES). Such as wind, solar and biomass energy. Besides the challenge of increasing the share of RES, the electricity sector faces several other challenges in maintaining a secure, reliable and affordable energy supply. In section 1.1, we introduce the reader to some of these challenges. Subsequently, we present the general outline of the Dutch electricity sector in section 1.2. In section 1.3, we present two solutions for addressing some of the challenges. Next, we describe the scope of this research. And finally, in section 1.5, we present the outline of this thesis.

1.1 Developments in the Dutch electricity sector

Development 1: Intermittency of wind and solar resources

The production of electricity by wind and solar resources can be characterised by its intermittent character. Unlike traditional power plants, their production cannot be accurately predicted, nor accurately controlled. This is problematic, because electricity systems require consumption and production to be balanced at all times. Currently, approximately 1% of the total energy consumption in Holland is covered by wind and solar resources [1]. Therefore, the problem of accommodating intermittent power production is not an issue yet. However, two major Dutch research institutes (TNO [2] and ECN [3]), have published reports stating that the current Dutch electricity system is not able to accommodate the increasing shares of solar and wind energy production without modifications.

Development 2: Decentralisation of energy production

The uptake of renewable energy has also given rise to the decentralisation of the energy sector. A part of the energy production takes places locally, turning consumers into so-called ‘prosumers’[2]. Consequently, electricity is no longer distributed unidirectional from a few central points (like large coal plants), but bi-directionally from multiple points. However, the electricity system and especially the management of these flows is currently not designed to cope with these bi-directional energy flows. Thus, the question is how to manage future electricity networks given increasing shares of locally produced (and intermittent) energy.

Development 3: Production and consumption discrepancy

Given decentralised solar energy production, there is often a time discrepancy between the production of solar energy and electricity consumption by a typical household. As shown in Figure 1.1, the electricity consumption by a typical households does not occur simultaneously with the production of solar energy. Consequently, excess solar energy is exported and used elsewhere. Given a low penetration of solar energy in some geographical area, this is not problematic. However, given an increasing penetration of solar installations, the distribution grid may not be able to accommodate this influx. For example, the financial support scheme for photovoltaic (PV) installations in Germany already includes guidelines that promote grid friendly operation [4].The guideline stipulates that, in order to qualify for financial support, only 60% of the nominal photovoltaic power installed can be fed back to the grid [4]. In order to address this problem, the question is how to utilise more solar energy locally, for example by temporarily storing solar energy. Hence, the question is how to match supply and demand.

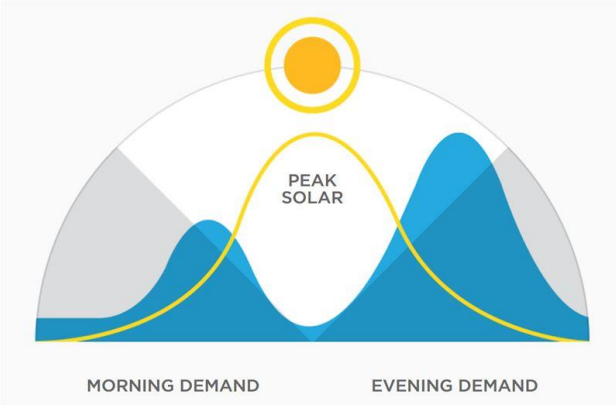

Figure 1.1: Residential energy consumption and solar production, adopted from [5]

Development 4: Electrification

Besides the increase of locally produced energy, we can also distinguish a trends towards electrification of transportation and heating. For example, the number of plug-in hybrid electric vehicles (PHEV), electric vehicles (EVs) and heat pumps (for space heating) has steadily increased over the past decade [6],[7]. A study on the impacts of electrification in the UK [8] shows that peak demand may increase by about 2-3 times. Consequently, grid reinforcements may be required to accommodate the increasing electricity demand and to prevent local power flow issues [8]. In the case of the UK, these reinforcements may cost tens of billions of pounds [7]. Hence, given the increasing electricity demand, the question is how to accommodate this growth, while avoiding excessively high network cost. Again, the question is how to match supply and demand. For example, by local cooperation of prosumers, through exchange of energy and/or by using EV's (cooperatively?) for storing solar energy.

Development 5: Managing distributed energy resources (DER)

The various new technologies that are/will be implemented locally have come to be known as distributed energy resources (DER). This include technologies such as solar and wind energy, referred to as distributed generation (DG), heat pumps (HP), electric vehicles (EV), but also electrochemical energy storage (EEG) or batteries for short, combined heat and power units (micro-CHP) or fuel cells (FC). Interestingly, some of these devices, such as heat pumps or batteries can be actively controlled. Hence, this raises the question how to manage these devices, for example to match supply and demand.

1.1.2 Summary of challenges

To summarise, we can distinguish the following developments.

- Energy production via RES will be more intermittent, requiring more balancing [2], [3].
- There is increasing penetration of (controllable) DER, such as electric vehicles, heat pumps, batteries and solar panels. The question is how to manage these DER [6],[7].
- Local power flow issues may occur as a result of increased local consumption and/or production [8]
- There will be bi-directional energy flows from multiple points in the distribution grid, for which it was not designed [4].

Given these developments, it follows that we require new methods for managing the increasing local electricity consumption, the increasing (local and/or intermittent) electricity production and the occurrence of bidirectional energy flows in the distribution grid. Two solutions to these challenges are discussed in section 1.3

1.2 The Dutch electricity sector

The developments as presented in section 1.1 occur in the context of the current electricity sector. To better understand the context, we now present a high level overview of this sector. The electricity sector can best be visualised by a physical and institutional layer. The two layers are presented in Figure 1.2

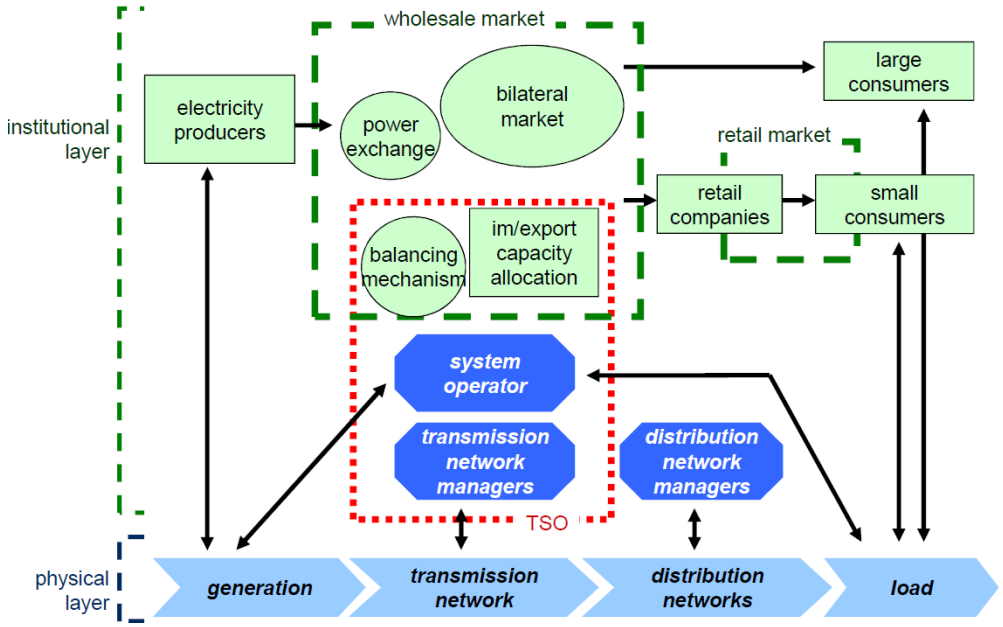

Figure 1.2: Diagram of the Dutch electricity, as discussed in section 1.2. Adopted from [9]

1.2.1 Physical layer

Transmission and distribution

Essentially, the electricity network consists of two parts, the transmission and distribution network. Each is being operated/managed by one or more entities. The transmission grid transports bulk energy over longer distances, whereas the distribution grid transports energy to each individual consumer. The transmission grid is operated by the transmission system operator (TSO). In the Netherlands this is TenneT. The distribution grid is operated by the distribution system managers/operators (DSO). In the Netherlands there are three companies (Alliander, Stedin and Enexis) that manage the majority of the Dutch distribution networks.

Generation and loads

Electricity was traditionally generated by several coal and gas power plants. Its bulk production is transported via the transmission lines and distributed to consumers via the distribution grid. On the other end of the lines are the loads (consumers). Large loads are (often) directly connected to the transmission grid, whereas small loads receive energy from the distribution grid. Nowadays, large solar and wind parks are also connected to the transmission grid. On the other hand, small wind turbines and particularly solar panels feed their production to the distribution grid.

1.2.2 Institutional layer

TSO and DSO

As seen in [10], the Dutch TSO TenneT has three tasks: '*to balance the injections and withdrawals of power in the transmission network, to manage the Dutch electricity transmission network and to manage import capacity.*' For the first task, TenneT operates various balancing mechanisms. Unlike the TSO, the DSO does not operate the network actively. Instead, the DSO performs maintenance, expansion and reinforcement of the distribution grid. Given the increasing penetration of DER, it is possible that DSOs will take a more active role in operating the distribution network. But for now, this is outside the scope of their activities and only occurs in some pilot projects.

Small and large scale consumers

Consumers with an interconnection capacity smaller than 55kW (3x80A) are designated small consumers ('kleinverbruikers'). Consumers with an interconnection capacity greater than 55kW are designated large scale consumers ('grootverbruikers'). Small consumers in the Netherlands currently enjoy the favourable feed-in tariff ('salderingsregeling'). This tariff applies to all small consumers that produce wind or solar energy themselves and 'behind their meter'. This means that any production is first used to meet consumption, before the superfluous production is fed to the grid. Given this scheme, small consumers can deduct their yearly energy production from their yearly energy consumption up to the point of having a net zero consumption/production. In contrast to small consumers, large scale consumers are not subject to the feed-in tariff. Instead, the price for supplying electricity to the grid is lower than the price for buying electricity. According to [10], the 'feed in price' is usually about 75% of the electricity price.

BRPs & E-programmes

Consumers, retailers and suppliers that wish to buy energy from or sell energy to the Dutch electricity network are obliged to enter into a balancing responsible party (BRP) contract with TenneT. Each purchase or sale, referred to as nominations, is communicated to Tennet via the BRP contract. Alternatively, market parties, such as large scale consumers, can designate a third party– being recognised by TenneT as a BRP – to make nominations on their behalf. Small scale consumers, like households, are obliged to contract an energy retailer (like Greenchoice/Eneco). These parties act on their behalf on the wholesale market. The energy retailer either contracts a third party BRP or is a BRP.

For each consecutive day, the BRP is responsible for notifying grid operators on their planned energy consumption, production and transport requirements. Based on this information (the nominations), BRPs produces a report, referred to as the E-programme (energy programme). The E-programme has a 15 minute resolution and spans an entire day. The 15 minute blocks are referred to as PTUs (per time unit). Each day, all BRPs communicate their E-programme for the next day to Tennet. These then serve as input for operating the transmission/distribution network the next day. If actual production and consumption deviate from the estimates in the E-programme, this leads to an imbalance. This can ultimately affect the reliability of the grid. TenneT resolves imbalances by utilising the balancing mechanisms described in section 1.2.3.

1.2.3 Wholesale market

For this study, we consider the power exchange and balancing mechanism. The power exchange (EPEX spot) includes the day-ahead market and the intraday market. The balancing mechanism contains various instruments. We can discriminate between two types of balancing mechanisms: active balancing and passive balancing. Active balancing mechanisms are actively controlled by TenneT. Passive balancing reserves are controlled by BRPs. Importantly, all national electricity networks in Europe are connected. A property of such a system is that the frequency is equal throughout the network. Consequently, any (local) perturbations affects the entire system and its frequency. Therefore, all TSOs across Europe jointly manage frequency perturbations within the European electricity system (synchronous area). Within the Netherlands (LFC area), part of the system control (mainly balancing) is carried out on a national level.

Day ahead and intraday market

In the day-ahead market, energy is traded per hour, in quantities of 0.1 MW (100 kW) or a multiple thereof. The hourly nominations are subject to physical delivery of electricity of a constant output on the electricity grid. Up to 1 hour prior to delivery, market parties can buy or sell electricity on the intraday market in quantities of 0.1MW or more. Market parties use the intraday market to optimise their position to reduce risks associated with unexpected imbalance prices charged by the TSO TenneT.

Active balancing

Four active balance mechanisms are available to the TSO, TenneT: *primary reserves, regulating capacity, reserve capacity and emergency capacity*. Each day, these mechanisms are continuously activated and deactivated. In case of a frequency disruption in the synchronous area, *primary reserves* are automatically activated within seconds. Their purpose is to contain the frequency within a certain safe operating range. On a slightly longer timescale (~30seconds or less), *regulating capacity* is actively controlled to maintain the balance between electricity supply and demand. *Reserve capacity* is primarily used to resolve local transmission restrictions, but may also be used for restoring the energy balance. Local transmission restrictions may occur if the electricity demand in some area exceeds the transmission line capacity that is used to supply electricity to that area. In case of insufficient *regulating and reserve capacity*, e*mergency capacity* is used to restore the electricity balance.

The *primary reserves* are often referred to as the frequency containment reserve (FCR). The other 3 regimes are often referred to as frequency restorations reserves (FRR). Within the FRR, we can distinguish between automated reserves: aFFR, (mostly regulating capacity) and manually operated reserves: mFFR (mostly reserve capacity). For an overview of all reserves, see Figure 1.3.

Passive balancing

BRPs can also help balance the electricity system by monitoring their portfolio imbalance and by responding to a real time system imbalance signal, broadcasted every minute by TenneT. This mechanism is referred to as the *replacement reserves (RR)*. Any BRP with an imbalance that helps reduce the system imbalance receives remuneration. Any negative contribution results in an imbalance penalty. Hence, **passive balancing** can be defined as: *The process whereby a BRP reduces or increases its portfolio imbalance by altering the energy consumption and/or energy production, based on a real time system imbalance signal broadcasted by TenneT, in order to balance the electricity system.*

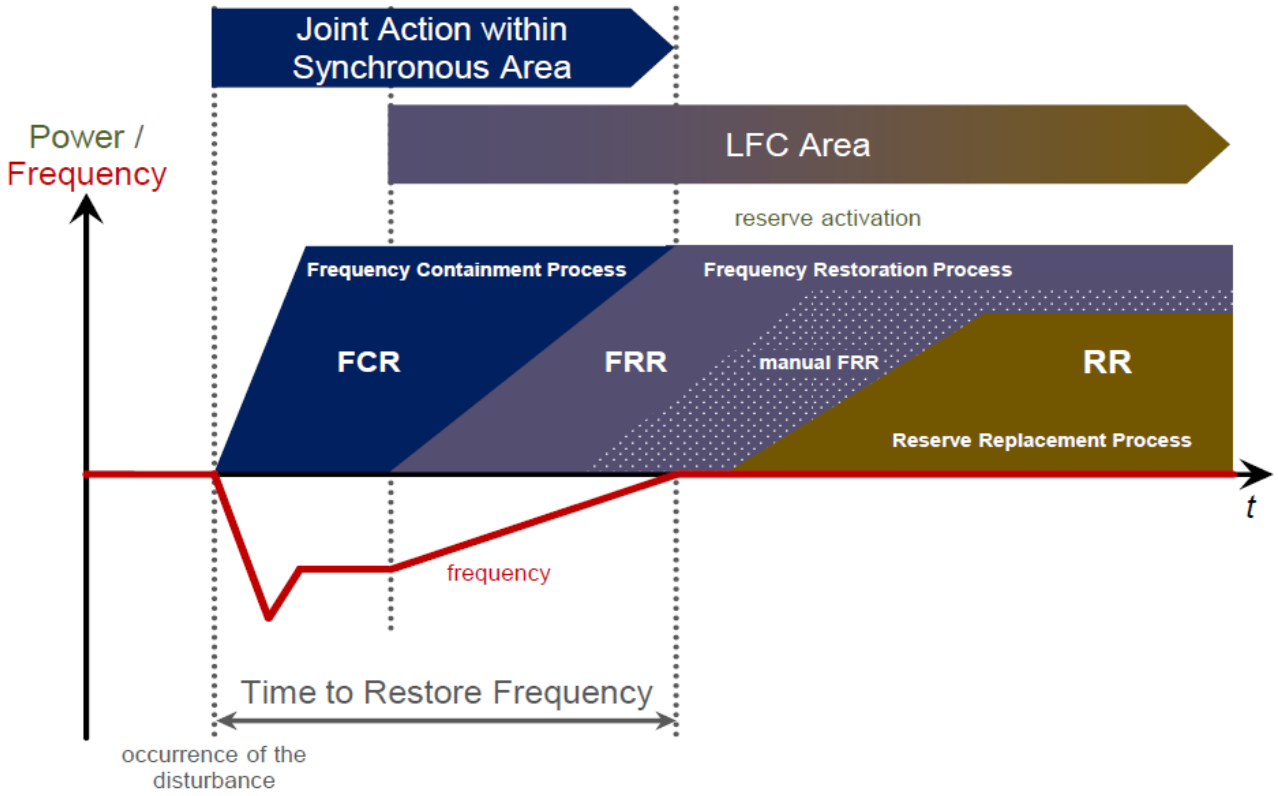

Figure 1.3: Balancing mechanisms in the Netherlands, adopted from [11].

1.3 Addressing the developments

Given the developments presented in section 1.1, the question rises how to address them. Various solutions are possible, of which two concepts are important to this study.

Flexibility

A solution to the intermittency and local power flow issues, is to increase the supply of flexibility. [2], [3]. **Flexibility** is the ability to rapidly modify the level of production and/or consumption. Flexibility can be used for balancing the grid, or to prevent local power flow issues, by altering energy production/consumption. Traditionally, production flexibility was used to maintain the system balance. Given varying demand, power plants continuously adjusted their output. However, given the increasing adoption of wind and solar, less production flexibility is available. Hence, the alternative is to add more load flexibility. For example by introducing electrical storage devices or by load shifting [1]. In load shifting, the overall energy consumption remains equal, but the time of consumption is manipulated.

Smart grids and microgrids

Often, the term *smart grid* is coined as a means to address the challenges as outlined in section 1.1. As stated by Fang et al. [12],'*The smart grid, regarded as the next generation power grid, uses two-way flows of electricity and information to create a widely distributed automated energy delivery network.' Hence,* the smart grid facilitates the exchange of information between (local) market parties in order to produce signals for operating DER and other units within the electricity system.

The microgrid (MG), can be considered as one of the more tangible smart grids solutions. Essentially, a microgrid is a small electricity grid, connected to the main electricity network via one interconnection. Within the microgrid, various production units and loads (possibly by different parties) are interconnected. In addition, the units are operated via an energy management system (EMS). The EMS and MG enable the exchange of local electricity and can help maximise consumption of local produced energy. The benefits of microgrids are manifold. According to Soshinskaya et al. [13], microgrids help reduce electricity transportation losses, increase energy efficiency and reduce CO2 emissions. Apart from the technical benefits, the adoption of the MG is also incentivised through socio-economic motives. According to Koirala et al. [14] '*the quest for autonomy and local community engagement are seen as important drivers, as well as an increased willingness to pay for local sustainable energy and a higher reliable supply.*'

The microgrid concept and related scientific research will be discussed in more detail in chapter 2.

1.3.2 Need for research into microgrids and flexibility services

Given the increasing need for flexibility [2][3] the question rises to what extent DER may be used to provide flexibility services in the context of a microgrid. Where [2] defines **flexibility services** as: ''Technically, an electric flexibility service can be defined as a power adjustment sustained at a given moment for a given duration from a specific location within the network.'

Research has already shown that microgrids can be used to address several of the challenges highlighted in section1.1, such as such power flow issues, increased penetration of DER and bi-directional power flows [13]. In addition, the operation of microgrids and connection with wholesale markets has been extensively researched.

However, the literature falls short in various aspects. Although various studies have defined scheduling strategies for market participation by microgrids, the provision of flexibility (services) is not considered sufficiently. Secondly, the goal of maximizing self-consumption, in conjunction with scheduling strategies for market participation is almost always neglected. Thirdly, the time resolution used by most researchers is 1 hour. Although this resolution is sufficient for estimating costs and benefits associated with the power exchange, it does not respect the 15 minute timescale of the imbalance markets. Lastly, the provision of flexibility to other market parties is currently subject to considerable barriers. These issues often remain unaddressed, but could affect the viability of some of the proposed market participation strategies.

1.4 Research question and scope

1.4.1 Topic of this study

The objective of this study is to investigate whether microgrids may offer flexibility services to the Dutch electricity system, while maximising solar self-consumption. In this study, the definition of flexibility services from Eid et al. [15] is used: *'Technically, an electric flexibility service can be defined as a power adjustment sustained at a given moment for a given duration from a specific location within the network.'* To investigate the provision of flexibility services by a microgrid, the Schoonschip microgrid serves as starting point for this research.

Schoonschip community microgrid

The Schoonschip project [16] is an ambitious initiative, aiming to become the most sustainable floating community within Europe to date. The Schoonschip microgrid will be situated in Buiksloterham, a neighbourhood in northern Amsterdam. It will consist of 30 floating houseboats that are equipped with solar PV, solar thermal collectors, heat pumps and thermal and electrical storage. The heat pumps can extract heat from the surrounding water using a heat exchanger that has been incorporated into the floating concrete structure of the houseboats. Each house is connected to the microgrid, to enable exchange of energy between the community members. The microgrid is connected to the main grid via one connection. The community is registered as a large-scale energy consumer ('grootverbruiker'), having a single energy retailer. The latter is possible, as the community is part of experimental legislation ('experimenteerwet'). This law grants the community the right to buy and sell electricity collectively, rather than individually per household. Peak shaving may be required to prevent overloading the interconnection. To that end, batteries are used. In addition, the batteries will be used to increase the solar-self consumption of the community.

Peak shaving is defined as: *The process of lowering electricity peak demand, through discharging batteries, shifting or curtailing the electricity demand*. **Solar-self consumption is defined as:** *The self-generated solar electricity that is not fed into the grid, but used directly or indirectly (via local batteries) within the community*.

To understand the difference between direct and indirect use of self-generated solar electricity, consult Figure 1.4. All solar electricity stored in the battery to be used later for serving demand is considered indirect solar self-consumption. Also, the battery is only used for storing solar energy, and not for storing energy that has been imported from the main grid.

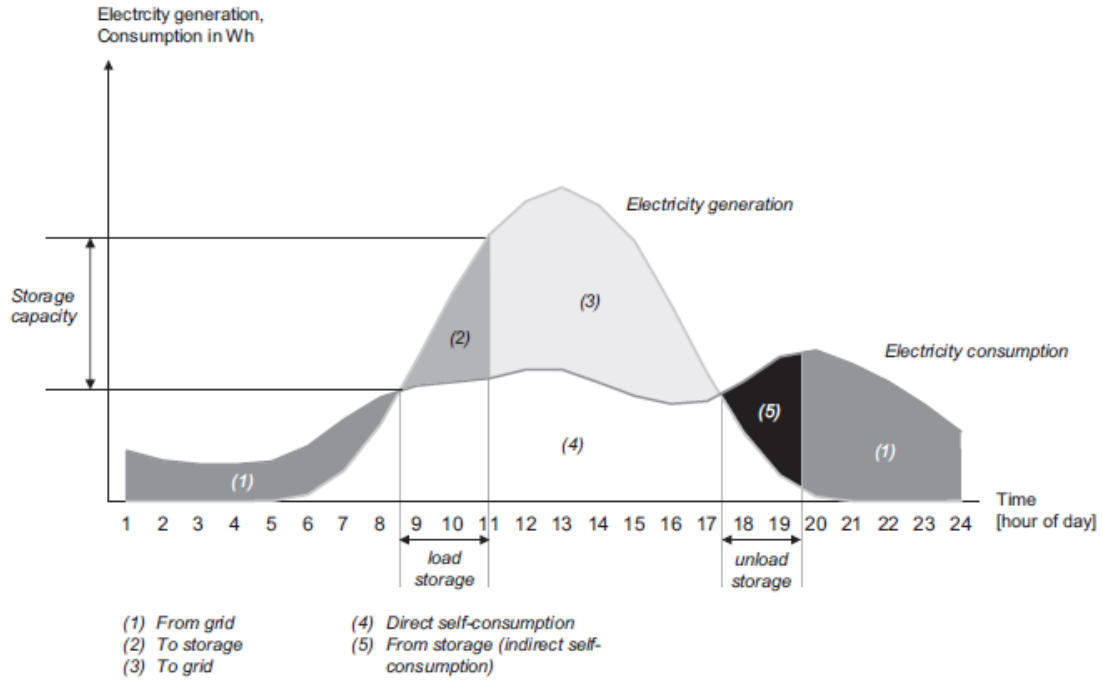

Figure 1.4: Direct and indirect solar self-consumption, adopted from [17].

Goal of Schoonschip

In the case of Schoonschip, the goal is to be as sustainable as possible and strive for collaboration among its residents. The economic exploitation is also of interest to the community. However, the maximisation of revenue is seen as a secondary objective. Therefore, profitable interactions with the energy market are subordinate to the main objective of maximising solar self-consumption.

1.4.2 Contributions of this study

The contribution of this study is to identify *if* and *how* flexibility services may be offered by a microgrid, such as Schoonschip. To that end, we consider the current Dutch electricity market and its regulations. The cost and benefits of exploiting flexibility services will be investigated. Thereby, we consider peak shaving and maximisation of self-consumption as two priorities.

Having defined the scope of this research, we can define the main research question:

> **Main research question (MRQ):** *How can a community microgrid provide flexibility-services to the current Dutch energy sector, while maximizing solar self-consumption, and what is the value of these services?*

1.5 Thesis structure

This thesis is structured as follows:

In chapter 2 we present a literature survey and market research on DER implementation, flexibility services, microgrids, market barriers and various other concepts that are closely related. The aim of chapter 2 is to identify which flexibility services can be offered by the Schoonschip microgrid, given the current Dutch electricity system, regulations and Dutch electricity market design. Informed by chapter 2, we present a problem setting in chapter 3 that describes the two flexibility services that will be analysed in this study. These include day-ahead portfolio optimization (participation to the day-ahead market) and passive balancing. In the problem setting, we have outlined the most important features of this research and the models that are to be constructed. Next, in chapter 4, we present a methodology for evaluating the value of both flexibility-services. Subsequently, in chapter 5, we present the Schoonschip case study and the data collections that have been used.

The core of this thesis revolves around chapter 6 and 7. In chapter 6, we provide the mathematical formulation of the day-ahead portfolio optimization problem. In this formulation, the goal is to maximize the solar self-consumption and secondly to minimize the net cost, using the flexibility of the battery systems. In chapter 6, we present an elaborate model to evaluate the electrical flexibility that can be provided by the thermal systems. That is, the electricity consumption by the heat pump and electrical back up heater coils, the latter being installed in the buffer tanks. Thermal models on the house, buffer tanks and heat pump serve as input for evaluating the electrical flexibility available for passive balancing (and peak shaving.

Next, in chapter 8, we present methods to forecast the electricity consumption and electricity production on a daily basis, with a forecast horizon of 36 hours. The forecasts techniques are used to produce production and consumption profiles for the day-ahead portfolio optimization problem.

In chapter 9, we present the results of chapter 6 and 7. In chapter 10, we present our conclusions and the limitations. Also we propose further research possibilities.

Chapter 2

Literature and market survey

In this chapter we present our literature and market survey. In section 2.1, we describe three solutions for integration of DER. Subsequently, in section 2.2, we present various types of flexibility services. In section 2.3, we describe 2 organisational designs for enabling flexibility services. Next, in section 2.4, we present the concept of microgrids and scientific research in the field of microgrids and market participation by microgrids. In section 2.5, we identify important market parties for enabling market access. Also, we identify market trends and opinions via various interviews. In section 2.6, we identify barriers for enabling flexibility services. Based on the previous sections, we identify which flexibility services are available to the Schoonschip microgrid community. Based on section 2.4 and 2.7, we identify several research opportunities in section 2.8

2.1 Literature survey: DER potential, challenges and integration

The energy transition is marked by a decentralizing energy sector, where increasing shares of energy are produced locally and distributed energy resources (DER) become available, turning consumers into so-called *''prosumers''.* With the adoption of DER, this presents challenges and opportunities for local and national management of the electricity grid. In 2.1.1, we briefly introduce the potential and issues of integrating DER. In section 2.1.2, we discuss three solutions for integrating DER into the electricity system.

2.1.1 DER potential and challenges

According to [15], some of the main benefits for adoption of DER are: the increase in local energy autonomy, the reduction of CO2 emissions, the reduction of peak demand requirements and the improved energy efficiency by reduction of transmission and distribution losses over electricity networks. In [18], the authors envision a future energy system where circa 50% of the energy production capacity and controllability of conventional centralised generators is covered by DER.

Currently, locally produced energy in the Netherlands is fed into the grid for favourable, government supported, feed-in tariffs, presenting prosumers with no incentive to take additional steps in raising energy autonomy and help improve energy efficiency. Moreover, operation of distribution networks may be hampered with increasing penetration of DER. As stated in [19], ''*increasing shares of DER are potentially problematic for grid stability and reliability due to congestion and voltage issues''.* In addition, the adoption of intermittent RES/DER, presents a challenge to cope with this volatility in a cost-efficient manner. According to [20], ''*Ensuring reliable electricity supply is a costly endeavour given the requirement for back-up flexible electric power generation combined with limited electricity transmission capacity*.'' Furthermore, various organisational designs aimed at integrating DER are prone to regulation barriers, as discussed in section 2.6. Hence, the integration of DER is hampered by technical barriers and, as we will see later, also by regulatory barriers requiring appropriate solutions.

2.1.2 Solutions for integrating DER

To address these issues, researchers in [21] distinguish three solutions for integrating more DER/RES: *''1) generation reserves, 2) demand-side management (DSM)/demand response (DR) and 3) DER integration from the distribution side''.*

1. Generation reserves

The idea behind generation reserves is to have back-up capacity available when electricity demand cannot be satisfied by (intermittent) production capacity. According to [21], ''*this approach is more traditional and due to limited availability of clean resources it is unlikely to play an important role.*''

2. Demand side management / demand response

The idea behind DSM is well explained by [22][22][22][23] ''*The concept of DSM includes all activities which target the alteration of the consumer's demand profile, in time and/or shape, to make it match the supply, while aiming at the efficient incorporation of renewable energy resources*.'' Hence, by smoothing the demand curve, demand elasticity is created, enabling electricity consumption to better match the intermittent electricity production. This will be important in a future with more intermittent RES capacity. According to [22], "*Demand response (DR) is considered one of main DSM activities being the most cost-effective and reliable option for smoothing of the demand curve, when the system is under stress'.* Thus, DR may also lower peak demand, reducing the need for (more) generation reserves and additional investments in transport capacity as pointed out by [20]: ''*Network-driven DR aims to maintain system reliability by decreasing demand in a short period of time and reducing the need to enhance generation or transmission capacity''.* Note that various demand response programs have been proposed in literature and implemented in practice (e.g. Volatis' BluePod implemented by more than 100,000 customers). However, these will not be covered as this is beyond the scope of this research.

3. DER integration from the distribution side

A third line of research focusses on *DER integration from the distribution side*, introducing new mechanisms for local coordination according to [21]. As argued by [15] and [23], the problem of integration DG in the distribution grid is the potential need for voltage- and congestion management. This is incentivised by the intermittent character of DG and potentially high solar production peaks. In light of these observations, the authors in [23] conclude that *''we expect to need new mechanisms for balancing and congestion management on the distribution grid''.* In section 2.2, these mechanisms have been explained shortly. In section 2.3, we will more thoroughly identify various configurations (and mechanisms) for local DER coordination.

2.1.3 Flexibility

In the context of DSM and local coordination strategies, scholar often refer to demand response, as ''load flexibility'' and/or ''production flexibility.'' A general definition on **flexibility** is presented in [24]: ''*On an individual level, flexibility, is the modification of generation injection and/or consumption patterns in reaction to an external signal (price signal or activation) in order to provide a service within the energy system.*'' Where [2] defines **flexibility services** as*: ''Technically, an electric flexibility service can be defined as a power adjustment sustained at a given moment for a given duration from a specific location within the network.'*

2.2 Literature survey: Flexibility services

Several flexibility services have been envisioned. The work in [22] and especially [25] provide a very comprehensive overview. DSO's, TSO's and BRP's are seen as potential customers of flexibility services. However, according to [25], prosumers can also utilise flexibility internally. That is, flexibility is used by the prosumer itself for behind the meter optimizations. We will refer to this application as *flexibility services for behind the meter.* The various flexibility services are summarised in Table 2.1

Table 2.1: Flexibility services

Flexibility services for:	**Type of flexibility services, according to** [25]
Behind the meter	• Time-of-use (ToU) optimization: load shifting from high price intervals to low price intervals and/or load shedding during high price intervals. • Peak shaving: Reduction of the maximum demand by shifting or shedding the electricity consumption • Self-balancing: creating value through the difference in the cost of buying/selling and generating electricity.
Balancing responsible party (BRP)	• Day-ahead portfolio optimization: shifting loads (in the portfolio of the BRP) from high price time intervals to low price time intervals, given a 24 hour time horizon. Conversely, production may also be shifted to high-price time intervals. • Intraday portfolio optimization: Similar to day-ahead portfolio optimizations, but the time window is 1 hour. • Passive-balancing: The process whereby a BRP reduces or increases its portfolio imbalance by altering the energy consumption and/or energy production, based on a real time system imbalance signal broadcasted by TenneT, in order to balance the electricity system. See chapter 1, section 1.2.3 • Generation optimization: Optimization of the electricity output by central production units when readjusting its output between two hourly planned production volumes.
Distribution system Operators (DSO)	• Congestion management and grid capacity management: Optimization of operational performance and reduction of the electricity peak load to avoid thermal overload of the system components. • Voltage problems: Voltage problems, due to a large influx of solar PV, can push up the voltage, but can be mitigated by employing flexibility services. As stated in [9] ''voltage problems typically occur when solar PV systems generate significant amounts of electricity, which can be resolved by using flexibility to increase the load or reduce generation''. In return, this mechanism may reduce the need for grid investments, according to [9].
Transmission System Operator (TSO)	• Primary, secondary and tertiary reserves are utilised to maintain constant frequency of 50 HZ within the transmission system, to relieve congested transmission lines and perform power quality management. Traditionally, large power plants provide these services, but as the energy mix contains increasing shares of RES, different providers are needed. According to [25], flexibility services from DER can be used for these purposes.

2.3 Literature survey: Enabling flexibility services

Given the potential of flexibility services, the question is how to enable these services. As argued in section 2.1.2, demand side management (DMS) and demand response (DR) are not sufficient to enable effective integration of distributed energy resources (DER). In this section, it is argued that to integrate DER and enable flexibility services, new organisational designs and entities are required for coordination and management. As will also be argued in this section, mechanisms for local coordination can be considered local energy management solutions. Where the definition by [26] on **local energy managemen**t solutions is as follows: *''the coordination of decentralised energy supply, storage, transport, conversion and consumption within a given geographical area.''*

Aggregation

According to [22], [23] and [25], a key notion in organising LEM is the concept of aggregation. According to [23], an **aggregator** is seen as an entity that collects the flexibility of local prosumers that own DER, to create ancillary services and offers these to other parties, such as the TSO, DSO or BRP. Aggregation is required, because individual prosumers may only offer limited capacity, flexibility and certainty of supply. As stated in [22][22][22][23] *''only large customers can easily sell flexibility and participate in the flexibility market today.''* Thus, by aggregating the flexibility volume of multiple customers, aggregators can reduce these existing barriers.

Two organizational designs for aggregation

The authors in [23], have identified two popular organisational designs in the context of smart energy systems (SES). Interestingly, both designs envision a different role for the aggregator. The **aggregator** is either seen as ***commercial party*** or as a ***local energy market*****.** Figure 2.1 schematically illustrates a simplified version of these two roles and presents the various entities that may use/deliver flexibility: In figure 2.2 *''direct trade''* resembles the use of local markets, whereas the *''aggregator/BRP route''* resembles the aggregator as commercial party. Note that *''the market''* either resembles the wholesale/imbalance market or a local market on the distribution side. In section 2.3.1 and 2.3.2. we describe both designs as discussed in [23]. For comparison, both designs are illustrated by discussing an actual pilot with each aggregator role in section 2.3.3. Using these cases, we also identify the key barriers in adopting these designs, given the Dutch energy retail market context.

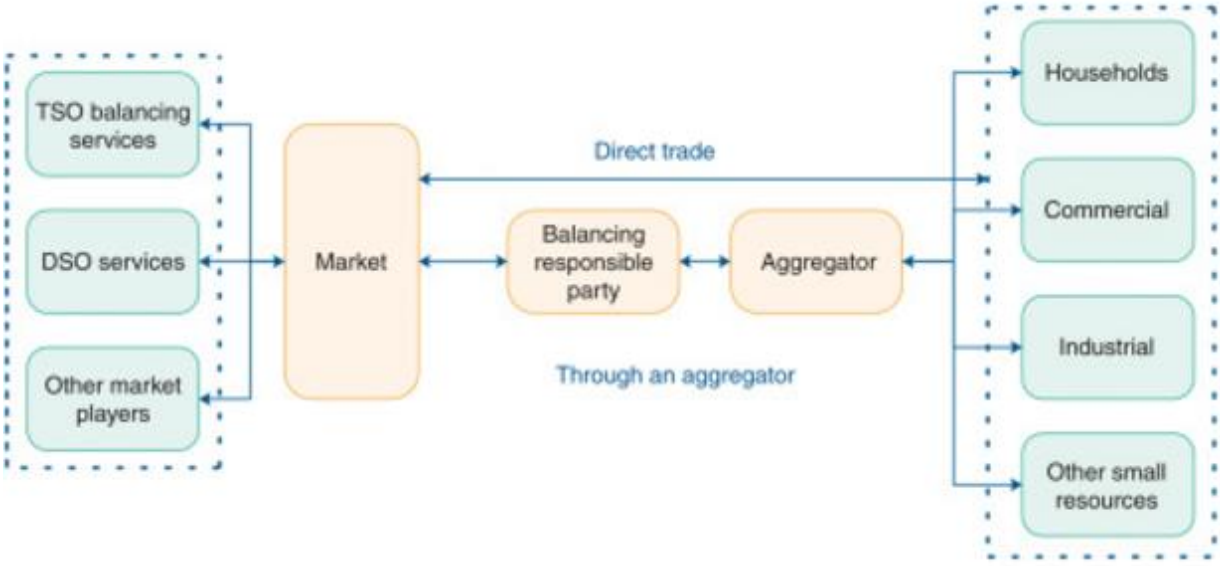

Figure 2.1: Aggregation through local market and commercial party, adopted from [27]

Different definitions, same ideas

Confusingly, authors use different definitions for categorising similar (aggregation) concepts. In [23], smart energy system (SES) and smart grids are used interchangeably, whereas in [26], various organisational models, including smart grids and SES are considered local energy management (LEM) concepts. According to [26], microgrids, VPP, smart grids, smart hubs & smart energy systems (SES) are all considered LEM solutions. However, in [21], only some specific concepts are considered key in enabling DER integration through aggregation: Microgrids, VPP and energy hubs.

LEM: a microgrid, smart grid, SES and more…

Next, we argue that the authors in [23] and [26] use different descriptions for similar organisational designs. Which implies that LEM, SES and smart grids all relate to the same concept. For example: in [26], four LEM pilots with different organizational models have been evaluated. In one of the pilots, the USEF (universal smart energy framework) design for enabling flexibility was applied. In [23], the authors used USEF to characterise the organisational design of a SES, in which the aggregator is seen as commercial party. Conversely, a local market based pilot called Power matching city (PMC) is evaluated by [26] and serves as example of a local market based aggregator, as described in [23]. Hence, organisational design for integration of DER in a distribution side context can be referred to as local energy management.

Henceforth, we will refer to *DER integration from the distribution side* as a Local Energy Management (LEM) solution.

2.3.2 Commercial party as aggregator

According to [23], this organisational design considers the aggregator to be a new type of retailer to which prosumers can offer their flexibility. The aggregator may have direct control over DER. As explained by [23], multiple aggregators may be active within a distribution grid area and prosumers may choose whether they want to contract a commercial aggregator, traditional retailer or both. The DSO remains responsible for balancing and congestion management within the distribution grid. Aggregators may be able to trade on the wholesale market, requiring them to appoint an existing BRP or become a BRP themselves. The latter would require the aggregator to purchase a BRP license & meet the requirements for assuming this role. On the distribution level, a similar construction could be possible, requiring the DSO to have a more dynamic mechanism for balancing and congestion management.

A prominent framework that has been developed to facilitate aggregation of flexibility services through commercial parties is USEF. The market structure and associated rules and tools have been described elaborately. In the work of [26], a USEF pilot, called energy front runners (‘’Energiekoplopers’’), was analysed. In Table 2.2: A commercial aggregator pilot: Energy frontrunners, the use case has been described; the mean barriers for adoption have been highlighted.

2.3.3 Local markets as aggregator

According to [23], a local market may act as aggregator of DER, allowing actors (i.e. prosumers, retailers, DSO) to offer their flexibility on the market. As stated in [23], *‘’The local market corresponds to (a part of) the distribution grid, where a DSO would be able to set local market prices for congestion and balancing.’’* BRPs may procure flexibility services on the local market and/or trade these further onto the national transmission system level imbalance market.

A prominent local market enabler is PowerMatcher [28]. In this design, agent-controlled DER clusters help balance supply and demand and provide flexibility services to a retailer & DSO. In [26], the application of a local market in combination with PowerMatcher is analysed: Power matching city. We present the use case and findings of this pilot in Table 2.3

2.3.4 Case studies

The case studies, as discussed in Table 2.2 and Table 2.3, illustrate the two aggregator roles. Also, the independent reviews by [26], underline some of the problems of adopting these LEM solutions, given the current market design. This is helpful to better understand which flexibility services may be offered by the Schoonschip microgrid. The results serve as input for section 2.6. There we present a comprehensive overview of the market & regulatory barriers.

Results of case studies

From the case study we can draw the following conclusions:

1. The DSO is not allowed, nor incentivised to procure flexibility, given the current market design.
2. Given the market design, the retailer nor the prosumer is allowed to sell flexibility in a local market.
3. In the context of retail competition and retail choice, a compensation mechanisms is needed to enable aggregators to utilise flexibility from prosumers, while compensating the retailers that are affected by these changes.
4. Given a local market, the coordination mechanism should be such that it is robust and does not require market parties to manage the process of allocating flexibility.

Table 2.2: A commercial aggregator pilot: Energy frontrunners
A first pilot using the USEF framework was the Energy koplopers project. According to Mr. Eric Woittiez, program manager of the Energy koplopers project, see [29], the aim of purchasing flexibility was to maximise the revenue of the BRP and return value to the prosumer for offering its flexibility. Flexibility was purchased to perform arbitrage and make use of the price differences between the retail price, flexibility price and day-ahead and imbalance market prices. The BRP functioned as an intermediary in order for the aggregator to create value in the wholesale and imbalance market. By using a link to the BRP systems, PowerMatcher was used to make a 'virtual power plant' of the available devices. The PowerMatcher allowed control over all devices as one or more subclusters.
Barriers for commercial aggregators, according to [26]
According to [26], the following barriers exist *1.* In the project, the aggregator was able to adjust the consumption pattern of individual households. However, since the households were free to choose their own retailer, the retailers would have been affected by the changes from the aggregator. As each retailer produces forecasts on the energy consumption within their portfolio (E-programme), they may be penalised by the TSO, in case these changes result in imbalance cost for the retailers. To resolve this problem and to maintain retail choice, a compensation mechanism should be devised for retailers that are affected by (sudden) changes to their E-programme. *2.* In this pilot, the DSO was allowed to procure flexibility, however, given the current market design, it is not incentivised nor allowed to procure flexibility.

Table 2.3: A local market as aggregator pilot: Power matching city (PMC)
Based on the PowerMatcher software, each device capable of delivering flexibility is presented by a software agent that bids flexibility into the local market. According to [26] **, *''consumers, energy suppliers and grid operators cooperate actively to balance the demand for and supply of energy in the grid''.*** The combined flexibility of all devices is aggregated by various aggregation agents located on a home and neighbourhood level. Also stated in [26]**, *''the local market is connected to the national power exchange through an auctioneer service enabling local and central energy supply systems supplement each other.'*** Finally, an auctioneer agent uses a multi-objective optimization to set a price for balancing power in the local market, taking grid constraints, national power exchange prices & DG (peak) production into account. Once the market is cleared, each device (agent) receives a signal. Based on the bid from the agent, the device is either activated or not.
Barriers for local markets, according to [26]
According to [26], the following barriers can be distinguished: 1. In this pilot, the energy retailer, DSO and prosumer were permitted to procure flexibility. Given the current market design, this is not possible as no market is located at the distribution level, nor is it permitted to engage in this type of interaction. 2. The coordination mechanism for allocating flexibility was not robust. As a result, flexibility could not be allocated. To resolve this problem, the energy supplier managed the allocation process. However, in the current market design, where every prosumer can choose its own retailer, the allocation process would be even more complex, requiring a better coordination mechanism. 3. Given the current market design, DSO's are not allowed to procure flexibility. Also, the current design provides DSOs with economic incentives that discourage the purchase of flexibility.

2.4 Literature survey: Microgrids

The organisational designs in which aggregators are seen as local markets or commercial parties provide a holistic description on the function of a LEM concept. Other LEM concepts such as the virtual power plant & microgrid concept may not be as holistic, but especially microgrids have received considerable attention amongst scholars. As stated by [30] *"Microgrids have been identified as a key component of the Smart Grid for improving power reliability and quality, increasing system energy efficiency."* Since Schoonschip is based on a microgrid we will mainly focus attention on the concept of microgrids. We will shed light on scientific work regarding microgrid management and market participation.

2.4.1 Microgrids (MG)

Another prominent LEM concept is the microgrid. According to [30], *"'A **microgrid** is a group of interconnected loads and DER within clearly defined electrical boundaries that acts as a single controllable entity with respect to the grid. A microgrid can connect and disconnect from the grid to enable it to operate in both grid-connected or island-mode."*

According to [30], [31] [32], microgrids present many benefits such as energy cost savings, greenhouse reductions, increased reliability and reduced grid congestion and transportation losses. These benefits are realised by the adoption of an energy management system (EMS). The EMS operates and coordinates the DER to provide energy to all participations within the microgrid. In order to fully exploit these benefits, microgrids require coordination and scheduling. According to [21], ''*The scheduling system must consider forecasted output of renewable DG and demand, market tariffs or forecasted electricity and fuel prices and the technical constraints on devices so as to plan and schedule within the microgrid as well as the relationships with the main grid in terms of market participation".*

Research on: Microgrid energy management & scheduling.

According to [33], ''*the optimisation of power flows, local dispatch and power purchases of microgrids is extensively researched."* In [34], day-ahead planning is optimised based on profit maximization considering system constraints and regulations. In [35], an EMS is presented to minimise the operational costs of microgrids by coordinating the power production by several devices and energy storage units. Alternatively, in [36] different pricing strategies, such as time of use & real time pricing, are adopted in conjunction with optimal day-ahead scheduling strategies. Centralised control is used to coordinate storage devices, satisfy load requirements and minimise the total operating costs of the microgrid. In [37], a method for determining the optimal hourly dispatch of an aggregated group of DER's is presented. The scholars in [37] have identified two market strategies for participation in a real-time market: Utilise local production as much as possible, or maximise the value of the MG. Depending on the market strategy, unit commitments/scheduling decisions are made. That is, the status (on/off) of power generation appliances is determined for each time period during some scheduling horizon.

Decentralised approaches have also been extensively investigated. In central design strategies, such as discussed in [34]- [37], DER are regulated by one central master controller. In decentralised control, often by the use of multi-agent systems (MAS), DER are controlled separately, each having an agent for control, operation and monitoring, while also communicating with other agents. For example in [38], a MAS is used for operation of a MG. Day-ahead and real-time generation scheduling is adopted. Real time scheduling updates are used to adjust the power settings of the DER. In [39], a MAS is also used, to provide a method for minimising energy costs and alleviating overall peak load of the system.

Research on: Microgrid wholesale market participation

The focus of [34]-[39] is primarily on the optimisation of MG operation itself. In more recent work, researchers have focused on the link between the external market and MG. In [40] & [41] researchers propose a bidding strategy that takes uncertainty from generation, demand & day-ahead market prices into consideration. Similar research, considering optimal day-ahead power scheduling is discussed in [42]. In this research, the adoption of flexible thermal loads is proved to be successful in compensating for the variable and intermittent behaviour of DG. The work in [40] is continued in [43] where hourly bidding curves for day-ahead markets are proposed as a trading technique for aggregators. In [44] the work in [43] is further extended to include intraday bidding, which is used to correct the positions taken in the day-ahead market. Similar work, including day-ahead market participation and intraday corrections is discussed in [45]. In [46] the research focuses on day-ahead power scheduling for aggregated prosumers in the electricity market. The work contributes to the existing line of research by taking the bidding process and market rules explicitly into account. In contrast to [40]-[46], the authors in [47] also take network conditions and physical constraints into account to obtain more realistic bids.

Research on: network constraints and losses

In this section we explore the research done on electrical network constraints, losses and other technical issues. In [48], the effects of increasing PV and HP penetration have been investigated for various feeder configurations, connecting 377 houses. The effects of varying feeder strength and increasing HP/PV penetration were evaluated. Given increasing penetration of PV/HP, the average annual Ohmic losses vary between 16.5 kWh to 225 kWh per house. Stronger feeders, having higher Ohmic resistances, result in more Ohmic losses, however, voltage quality is less of a concern. According to [48], weak feeders require PV curtailment to prevent feeder voltage reach impermissibly high values. For HP/PV penetration between 60-100%, the average annual curtailment losses increase from 0 kWh to 817kWh per house.

In [49], the main bottlenecks for implementing net zero-energy buildings (ZEB) have been investigated.. As stated in [49], ''the feeder voltage fluctuations and possible transformer overload are quantified as bottlenecks.'' As stated by the authors in [49], *When all dwellings are intended to achieve a ZEB status, (i) a fraction of 14 to 47% of local PV supply is wasted by inverter curtailing, depending on the feeder strength, while (ii) the peak transformer load is found to be 3.3 kVA per dwelling which may affect power security in existing feeder designs''*

Hence, from [48] and [49], it follows that PV curtailing, feeder strength, and transformer capacity affect the electrical losses and viability of implementing ZEB. According to [49], solutions can be implemented on a building and feeder level. As mentioned in [49] and [47], the implementation of battery storage and/or (more) heat storage can (partially) elevate inverter curtailment losses. Finally, new advanced inverter controls and distribution system management (DMS) can alleviate the problems even further. As discussed in [50], the implementation of DMS and advanced inverters can contribute to power quality and acceptable voltage levels, as a result of power factor corrections and voltage modulations. As seen in [48] and discussed in [49], an obvious way to mitigate problems is to increase feeder strength and/or increase transformer capacity.

Research on: network conditions/physical constrains in scheduling problems

Many researchers [40]-[46], neglect the network conditions and physical constraints in their microgrid scheduling strategy. However, the analysis by [48] and [49], raise suspicion whether these constraints can be neglected in scheduling optimizations. In [47], the importance of including network conditions and physical constraints into a scheduling problem has been shown. As stated in [47] *''the actual power flow in the line connecting the main grid and microgrid may deviate significantly from the day-ahead bids, if the bids are determined without consideration of the real-time adjustment through active network management, which will lead to a substantial imbalance cost.''* To mitigate these problems, the following considerations when formulating the optimization problem have been made by [47]:

- Active and reactive power flows in the distribution and connecting line should not exceed their respective line capacities
- The power flow in the connecting line should be maintained within the power factor range permitted by the contract with the DSO
- The voltages of all busses should be within the regulation range.

2.5 Market survey: Market parties, trends and opinions

To acquire a better understanding of the possibilities and developments in the energy sector, we review some market parties enabling access to wholesale markets. A short description about some interesting companies and their services follows in section 2.5.1 Subsequently, in section 2.5.2, we discuss some recent developments in the energy sector. For this market survey, we review information from various websites. [51]–[57]. Also, various interviews have been conducted to acquire a better understanding [29], [58]–[61], [62]–[64]. All interviewees have given their permission to incorporate (edited) quotes in this research document.

2.5.1 Market parties enabling market access and their views/opinions

Various entities enable access to wholesale markets for prosumers. An overview follows:

Jules energy [53]

Jules energy is a BRP that focuses on prosumers with more than 100 KW of installed DG capacity. Via an online web based transaction platform Jules enables access to the wholesale electricity market.

ETPA [54]

ETPA enables large consumers (>0.5 MW) to trade energy capacity via the intraday market through their platform. According to [65]: ''*ETPA could provide a potential solution as a trading platform capable of providing access to flexible capacity with opportunities to conclude short-term intra-day contracts".* This allows aggregators to provide flexibility services to other market parties. This claim is supported by Mrs. Gerda de Jong, Electricity market developer at Tennet. According to Mrs de Jong, interview [63]: *''TenneT is shareholder of ETPA, because TenneT thinks it will unlock flexibility in the market."*

An advantage of using ETPA is that no (large) entry fee and retail license are required to start trading on the EPEX spot. Instead, small fees are charged per transaction. It follows from [66] that the cost of trading via ETPA consist of a monthly license fee of € 150 and a variable fee of € 0,25 to € 0,75 per MWh. Customers that wish to trade energy via ETPA are not required to switch energy supplier [67]. Interestingly, this is possible as ones retailer is not affected if its client trade via the ETPA. According to [67], this is because of the following: Energy trading via ETPA is facilitated through Single-sided transactions (SST), that are used to make changes to the E-programmes of the client's BRP/retailer program. The changes are processed by TenneT. Thereby, TenneT automatically adjusts the E-programme of the clients BRP. To make use of SST, TenneT needs to receive approval from ones retailer/BRP, before SST and mutations in its E-programme can be applied by TenneT.

Dynamo [55]

Despite the limitations of the current market design, Dutch DSO Alliander is looking to close bilateral contracts with (large) commercial customers for the purchase of flexibility in the coming years. Also, some experiments with dynamic connection and distribution tariffs will be introduced.

E.X.E [56]

E.X.E is a BRP enabling customers access to the wholesale market through their online platform (EAN to EPEX). Note, the European Article Number (EAN) is the identification number of an electricity connection. Also bilateral energy deals between electricity connections are possible (EAN to EAN). No access to the imbalance market is yet provided. By entering in a service contract with E.X.E., electricity exchange with the grid is covered through their BRP position. Since E.X.E. is owned by Alliander (DSO), they are not allowed to trade or sell energy. Hence, E.X.E merely provide access to the wholesale market, requiring customers to have an EPEX retail license. Noteworthy to mention is that, according to Mr. George Trienekens, business manager at E.X.E, interview [62], the platform could potentially allow nominations to be made of less than 100kW, using intermediate parties.

E.D.mij [57]

E.D.mij is a BRP and retailer enabling clients to exploit fluctuating prices in the day ahead market and strongly fluctuating imbalance prices. E.D.mij was also the first party to provide *collective* emergency power by aggregating capacity, with a minimum of 0.5MW per client. E.D.mij charges a fixed monthly fee and flexible market prices depending on the energy volume that was traded. Interestingly, according to Mr. Heine Prins, co-founder and board member at E.D.mij, interview [61], E.D.mij has developed an algorithm enabling them to predict the direction of the system imbalance for every PTU. Based on this information, customers are instructed to ramp up or down their energy demand/production, yielding lower imbalance cost and higher imbalance revenues.

2.5.2 Developments

Although the energy sector is gradually developing, it is noteworthy to mention some of the (recent) developments.

Imbalance market [51]

In 2017, Tennet is running pilots for frequency containment reserves (FCR) and automatic frequency restoration reserves (AFRR). The goal is to uncover possibilities for smaller actors to provide balancing services. Usually, Tennet asks for a minimum of 1 MW, see table 2.3, whereas in these pilots, the providers are allowed to supply 0.1 MW. One of the pilots, see [68], includes the New Motion, a company that owns charging stations for electric vehicles. By charging faster or slower depending on the needs of the TSO, the New Motion provides FCR. The ultimate goal is to set up a competitive market allowing all market parties access to the imbalance market. For now, the limit is still at 1MW, except for the participating piloting parties.

Multiple retailers per connection point [52]

A development with respect to changing regulations is a recently published draft by the Dutch energy regulator ACM (Autoriteit Consument & Markt). The draft states that both companies and consumers may contract multiple retailers per connection point, by requesting a secondary allocation point and installing a separate measuring device. This allows customers to contract 1 retailer for the electricity consumption, and possible another for selling excess energy. This could result in more competition promoting the adoption of distributed renewable energy. See section 2.6 for a review on the limitations of this regulation. The regulation started in 2018 onward.

Shift to more liquid wholesale market

According to Mr. Eric Woittiez, program manager of the ‘’Energy Koplopers’’ project, interview [29], the intraday market was too illiquid to profit from price differences in the ‘’Energy Koplopers’’ project. Mr. Matthijs van Rijn, former project manager at Alliander, interview [59], acknowledges this claim and also points out that the intraday market is still too illiquid. Furthermore, according to Mr. van Rijn, the need for portfolio balancing products is limited, because the uptake of solar panels in the Netherlands is too small to cause significant imbalances. Therefore, BRPs are still able to resolve most system imbalances within their own portfolios, rather than having to rely on external parties.

From a 2016 market review by Tennet, it shows that: ‘’the volumes on intraday markets are only about 1.8% of the day-ahead volumes for EPEX spot [69]. The Dutch intraday market is much smaller than the German market because of the following four aspects: ‘’a) the smaller size of the market in the Netherlands; b) a lower amount of intermittent renewable capacities; c) a different balancing market which allows to trade; and d) ex-post trading capabilities.’’ However, according to Mr. Phillippe Vassilopoulos, head of product design at EPEX SPOT, [64], the markets of the future will increasingly revolve around intraday and closer to real time markets. Already, the intraday market is becoming more liquid month by month. According to Mr. Vassilopoulos the liquidity has been increasing for years now, mostly due to uptake of RES. The claims by Mr. Vassilopoulos are supported by research on the development of Dutch wholesale markets. According to a TNO report in [70]: *‘’The increasing need for balancing, either within portfolios or on the intraday market, will not only provide additional demand for ramping up of conventional production, it will also drive up the price on the intraday market for additional power to compensate a shortfall in production from renewables.’’* This result is supported by evidence from Great Britain’s electricity market. According to [27]: ‘’*with more uptake of variable generation, the real-time price volatility increases much faster than the day-ahead price volatility and flexible resources can take the advantages of this volatility’’*

Intraday not easily achievable

Participation to the intraday market is difficult to achieve. As pointed out in [46] ***’’****intraday trading may involve costly and time consuming task, such as replanning and communicating these revised plans to the market operator and involved departments’’* This remark is partially supported by Mr. Heine Prins, co-founder and board member of E.D.mij, interview [61]. According to Mr. Prins, intraday prices are hard to predict, as it requires a continuous acquisition of weather data, market information and analysis. Moreover, Mr. Prins states that successful intraday market participation is also influenced by a certain amount of ‘’gut feeling’’. E.D.mij uses algorithms to do the intraday planning, but this is followed by human confirmation. Hence, this would hamper the possibility to fully automate trading, without the help of advanced machine learning algorithms.

2.6 Market survey: Barriers for flexibility services

The possibilities for providing flexibility services and participation to the wholesale market are limited. Several issues are outlined hereunder:

Retail competition & BRP's

One of the problems hampering utilisation of flexibility services in the Dutch retail market design, is that no competition over demand-side services is allowed. According to [71], ''*Every small prosumer/aggregator is bound to a retail contract and its balancing responsible party*.'' Therefore, aggregators can only trade on the market through their BRP, hampering free trade on the wholesale- and imbalance market. The only possibility for unlocking flexibility seems to switch retail/BRP contract as stated in [71], ''*Prosumers that wish to unlock their flexibility can either accept the combined BRP/retail offer or renegotiate their entire contract with another supplier.''*

Compensation schemes to enable aggregation of flexibility services through commercial parties.

According to [24] & [26], aggregation of flexibility services through a commercial party is not (yet) possible in the context of retail competition. As seen in the case study in table 2.1, compensation schemes are required to reimburse retailers that are affected by sudden changes in their portfolio.

Lacking ICT infrastructure

According to Mr. Guy Rutten, energy consultant at SIA partners, interview [60], ''*Large energy retailers have difficulties adjusting their IT systems to deal with the increasing influx of data coming from smart meters. Notice that this problem does not apply to new market entrants.''* In addition, the aggregation and utilisation of flexibility from small scale consumers would require more extensive administration. However, the mutations that follow from utilisation of DER is again something that is not yet supported by retailers. Mr Rutten points out that the adoption of Microgrids, having a single connection, may address part of these issues. Although, according to Mr. Rutten, ''*retailers would probably not be interested still, as it would also require investments in new IT systems, while there is no clear business case for this investment.''* He states that microgrids make local distribution more efficient, so in the end there is less volume to sell for the large retailer and therefore it is harder to make a profit with the current low margins. As a result of these IT barriers, only large consumers with power requirements in the order of MW's are the ones that provide various flexibility services today. This claim is supported by the work in [22], *''only large customers can easily sell flexibility and participate in the flexibility market today.''*

DSO position

The provision of flexibility services to DSO's is hampered by the current market design. To enable market access, the position of the DSO needs to be reviewed. According to [26], ''*the DSO is not allowed to procure ancillary services, because it is a monopoly party and so the price of flexibility cannot be set competitively''.* Also, as stated in [26] DSO's are forced to annually decrease operational expenditures, whereas the procurement of flexibility services would potentially increase these expenditures. However, possibilities exist to participate in pilot projects. For example, Alliander has designated several locations requiring congestion management and voltage control [53]. However, Buiksloterham (the neighbourhood where Schoonschip is located) is not one of them. Therefore, we will not further elaborate on this.

Multiple retailers restrictions

The possibility to issue multiple retailers per connection point may present interesting opportunities. However, the possibilities seem limited in the Schoonschip context. According to a senior enforcement official at ACM, see interview [58], a new delivery contract (also the second or third) will be closed for each individual allocation point. An allocation point can contain one or multiple DER/loads; within an allocation point one can produce and consume. In that case, one's production can be utilised for self-consumption. However, if production takes place at an allocation point and consumption at another allocation point, it is not possible to use the electricity production for self-consumption. Hence, Schoonschip cannot maintain a traditional retail contract for its energy consumption , while utilising the PV production for self-consumption and having a second allocation point and retailer to sell excess energy.

Flat energy tariffs

Most traditional retail contracts provide little or no incentive to utilise/aggregate the flexibility of prosumers. In most cases prosumers are subject to flat energy tariffs and do not respond to price signals. However, as of 2017, it is possible to contract APX based tariffs (e.g. NUON and EasyEnergy) for small business and consumers (with a connection smaller than 45kW)

Imbalance market participation

According to [19], requirements such as a minimal bid size, bid duration, penalties on non-supplied services and high entrance fees for assuming the role of BRP/supplier create more barriers for (small) aggregators. As can be seen in Table 2.4, the primary, secondary, tertiary and emergency reserves have a minimum capacity requirement of at least 1 MW. Given the Schoonschip interconnection capacity of 136 kW it is impossible to directly participate in any of these regimes, without further aggregation. As previously outlined in section 2.5.2, Tennet only recently initiated some first pilots, see [51], to explore the opportunities of utilising aggregated DER capacity for balancing services in the primary and secondary reserve domain.

Another problem is the uncertainty about when and how much capacity will be required once participating in the primary, secondary or tertiary regimes. Participation would involve considerable uncertainty, which makes it hard to schedule energy imports/exports for a microgrid while fulfilling self-consumption and maximising profit. In addition, penalties on non-delivered services pose a serious problem in conjunction with this uncertainty. For example, the penalty involved in failing to meet commitments for FCR are 10 times bigger than the potential revenue.

The only feasible option is to make use of the restoration reserves. For example, E.D.mij grants indirect access to the restoration reserves by signalling its clients to ramp up or down their consumption.

Wholesale market participation

In contrast to the imbalance market, the day-ahead and intraday market are more easily accessible. These markets require a minimum of 0.1 MW nominations or potentially even less , as is suggested by Mr. George Trienekens, in section 2.5.1. participation into the day-ahead market requires a BRP license. A BRP license is extremely costly (>1.0 E6 euro), hence it is more feasible to contract a third party BRP. Finally, access to the wholesale market requires a retail license.

Table 2.4: Characteristics of the wholesale market

Day-ahead market:

- 1 hour intervals
- Minimal bid size is 0.1 MW [72]
- Requires entrance fee, retailer license and (third party) BRP license

Intraday market:

- 1 hour intervals [69]
- Minimal bid size is 0.1 MW[72]
- Requires entrance fee, retailer license and (third party) BRP license

Primary reserves (FCR)

- Contracted for one week [73]
- Minimum bid size is 1 MW [73]
  - Except for the case of this year's Tennet pilot, as referred to in section 2.5
- Automated frequency control [73]
- 100% availability within 30 seconds [73]Full activation frequency deviation: +/- 200mHz [74]
- Technical unit or pool of units [74]
- Penalty on non-delivered services for the period capacity is not available [75]
  - 10x bid price * volume [75]
- Limited resources, such batteries, fly wheels, water reservoirs, etc., are also allowed. [74]
- Minimum supply period for limited resources is 30 minutes. [74]

Automated frequency restoration reserves (aFFR)

- Parties that consume or produce more than 60MW have an obligation to participate.
- Minimum bid size is 4 MW. [73]
- Aggregation is possible [73]

Manual frequency restoration reserves (mFFR)

- Minimum bid size is 4 MW. [76]
- The minimum up and downward regulating rate per minute needs to be at least equal to 7.0% of the total capacity. [76]
- The activation time is smaller than 1 minute. [76]
- Reserve capacity offered on the imbalance market should be available for a duration of 15 minute (referred to as 1 PTU.) [77]
- The bid price and capacity can be adjusted up to an hour prior to delivery. [77]

Emergency capacity

- Minimum volume of 20 MW [73]
- Aggregation is possible [73]
- 24/7 stand-by [73]

Passive balancing reserves

- Per 15 minutes / PTU.
- Requires access and integration with portfolio management system of a BRP

2.7 Market survey: Selecting flexibility services

In this section, we describe the available research opportunities and identify which flexibility services are available to the Schoonschip microgrid. In section 2.7.1,we identify how direct market access can be obtained by the Schoonschip microgrid. In section 2.7.2, we discuss which flexibility services can be provided by the Schoonschip community.

2.7.1 Enabling market access

Barriers for enabling market access

Based on section 2.6, six barriers can be distinguished that hamper direct market access for prosumers and prosumers that are part of a microgrid.

1. Aggregation of flexibility services through a commercial party is not (yet) possible, because this requires compensation schemes to reimburse retailers that are affected by (sudden) changes in their portfolio.
2. Assuming the role of BRP/supplier involves high entrances fees, which create barriers for adopting the role of commercial aggregator.
3. Requirements such as a minimal bid size, bid duration, penalties on non-supplied services create barriers for participating in the imbalance market.
4. Retailers do not (yet) require portfolio balancing/optimization.
5. The IT systems of (large) retailers are (probably) not ready yet for portfolio optimization by external parties.
6. DSO's are not allowed to procure flexibility.

Market parties for enabling energy market access

Based on section 2.5, we identify options and possible bottlenecks to enable market access for microgrids like Schoonschip.

1. A potential solution would be use ETPA. ETPA allows her clients to maintain its retail contract, while trading on the energy market. Importantly, ETPA needs approval from one retailer/BRP to apply their services. Moreover, ETPA requires a minimal capacity of 0.5MW, which is more than the maximum interconnection capacity of the Schoonschip microgrid.
2. The possibility to issue multiple contracts per connection point may also aid wholesale market trading. However, as was discussed in section 2.5. the restriction on exchanging power between two allocation points prevents implementation.
3. The final option is to contract a BRP/retailer to facilitate direct market access and trading capabilities. Given the experimental legislation (''experimenteerwet''), the households within Schoonschip do not each require a separate retailer/BRP contract, but can all be part of the same retailer/BRP contract. In addition, the minimum volumes required for trading are within range of the interconnection capacity. For example, Jules Energy requires a minimum nomination capacity of 0.1 MW, see [53], whereas E.X.E. potentially allows for even smaller nominations, as found in an interview with Mr. George Trienekens, see [62].

Selecting a market party

We can conclude that option 1 and 2 are not feasible, because of the minimal capacity requirements (option 1) and limitations on having multiple connection points (option 2). However, option 3 is feasible, because it is conceivable that Schoonschip can trade via E.X.E, Jules Energy, Ed.mij or similar BRPs/retailers. These type of BRPs/retailer closely resemble the *aggregator as commercial party* (as discussed in section 2.3). Thus, a commercial aggregator (like E.D.mij or Jules energy) may act as market participant on behalf of Schoonschip.

Thereby, barrier (1) is circumvented because only one retailer/BRP is supplying all households within Schoonschip. This is possible given the experimental legislation that Schoonschip is part of. Barrier (2) is also circumvented given the low financial barriers of contracting these type of market parties. Finally, barriers (4) and (5) are also less of a concern, as these market parties have new IT systems to enable demand side management. Hence, given these new type of BRPs/retailers, only barriers (3) and (6) are of importance. These will be considered in the next section, when selecting suitable flexibility services

2.7.2 Enabling flexibility services

As discussed in section 2.2, we can discriminate between four types of flexibility services: Flexibility services for the TSO, DSO, BRP and for behind the meter. In this section we identify which flexibility services may be offered by Schoonschip.

Flexibility services for behind the meter

It follows that all options for utilizing flexibility behind the meter can be executed given a traditional retail contract. Most notably, *peak shaving* can be used to reduce the contracted interconnection capacity thereby reducing grid connection cost. Also, some retailers already offer variable retail tariffs. Given these flexible tariffs, it is possible to benefit from *ToU optimization.* However, the use of flexibility behind the meter does not enable market interactions. Therefore, we also turn our attention to the other three types of flexibility services.

Flexibility services for the DSO and TSO

Given barriers (3) and (6), we conclude that individual microgrids cannot (easily) provide flexibility services to the DSO or TSO, directly. The DSO is simply not allowed to procure flexibility, hampering this possibility. Participation to the imbalance market is currently not possible given the capacity requirements. Participation via an innovative BRP/retailer is, however, possible if flexibility from multiple microgrids is aggregated. However, this is beyond the scope of this research.

Flexibility services for the BRP

Given barriers (4) and (5), traditional retailers / BRP's are either not ready for this kind of services and/or do not require flexibility services yet. However, relatively new market parties such as Jules Energy, E.X.E. or E.D.mij allow for a wider range of flexibility services. Consequently, it is conceivable that the following flexibility services can be enabled given the current market design: *day-ahead-portfolio optimization*s, *intraday- portfolio optimizations* and *passive balancing*.

Inspection reveals that intraday portfolio optimization is not yet feasible. As discussed in section 2.5, the intraday market is not yet liquid, although it is likely to become increasingly liquid over the coming decade. In any case, intraday market participation is difficult to achieve: automated participation requires continuous weather forecast updates, data analyses, machine learning & serious computational power to be of any interest. As this is beyond the scope of this research, we will not further elaborate on this.

Thus, day-ahead portfolio optimizations and passive balancing are the only options left. It follows that day-ahead portfolio optimization can be accomplished fairly easily. New BRP's like E.X.E allow their clients to freely trade on the day-ahead market. Also they allow for smaller nominations than normally accepted. Passive balancing is also possible, given state of the art IT systems, which allow BRP's to control flexibility of their clients. Examples are Ed.mij and E.X.E.

2.8 Summary: Research opportunities

The literature and market survey has revealed several local energy management (LEM) approaches to integrate DER from the distribution side. One of these approaches is the microgrid (MG). Interestingly, most scheduling optimizations [40]-[46] do not include an optimisation for solar self-consumption. To the best of our knowledge, no study has yet considered maximisation solar self-consumption as a constraint for scheduling energy in the wholesale market. Although [37], considers self-consumption and real-time market prices, no overall optimization on scheduling energy in the energy market is conducted.

Another void in microgrid scheduling relates to the consideration of network constraints in formulating optimization problems. The need of including these was first shown by [47]. Ideally, the optimization should include these constraints to identify how much capacity is available for export or import of energy.

The possibility to use microgrids for day-ahead portfolio optimizations in combination with passive balancing and peak shaving provides excellent opportunities to provide flexibility services to both BRP's and the transmission system. However, little attention has yet been directed towards this type of market interaction. To the best of our knowledge, only the scholars in [42] investigated the possibility to utilise thermal flexibility for balancing purposes. However, the scholars have not considered an actual market and only perform corrections with a 1 hour time window.

Finally, many researchers [40]-[43],[46] consider hourly data on production and consumption. Thereby, neglecting uncertainty about the intra hourly variations. To appreciate this stochastic behaviour and to address imbalances settlements over 15 minute time periods, a smaller time resolution is required.

Chapter 3

Problem setting

In this chapter, we present three research questions. The questions follow from the literature and market survey and serve as a guideline for answering the main research question.

3.1 Project description

For this research, we consider a collaborative energy community, inspired by the Schoonschip project in Amsterdam north. The community contains 30 floating houseboats, equipped with PV panels, modulating heat pumps, thermal collectors and battery storage. The heat pumps can extract heat from the surrounding water using a heat exchanger that has been incorporated into the floating concrete structure of the houseboats. The DER (distributed energy resources) are integrated via a MG (microgrid) and centrally controlled by an EMS (energy management system). The microgrid is connected to the local distribution grid via interconnection of 136kW and registered as large-scale consumer (''grootverbruiker''). The community receives its energy from a single energy retailer/aggregator. The aggregation of DER via a MG requires collaboration between its users.

3.1.1 Percentage of solar self-consumption

The main drivers for the adoption of the Schoonschip microgrid are community sustainability and increased collaboration amongst its members and their assets. The utilisation of locally produced solar energy is seen as the main objective, yielding higher energy efficiency, energy autonomy and lower transportation losses.[30]

The gross solar self-consumption percentage, SSC_{gross}^{day} is given by equation (3.1). In this case, all solar energy that is produced within the microgrid is also is consumed within the microgrid.

$$SSC_{gross}^{day} = \frac{E_{PV}^{day}}{E_{consumption}^{day}} \cdot 100\% \tag{3.1}$$

With $E_{consumption}^{day}$, the total energy consumption for some day and E_{PV}^{day},the total PV production that day.

In practice, the ability to consume all solar energy may be limited. In that case, the maximum direct and indirect solar self-consumption percentage per day is given by equation (3.2).

$$SSC_{max}^{day} = \frac{E_{PV,direct}^{day} + E_{PV,indirect}^{day}}{E_{consumption}^{day}} \cdot 100\% \tag{3.2}$$

With $E_{PV,direct}^{day}$ the direct solar self-consumption and $E_{PV,indirect}^{day}$ the indirect solar self-consumption.

3.2 Research questions (RQ)

3.2.1 Main research question (MRQ)

Based on chapter 2, *the first part* of the main research question can be answered.

> **Main research question:** *How can a community microgrid provide flexibility-services to the current Dutch energy sector, while maximizing solar self-consumption, and what is the value of these services?*

In chapter 2, two options for providing external flexibility services by the Schoonschip microgrid have been identified: *Day-ahead portfolio optimizations and passive balancing.* Here, *passive balancing* is the process whereby a BRP reduces or increases its portfolio imbalance in order to balance the electricity system and reduce its imbalance cost and/or increase imbalance remunerations. *Day-ahead portfolio optimization* aims to shift energy imports to low-price time intervals and energy exports to high-price time intervals. To enable *both* services, the community must participate in the day-ahead market and contract a retail/BRP party that can enable these services.

To evaluate the value of both flexibility services, we assume the community can appoint an aggregator. The aggregator acts on behalf of the energy community as market participant and has full control over the DER. Also, we assume the aggregator has access to the electricity markets via a third party BRP. Thereby, we assume the BRP portfolio only comprises the Schoonschip MG. Consequently, the value of microgrid flexibility for day-ahead portfolio optimizations and passive balancing can be assessed explicitly. To identify the value of both services, we have defined three research questions:

3.2.2 Research question 1 (RQ1)

On a daily basis, the aggregator performs an optimization for the next day to identify the optimal bids for energy imports and exports in the day-ahead market. As input for this optimization, we assume that the aggregator uses imperfect day-ahead forecasts on the energy consumption and production within the Schoonschip microgrid. We assume battery flexibility to be the main source of flexibility in performing portfolio optimizations. Load shifting is left an open problem, to avoid making the analysis too complex.

> ***Research question 1:*** *What is the value of day-ahead portfolio optimizations with respect to the day-ahead market prices, using battery flexibility?*

RQ1: Sub questions

1. *What are the yearly cost and revenue of day ahead market participation?*
2. *What is the forecasted percentage of solar self-consumption?*
3. *What is the level of cyclic battery aging?*

3.2.3 Research question 2 (RQ2)

As a result of imperfect forecasts in the day-ahead portfolio optimization, imbalances will occur, resulting in portfolio imbalances $P^{t}_{imbalance,R}$. As a result of the imbalances, the real time peak demand may exceed the capacity of the interconnection. In addition, imbalances are to be managed through passive balancing. Since the imperfect forecasts may bring about considerable imbalances, much flexibility is required. We note that only the batteries and thermal systems are capable of delivering this amount of flexibility continuously throughout the day. However, most battery flexibility is already used for day-ahead portfolio optimizations. Therefore, we assume that thermal flexibility is utilised for peak shaving and passive balancing. That is, the thermal flexibility related to shifting the electricity consumption of heat humps (HP) and electrical coils.

> ***Research question 2:*** *What is the value of passive-balancing, using thermal flexibility from heat pumps and electrical coils?*

RQ3: sub questions :

1. *What are the yearly imbalance costs and revenues associated with passive balancing?*
2. *Can violation of the interconnection be prevented using thermal flexibility?*
3. *What is the percentage of solar self-consumption?*

3.2.4 Research question 3 (RQ3)

In chapter 2, one option for providing internal, 'behind the meter' flexibility services has been identified: ToU optimization for reducing electricity cost with respect to a dual or dynamic electricity tariff.

To evaluate whether it is useful to pursue day-ahead portfolio optimization and passive-balancing, the results of RQ1 and RQ2 will be compared with the use of ToU optimizations. To that end, we evaluate the value of Time of Use (ToU) optimizations with respect to a dual electricity tariff from a traditional energy retailer. The price for feeding electricity to the network is set to 100% of the dual tariff prices charged by the retailer. Also, we assume that the community owns batteries to maximise their solar-self consumption.

> **Research question 3:** *What is the value of Time of Use (ToU) optimizations with respect to a dual electricity tariff, using battery flexibility ?*

Chapter 4

Methodology

In this chapter we present the research methodology. In section 4.1 we present a method to evaluate the value of day-ahead portfolio optimizations Subsequently, we present the methodology for evaluating the cost and benefits of a traditional energy retailer in section 4.2. In section 4.3 we present the methodology for evaluating the potential of peak shaving and value of passive balancing. Finally, in section 4.4 we present schematic overview of the thermal models used to quantify the thermal flexibility. Also we present a general schematic overview of the entire simulation model. Furthermore, we describe the modularity of the various models and decision software.

4.1 RQ1: Day-ahead portfolio optimizations

4.1.1 The day ahead market

In the EPEX day ahead market, sales and purchase bids are submitted for every hour of the next day via a double sided blind auction. According to [78] energy bids should stipulate a volume and price. The day before delivery, the day-ahead market opens at 00:30 and closes at 12:00. After closure, the market prices are determined for each hour. The marginal price determines the market price. At 12:55 the market prices for each hour of the next day are published [78]. Once a bid is accepted, the owner is obliged to follow through on their bid [72].

Scheduling

According to [79], scheduling problems are often solved under the assumptions of *perfect foresight* and ‘’*price taker”.* With perfect foresight, total knowledge on future energy prices/energy flows is assumed. The price taker assumption implies that the scheduled bids are too small to significantly affect the market prices. Thus, under this assumption, the market prices may be used for calculating the cost and benefits of scheduling. According to [79], optimization problems are usually defined as a deterministic or non-deterministic problem The deterministic approach relies on the assumption of perfect foresight. Non-deterministic approaches can also cope with imperfect information.

4.1.2 Approach for answering RQ1

For day-ahead portfolio optimizations, we consider a scheduling horizon of 24 hours: 00:00-24:00 and a resolution of 15 minutes. We assume that the aggregator can buy and sell electricity to/from the day-ahead market. In addition, we assume that the bid size can vary between zero and the maximum interconnection capacity. Only the batteries are used for scheduling in the day-ahead portfolio optimization problem. The cost and benefits of selling and buying electricity are evaluated over the course of an entire year.

We assume that the aggregator is a *price taker*, because it is assumed that the microgrid is too small to affect the market prices. In addition, we assume that the aggregator has *perfect foresight* about the hourly day ahead market prices for upper bound valuation of the revenue/cost. According to [80], day-ahead market prices are expected to remain at the current price level until 2020. Hence, for this study, historic day ahead market prices may serve as reference for buying and selling energy. Day-ahead market prices from 2015 and 2016 are used. Finally, no *perfect foresight* is assumed with respect to most energy flows. The various energy flows are discussed in more detail in section 4.4.

We adopt a deterministic optimization approach for solving the day-ahead portfolio optimization problem. The use of more advanced optimization techniques is left an open problem. The implementation of power flow constraints in the microgrid schedule is also left an open problem. The day-ahead portfolio optimization problem is solved using lineair programming (LP).

4.2 RQ2: Passive balancing and peak shaving

4.2.1 Passive balancing

BRP's can help balance the system by responding to a real time system imbalance signal, referred to as the ''balans delta''. The balans delta represent the total system imbalance. It is publicly made available and updated every minute. BRP's can act upon the balans delta by adjusting their portfolio imbalance. Any BRP with a portfolio imbalance that positively contributes to resolving the system imbalance receives remuneration. Any negative contribution results in an imbalance penalty.

System imbalances are resolved by Tennet and the cost (or remuneration) are passed on to BRP's. The financial settlements are processed by the TenneT per time unit (PTU) of 15 minutes. To that end, a marginal upward or downward settlement price is calculated per PTU ex ante. Essentially, the settlement prices represent the need for upward or downward capacity and can be used as reference of the system imbalance for some day/PTU. Importantly, the overall portfolio imbalance of any BRP (in MWh), is penalised/remunerated in €/MWh and not in €/MW.

4.2.2 Approach for answering RQ2

We assume that the result of the day-ahead portfolio optimization may be used as E-programme, whereby the E-programme contains the scheduled energy imports and exports. The MG imbalance is defined as the difference between the E-programme and the actual energy production/ consumption. Whereby, we assume that the battery is operated based on the scheduled charge and discharge events from the day-ahead optimization problem. For passive balancing, we assume perfect knowledge, with a 15 minute horizon (1 PTU), on imbalance settlement prices and energy flows with the Schoonschip microgrid. These assumptions are reasonable because:

1) it is feasible to accurately predict consumption/production with a 15 minute horizon.
2) algorithms can be devised to forecast the system imbalance for the next PTU. For example, the Dutch BRP/retailer E.D.mij has already developed such an algorithm, see interview [61].

E-programme and microgrid imbalance

The E-programme is given by equation (4.1). The MG imbalance is given by equation (4.2). The total electricity consumption, given by equation (4.3). We use superscript *h* to indicate hourly time intervals, superscript *t* to indicate quarterly time intervals subscript *F* to indicate that variables are based on the results of the imperfect day-ahead portfolio optimization and subscript *R* to indicate that variables are based on actual values.

$$\hat{P}^{h}_{Eprogramme,F} = \hat{P}^{h}_{Import,F} - \hat{P}^{h}_{Export,F} \text{ for every h} \tag{4.1}$$

With $\hat{P}^{h}_{Import,F}$ scheduled power imports, $\hat{P}^{t}_{Discharge,F}$ scheduled battery discharging, $\hat{P}^{h}_{Export,F}$ scheduled power exports and $\hat{P}^{t}_{Charge,F}$ scheduled battery charging.

$$\hat{P}^{t}_{imbalance,R} = \hat{P}^{h}_{Eprogramme,F} + P^{t}_{PV,R} - \hat{P}^{t}_{load,R} + \hat{P}^{t}_{Discharge,F} - \hat{P}^{t}_{Charge,F} \text{ with } h = \left\lfloor \tfrac{t}{4} \right\rfloor \tag{4.2}$$

With $P^{t}_{PV,R}$ the PV production and $\hat{P}^{t}_{load,R}$ the electricity consumption.

$$\hat{P}^{t}_{load,R} = P^{t}_{Electricity} + \hat{P}^{t}_{HP} + \hat{P}^{t}_{back-up} \text{ for every t} \tag{4.3}$$

With, $P^{t}_{Electricity}$ the *non-thermal based electricity consumption* by appliances and other devices, $\hat{P}^{t}_{HP}$ the *thermal based electricity consumption* of the heat pump and $\hat{P}^{t}_{coils}$ the *thermal based electricity consumption* of the electrical coils in the buffer tanks.

Thermal flexibility

From equation (4.3), it follows that local microgrid imbalances can be managed in various ways. For example, by curtailing the PV production or by reducing the electricity consumption via load shifting. Also, battery flexibility can be used to alter the microgrid imbalance. However, as assumed in chapter 3, these options will not be considered. Instead, we only consider the alteration of the power consumption by heat pumps $\hat{P}^{t}_{HP}$ and electrical coils $\hat{P}^{t}_{coils}$. Now, the electrical flexibility of the heat pumps and back up heaters is directly linked with the thermal flexibility. Two sources of thermal flexibility can be identified:

1. the allowable temperature variance around the set-point temperature of the house.
2. the buffer tanks that can store warm water.

Thus, the thermal flexibility is dependent on the temperature in the house and the temperature of the buffer tanks. As a result of managing imbalances, the power fed to the HP and back up heaters is altered. This affects the temperature in the buffer tanks and ultimately the house temperature. Also, adjustments made to the thermodynamic state of the house and heat storage tanks affect the temperatures in consecutive states. Hence, the temperature in the house and storage tanks are time dependent. Therefore, a dynamic model is required to describe the thermal systems.

To quantify the value of thermal flexibility and potential of peak shaving, we adopt five settings. For each, we evaluate the violation of the interconnection, the percentage of solar self-consumption, the imbalance cost and imbalance revenue per PTU. The evaluation is done over the course of an entire year. The imbalance settlement prices of 2015 and 2016 thereby serve as a reference. The 5 settings are as follows:

1. **No action**
2. **Peak shaving only**: Thermal flexibility is utilised for peak shaving in case the average power demand exceeds the interconnection capacity. No passive balancing is applied.
3. **Passive balancing in one direction:** Thermal flexibility is utilised to reduce local imbalances that yield imbalance cost. Thereby, the imbalance settlement prices serve as reference. Local imbalances that yield revenue are maintained.
4. **Passive balancing in two directions:** Here, thermal flexibility is utilised to reduce local imbalances that yield imbalance cost. Unlike setting 2, thermal flexibility is also utilised to increase local imbalances, yielding more revenue.
5. **Reduce all imbalances:** For this setting, all imbalances are reduced, regardless of the imbalance settlement prices.

Algorithms for control.

The thermal components are modelled and implemented in Matlab (R2016a). In addition, we devise two algorithms. One is used for controlling the temperature in the house and buffer tanks. .The second algorithm is used for performing passive balancing and peak shaving.

4.3 RQ3: Time of use optimizations

4.3.1 Approach for answering RQ3

For the estimation of the cost and benefits associated with Time of use (ToU) optimizations with respect to a dual electricity from a traditional energy retailer, we assume that the Schoonschip community has a traditional energy retail contract. Given the size of the interconnection (136kW), Schoonschip is a large scale consumer (‘’grootverbruiker’’). Hence, the community cannot make use of the favourable feed-in tariff (‘’salderingsregeling’’). Consequently, the price for feeding electricity to the network is lower. We assume that the feed-in price is equal to the dual tariff prices. For ToU optimizations, we assume that the community aims to maximise the solar self-consumption using the battery systems. The ToU optimization is implemented by using the day-ahead portfolio optimization formulation. However, instead of day-ahead market prices, we implement a dual electricity tariff

In addition, we evaluate the cost and benefits of a dual electricity tariff, when only optimizing for a maximisation of the solar self-consumption. Finally, we also evaluate the cost and benefits for a dual electricity tariff when no batteries are available for a maximisation of the solar-self consumption.

4.4 Overview

4.4.1 The thermal models

In Figure 4.1, we present a schematic overview of the thermal systems and energy flows. Central are the buffer tanks that contain hot water for domestic hot water (DHW) and heating. The buffer tank is modelled as two separate tanks. The buffer tanks receive heat from the solar collector, back up heater coils and the heat pump $Q_{hp1,}$ $Q_{hp2.}$ The heat pump and back up heater coils receive electricity from the microgrid $P_{HP,}$ $P_{S1,coils}$ and $P_{S2,coil}$. Both buffer tanks deliver heat for DHW. The house exchanges heat with the floor and the environment, whereby the external air temperature and incoming solar irradiance serve as exogenous variable. The floor heating systems receives heat, Q_{heat}, from buffer tank S2 and emits heat to the house via natural convection $Q_{convection}$ and radiation $Q_{radiation}$. The water duct temperature serves as reference for characterising the demand for DHW. The solar irradiance serves as reference for characterising solar collector production. The external water temperature serves as reference for characterising the performance of the heat pump.

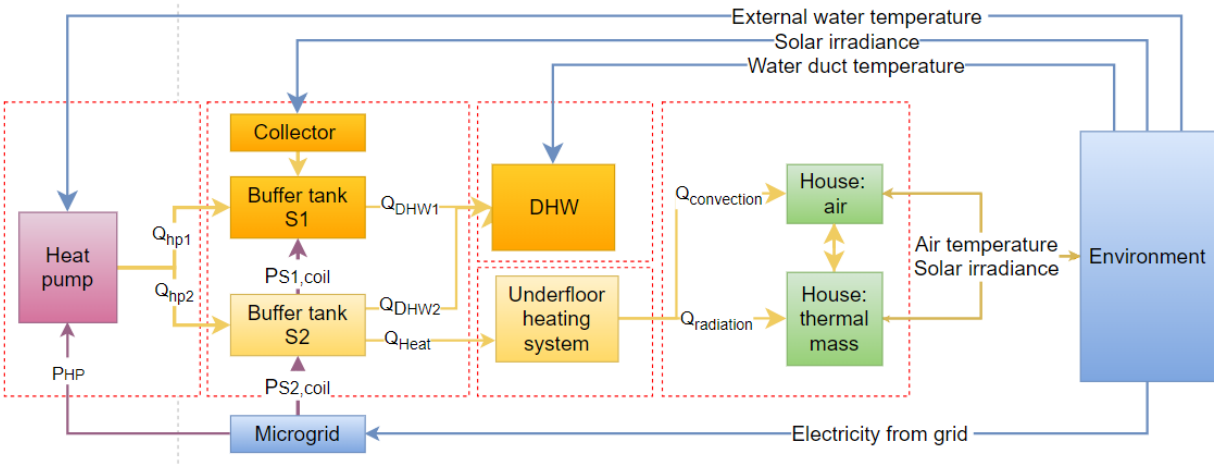

Figure 4.1: The thermal models and energy flows

4.4.2 Schematic overview of simulation model and decision software

In Figure 4.2, we present a schematic overview of the information exchange between the simulation models (green) and decision software (yellow) . The input data and input variables (grey) are supplied to the forecast tools, simulation models and control logic. The output of the forecast tools is fed directly to the day-ahead optimization and indirectly via the thermal models. The day-ahead optimization is used for portfolio optimizations using the battery model. The output of the thermal models and day-ahead optimizations serve as input to the flexibility control unit. The flexibility control unit is used for real time passive balancing and peak shaving. Output data (red) is gathered from the day-ahead optimization, the thermal models, temperature control and flexibility control.

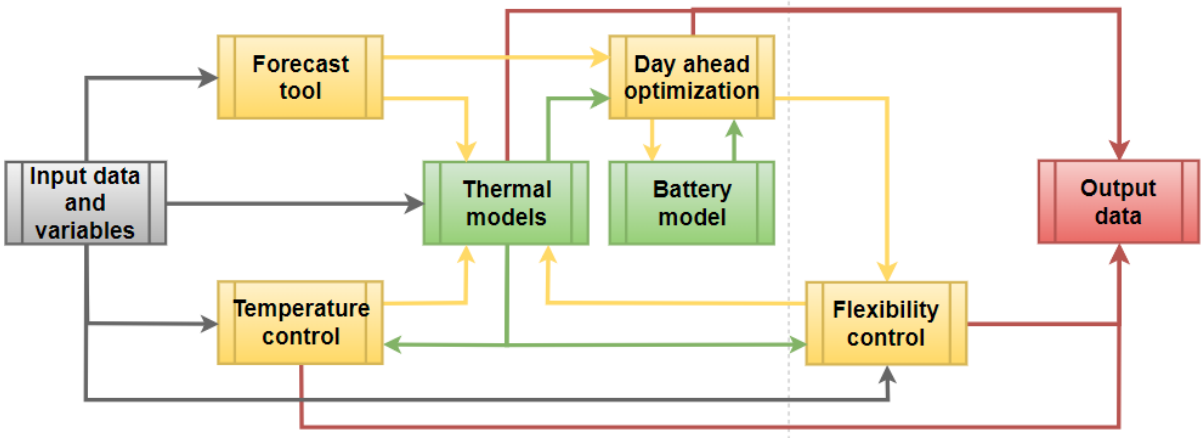

Figure 4.2:The information exchange between simulation models and decision software

4.4.3 Model modularity

The aim of this study is to come up with a complete methodology for evaluating the potential of day-ahead portfolio optimizations, passive balancing and peak shaving. However, given the broad scope of this research, most models are open to improvements. Therefore, the design of most models (1-8) is such that it allows scholars to replace or modify the models proposed in this study. The proposed methodology includes 8 different sub-models:

1. The house model
2. The underfloor heating system model
3. The demand for DHW
4. The stratified buffer tank model
5. The (ground source) heat pump model
6. Forecast tools for various types of energy flows
7. The deterministic day-ahead optimization
8. The control logic for performing temperature control, passive balancing and peak shaving

We present the relations between the sub-components of the thermal model in Figure 4.3and the relations between all main components in Figure 4.4.

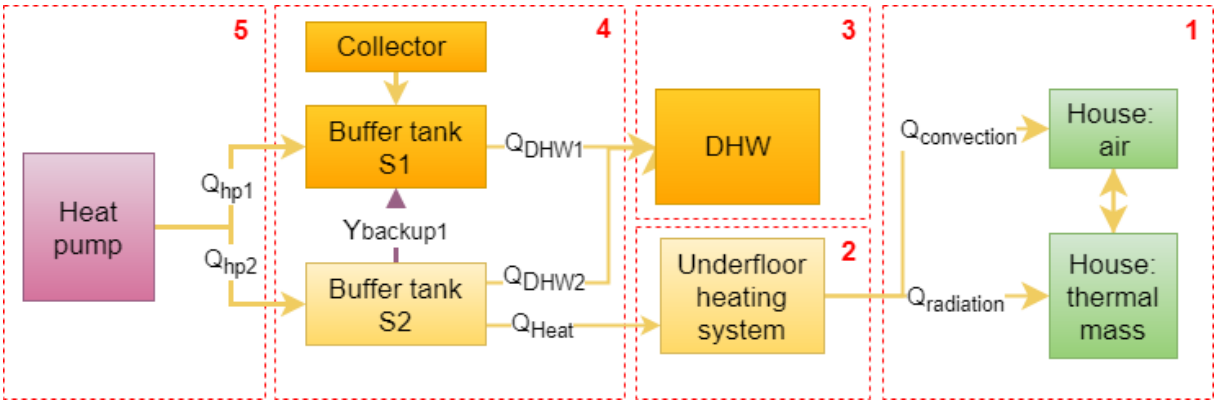

Figure 4.3: Modularity of thermal models, with 5 different sub-models

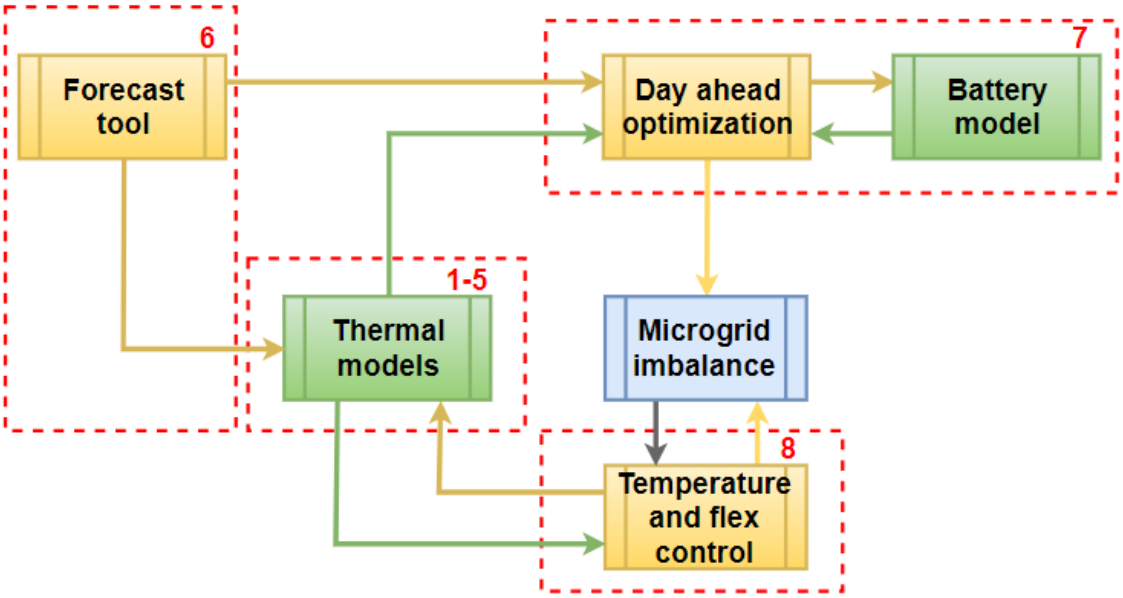

Figure 4.4: Modularity of day-ahead portfolio optimization phase and passive balancing phase

Chapter 5

Case description and data

In this chapter, we present the characteristics of the Schoonschip case study. In addition, we present the sources and methods for acquiring the data the electricity consumption and production within the Schoonschip community. Together, the characteristics and acquired data serve as input for the day-ahead portfolio optimization described in chapter 6, the passive balancing and peak shaving process described in chapter 7, and the forecasts as described in chapter 8.

5.1 Schoonschip community microgrid

For this research we consider a microgrid, inspired by the Schoonschip project in Amsterdam North. The microgrid contains 46 households, divided over 30 lots, equipped with PV panels, heat pumps, thermal solar collectors and battery storage. The Distributed Energy Resources (DER) are integrated via a microgrid (MG) and centrally controlled by an Energy Management System (EMS). The radial distribution network of the microgrid, containing 5 branches that connect several dwellings, is shown in Figure 5.1: Outline of the Schoonschip microgrid

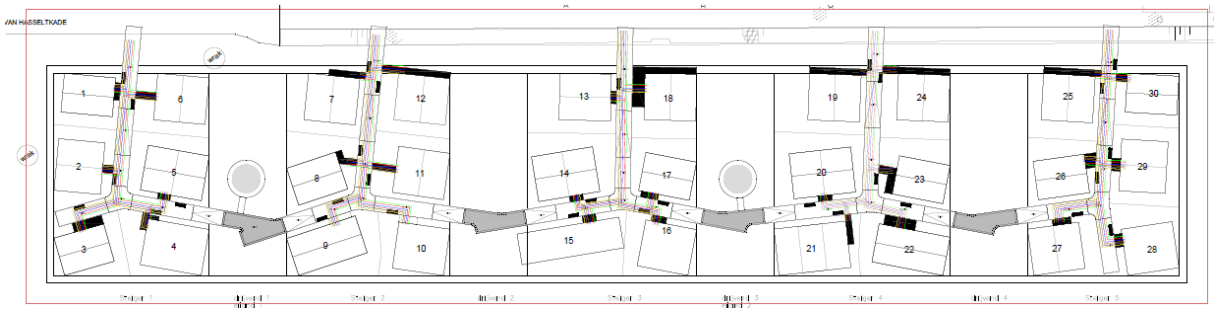

Figure 5.1: Outline of the Schoonschip microgrid, adopted from [16]

5.1.1 Schoonschip microgrid

In Figure 5.2, a graphical representation of the microgrid is given. The microgrid feeder contains 5 branches. Each branch contains several nodes connecting all 30 lots. The microgrid is connected with one interconnection to the main distribution grid of a Dutch DSO, Alliander.

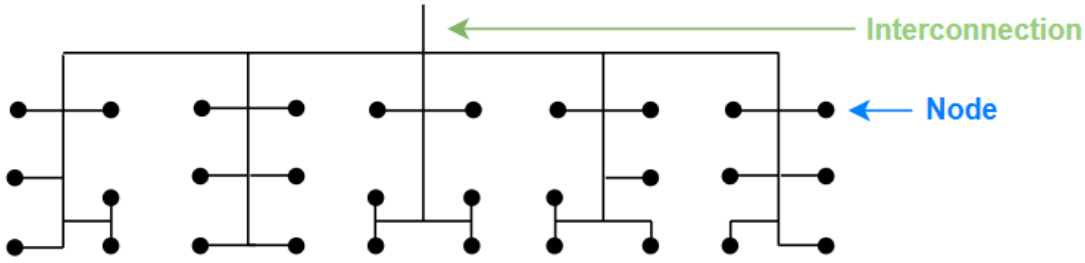

Figure 5.2: Schematic outline of microgrid Feeder and nodes connecting all houses

5.1.2 Schoonschip smart home

Each node contains a smart home in which several devices are installed. A schematic overview of all devices and the electrical power exchange between the devices, the microgrid and the distribution grid is shown in Figure 5.3. Energy is imported ($\hat{P}^{t}_{import}$) and exported ($\hat{P}^{t}_{export}$) between the microgrid and the distributed grid. The import and export is dependent on the energy consumption of all 46 houses, divided over the 30 lots. The import and export of energy is governed by the central energy management system (EMS). The central EMS can adjust the import and export by altering the power injection/withdrawal from the various devices in each lot. Thus, for each lot, the central EMS controls the PV inverter settings, the battery converter, the heat pump and the electrical back up coils in the buffer tanks.

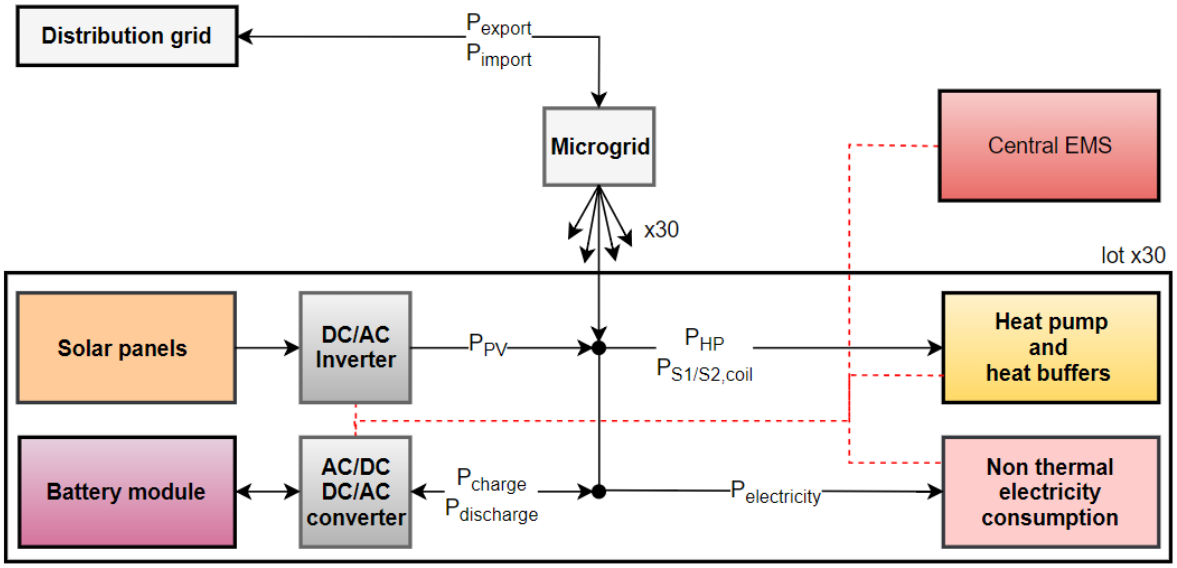

Figure 5.3: Schematic overview of the devices in each Schoonschip lot.

5.1.3 Building lot 5: thermal systems

A high level overview of the various thermal system components and energy flows is presented Figure 5.4. As seen in Figure 5.4, the heat pump extracts heat from the surrounding water using a heat exchanger that has been incorporated into the floating concrete structure. The heat that is produced by the heat pump is fed to a buffer tank. In addition, the buffer tank receives heat from the solar collector and back up heaters. The buffer tank supplies heat for DHW and heating purposes. The underfloor heating system supplies heat to the air within the building and the thermal mass of the building. According to [81]: The thermal mass of a building is defined as: ‘’*a property of the mass of a building which enables it to store heat, providing "inertia" against temperature fluctuation.*’’ Finally, the house is subject to various heat losses to the surroundings and internal and external heat gains.

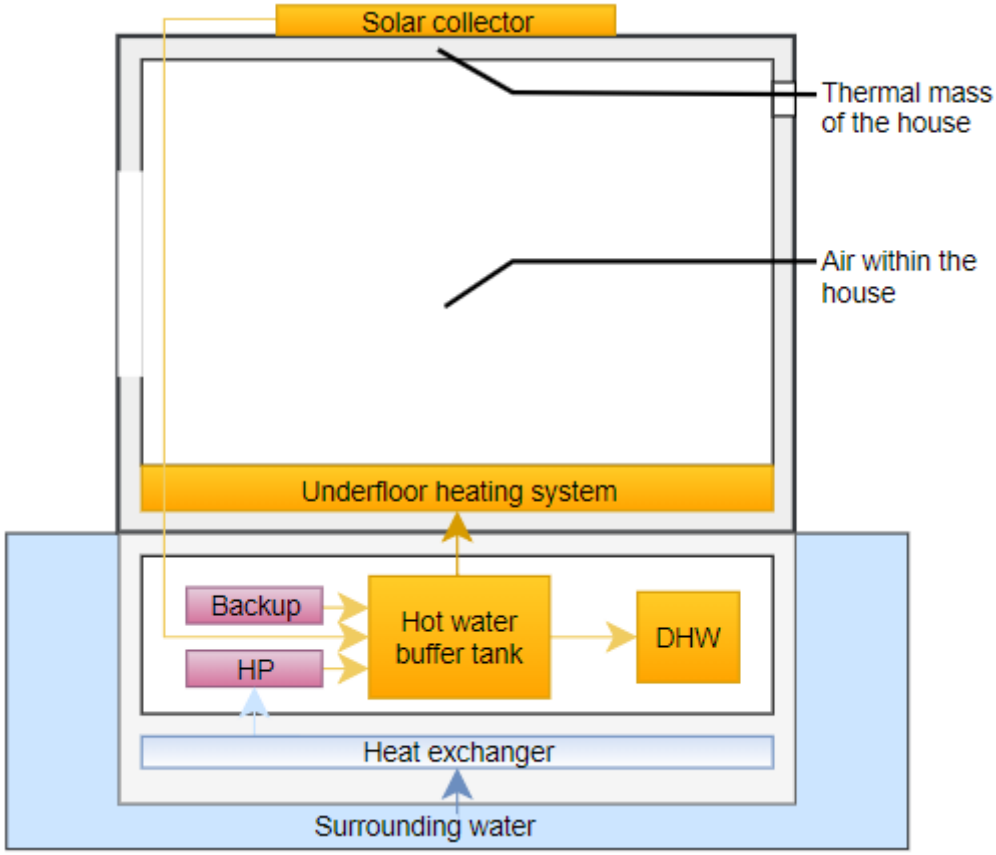

Figure 5.4: High level overview of the thermal systems and energy flows

5.2 Schoonschip building characteristics

For every house in Schoonschip, an EPC report [82], (energy performance coefficient) has been produced. Amongst others, the reports contain information regarding the yearly heat demand of each Schoonschip house. Based on the yearly heat demand of all houses in Schoonschip, 7 lots have been selected that form a good representation of most houses in Schoonschip. The 7 lots are presented in Table 5.1. By inspection of Table 5.1, we conclude that the heat demand of lot 5 is approximately equal to the total average of the entire community. Therefore, lot 5 has been selected for further analysis.

Heat demand of typical house (lot 5)

Based on the EPC report of Schoonschip lot 5 [1], the yearly thermal and electricity demand characteristics are as follows:

- Yearly heat demand: 9.4 MWh.
- Yearly electricity consumption heat pump: 5.8 MWh.
- Yearly electricity consumption by auxiliary systems (such as back up heater coils): 0.45 MWh.

These energy demand characteristics will be used as input in the simulations described in chapter 5-7.

Table 5.1: Heat demand of different lots (‘kavels’) in Schoonschip

Kavel no.		16	17	28	5	27	25	21
Yearly heat demand	[MWh]	5.3	6.7	8.40	9.40	8.60	10.5	13.4
Number of houses with similar heat demand	[-]	2	5	3	8	8	3	1

5.3 Schoonschip resource specifications

Information regarding the devices in lot 5 have been used as input for the models. In Table 5.2, this information is presented. The characteristics of the batteries, heat pumps and solar thermal collectors are based on the EPC report of lot five [82]. The PV panel specifications have been given for the entire Schoonschip microgrid. More information regarding the PV panels is presented in section 5.4.3.

Table 5.2: Parameters

Schoonschip community	
• 46 households → divided over 30 buildings → some contain two households • 100 people in total	
Photovoltaic (PV) panels [82]	
• DC-AC inverter efficiency • Total surface area Schoonschip • Capacity • Tilt angles (inclination angles): • Panel orientations (azimuth angles):	• 95% • 827 m^2 • 160 – 200 Watt-peak (W_p) • 0 – 90 degrees • S/SE/SW/NE/NW
Solar thermal collectors [82]	
• Surface area • Yearly yield • Daily yield	• 3.2 m^2 • 1055 kWh/y • 110 liters/day (10-60 °C)
Lithium Ion Battery (LG Chem RESU10) [83]	
• Number of batteries • Battery capacity • Depth of discharge: • Community capacity • Round trip efficiency • Battery charge/discharge efficiency: • Maximum charge/discharge rate: • Maximum battery life time • Battery cycle life at 90% depth of discharge • Capacity after 6000 cycles @ 90% depth of discharge • Minimum throughput	• 30 • 9.8 kWh • 90% • 265 kWh (9.8*30*90%) • 95% • 98% • 150 kW • 15-20 years • 6000 cycles • 60% • 30 MWh
Heat pump (Nibe FC1255 PC) [84]	
• Type of heat pump • Heating capacity • Maximum supply temperature	• Water –water/ closed cycle ground loop • 1.5-6 kW • 65º Celsius
Hot water stratified buffer tank	
• Capacity • Insulation EPS • Insulation thickness	• 600 litre • 0.040 W/mK • 100 mm
Interconnection capacity	
• Connection type • Active power capacity	• 160 kVA • 136 kW
Dual electricity tariff traditional energy retailer	
• Peak price • Off-peak price	• 0.0435 €/kWh (07:00-23:00) • 0.0318 €/kWh (23:00-07:00)

5.4 Simulation model: datasets

For simulating the energy consumption and production within the Schoonschip community, various data collections are required. The data collections and specifications are presented in Table 5.3. We will discuss the content and composition of each dataset in detail in sections 5.4.1-5.4.7. The various datasets are used for the following purposes:

- Day-ahead market → day-ahead portfolio optimization
- Imbalance settlement prices → real time passive balancing
- Solar irradiance → heat demand, PV production, Solar thermal production
- External air temperature → heat demand
- Surface water temperature → heat pump performance
- Non thermal electricity demand → electricity consumption by Schoonschip community
- DHW Demand → heat demand
- PV production/ realisation → forecasts on PV production

Table 5.3: Datasets and specifications

Data type	Level of application	Location / region	Resolution	Period	Source
Day-ahead market prices	Community level	Dutch power exchange	1 hour	2015 and 2016	ENTSO-E Transparency platform [85]
Imbalance settlement prices		Dutch imbalance market	15 minutes		TenneT Dutch TSO [86]
Direct and diffuse solar irradiance, solar azimuth/altitude	Community and house level	Amsterdam	1 hour	One year	IWEC weather data by ASHREA [87]
External air temperature	House level				
Surface water temperature	House level	Amsterdam IJ	24 hour	One year	Waterbase.nl [88]
Non thermal electricity demand	House level	Field trials in the Netherlands	15 minutes	One year	Liander Dutch DSO [89]
DHW demand	House level	None	1 minute	Specific days	CREST [90]
PV production forecasts	Community and house level	Brussel	15 minutes	2016	ELIA Belgium TSO [8]
PV production realisation					

5.4.1 Wholesale market information

The day-ahead market prices will be used for the portfolio optimization problem as discussed in chapter 6. The imbalance settlement prices serve as input for passive balancing in chapter 7.

Validation

From inspection, it follows that some timeslots are missing in the day ahead market dataset as published on the ENTSO-E Transparency platform [85]. These timeslots have been listed hereunder. The missing timeslots have been replaced by other days/weeks, as also listed hereunder. Although not ideal, this is reasonable because the day-ahead market is not volatile. As a result, the prices for one day or one week do not vary significantly and so other days/weeks are sufficiently representative.

- Day ahead market prices for 2015:
  - Missing data for the hourly timeslots: h=1-121.
  - Missing data replace with replaced with week after: h=169-289.
- Day ahead market prices for 2016:
  - Missing data for hourly timeslots: h=554-577, h=5978-6001,h=7562-7585.
  - Missing data replaced with the day before.

5.4.2 IWEC weather data

The local air temperatures and local direct and diffuse solar irradiance have been derived from International Weather for Energy Calculation (IWEC) weather files. IWEC weather data files have been composed in the year of 2000, by the American Society of Heating, Refrigerating and Air Conditioning Engineer (ASHREA) [91]. According to [9], the composite IWEC weather file is based on 18 years of hourly weather data measurements (for most locations 1982-1999). For clarity, the IWEC weather file does not contain averages of the 18 years' worth of data, but forms a simulated representation of a typical year and location, that has been based on 18 years of data.

5.4.3 PV production using DesignBuilder and IWEC data

PV production patterns for the area of Schoonschip, have been simulated using DesignBuilder [92]. By default, DesignBuilder software uses IWEC weather data [87] to produce PV production profiles. The software environment enables users to define the solar panel surface area, azimuth angle and orientation of PV panels to determine the net solar irradiation received by a PV panel [93]. Given a certain irradiance, the total power output of the panels is directly proportional to the effective surface area and nominal conversion efficiency. Depending on the orientation of the panels and their inclination (tilt angle) the power output is calculated. Thereby, the efficiency of the PV panels is assumed to be independent of the outer temperature. In reality, however, this is not the case as the efficiency of PV panels decreases with increasing temperature [94].

Assumption on modelling PV production

For the creation of solar energy production profiles we use information from the Schoonschip community on the positioning of solar panels. This information includes specifications on the orientation (azimuth), surface area, panel inclination (tilt angle) and efficiency of the PV panels that will be installed. To aid the modelling we make some simplifications. We assume all solar panels have similar inclinations. The inclination of all panels is set to 20 degrees. This is the average inclination angle of all the PV panels that will be installed at Schoonschip. Also, we assume a standard efficiency of 18%. Again, this is the average efficiency of all PV panels at Schoonschip. The effective surface area is set to 90% of the total surface area. The inverter efficiency is set to 95%. No cable losses are considered. Finally we assume the orientation of the solar panels can be divided over 5 orientations: South, South-west, South-east, North-east and North-west. Based on information from all the EPC reports [82], the total surface area (827.21 m^2) is divided over all 5 orientations as follows:

- South: 16% of total surface area
- South-west: 56% of total surface area
- South-East: 13% of total surface area
- North-East: 8% of total surface area
- North-West: 7% of total surface area

The output resolution of the PV production profile generated by DesignBuilder is 1 hour. The dataset expanded to quarterly hour timeslots, by duplicating the hourly values.

Validation of DesignBuilder results

Research shows that the amount of direct solar irradiance in the IWEC weather data is 20-40% lower than in practise for northern European countries [95]. The researchers did not specify for which northern European countries this bias occurs. Thus, to determine whether such a negative bias is present for the Netherlands, we compare the specific energy yield for typical solar systems in the Netherlands [96], [97] to the specific energy yield as calculated with DesignBuilder. According to [96], [97], the total yearly energy yield for typical PV systems in the Netherlands, equals 875 kWh/kWp. The total specific energy yield for the PV panel fleet of Schoonschip, as calculated with DesignBuilder, equals 840 kWh/kWp. Thus, no strong negative bias is present Therefore, the PV production profile is assumed valid.

5.4.4 Solar thermal collector using IWEC data

For simulating the production of solar thermal energy at the Schoonschip site, we use a simplified representation of a solar thermal collector. We neglect conversion losses and assume the thermal production to be proportional to the incident solar irradiance and surface area. To account for the conversion losses, the surface area of the solar collector is considered twice as small, equalling 1.6m2. For calculating the incident irradiance on a solar thermal collector, the formulas for calculating the incident irradiance on windows, as discussed in appendix A11.1, are adopted.

Simple method for producing a production profile on solar thermal energy

The hourly solar thermal production, for a period of 1 year, is calculated using the IWEC weather data and the formulas from appendix A11.1. Given a solar thermal collector, oriented south-west, having a 30^{o} inclination and surface area of 1.6 m^2, the annual thermal energy yield equals 1071.5 kWh.

Validation of dataset

The estimated solar thermal production is validated using manufacturer data on the solar thermal collector that will be installed at the Schoonschip houses. Based on Table 5.2, the annual energy yield of the solar thermal collector system equals 1055 kWh, being orientated south, with 45^{o} inclination and a surface area of 3.2 m2. Thus, the estimated yearly yield (of 1071.5 kWh), deviates by only 1 percent from the actual annual production. Therefore, we conclude that our simple method gives a reasonable approximation of the expected solar thermal energy production per hour.

5.4.5 External air and water surface temperature

The external air temperatures follows from the IWEC weather dataset for the region of Amsterdam [87]. The Schoonschip houses are floating structures (houseboats) that extract heat (with the water-water heat pump) from the surface water. Therefore, a dataset is required on the water surface temperature at the Schoonschip sight. To that end, we adopt a dataset from the live.waterbase.nl website [88]. This dataset describes the temperature of the IJ over multiple years. The year of 2016 is selected. The dataset has a 24 hour resolution. Given the large thermal capacity of the surface water, it's surface temperature only varies slightly over the course of a day. Therefore, the temperature for each 15 minutes is set equal to the daily value.

5.4.6 Non thermal electricity consumption profiles

Multiple empirical datasets on the electricity and gas consumption of various Dutch households is used to represent the non-thermal electricity consumption $P^{t}_{electricity}$ of the Schoonschip community.

The datasets have been retrieved from the website of the Dutch DSO, Liander [89]. The datasets contain the electricity demand of 80 different households, with a 15 minute resolution expressed in Wh. The measurements were performed from 01-05-2012 to 07-03-2014. For the simulation we only use data for 2013. For every household, the type of house (semi-detached, terrace, etc.), construction year and family composition is known. The family composition category differentiates between ''Single'', ''Couple without children'' and ''family with children''.

Approach

It is found that some datasets contain missing data points. These datasets have not been considered, yielding only 47 complete datasets. The number of people, as indicated by 'family composition with children' has not been specified. Therefore, we assume an average of 3.5 people, in case of a *family composition with children*. Together with the other datasets ('Single'' and 'Couple without children'), this results in a headcount of 103.5 people. Given the amount of households within Schoonschip (46) and amount of people (~100) we conclude this dataset will give a reasonable impression of the non-thermal electricity consumption profile of the entire community.

Induction cooker profiles

The datasets on gas consumption, as given by the Liander dataset [89], describe the gas consumption per household. Inspection of all datasets reveals that all households use gas. The gas is used for cooking, room heating and domestic hot water (DHW). Since the houses within Schoonschip are highly energy efficient buildings, the demand for room heating will be much lower. Hence, the gas consumption profiles cannot be used. This means that representative profiles for induction cookers and domestic hot water (DHW) need to be devised. The latter is discussed in section 8.4.7. For estimating the daily electricity consumption by induction cookers, we estimate the daily electricity consumption for every timeslot. To that end, we assume that the electricity/induction cookers are used only in the morning and evening. Also, we assume that the highest peak occurs in the evening. The electricity consumption by induction cookers of the Schoonschip community for every timeslot t, is presented in Figure 5.5.

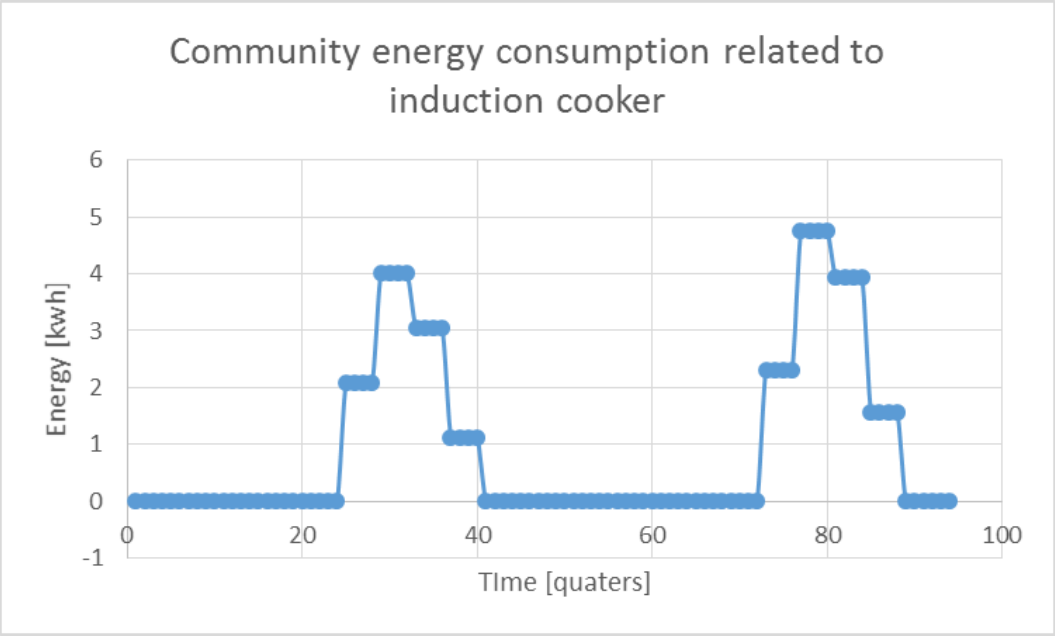

Figure 5.5: Daily community energy consumption by induction cookers.

5.4.7 Domestic hot water profiles (DHW)

For producing DHW profiles, we use the demand model that has been developed by the Centre For Renewable Energy Systems Technology (CREST) [90]. According to [98], the CREST model is a validated high resolution stochastic model for simulating the domestic thermal and electricity demand. Amongst other, the model accounts for randomised occupancy by residents, derived from time-use survey data. The latter will be used to produce lifelike DHW consumption profiles for various family composition.

Approach

Using the CREST model [90], we create 5 DHW consumption profiles, with 1 minute resolution and a period of 1 week. The reason for creating 5 profiles is because the CREST model creates a different profile for each entry. Thus, to obtain a realistic profile, we produce multiple datasets and select only one dataset that matches our criteria.

For creating 5 profiles, we vary the number of occupants (in the CREST model) between 2 to 5 people. Also, we differentiate between weekend and week days. Thus, each dataset is composed of 5 equal weekdays and 2 equal weekend days. Each having a different family composition. Each dataset has been converted to 15-minute resolution data by taking the sum of every 15 minute interval. A yearly consumption profile is generated by using the dataset for each week of the year. The average DHW consumption per year per household and per person is presented in Table 5.4.

Table 5.4: Yearly DHW demand by CREST model

	Unit	Dataset 1	Dataset 2	Dataset 3	Dataset 4	Dataset 5
Number of occupants	[-]	2	2	3	5	5
Water consumption	[m^3/year]	34.3	65.5	60.0	113.4	56
	[m^3/year/person]	17.1	32.7	20.0	22.7	11.2

Validation CREST data

For validation of the CREST datasets, key figures on Dutch DHW consumption are considered. According to milieucentraal.nl [99], the average water consumption per person per day in the Netherlands for 2013, equalled 119 litres. Now, according to [99], 50% of the water consumption is used for DHW purposes. Hence, the yearly DHW consumption for an average Dutch person equals **21.7 m^3/year/person**.

It follows that dataset 1, 3 and 4 are in the same order of magnitude. However, the consumption pattern for every quarterly timestep *t*, is significantly different. Whereas dataset 1 and 3 only show a few peaks in DHW consumption, dataset 4 shows multiple peaks per day. Although the latter may occur during some instances, it is not likely to occur frequently. Given this analysis, we discard dataset 2, 4 and 5.

Given the Schoonschip population (100 people) and the number of buildings (30), there is an average of 3.33 people living in each lot. Lot 5 contains two households. Hence, we would expect at least 2 occupants and a maximum of 6-8. Since the family composition of both households is unknown, we assume that the total number of occupants in lot 5 is equal to 5. As an approximation, we combine dataset 1 and 3 for simulating the total DHW demand of lot 5.

Chapter 6

Day ahead portfolio optimization

In this chapter, we present the mathematical formulation of the day-ahead portfolio optimization process. In section 6.1, we present a mathematical formulation of the microgrid system constraints. Next, in section 6.2, we provide a mathematical formulation of the solar-self consumption requirement and a formulation of two strategies for day-ahead market participation. Section 6.3 explains the strategy for solving the day-ahead portfolio optimization problem. Finally, section 6.4, gives the mathematical formulation of the day-ahead portfolio optimization approach.

6.1 System constraints

Similar to [40]-[46], various constraints regarding the operation of the battery system are included. Also, some microgrid and interconnection constraints are considered.

6.1.1 Maximum interconnection capacity

The first constraint relates to the interconnection between the microgrid and the distribution grid. The active power flow is limited and of equal magnitude for import and export. Let P_{inter}^{max} denote the maximal active power capacity of the interconnection. In the case of Schoonschip: $P_{inter}^{max} = 136\text{kW}$.

6.1.2 Internal power balance

The power consumption and production within the microgrid should be balanced. To maximise the PV production, we assume that PV curtailment is not possible. Also, load curtailment is not considered, to avoid dissatisfaction among the residents. Note that load flexibility is considered for passive balancing and peak shaving. However, this only includes the heat pump and back up heater. Hence, the following condition should hold:

$$P_{PV}^{t} + \hat{P}_{discharge}^{t} + \hat{P}_{import}^{h} - P_{load}^{t} - \hat{P}_{charge}^{t} - \hat{P}_{export}^{h} = 0 \tag{6.1}$$

With P_{PV}^{t} ,the PV power production, $\hat{P}_{discharge}^{t}$ battery discharging, $\hat{P}_{import}^{h}$ the rate at which energy is imported from the main grid, P_{load}^{t} , the power consumption, $\hat{P}_{charge}^{t}$ battery charging and $\hat{P}_{export}^{h}$ the rate at which energy is exported to the main grid.

6.1.3 Peak shaving

During some instances the peak demand may exceed the interconnection capacity. This problem can be addressed by either increasing interconnection capacity, or by *reducing peak demand,* referred to as *peak shaving*. See chapter 1, section 1.4, for a definition on peak shaving. However, during day-ahead scheduling, this problem does not arise, as the maximum interconnection capacity can be included in the scheduling problem. Instead, the problem does arise during the passive balancing phase. As a result of imbalances, the demand and peak demand deviate from the schedule. Consequently, the peak demand may then exceed the interconnection capacity. The solution to this problem is addressed in chapter 7. So, in this chapter on day-ahead portfolio optimizations, it is not included.

6.1.4 Battery constraints

The battery charge/discharge power rates are limited and of equal magnitude, denoted by P_{Bat}^{max}. Battery charging/discharging is not 100% efficient, hence we account for battery specific charge/ discharge efficiency, denoted by η_{Bat}. This includes the inefficiencies of the inverter to convert direct current (DC) to alternating current (AC). To prevent accelerated battery degradation as a result of deep discharging and/or overcharging, we assume only part of the battery capacity may be utilised. We define the effective battery capacity as E_{SOC}^{max} A minimum state of charge (SOC) is assumed and set equal to 0. The maximum state of charge is equal to the effective battery capacity E_{SOC}^{max}. The state of charge, denoted by the endogenous variable E_{SOC}^{t}, can take any value between the minimum and maximum state of charge. Battery self-discharging is not considered.

6.1.5 Battery aging

Batteries are subject to different forms of degradation. Therefore, an activation cost function is needed to assess the impact of aging on the battery life. Battery aging, in lithium ion batteries, is subject to two forms of degradation: calendric & cyclic aging. Calendric aging is correlated to wear and tear. Cyclic aging depends on various operational aspects. According to [100], cycle aging is related to: operating temperature, depth of discharge, number of completed cycles and the charge/discharge voltage. However, most studies on scheduling [40], [47], [42] [101],[102] neglect these dependencies and assume cost of operation to be linearly depended on the discharge power. Unlike the cyclic aging, the calendric aging cannot be expressed in a cost parameter. Instead, as a result of calendric aging, the battery capacity declines over time. To account for this phenomena, we can vary the effective battery capacity E_{SOC}^{max} and assess the impact on self-consumption, cost and benefits.

Inspired by [40], [47], [42] [101],[102], we assume that the battery degradation scales linearly with the power discharged for some time interval t. The cyclic degradation costs, C_{Bat}^{t} for some quarter are then given by:

$$C_{Bat}^{t} = \frac{p_{Bat}^{deg} \cdot \hat{P}_{discharge}^{t} \cdot \frac{1}{4}\delta q}{\eta_{Bat}} \tag{6.2}$$

With p_{Bat}^{deg} virtual cost of cyclic battery degradation, η_{Bat} the discharge/charge efficiency of the battery and the inverter, $\hat{P}_{discharge}^{t}$ the rate of discharge [J/s], and $\frac{1}{4}\delta q$ a quarterly time interval.

6.2 Optimization constraints

Two constraints are important for day-ahead portfolio optimizations:

1. to maximise the solar self-consumption by using the battery;
2. to optimise participation in the day-ahead market.

In this section, we first define two benchmarks for maximising the solar self-consumption. Secondly, we propose a method to quantify the percentage of solar-self consumption. Finally, we propose two functions that may be used as objective function for the day-ahead portfolio optimization problem: a net profit function and a net cost function.

6.2.1 Maximizing solar self-consumption

Given a battery for maximising the solar-self consumption, the maximum percentage of solar-self consumption, $\mathrm{SSC}_{\mathrm{max}}^{\mathrm{day}}$ is given by equation (6.3). Where we assume that the batteries are only used for storing solar energy and not for storing energy that has been imported from the main grid. See chapter 1, section 1.3 for a graphical representation.

$$\mathrm{SSC}_{\mathrm{max}}^{\mathrm{day}} = \frac{\mathrm{E}_{\mathrm{PV,direct}}^{\mathrm{day}} + \mathrm{E}_{\mathrm{PV,indirect}}^{\mathrm{day}}}{\mathrm{E}_{\mathrm{consumption}}^{\mathrm{day}}} \cdot 100\% \tag{6.3}$$

Where $\mathrm{E}_{\mathrm{PV,direct}}^{\mathrm{day}}$ and $\mathrm{E}_{\mathrm{PV,indirect}}^{\mathrm{day}}$ represent the direct solar self-consumption and the indirect solar self-consumption respectively.

Strategy for maximising solar self-consumption

The simplest strategy to maximise the solar self-consumption when using a battery, is by applying rules 1 up until 5. It is evident that this will maximise the solar self-consumption, as discussed in [4], [17].

1. The battery is charged for any t, where $\mathrm{P}_{\mathrm{PV}}^{\mathrm{t}} > \mathrm{P}_{\mathrm{load}}^{\mathrm{t}}$ and $\mathrm{E}_{\mathrm{SOC}}^{\mathrm{t}} < \mathrm{E}_{\mathrm{SOC}}^{\mathrm{Max}}$
2. The battery is discharged for any t, where $\mathrm{P}_{\mathrm{PV}}^{\mathrm{t}} < \mathrm{P}_{\mathrm{load}}^{\mathrm{t}}$ and $\mathrm{E}_{\mathrm{SOC}}^{\mathrm{t}} > 0$
3. The battery SOC remains constant, if $\mathrm{P}_{\mathrm{PV}}^{\mathrm{t}} = \mathrm{P}_{\mathrm{load}}^{\mathrm{t}}$
4. Solar energy is exported for any t, where $\mathrm{P}_{\mathrm{PV}}^{\mathrm{t}} > \mathrm{P}_{\mathrm{load}}^{\mathrm{t}}$ and $\mathrm{E}_{\mathrm{SOC}}^{\mathrm{t}} = \mathrm{E}_{\mathrm{SOC}}^{\mathrm{Max}}$
5. Solar energy is imported for any t, where $\mathrm{P}_{\mathrm{PV}}^{\mathrm{t}} < \mathrm{P}_{\mathrm{load}}^{\mathrm{t}}$ and $\mathrm{E}_{\mathrm{SOC}}^{\mathrm{t}} = 0$

It is important to emphasise that rules 1 up until 5 only apply for maximising the solar self-consumption if no energy imports are used for charging the battery.

Benchmark 1: Minimise energy exports

Given rules (1-5), the sum of all energy exports resembles the maximum amount of solar energy that can be exported for that day, where $\mathrm{E}_{\mathrm{export}}^{\mathrm{day,max}}$ denotes the maximum constrained solar energy export for some day. Essentially, this implies that if more energy is exported than this constrained maximum, the percentage of solar self-consumption, related to the use of direct and indirect solar energy, deteriorates. Hence, any *scheduling strategy* that results in more energy exports than the constrained maximum energy export $\mathrm{E}_{\mathrm{export}}^{\mathrm{day,max}}$, results in a lower percentage of solar self-consumption. Given these findings, it can be concluded that the constrained maximum amount of energy exports for a particular day resembles a solar self-consumption benchmark. We refer to this as benchmark 1.

Benchmark 2: minimise energy imports

The same line of reasoning with respect to the constrained energy exports holds for the import of energy. Given a strategy that maximises the solar-self consumption (rules 1-5), the import of energy is minimised. Hence, a minimisation of the energy imports can also result in a maximisation of the solar-self consumption. We refer to this as benchmark 2.

Solar self-consumption benchmark applications

The solar self-consumption benchmark can be used for two applications. Firstly, the benchmarks can serve as a constraint for the day-ahead portfolio optimization problem. This is shown in section 5.3.1. Secondly, it is shown that benchmark 1 can be used to calculate the maximum percentage of solar self-consumption SSC^{day}_{max}.

Calculating the maximum energy export for some day

Let E^{t}_{export} denote the energy exports for a certain timeslot t during some day. Then, given rules (1-5), the maximum constrained amount of energy exports for this day, $E^{day,max}_{export}$ is given by equation (6.4).

$$E^{day,max}_{export} = \sum_{t=0}^{95} E^{t}_{export} \text{ for any t where } P^{t}_{PV} > P^{t}_{load} \text{ and } E^{t}_{SOC} = E^{Max}_{SOC} \tag{6.4}$$

6.2.2 Quantifying the maximum percentage of solar self-consumption

In case the battery is used for maximising the solar self-consumption, the total amount of energy exports is minimised. Hence, equation (6.5) expresses the maximum percentage of solar self-consumption, SSC^{day}_{max}.

$$SSC^{day}_{max} = \left(\frac{E^{day}_{PV} - E^{day,max}_{export}}{E^{day}_{consumption}} \right) \cdot 100\% \tag{6.5}$$

With E^{day}_{PV} the total solar electricity production for some day. Note that equation (6.5) is different from equation (6.3). Yet, based on the argumentation in 5.2.1, we can state that the numerator in equations (6.3) and (5) are equal, as in equation (6).

$$E^{day}_{PV,direct} + E^{day}_{PV,indirect} = E^{day}_{PV} - E^{day,max}_{export} \tag{6.6}$$

6.2.3 Day-ahead market participation

Having defined all requirements, an equation (6.7) can be formulated that captures the cost and benefits of day-ahead market participation. The goal of the aggregator is to schedule energy exports at high market prices and schedule energy imports at low market prices, whilst first maximising solar-self consumption and respecting the operational requirements (as seen in section 5.1.2). As will become clear in section 5.3.3, the net cost function does not yet fully describe the goal of the aggregator. This shortcoming will become clear when we formulate the objective function.

Net cost function

The net cost function is given by equation (6.7).

$$\mathbb{C}^{day}_{netto} = \sum_{h=0}^{23} \left[p^{h}_{DA} (\hat{P}^{h}_{import} - \hat{P}^{h}_{export}) \cdot \delta q + \sum_{t=4h}^{4h+3} \left[p^{deg}_{Bat} \cdot \hat{P}^{t}_{discharge} \cdot \tfrac{1}{4} \delta q \right] \right] \tag{6.7}$$

With p^{h}_{DA} as the day ahead market price per hour h, $\hat{P}^{h}_{export}$ and $\hat{P}^{h}_{import}$ representing the scheduled exports and imports per hour h respectively, $\hat{P}^{t}_{discharge}$ indicating the rate of discharge per quarter t, p^{deg}_{Bat} the battery degradation cost, $\frac{1}{4}\delta q$ a quarterly time interval and δq an hourly time interval.

6.3 Optimisation approach

6.3.1 Decision variables to the optimisation problem

Optimisation problems require an objective function, a set of decision variables and a set of constraints. The objective function is given by the net cost function (6.7). The system and optimizations constraints have been defined in section 6.1 and 65.2. The decision variables for the optimization problem are as follows:

Decision variables

The following variables are set as decision variables to the objective function: The battery charge rate, the battery discharge rate, hourly grid imports and hourly grid exports.

- Charge rate $\hat{P}^{t}_{charge} \in \mathbb{R}^{+}_{0}$
- Discharge rate: $\hat{P}^{t}_{discharge} \in \mathbb{R}^{+}_{0}$
- Grid import: $\hat{P}^{h}_{import} \in \mathbb{R}^{+}_{0}$
- Grid export: $\hat{P}^{h}_{export} \in \mathbb{R}^{+}_{0}$

Note that each variable can only take positive values. In addition, the charge and discharge variable are restricted by the maximum charge/discharge rate P^{max}_{Bat} . The import and export variables are restricted by the interconnection capacity.

Charge and discharge decision variable

We define the decision variables $\hat{P}^{t}_{charge}$, $\hat{P}^{t}_{discharge}$ as the gross power that is fed or extracted from the battery systems. Given the battery- and inverter efficiency, $0 < \eta_{Bat} \leq 1$, the net power that is fed or extracted from the battery differs from the gross power. For charging, the net power is smaller and equals $\eta_{Bat} \cdot \hat{P}^{t}_{charge}$. For discharging, the net power is larger and equals $\hat{P}^{t}_{discharge} / \eta_{Bat}$. Hence, to accurately describe the battery state of charge, we require two decision variables for charging and discharging. This distinction can be seen in equation (6.19), in section 6.4.2.

Import and export decision variable

Both import and export decision variables are introduced to discriminate between importing and exporting energy. This is needed to enforce maximisation of the solar self-consumption. Maximisation of the solar-self consumption can be achieved in two ways:

1. By enforcing a limit on the export of energy per day (benchmark 1)
2. By penalizing the import of energy. (benchmark 2)

The implementation of both approaches is presented in section 6.3.3.

6.3.2 Linear programming (LP)

We observe that the decision variables $\hat{P}^{h}_{import}$ $\hat{P}^{h}_{export}$, $\hat{P}^{t}_{charge}$, $\hat{P}^{t}_{discharge}$ can take any value between 0 and some upper boundary. Hence, these decision variables are continuous. From inspection of the system constraints, see 6.1.2, it follows all (in)equality constraints are linear. Hence, all decision variables and constraints per hour/quarter are continuous. Therefore, the optimization is purely linear. We conclude that linear programming (LP) is required to solve the optimization problem.

Linear programming formulation

A LP problem consists of a set, containing all feasible points that satisfy all constraints. The use of a LP allows us to find (or approximate) the global optimum solution. If the LP problem is infeasible, it is impossible to satisfy all constraints. Also, the problem may be unbounded, in which case the constraints do not define a closed solution space. The LP problem may implemented in a solver to calculate the global optimum. A LP optimization in standard form is denoted as follows:

$$\begin{aligned} &\min_{x} z \triangleq c^{T}x \\ &s.t.\ Ax \begin{Bmatrix} \leq \\ = \\ \geq \end{Bmatrix} b \\ &x_{min} \leq x \leq x_{max} \end{aligned} \tag{6.8}$$

With x, the continuous decision variables, A and b exogenous parameterisation variables and x_{min}, x_{max} the lower and upper bounds of the decision variables.

6.3.3 Maximizing solar self-consumption in LP problem

The use of two solving strategies for maximising solar self-consumption in the LP problem is examined. The first solving strategy is to minimise the import of energy, using a fixed constraint. The second strategy is to penalise the import of energy. In both cases the first goal is to maximise solar self-consumption, the second goal is to minimise the net cost $\mathbb{C}^{day}_{netto}$.

Strategy 1: enforce a maximum on the export of energy per day

To enforce maximisation of the solar self-consumption, an additional constraint is added to the operational constraints. This constraint is given by equation (6.9), which utilises benchmark 1, as seen in section 5.2.1. The constraint ensures that the solar self-consumption is maximised by limiting the export of (solar) energy for some day.

$$\sum_{h=1}^{24} \hat{P}^{h}_{export} \cdot \delta q \leq E^{Day,max}_{Export} \tag{6.9}$$

With $\hat{P}^{h}_{export} \cdot \delta q$ the energy import for some hour.

Strategy 2: penalise the import of energy

The first strategy yields many insolvable optimization problems. Ultimately, this is the result of using a fixed constraint for maximising the solar self-consumption. Therefore, we propose the use of an import penalty, p_{fine} for maximising the solar self-consumption. Given a sufficiently large fine, the import of energy is minimised, resulting in a maximisation of the solar self-consumption. To relax the operational constraints when needed, for every t a slack variable, $\hat{P}^{t}_{slack}$ is added to the net cost function (6.7). The slack variables are assigned a virtual cost parameter, p_{slack}. This results in equation (6.10).

$$\min_{h\in\{0,..,23\}} = \sum_{h=0}^{23}\left[(p^{h}_{DA} + p_{fine}) \cdot \hat{P}^{h}_{import} - p^{h}_{DA} \cdot \hat{P}^{h}_{export} + \sum_{t=4h}^{4h+3}\left[p^{deg}_{Bat} \cdot \hat{P}^{t}_{discharge} + p_{slack} \cdot \hat{P}^{t}_{slack} \right] \right] \tag{6.10}$$

Slack variables

To ensure that the solver first explores the solution space as given by the operational constraints, the virtual cost parameter is assigned a high value, with $p_{slack} >> p_{DA}^{h}$. The slack variables are added to the power balance, as given by equation (6.11). The power balance serves as equality constraint to the LP problem.

$$P_{PV}^{t} + \hat{P}_{discharge}^{t} + \hat{P}_{import}^{h} + \hat{P}_{slack}^{t} - P_{load}^{t} - \hat{P}_{charge}^{t} - \hat{P}_{export}^{h} = 0 \quad (6.11)$$

Note that for every t, the slack variable is a decision variable that is continuous and strictly positive. Consequently, it can be added to the LP objective function without problems. Also note that utilisation of the slack variable inflicts an imbalance in real time.

Solvability

Strategy 2 is found to be more effective than strategy 1, as strategy 2 results in less insolvable LP problems. This is because the solution space is less firmly constrained by penalising the import of energy, than by restricting the import of energy. Nonetheless, some LP problems are still insolvable. The solver can cope with this problem by relaxing the operational constraints, using the slack variable.

It is found that the slack variable is rarely needed to relax the operational constraints, as to find a feasible solution to the optimisation problem. It is also found that the need for relaxing the operational constraints is inversely proportional to the interconnection capacity P_{inter}^{max}. Thus, given a smaller interconnection capacity, the operational constraints need to be relaxed more frequently to find feasible solutions.

6.3.4 Solving the LP: exact vs. heuristic method

The LP problem may be solved using an approximation (heuristic approach) or by calculating the exact solution. The former relies on a problem solving strategy that approaches the global optimum, but not exactly yield the global optimum. The heuristic method may be able to find a fairly accurate answer, within a reasonable amount of time, however, the solution may not be the global optimum. The advantage of using an exact approach is that identifies the global optimum. However, the disadvantage is that the computational burden is larger.

6.4 Mathematical formulation

6.4.1 Objective function

The objective function is formulated as a net cost minimisation function. Note that a solution to this objective function is produced for all 365 days of the year. The function is given by equation (6.12) .

$$\min_{h\in\{0,..,23\}} = \sum_{h=0}^{23}\left[(p^{h}_{DA}+p_{fine})\cdot\hat{P}^{h}_{import}-p^{h}_{DA}\cdot\hat{P}^{h}_{export}+\sum_{t=4h}^{4h+3}\left[p^{deg}_{Bat}\cdot\hat{P}^{t}_{discharge}+p_{slack}\cdot\hat{P}^{t}_{slack}\right]\right] \quad (6.12)$$

$$\text{with } h=\left\lfloor\tfrac{t}{4}\right\rfloor \text{ for } t\in\{1,..,95\}=t\in T$$

With $\hat{P}^{t}_{export}$, $\hat{P}^{h}_{import}$, $\hat{P}^{t}_{discharge}$ and $\hat{P}^{t}_{slack}$ the decision variables that have been assigned a price / cost. The other decision variables, $\hat{P}^{t}_{charge}$, has not been assigned any cost. As a result, it is not considered in the objective function. With p^{h}_{DA} the day ahead market price, p_{fine} a fine imposed on the import of energy, p^{deg}_{Bat} the virtual cost of cyclic battery degradation and p_{slack} the virtual cost assigned to the slack variable.

6.4.2 Constraints

The objective function is bound by several constraints, which are formulated as follows:

Internal power balance constraint

The power inputs and outputs to the microgrid must be balanced at all times. Therefore, the power inputs and outputs must be chosen such that the total sum is equal to zero. See expression (6.13).

$$P^{t}_{PV}+\hat{P}^{t}_{discharge}+\hat{P}^{h}_{import}+\hat{P}^{t}_{slack}-P^{t}_{load}-\hat{P}^{t}_{charge}-\hat{P}^{h}_{export}=0 \quad (6.13)$$

$$\text{with } h=\left\lfloor\tfrac{t}{4}\right\rfloor \text{ for } t\in T$$

Where P^{t}_{PV} and P^{t}_{load} the only exogenous variables denoting PV power production and electricity power consumption at any t.

Maximum interconnection capacity constraint

The import and export of energy is confined by the interconnection capacity.

$$0\le\hat{P}^{h}_{export}\le P^{max}_{inter} \text{ with } h=\left\lfloor\tfrac{t}{4}\right\rfloor \text{ for } t\in T \quad (6.14)$$

$$0\le\hat{P}^{h}_{import}\le P^{max}_{inter} \text{ with } h=\left\lfloor\tfrac{t}{4}\right\rfloor \text{ for } t\in T \quad (6.15)$$

With P^{max}_{inter} the maximum interconnection capacity and with P^{max}_{inter} =136 kW.

Slack constraint

The slack variables can only take positive values.

$$0\le\hat{P}^{t}_{slack}\le M \text{ for } t\in T \quad (6.16)$$

With M a large number, where M is in the order of magnitude of the interconnection capacity P^{max}_{inter}.

Battery constraints

In (6.17), the battery charge and discharge powers are confined by the maximum charge and discharge capacity, denoted by P_{Bat}^{max}. In the case study it is equal to 135 kW.

$$\hat{P}_{charge}^{t} \leq P_{Bat}^{max} \quad \text{for } t \in T \tag{6.17}$$

$$\hat{P}_{discharge}^{t} \leq P_{Bat}^{max} \text{ for } t \in T \tag{6.18}$$

In (6.19) the battery state of charge (SOC) is updated for every charge or discharge event.

$$E_{SOC}^{t+1} = E_{SOC}^{t=0} + E_{SOC}^{t} + \tfrac{1}{4}\delta q \cdot \hat{P}_{charge}^{t} \cdot \eta_{Bat} - \tfrac{1}{4}\delta q \cdot \frac{\hat{P}_{discharge}^{t}}{\eta_{Bat}} \text{ for } t \in T \tag{6.19}$$

With $E_{SOC}^{t=0}$ the battery state of charge at the beginning of the day, where the state of charge is equal to the final state of charge at the end of the previous day (6.20).

$$E_{SOC}^{t=0} = E_{SOC}^{t=95} \text{ of the previous day} \tag{6.20}$$

For initialising the LP (6.21) , the state of charge at the beginning of the year is set equal to zero

$$E_{SOC}^{t=0} = 0 \text{ for day 1 of 365} \tag{6.21}$$

In (6.22) the charge and discharge capacity is confined by the minimum and maximum state of charge.

$$0 \leq E_{SOC}^{t} \leq E_{SOC}^{max} \text{ for } t \in T \tag{6.22}$$

Chapter 7

Thermal models and control logic

In this chapter we present the models for simulating the supply of heat and heat demand. In section 7.1, we present an overview of the various models that are developed. Subsequently, in section 7.2, we present the house model. In section 7.3 we present the buffer tank model and in section 7.4 we present the heat pump model. In section 7.5 we present the temperature control logic and finally in section 7.6 we present the logic for controlling the thermal flexibility for passive balancing and peak shaving.

7.1 Overview

7.1.1 Modelling approach

To develop an accurate thermal systems model, we build on the work of others. For quantifying the heat gains/losses, an EPC equation structure is used, see [103]. For calculating the contribution of heat gains, due to incident solar irradiance, the mathematical equations by [104] have been adopted. Characteristics of the Schoonschip houses and systems are obtained from EPC reports, see [82]. Inspired by [105], the underfloor heating system is modelled as a flat slab. Formulas by [106] and [107] are used to characterise heat exchange between the floor, air and thermal mass of the house. Profiles on domestic hot water consumption (DHW) are obtained from [98]. For characterising the hot water buffer tank, the work in [108] and [109] is used. For characterising heat pump performance, [110] was used. A literature survey on closed cycle ground source heat pumps was conducted, to better understand its characteristics. To summarise, the following resources have been used:

1.	Heat losses/gains calculations according to EPC	[103]
1.	Incident irradiance on windows	[104]
1.	House characteristics by EPC report	[82]
2.	Underfloor heating system	[105], [106] and [107]
3.	DHW demand	[98]
4.	Buffer model	[108] and [109]
5.	Ground source heat pump model	[110]
5.	Literature survey on heat pumps systems	Appendix A11.2

A detailed overview of all components and energy/heat flows is presented in Figure 7.1. The red boxes and numbers indicate which papers have been used to obtain a mathematical formulation of each component.

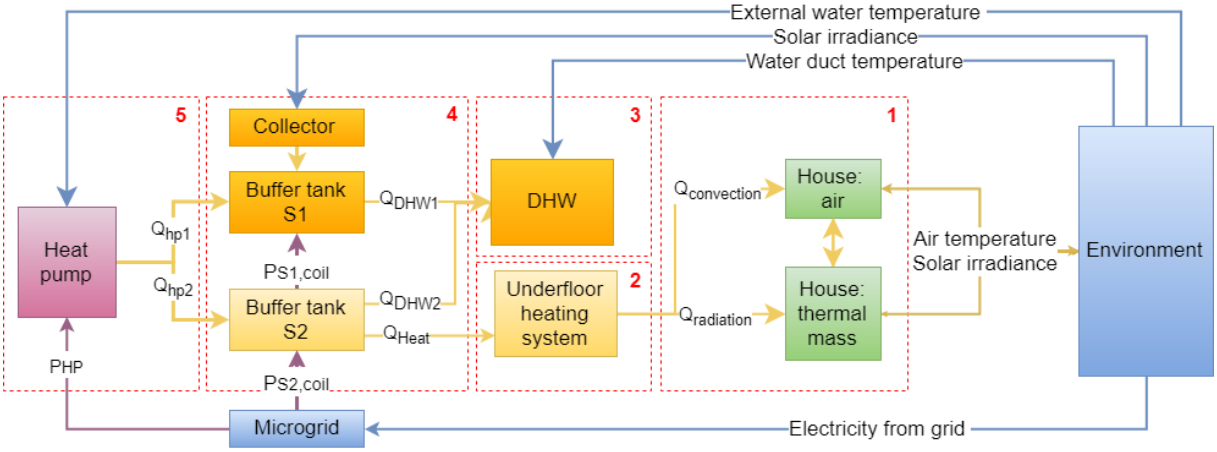

Figure 7.1: Schematic overview of thermal system models and energy flows

7.1.2 Main assumptions

The following assumptions have been made to aid modelling the thermal systems:

- To simplify modelling, we assume all houses to be identical, having the same demand for heat and DHW.
- To simplify modelling, the house is considered a single volume, having a single thermal enclosure containing a single volume of air.
- The house is modelled as three components: One model represents the internal energy of the air. The second model represents the internal energy contained by the thermal mass of the house. The third model represents the underfloor heating system.
- To simplify modelling, and similar to [9] and [10], the exchange of heat between the various thermal components is modelled using energy flows.
- Inspired by [105], the underfloor heating system is modelled as a flat slab. The approach by [105], is useful, as no detailed underfloor heat system model is required. Also, this approach allows the use of energy flows, rather than supply and return temperatures.
- The thermal buffer is modelled as a stratified tank consisting of two layers. Each layer is modelled as a separate tank, having its own uniform temperature.
- The performance and characteristics of the heat pump have been simplified. The performance of the heat pump can be expressed using the correlation by [110].

7.1.3 Differences with respect to [108] and [109].

Next, we identify three differences between our study and that of [108] and [109]. This forms the motivation to adopt other sources as previously listed.

- The researchers in [108] and [109] have investigated the use of air source heat pumps. However, in Schoonschip, ground source heat pumps will be implemented. Hence, the performance characteristics are different. To that end, we adopt the correlation found by [110].
- In [108] and [109], the heat supplied to the building is assumed to be dissipated instantly. However, in our case, the house is equipped with an underfloor heating system. Given the thermal inertia of such a system, there is a delay between the delivery and dissipation of heat to the house. Therefore, the underfloor heating system should be modelled separately.
- In [108] and [109], a simplified model was used to calculate the indoor temperature in the building. As input to the simplified building model, a predefined heat profile was used. The profile was based on accurate simulations of the building under consideration. Hence, the heat demand is considered fixed. However, in this study, the aim is to quantify the amount of thermal flexibility. Now, both the heat demand and thermal flexibility are, amongst others, a function of the temperature of the air within the house, the temperature of the thermal mass of the house and the temperature of the floor. Hence in order to quantify the availability of thermal flexibility, the heat demand should be a function of time and temperatures of the various masses.

7.1.4 Compatibility of papers

By combining several models, it is important to insure coherency between the models. Three problems are discussed and solutions or simplifications are proposed.

Buffer tank and underfloor heating system

The first problem relates to the interaction between the underfloor heating system and buffer tanks. Given the assumption of energy flows, the exchange of heat is no longer characterised by the flow rate and temperatures of both components. However, in practise, the supply temperature should be such that sufficient amount of heat can be transferred from the floor to the house. To that end, heat pump manufacturers use heating curves that prescribe the required heat pump outlet temperature as a function of the outdoor air temperature. In our case, the buffer tanks should supply water at sufficiently high temperatures. To account for this, we do not use a heating curve. Instead the temperature in the buffer tank is kept above a certain minimum temperature. In addition, to account for flow rate limitations, a maximum is imposed on the heat being transported from the buffer tank to the floor.

Buffer tank and solar collector

Another difficulty relates to the distribution of heat from the solar collector across the two buffer tanks. In [108] and [109], the distribution of heat across both tanks is actively controlled, depending on the temperature of the water coming from the collector. However, in our work, we assume heat is distributed equally across each buffer tank. This simplification may lead to a slightly inaccurate representation of the tank temperatures. For including a more detailed representation, we refer to the work by [108] and [109]. A detailed description of our assumptions is given in section 6.4.1 and 6.4.2

Heat pump type and performance characteristic

Another problem relates to the combination of the buffer tank model by [108] and [109] and the heat pump model by [110]. In [108] and [109], the heat pump is modelled as two separate devices. One for supplying hot water to buffer tank S1 and one for supplying warm water to buffer tank S2. The outlet temperature of each HP device is characterised by the temperature of each tank. Whereas in [110], the outlet temperature of the HP is taken as a weighted average. The average outlet temperature is dependent on the heat requirement for DHW and heating and the temperature of each heat flow. To combine the models by [108], [109] and [110], we disregard the two device approach. Instead, we assume that the heat pump supplies heat to both buffer tanks. Where we require that, for any timeslot t, the heat pump can only supply heat to one buffer tank.

7.2 House model

In this section, we present the thermal dynamics model of the house. This concerns the various components and heat flows as presented in Figure 7.2. In section 7.2.1 we conduct a small literature survey on modelling the thermal dynamics of a house. In section 7.2.2, we present our assumptions and assumptions by [103] and [104]. In section 7.2.3, we present an schematised overview of the Schoonschip house model, informed by the literature survey in section 7.2.1 and the assumptions in section 7.2.2. Finally, in section 7.2.4, we present the mathematical formulation of the house model.

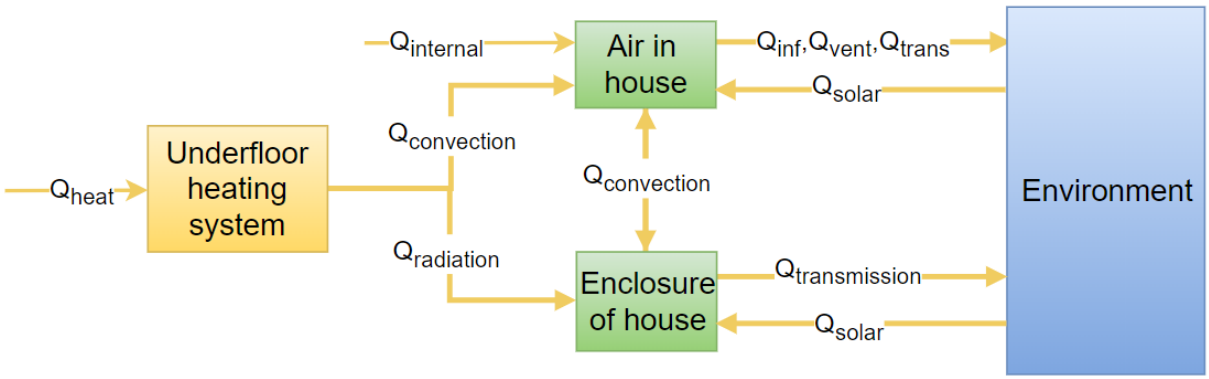

Figure 7.2: Heat flows between the various house system models and environment

7.2.1 Literature on thermal dynamic house models

Simulation of the dynamic thermal behaviour in residential buildings is a well-developed field. We can distinguish two approaches: Low/reduced order models (LOM/ROM) and high order models (HOM).

High order models

Very sophisticated packages, like EPS-r or EnergyPlus, are available that can accurately describe the dynamic thermal behaviour of a building. According to [111], the level of detail in these packages contributes to the accuracy of the simulation, but also requires very detailed input. Also, the packages can have excessive computational runtimes.

Low order models

According to [112], three types of low order models can be used: White-box, Grey-box, and Black-box models. As stated in [112], *"white-box models are represented by physical models that simulate the heating demand by simplified physical equations using solely physical knowledge about the system and material properties."* As stated in [112], "*Grey-box models rely on physical knowledge about the system dynamics to define the model structure using stochastic differential equations. Statistical methods are then used to estimate the unknown parameters"* According to [112], black-box models rely on statistical data analysis, based on statistical input-output models.

According to [112], white box models allow analysing the physical behaviour of buildings, yielding sufficiently accurate results for research purposes. However, according to [112], the use of white box models has not been satisfactory for accurate temperature control in real houses. Therefore, scholars often use grey-box models. By calibrating the grey-model with respect to a high order model or empirical data, a high level of accuracy and accurate control can be obtained. This allows for implementation of grey box models in actual buildings to enable demand-side management (DSM).

In the case of white-box and grey-box models, lumped thermal capacity models are commonly used. Very often, these models are represented by electric network analogies. In this approach, the following phenomena are assigned an electrical component: thermal masses (capacitances), heat flows (currents), temperatures (voltage), heat transfers rates (resistances) and heat sources (current sources).

Modelling complexity of reduced order models

In a study on suitable grey-box models by [113], the required level of modelling complexity has been evaluated. Based on [113], it follows that 3^e order models are considerably more accurate than 2^e order models, whereas 4^e order models do no show a significant increase in accuracy. Hence, both [111] and [113], conclude that a 3^e order models is sufficient for modelling the thermal dynamics of a building. When modelling a building as a 3^e order model, the following capacitances (thermal capacities) should be included according to [113]:

1. the thermal capacity of the building envelope
2. the thermal capacity of the air within the envelope
3. the thermal capacity of the heat emitting unit(s).

Accuracy of 3^e order models

Given a 3^e order grey box model, the authors in [3] note that deficiencies may occur for a high influx of solar heat. Also, the scholars in [113] found that their 3^e order grey-box model does not pass the white noise test for one-step predictions. The authors in [112] found that over long time periods, their 3^e order grey-box model shows a significant drift from the validation data. Indicating, that only over short time periods (~1000h), the grey box model performs adequately. However, in [111], the authors did not identify such a deviation for longer time periods, in their 3^e order grey-box model.

7.2.2 Assumptions

Assumptions and changes to [103]

Based on [103], we will consider the following heat losses and heat gains.

- *Heat losses:* infiltration (Q_{inf}), ventilation (Q_{vent}), transmission through walls/roof ($Q_{transmission}$).
- *Heat gains:* radiation through windows (Q_{solar}), internal gains by devices and people ($Q_{internal}$).

We propose three changes with respect to [103]. This includes changes to the time resolution, temperature setpoint and ''the heat gain utilisation factor''. The time resolution is increased to 15 minutes, instead of one month. Based on ISSO 51 standards, see [114], the temperature setpoint, during the heating season, is set to 20° Celsius, instead of 18° Celsius. The heating season is assumed to lasts from September t/m April. From [114], it follows that the average comfortable indoor temperature T_{res} depends on the average air temperature T_{air} and radiation temperature, T_{rad} . Where the radiation temperature is the average surface temperature of walls and objects in the room. As seen in Figure 7.3, some variation around T_{res} is allowed. In addition, it follows from [115] that residents do not notice temperature changes up to 1.5° Celsius per hour. The heat gain utilisation factor is a factor that expresses the extent to which a building is able to absorb solar heat and internal heat during some month. Unlike in [103], our model includes a detailed description of the interplay between thermal masses, heat losses and heat gains, on a 15 minute interval basis. Consequently, no utilisation factor needs to be included.

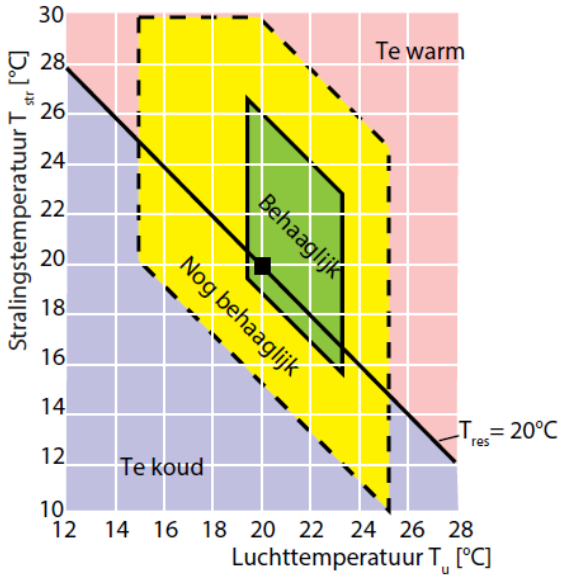

Figure 7.3: Comfortable indoor temperatures for T_{air} and T_{rad}, adopted from [12]

Assumptions with respect to [104]

The work in [104] describes a set of mathematical formulas that can be used to estimate the incident irradiance on solar modules. In our case, the mathematical formulas are used to assess the incident irradiance on windows. This assumption is valid, since the mathematical formulas are generic and applicable to any object that receives solar irradiance. We assume all windows are positioned vertically.

Additional assumptions

For modelling the Schoonschip community and houses, we introduce some major assumptions: We assume a single house to be representative for all other houses within Schoonschip. To that end, the thermal properties of kavel 5 serve as guideline for modelling the house. A motivation for selecting kavel 5 can be found in chapter 5. As seen in Figure *7.4*, kavel 5 is a two story building. The top floor contains two living quarters with floor area A1 and A2 and volume V1 and V2. Both are equipped with underfloor heating systems. For simplicity, we only consider the top floor for modelling the heat demand of the house. The configuration of kavel 5 has been simplified to aid modelling. The simplifications are presented in Figure 7.5.

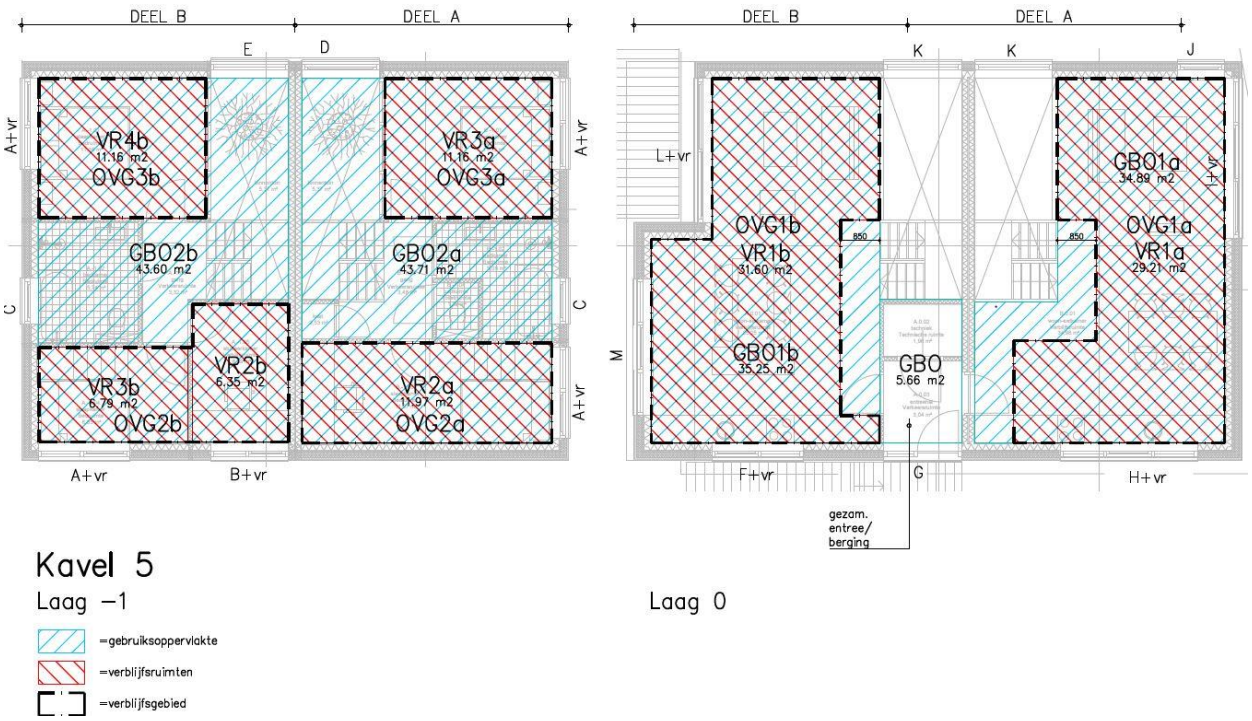

Figure 7.4: Lot 5: a two story floating house, with two households, adopted from [4]

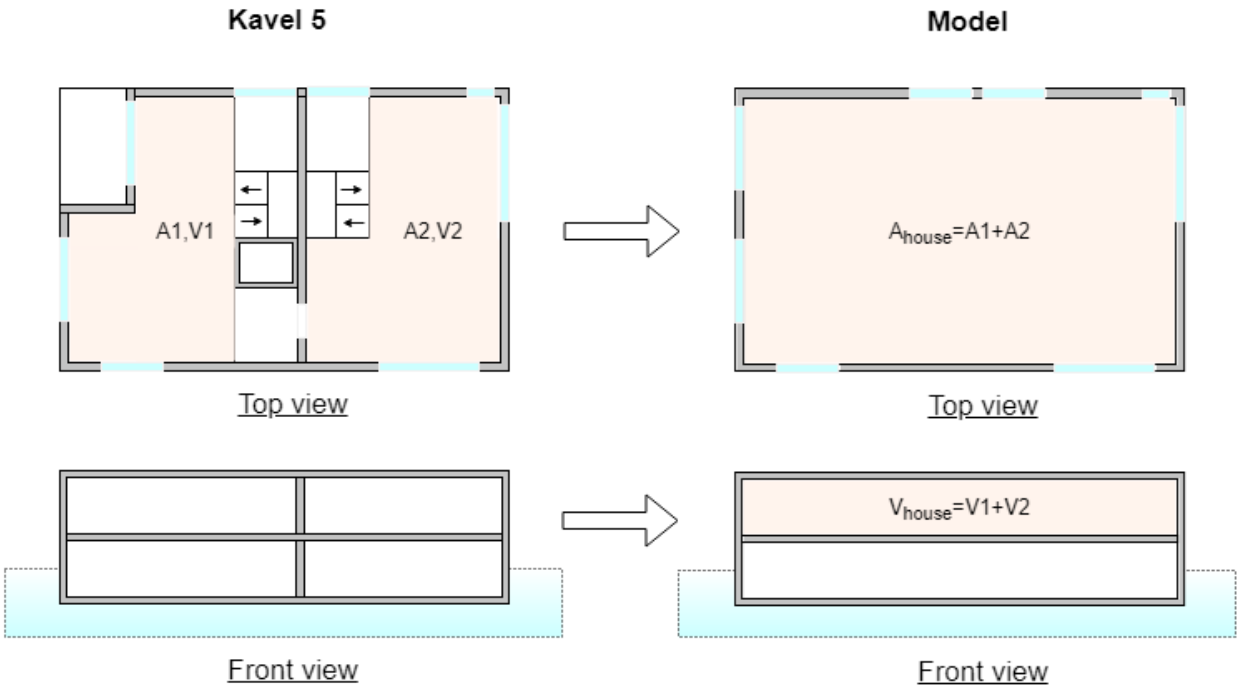

Figure 7.5: Schoonschip lot 5: simplified model outline

Assumptions on thermal dynamics

An overview of assumption on various thermal dynamic properties and variables are now listed. We present a final overview of the thermal characteristics in Table 6.1.

Heat losses: Ventilation, infiltration

- According to [82], house 5 is equipped with unbalanced ventilation. No heat recovery is included.
- Based on [82], the infiltration rate is set to 8dm3/s, the ventilation rate is set to 40dm3/s.

External heat gains: solar irradiance through windows

- The heat gains by irradiance, as received through the windows, are dependent on their orientation, inclination, surface area and total irradiance.
- The normal incident solar irradiance per window, is based on the formula's in [22].
- The window surface area, orientation, inclination and ZTA (zonnetoetredingsfactor) are derived from [103].
- Based on [116], the convection factor (C_f) is set to 0.15. Hence, 15% of the incident solar irradiance is immediately released into the air by convection.
- The solar absorption coefficient by white walls/ceiling in the interior is set to 0.15.

Underfloor heating system

- The underfloor heating system is assumed to be perfectly isolated. Consequently, heat is only transmitted via its upper surface.
- We assume the underfloor heating system transmits heat via natural convection and radiation to the air and house enclosure
- The underfloor volume is assumed equal to the floor surface and thickness.

Distribution efficiencies

- Based on [82], the supply and distribution efficiencies of the heating system are set equal to 1.
- Based on [82], the supply efficiency for DHW is set to 87%.

Thermal mass of floor and house

The thermal mass of the floor is set equal to the specific heat capacity of concrete, the density of concrete and some volume [82]. The EPC report in [82], only specifies the *building mass* of the Schoonschip house. The building mass is considered ''mixed light''. According to [114], the building mass is considered an indirect measure of the thermal mass. As stated in NEN7120, see [117]: ''*The thermal mass of a building is large, if much building mass is present in the building, such as concrete and stone, and the mass is not isolated from the inside air.* It follows from [17] that, mixed light buildings, as seen in Schoonschip, are constructed from wood, having solid floors, but no solid separating walls. Hence, the thermal mass of the Schoonschip houses is relatively small. Now the ISSO 51 standard, see [118], discriminates between three categories of thermal masses: ''light'', ''average'' and ''heavy''. Hence, given the low thermal mass of the Schoonschip house, we assume the thermal mass to be ''light''. Based on [118], the thermal mass c_{house} of *light buildings* amounts to 54000J/K·m3. In our model the thermal mass is considered proportional to the surface area of the enclosure, multiplied by some thickness. The thickness, $l_{enclosure}$ is set to 0.3 m, to account for the mass of the internal walls, objects and exterior wall

Residence behaviour

The temperature set points and internal heat gains are dependent on the occupancy of the residence. However, this effects are left out of scope. Instead, a fixed value on average heat gains has been adopted. The temperature setpoint is assumed to be constant. Based on [116] the internal heat gains $q_{internal} = 6W/m2$ are proportional to the floor surface.

Average indoor temperature

From [12], it follows that the average comfortable indoor temperature depends on the average air temperature and average radiation temperature. Hence, we define the average indoor temperature $\bar{T}^t_{house}$ as:

$$\bar{T}^t_{house} = (\bar{T}^t_{i,air} + \bar{T}^t_{e,enclosure}) / 2 \qquad (6.23)$$

7.2.3 Schematic representation of house model

Given the findings in section 7.2.2, we use a 3e order white box model for sake of simplicity. The use of more advanced (high order modelling) packages is not pursued, because of the high computational burden and detailed input data requirements. Also, the use of high order models hampers integration with the other thermal models. In this thesis, we leave validation of the 3e order white box model an open problem.

In the 3e order white-box modelling approach, three thermal capacitances are used to represent the building: The house enclosure, the internal air, and the underfloor heating system. Each thermal capacity is assumed to have an uniform temperature. According to [10], the average temperature within such a system can be approximated using a lumped thermal capacity model. Consequently, changes to the internal energy of each system, can be expressed in terms of a change in the temperature.

Building thermal model overview

In Figure 7.6, we present an electrical circuit analogy to illustrate the relations between the thermal capacities more specifically. Here, the voltage source T_O, represents the varying outside air temperature, T_e, the enclosure temperature, T_{fl} the floor temperature and T_i the internal air temperature. Capacitances C_e, C_{fl}, C_i represent the heat capacities of the enclosure, air and floor. Current sources are used to represent the various heat gains. With q_{ig} the internal heat gains, $C_f \cdot \varphi_S$ the solar radiation gains to the air, $(1-C_f)\cdot\varphi_S$ the solar radiation gains to the enclosure and φ_{fl} the underfloor heat gains. Resistances are used to describe the heat resistance to heat transfer between the thermal capacitances and the outside air.

With R_{vent} the heat transport through ventilation, where the rate of ventilation is strictly not a resistance, but rather a current source. With R_{inf} the heat resistance to infiltration, R_{trans1} the heat resistance to transmission by windows, R_{trans2} the heat resistance to transmission via the building envelope (walls and roof), R_{rad} the heat resistance to radiation from the floor to the enclosure, R_{conv1} the heat resistance to convection from the internal air to the enclosure and R_{conv2} the heat resistance to convection from the floor to the internal air.

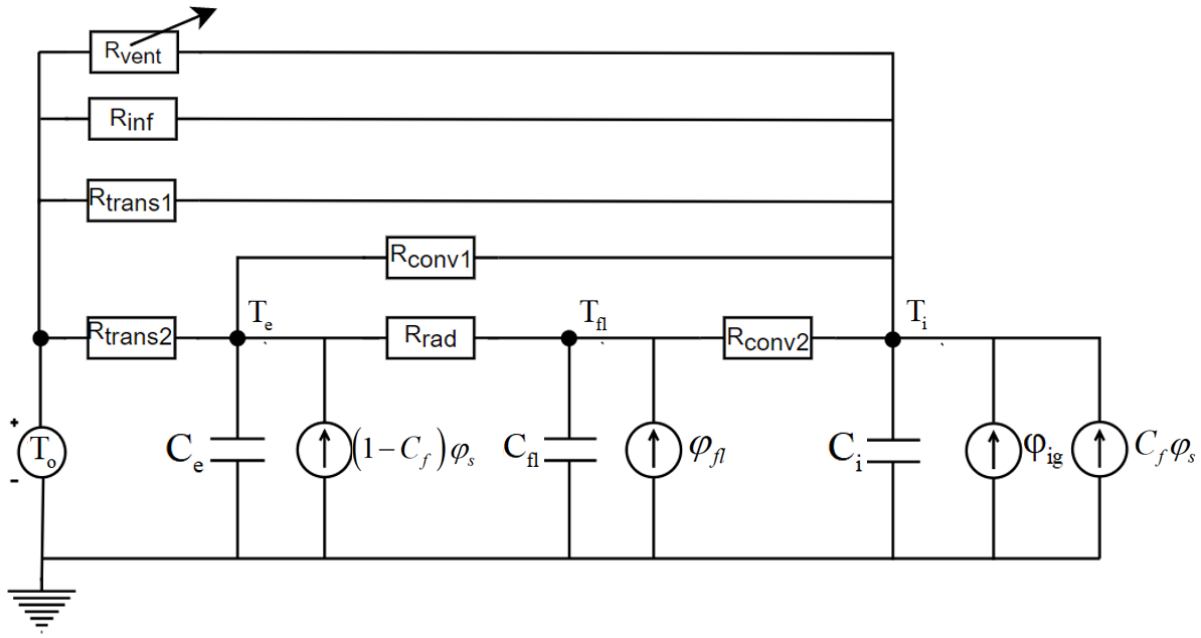

Figure 7.6: Electrical circuit analogy of the 3e order white box model to represent the house

7.2.4 Mathematical formulation

Using the lumped thermal capacity modelling approach, the average temperature change in each volume is given by equations (6.24)-(6.26). We present the mathematical equations for calculating the individual heat gains and losses in appendix A11.1.

Temperature change of the internal air

The average temperature change of air within the enclosure is given by equation (6.24).

$$c_{p,air} \cdot \rho_{air} \cdot V_{air} \cdot \frac{d\bar{T}_i^t}{dt^*} = Q_{i,gains}^t - Q_{i,losses}^t \quad (6.24)$$

Temperature change of the enclosure

The average temperature change of the house enclosure is given by equation (6.25).

$$C_{enclosure} \cdot A_{enclosure} \cdot h_{enclosure} \cdot \frac{d\bar{T}_e^t}{dt^*} = Q_{e,gains}^t - Q_{e,losses}^t \quad (6.25)$$

Temperature change of the floor

The average temperature change of the underfloor heating system is given by equation (6.26).

$$c_{p,floor} \cdot \rho_{floor} \cdot V_{floor} \cdot \frac{d\bar{T}_{fl}^t}{dt^*} = Q_{heat}^t - Q_{fl-i,Convection}^t - Q_{fl-e,Radiation}^t \quad (6.26)$$

With $\bar{T}_i^t$ $\bar{T}_e^t$, and $\bar{T}_{fl}^t$ the average temperature of the internal air, enclosure and floor. $Q_{e,lossses}^t$ the heat losses from the enclosure and $Q_{e,gains}^t$ the heat gains to the enclosure, $Q_{i,losses}^t$ the heat losses from the internal air and $Q_{i,gains}^t$ the heat gains to the internal air, $Q_{fl-i,Convection}^t$ the heat supplied through natural convection from the underfloor heating system to the internal air, $Q_{fl-e,Radiation}^t$ the heat loss through radiation from the underfloor heating system to enclosure. Here, the floor heat gains, φ_{fl} equals $Q_{fl-i,Convection}^t + Q_{fl-e,Radiation}^t$ Finally, Q_{heat}^t is the heat supplied by buffer tank, to the underfloor heating system. Each term is given in Joules/s. t^* is the time of one time interval equal to 1 quarter (900 seconds). The thermal properties are given by Table 7.1.

Internal air: heat gains and losses

The heat losses and heat gains to and from the internal air are given by equations (6.27) and (6.28).

$$Q_{i,losses}^t = Q_{i-o,Infiltration}^t + Q_{i-o,Ventilation}^t + Q_{i-o,Transmission}^t + Q_{i-e,Convection}^t \quad (6.27)$$

$$Q_{i,gains}^t = Q_{Internal} + Q_{i,Irradiance}^t + Q_{fl-i,Convection}^t \quad (6.28)$$

With, $Q_{i-o,Infiltration}^t$ the infiltration losses to the surrounding outside air $Q_{i-o,Ventilation}^t$ the ventilation losses to the surrounding outside air, $Q_{i-o,Transmission}^t$ the heat losses through transmission via windows, $Q_{i-e,Convection}^t$ the heat losses through natural convection from the internal air to the house enclosure, $Q_{Internal}$ the internal heat gains to the air. With, $Q_{i,irradiance}^t$ the radiation heat gains to the internal air, $Q_{fl-i,Convection}^t$ the radiation heat gains via convective heat transfer from the underfloor heating system to the internal air.

Heat losses from the house enclosure

The heat losses and heat gains to and from the internal air are given by equations (6.29) and (6.30).

$$Q^{t}_{e,losses} = Q^{t}_{e-o,Transmission} \tag{6.29}$$

$$Q^{t}_{e,gains} = Q^{t}_{i-e,Convection} + Q^{t}_{e,Irradiance} + Q^{t}_{fl-e,Radiation} \tag{6.30}$$

With $Q^{t}_{e-o,transmission}$ the heat losses through transmission via the enclosure to the external air, $Q^{t}_{i-e,Convection}$ the heat gains through natural convection from the internal air to the house enclosure, $Q^{t}_{e,irradiance}$ the solar radiation heat gains to the enclosure and $Q^{t}_{fl-e,Radiation}$ the radiation heat gains via radiative heat transfer from the underfloor heating system to the enclosure. Each heat loss/ heat gain is given in Joule/second.

Table 7.1: Thermal properties of lot 5

Characteristics	Variable	Units	Value
Height of house	$h_{enclosure}$	[m]	3
Thickness of floor slab	l_{floor}	[m]	0.1
Thickness of enclosure	$l_{enclosure}$	[m]	0.3
Floor surface (heated area)	A_{floor}	[m2]	110
Surface of house enclosure	$A_{enclosure}$	[m2]	250
Volume of floor slab	$V_{floor} = A_{floor} \cdot l_{floor}$	[m3]	7
Volume of house/air in house	$V_{air} = A_{floor} \cdot h_{enclosure}$	[m3]	330
Volume of enclosure	$V_{enclosure} = A_{enclosure} \cdot l_{enclosure}$	[m3]	75
Window area * ZTA	$ZTA \cdot A_{window,orientation:ZO}$	[m2]	3.9
Window area * ZTA	$ZTA \cdot A_{window,orientation,ZW}$	[m2]	16.9
Window area * ZTA	$ZTA \cdot A_{window,orientation,NW}$	[m2]	4.5
Window area * ZTA	$ZTA \cdot A_{window,orientation,NO}$	[m2]	4.8
Infiltration rate	$\varphi_{infiltration}$	[m3/s]	0.004
Ventilation rate	$\varphi_{ventilation}$	[m3/s]	0.05
UA value, total surface windows	$\sum A_{window,orientation} \cdot (R_{trans1})^{-1}$	[W/K]	77
UA value, total surface enclosure	$\sum A_{enclosure,orientation} \cdot (R_{trans2})^{-1}$	[W/K]	30
Internal heat gain per floor area	q_{ig}	[W/m2]	6
Convection factor	C_f	[-]	0.3
Absorption coefficient white walls	α_{abs}	[-]	1
Inclination angle of windows	θ_W	[deg]	0
Solar radiation through windows	φ_S	[J/s]	[-]

7.3 Underfloor heating model

In this section we present the model of the underfloor heating system. In section 7.3.1, the modelling approach is outlined. In section 7.3.2 and 7.3.3 we present formula's for calculating the radiative and convective heat transfer coefficients. In addition, we also supply an expression for calculating the convective heat transfer between the internal air and the house enclosure. Finally, we perform some validation of the heat transfer coefficients. A simple graphical representation of the underfloor heating model is given by **Fout! Verwijzingsbron niet gevonden.**.

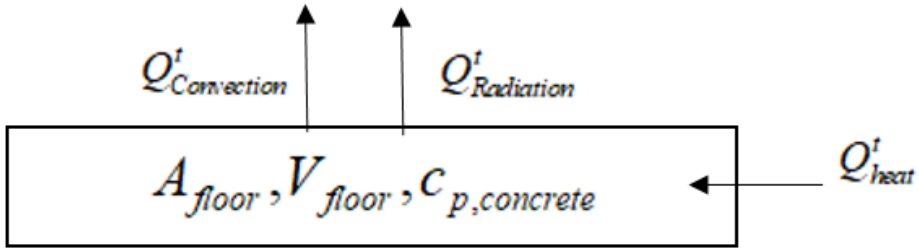

Figure 7.7: Lumped thermal capacity model of the underfloor heating system

7.3.1 Modelling approach

The floor is modelled as a flat slab, having a surface area, heat capacity, volume and time dependent temperature. The influx of heat from the buffer tank to the underfloor heating system is given by Q^t_{heat}. The flat slab is assumed to be perfectly insulated. Hence, heat is only exchanged with the house. The heat transfer of heat from the underfloor heating system to its surroundings are governed by natural convection and radiative heat transfer. These are given by equation (6.31) and (6.32).

$$Q^t_{fl-i,convection} = h^t_{R,fl-i} \cdot A_{floor} \cdot (\bar{T}^t_{fl,floor} - \bar{T}^t_{i,air}) \quad (6.31)$$

$$Q^t_{fl-e,radiation} = \bar{h}^t_{R,fl-e} \cdot A_{floor} \cdot (\bar{T}^t_{fl,floor} - \bar{T}^t_{e,enclosure}) \quad (6.32)$$

With $Q^t_{fl-i,convection}$, the heat transfer through natural convection from the floor to the surrounding air, $Q^t_{fl-e,radiation}$ the heat transfer through radiation from the floor to the house enclosure. With $\overline{h^t_C}$ the average time dependent heat transfer coefficient by convection, $\overline{h^t_R}$ the average time dependent heat transfer coefficient by radiation, A_{floor} the area of the floor containing the underfloor heating system, $\bar{T}^t_{fl,floor}$ the average surface temperature of the floor, $\bar{T}^t_{i,air}$ the average temperature of the internal air and $\bar{T}^t_{e,enclosure}$ the average house enclosure temperature. Each term is given in Joule/second.

Heat transfer coefficients

The heat transfer coefficients for radiation between the floor and enclosure, $\bar{h}^t_{R,fl-e}$ and natural convection between the floor and internal air, $\bar{h}^t_{C,fl-i}$ are not static. The same holds for the heat transfer coefficient, $\bar{h}^t_{C,i-e}$ between the internal air and the house enclosure. Depending on the temperature of each volume, the coefficients differ. Based on [106] and [107], heat transfer coefficients have been derived. This derivation is presented in the next sections

7.3.2 Radiative heat transfer coefficient

According to [119], 75–80% of the heat emission from the underfloor heating system takes place through radiation. The remaining heat transport is governed by natural convection. To account for these phenomena, we present approximations of natural convection and radiation using formula's by [106] and [107]. According to [107], the average radiative heat transfer coefficient $\bar{h}^t_{R,fl-e}$ between the floor and enclosure, may be estimated using equation (6.33).

$$\bar{h}^t_{R,fl-e} = 4 \cdot \varepsilon_{eff} \cdot \sigma \cdot \overline{T^t_R}^3 \tag{6.33}$$

With ε_{eff} ,the effective emission coefficient, σ the Stefan-Boltzmann constant. $\overline{T^t_R}$ is defined as the average surface temperature (in Kelvin) of the floor and surface temperature of the building. The average temperatures is given by equation (6.34).

$$\overline{T^t_R} = \tfrac{1}{2}(T^t_{fl,floor} + T^t_{e,enclosure}) \tag{6.34}$$

The effective emission coefficient, ε_{eff} is a function of the emission coefficients of the objects within the house. According to [107], the coefficient can be neglected if the following condition holds: An object (1) is completely enclosed by its environment (2) with A2>>A1. In our case, this condition holds, as almost all radiation produced by the floor, is received by the walls and ceiling of the enclosure. Consequently, we may assume the emission coefficient to be equal to 1.

7.3.3 Natural convective heat transfer coefficients

In general, the average natural convective heat transfer coefficient, is a function of the average Nusselt number, given air and some plate. An expression is given by equation (6.35)

$$\bar{h}^t_C = \frac{k}{L} \cdot \overline{Nu_L}^t \tag{6.35}$$

With L the characteristic length of the solid surface, k the thermal conductivity coefficient of air, evaluated at the film temperature and $\overline{Nu_L}^t$ the average Nusselt number. The average Nusselt number is the ratio of the actual heat transfer with respect to the heat transfer by natural convection. According to [107], free convection below or above a horizontal plate can be expressed as in equation (6.36), whereas the natural convection along a vertical plate is given by equation (6.37)

Horizontal plate: $\overline{Nu_L} = 0.17 Ra_L^{1/3}; \quad \text{providing that } Ra_L > 3\times10^8$ (6.36)

Vertical plate: $\overline{Nu_L} = 0.12 Ra_L^{1/3}; \quad \text{providing that } Ra_L > 1\times10^8$ (6.37)

The Rayleigh number is given by equation (6.38).

$$Ra_L^{1/3} = \left(Gr^t \cdot Pr\right)^{1/3} = \left(\frac{\beta^t \cdot \Delta T^t_C \cdot g \cdot L^3}{\nu^2} \cdot \frac{\nu}{\alpha}\right)^{1/3} \tag{6.38}$$

With $\Delta T^t_C = \bar{T}^t_{plate} - \bar{T}^t_{air}$, g the gravitational acceleration coefficient, L the characteristic length of the solid mass, ν the kinematic viscosity, α, the thermal diffusion coefficient and β^t, the volumetric coefficient of expansion.

According to [106], the characteristic length L is given by the shorter side of rectangular plate. According to [106], the volumetric coefficient of expansion β^t is defined as $\beta^t = 1/\overline{T_C}^t$ with $\overline{T_C}^t$ the absolute film temperature between the air and temperature at the surface of the plate. The film temperature is given by equation (6.39).

$$\overline{T^t_C} = \tfrac{1}{2}\left(\bar{T}^t_{air} + \bar{T}^t_{plate}\right) \tag{6.39}$$

Natural convective heat transfer between enclosure and internal air

From equation (6.36)and(6.37), it follows that the Nusselt number is different for vertical walls and horizontal ceilings. For vertical plates (walls), the multiplication factor equals 0.12, whereas for horizontal plates (ceiling) the multiplication factor equals 0.17. Given the small difference, we assume this difference to be negligible. As an approximation, we set the multiplication factor equal to 0.15. Hence, the natural convective heat transfer coefficient, $\bar{h}^{t}_{C,i-e}$ between air and the enclosure is given by (6.40)

$$\bar{h}^{t}_{C,i-e} = \frac{k}{L_{wall/roof}} \cdot 0.15 \cdot Ra^{1/3}_{L_{wall/roof}}; \quad \text{providing that } Ra_L > 3\times10^8 \tag{6.40}$$

With k the thermal conductivity coefficient of air and $L_{wall/roof}$ the characteristic length of the walls and roof. This value is set to 5m as an average between the characteristic length of the wall: 3m and the characteristic length of the roof: 6m.

Natural convective heat transfer between the floor and internal air

The natural convective heat transfer coefficient between the floor and the air is given by equation (6.41)

$$\bar{h}^{t}_{C,fl-e} = \frac{k}{L_{floor}} \cdot 0.17 \cdot Ra^{1/3}_{L_{floor}}; \quad \text{providing that } Ra_L > 3\times10^8 \tag{6.41}$$

With k the thermal conductivity coefficient of air and L_{floor} the characteristic length of the floor heating system. This value is set to 6m.

7.3.4 Validation of heat transfer coefficients

Given that equations (6.36) and(6.37), are only valid for a specific range of the Rayleigh number, we must evaluate whether this condition is met. Thereto, we vary the average air temperature and floor temperature and evaluate the Rayleigh number. The following air/floor temperatures are selected: 18°/29°, 24°/29° and 22.9°/23° and 20°/22° Celsius. The characteristic length of the floor heating system is set to 4.4m, which is half the length of house number 5. Based on these variables, the Rayleigh number was calculated using (6.36). This yields approximately the following Rayleigh numbers: $9\cdot10^{10}$, $4\cdot10^{10}$, $8\cdot10^{8}$ and $2\cdot10^{10}$. For larger characteristic lengths, the Rayleigh number even increases. Hence, equation (6.36) and(6.37), hold and may be used.

Given the same temperatures and characteristic length, the convective heat transfer coefficients amount to respectively 4.5, 3.46, 0.94 and 2.56 W/m2K. For a wall temperature of 20° Celsius, the radiative heat transfer coefficients amount to 5.9, 6.2, 5.9 and 5.8 W/m2 K.

Convection versus radiation

Observe that for reasonable air, floor and wall temperatures, 56% of the total heat transfer is governed by radiation. In general, we expect a smaller contribution from natural convective heat transfer. Given the fact that air heats up quickly, the convective heat transfer coefficient will decrease rapidly. Indeed, this will lead to a larger contribution of radiative heat transfer, as this transfer coefficient is relatively constant for any temperature difference.

7.4 Stratified buffer tank model

In this section, we present a stratified buffer tank model. In section 7.4.1, we present the assumptions by [108] and [109] on modelling a stratified buffer tank. In section 7.4.2, we present our assumptions and alterations with respect to the work in[109]. Finally, in 7.4.3 we present the mathematical formulation of the stratified buffer tank model by [109].. A graphical overview of the stratified buffer tank model is shown in Figure 7.8.

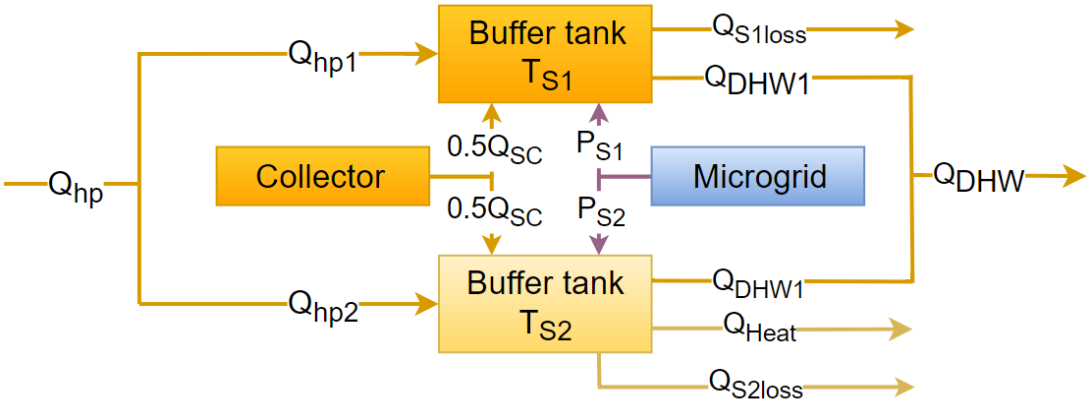

Figure 7.8: A graphical representation of the buffer tank components and energy flows

7.4.1 Assumptions by [108] and [109]

In [108] and [109] the stratified buffer tank is modelled as two separate buffer tanks: Tank S1 and tank S2. No heat exchange between the two tanks is considered. And the temperature in buffer tank *S2*, cannot exceed the temperature in buffer tank S1. The water in each tank is assumed to be perfectly mixed, having a single uniform temperature. Tank S1 is primarily used for DHW purposes. Tank S2 is used for DHW and heating purposes. Energy for DHW purposes is taken proportionally from both tanks. Heat loss from each tank are dependent on transmission losses. The heat production by the solar collector is distributed across both tanks. The distribution is regulated by a controller which takes into account the collector supply temperature and buffer tank temperatures. The minimum temperature of tank S2 is government by a heating curve. The heating curve prescribes the required supply temperature to the heating system, as a function of the outdoor air temperature. The stratified buffer tank model by [108] has been validated by the authors. It is found in [109] that the stratified buffer tank model is sufficiently accurate for most operational modes. However, the mean temperature deviates by circa +5^{o} Celsius. The authors account for this deficit by increasing the supply temperature of the heat pump by 5^{o} Celsius [109].

7.4.2 Our assumption and modifications

The stratified buffer tank model that is proposed by [109] is also used in our study. However, various simplifications and alterations are proposed. Unlike the authors of [109], we assume for simplicity that the heat production of the solar collector is equally divided over both buffer tanks. Furthermore, we assume that both buffer tanks are equipped with electrical coils. The electrical coils represent an electrical boiler that comes preinstalled installed with the NIBE heat pump system [84]**,** used in the Schoonschip houses. The electrical capacity of each coil is set to 1.5kW, which is in the same order of magnitude as the electrical boiler. Finally, we assume 100% conversion of electricity to heat.

Similar to [109] , the maximum temperature of buffer tank S1 T_{S1}^{max} is set to 75^{o} Celsius. The minimum temperature of buffer tank S1 T_{S1}^{min} is set to 55^{o} Celsius, to mitigate the risk for legionella infections, as discussed in [109]. In addition, we demand that the temperature is frequently raised beyond 60^{0} Celsius. Similar to [109], we assume that the maximum temperature of S2 should remain below that of tank S1. However**,** unlike in [109], we assume that the minimum temperature of S2 is not governed by a heating curve. Instead, a fixed value is used. According to [110] , the supply temperature of underfloor heating systems varies between 30^{o} and 45^{o} Celsius and according to [114], a supply temperature of 30^{o} Celcius is often feasible in well insulated dwellings. Given that the Schoonschip houses are well insulated, the minimum temperature of tank S2 is set to 30^{o} Celsius T_{S2}^{min} .

7.4.3 Stratified buffer tank model

The temperature dependent heat losses are small with respect to the heat extracted from buffer tank S1 and S2. Therefore, the linear differential equations proposed by [109] can be linearized. The average temperature change in each buffer tank is given by (6.42) and (6.43). Each term is given in Joules/second.

$$\bar{T}_{S1}^{t+1} = \bar{T}_{S1}^{t} + \frac{(Q_{QHP1}^{t} + 0.5 \cdot Q_{SC}^{t} + \hat{P}_{S1,coil}^{t} - Q_{DHW1}^{t} - Q_{S1loss}^{t}) \cdot t^{*}}{c_{p,water} \cdot \rho_{water} \cdot V_{S1}} \tag{6.42}$$

$$\bar{T}_{S2}^{t+1} = \bar{T}_{S2}^{t} + \frac{(Q_{HP2}^{t} + 0.5 \cdot Q_{SC}^{t} + \hat{P}_{S2,coil}^{t} - Q_{Heat}^{t} - Q_{DHW2}^{t} - Q_{S2loss}^{t}) \cdot t^{*}}{c_{p,water} \cdot \rho_{water} \cdot V_{S2}} \tag{6.43}$$

With $V_{S1,}$ V_{S2} the volume of the buffer tanks, T_{S1}^{t}, T_{S2}^{t} temperature of tank S1 and S2, Q_{HP1}^{t} and Q_{HP2}^{t} the heat supplied by the heat pumps Q_{SC}^{t} ,the heat supplied by the solar collector Q_{DHW1}^{t}, Q_{DHW2}^{t} the heat for DHW that is extracted from each tank. $\hat{P}_{S1,coil}^{t}$, $\hat{P}_{S2,coil}^{t}$ the heat supplied by the electrical coils, Q_{Heat}^{t} the heat required for heating the building and Q_{S1loss}^{t}, Q_{S2loss}^{t} the heat losses from the storage tanks to their surroundings. And t^{*} the time equal to 1 quarter (900 seconds).

DHW demand

The demand for DHW is governed by the DHW demand profiles and the distribution losses. The demand for DHW in [J/s], is given by equation (6.44).

$$\dot{Q}_{DHW}^{t} = \frac{\phi_{V,DHW}^{t} \cdot c_{p,water} \cdot \rho_{water} \cdot (\bar{T}_{S1}^{t} - \bar{T}_{Waterworks}^{t})}{\eta_{DHW}} \tag{6.44}$$

With η_{DHW} the distribution system losses, $\phi_{V,DHW}^{t}$ the hot water flow rate in [m3/s] that is obtained from the CREST model [98], $c_{p,water}$ the specific heat capacity of water, ρ_{water} the density of water, T_{S1}^{t} the average temperature of buffer tank S1 and $\bar{T}_{Waterworks}^{t}$ the average water work supply temperature.

DHW extraction

Similar to [110], we assume that heat for DHW is extracted from buffer tank S1 and S2 as given by (6.45) and (6.46).

$$Q_{DHW1}^{t} = Q_{DHW}^{t} \cdot \frac{(\bar{T}_{S2}^{t} - \bar{T}_{S1}^{t})}{(\bar{T}_{Waterworks}^{t} - \bar{T}_{S1}^{t})} \tag{6.45}$$

$$Q_{DHW2}^{t} = Q_{DHW}^{t} \cdot \frac{(\bar{T}_{Waterworks}^{t} - \bar{T}_{S2}^{t})}{(\bar{T}_{Waterworks}^{t} - \bar{T}_{S1}^{t})} \tag{6.46}$$

Water work temperature

According to [120], the average temperature in the Dutch water work system $\bar{T}^{t}_{Waterworks}$ varies between roughly 5° and 20° Celsius, reaching its lowest temperature in February. In addition, it follows from [121] that the average water work temperature throughout the year can be described by a sinusoidal function. Therefore, the waterworks temperature is modelled as a sinusoid, having an average temperature of 12°C, an amplitude of 7° C, a period of one year and a phase offset of 0.7π. The phase offset results in a minimum temperature mid-February. The water work temperature is given by equation (6.47).

$$T^{t}_{Waterworks} = 12 + 7\sin\left(\frac{2\pi}{35040}\cdot t - 0.7\pi\right) \tag{6.47}$$

Buffer tank losses

Similar to [110], we assume that the heat losses from the buffer tanks are proportional to the heat transfer coefficient of EPS insulation material, $h_{S1/S2}$, the tank surface areas A_{S1}, A_{S2} and the temperature difference between the tank and the indoor air temperature $T^{t}_{i,house}$. The losses of each tank are given by equation (6.48) and (6.49).

$$Q^{t}_{S1loss} = h_{S1/S2}\cdot A_{S1}\cdot\left(\bar{T}^{t}_{S1} - \bar{T}^{t}_{house}\right) \tag{6.48}$$

$$Q^{t}_{S2loss} = h_{S1/S2}\cdot A_{S2}\cdot\left(\bar{T}^{t}_{S2} - \bar{T}^{t}_{house}\right) \tag{6.49}$$

Underfloor heat transport limitations

Based on [121], typical flow rates in underfloor heating systems vary between 1-6 litres per minute during continuous operation. To account for flow rate limitations, a maximum is imposed on the heat that can be transported per quarter t. The maximum flow rate, $\phi^{t}_{V,maxheat}$ is set to 90 litres per quarter. The volume flow per quarter t can be evaluated using equation (6.50)

$$\phi^{t}_{V,heat} = \frac{Q^{t}_{heat}\cdot t^{*}}{\rho_{water}\cdot cp_{water}\cdot\left(T^{t}_{S2} - T^{t}_{e,floor}\right)} \quad \text{with } \phi^{t}_{V,heat} < \phi^{t}_{V,maxheat} \tag{6.50}$$

With T^{t}_{S2} the temperature of buffer tank S2, T^{t}_{floor} the floor temperature, Q^{t}_{heat} the heat demand and t^{*} the time equal to 1 quarter t (900 seconds).

7.5 Heat pump model

In this section, we present the heat pump system model. A schematic overview of this model is presented in Figure 7.9. In section 6.5.1, we introduce the formulas by [110] a In section 6.5.2. we present our assumptions.

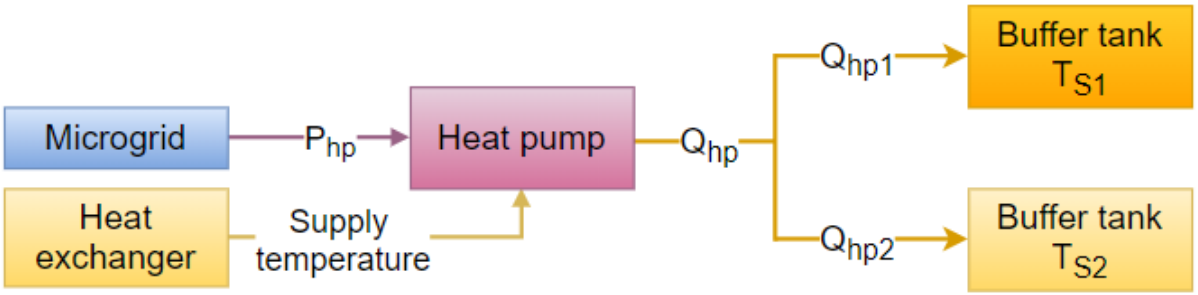

Figure 7.9: The heat pump system and energy flows.

7.5.1 Formulas

Heat pump performance

According to [11], the heat pump performance is a function of the temperature difference ΔT^t between the temperature T^t_{out} supplied by the heat pump and the water supply temperature T^t_{supply} to the heat pump by the heat exchanger in the floating concrete structure. The temperature difference (lift) is expressed as in equation (6.51).

$$\Delta T^t = T^t_{out} - T^t_{supply} \tag{6.51}$$

The study in [11] has found an empirical relationship between the COP and temperature difference. For ground source heat pumps (GSHP) this relation is given by equation (6.52)

$$COP^t_{GSHP}(\Delta T^t) = 8.77 - 0.150 \cdot \Delta T^t + 0.000734 \cdot (\Delta T^t)^2 \text{ for } 20 \leq \Delta T^t \leq 60 \tag{6.52}$$

Validation of correlation

The correlation in equation (6.52) is compared with the characteristics of the heat pump used in Schoonschip (NIBE F1255-PC). A detailed comparison is presented in appendix A11.3. It follows that the correlation reflects the system-COP quite accurately, at a supply temperature of 0 degrees. However, at a supply temperature of 10 degrees, the estimated COP is too small. Throughout the year, the supply temperature will vary between 0° and 25° Celsius. Therefore, the use of equation (6.52) is conservative, indicating lower performance by the heat pump in our model, than encountered in practise.

7.5.2 Model assumptions

Supply temperatures

The Schoonschip houses have been equipped with a heat exchanger that has been incorporated into the floating concrete structure. The heat exchanger is connected to the heat pump for extracting heat from the surrounding surface water. For estimating the heat pump supply temperature T^t_{supply}, we assume the evaporator temperature is equal to the surrounding water temperature.

Heat pump model

The system COP of a heat pump does not solely depend on the temperature lift, but also on the compressor and circulation pump load ratio. However, the correlation only accounts for the temperature dependent performance changes. Unfortunately, NIBE has not published characteristics on the frequency/heat dependent system COP. Therefore, we leave this an open problem and assume that the COP is only dependent on the temperature lift ΔT^t and heat output Q^t_{HP}.

To further simplify the heat pump model, we neglect the compressor ramp rates and transient response characteristics at start up. Instead, the heat output Q^t_{HP} and electrical input $\hat{P}^t_{HP}$ reach there designated values instantaneously. In addition, we assume that the cyclic losses may be neglected. This assumption is motivated by the fact that the standby and start-up losses are relatively small: <70W [122].

To further simplify modelling, we also neglect the quasi steady state behaviour of the heat pump, as outlined in appendix A11.2.4 Hence, the heat output does not change as a function of the temperature at the inlet of the condenser. Also, we assume that the output temperature of the heat pump T^t_{out} is confined by some maximum output temperature T^{max}_{HP}.

Finally, the on/off cycle time of the heat pump is set to 20min, as discussed in appendix A11.2.5.

7.5.3 Heat pump control

Given these assumptions, the heat pump power is a function of the heat output and the temperature lift. For controlling the heat pump, the control logic will compare the heat requirements of both buffer tanks. For any t, heat is supplied to the buffer tank with the largest heat requirement. Using the COP, the electrical power consumption is given by equation (6.53).

$$\hat{P}^t_{HP} = \frac{Q^t_{HP1}}{COP^t_{GSHP}(\Delta T^t)} \text{ or } \frac{Q^t_{HP2}}{COP^t_{GSHP}(\Delta T^t)} \tag{6.53}$$

With $\hat{P}^t_{HP}$, the electrical input to the heat pump and $COP^t_{GSHP}(\Delta T^t)$ the temperature lift dependent COP as in equation (6.52).

7.6 Decision software: Temperature control

In this section we present the control logic for controlling the house temperature and buffer tank temperature. In section 7.6.1, we define the temper control design parameters. Subsequently, in section 7.6.2, we introduce the temperature control algorithms. Finally, in section 7.6.3, we a pseudo code of the entire temperature control algorithm.

7.6.1 Design parameters

In the previous sections, we have defined various design parameters for controlling temperatures and for controlling the heat pump. These have been summarised in Table 7.2. Note that the buffer tank volume has not yet been set. An appropriate buffer tank volume will be determined in chapter 9. The heat pump design parameters have been derived from specifications of a commercially available ground source heat pump: the NIBE F1255-PC.

Table 7.2: Parameters for temperature control and heat pump control

Characteristics	Variable	Value	Units	Source
House temperature setpoint	$\bar{T}^{setpoint}_{house}$	20°	[C]	Section 7.2.1
Max. temperature variation house	$\Delta\bar{T}^{dev}_{house}$	1°	[C]	Section 7.2.1
Minimum temperature tank S1	$\bar{T}^{min}_{S1}$	55°	[C]	Section 7.4.2
Maximum temperature tank S1	$\bar{T}^{max}_{S1}$	75°	[C]	Section 7.4.2
Minimum temperature tank S2	$\bar{T}^{min}_{S2}$	30°	[C]	Section 7.4.2
Maximum temperature tank S2	T^{max}_{S2}	$\bar{T}^{t}_{S1}$	[C]	Section 7.4.2
Maximum avg. temperature floor	$\bar{T}^{max}_{floor}$	29°	[C]	[114]
Maximum floor supply rate	$\phi^{t}_{V,maxheat}$	6	[L/min]	Section 7.4.2
Stratified buffer tank capacity	$V_{S1}+V_{S2}$	600	[L]	Chapter 5
Minimum heat pump output	Q^{min}_{HP}	1.5	[kW]	[122]
Maximum heat pump output	Q^{max}_{HP}	6	[kW]	[122]
Maximum supply temperature	T^{max}_{HP}	65°	[C]	[122]
Minimum on/off cycle time	$t^{min}_{hp,on/off}$	20	[min]	Appendix A11.2.5

7.6.2 Temperature control

Indoor temperature control

The setpoint for supplying heat to the house is given by equation (6.54). With $\overline{T}_{house}^{setpoint}$, the temperature setpoint of the house.

$$\text{if } \overline{T}_{house}^{t} - 0.5 \leq \overline{T}_{house}^{setpoint} \text{ then } Q_{heat}^{t} > 0 \tag{6.54}$$

The supply of heat from tank S2 to the underfloor heating system is confined by the maximum average floor temperature $\overline{T}_{fl,floor}^{max}$ as given by equation (6.55). This maximum is imposed to maintain a comfortable floor surface temperature [114].

$$\text{if } \overline{T}_{fl,floor}^{t} > \overline{T}_{fl,floor}^{max} \text{ then } Q_{heat}^{t} = 0 \tag{6.55}$$

Buffer tank temperature control

For controlling the temperature in the buffer tanks, we consider four control parameters: the set point for which heat is supplied by the heat pump to one of the buffer tanks $T_{S1,HP}^{setpoint}$ $T_{S2,HP}^{setpoint}$ and the set points for which heat is supplied by the electrical back up coils $T_{S1,coil}^{setpoint}$, $T_{S2,coil}^{setpoint}$.

The control logic for governing the supply of heat to the buffer tanks is given by equation (6.56) and equation (6.57). Note that for any timeslot t, the heat pump can only supply heat to one buffer tank. Therefore, the heat control logic will evaluate the magnitude of the heat demand. Informed by the control logic, the heat pump will supply heat to the buffer tank with the highest heat demand. This condition is given by equation (6.58).

$$\text{if } \begin{Bmatrix} \overline{T}_{S1}^{t} \leq T_{S1,HP}^{setpoint} & \text{then } Q_{HP1}^{t} > 0 \\ \overline{T}_{S1}^{t} \leq T_{S1,coil}^{setpoint} & \text{then } \hat{P}_{S1,coil}^{t} > 0 \end{Bmatrix} \tag{6.56}$$

$$\text{if } \begin{Bmatrix} \overline{T}_{S2}^{t} \leq T_{S2,HP}^{setpoint} & \text{then } Q_{HP2}^{t} > 0 \\ \overline{T}_{S2}^{t} \leq T_{S2,coil}^{setpoint} & \text{then } \hat{P}_{S2,coil}^{t} > 0 \end{Bmatrix} \tag{6.57}$$

$$\text{if } \begin{Bmatrix} Q_{HP1}^{t} < Q_{HP2}^{t} & \text{then } Q_{HP1}^{t} = 0 \\ Q_{HP1}^{t} \geq Q_{HP2}^{t} & \text{then } Q_{HP2}^{t} = 0 \end{Bmatrix} \tag{6.58}$$

Temperature constraints

The set points for supplying heat to the buffer tanks should be chosen such that the constraints in equation (6.59) and (6.60) are satisfied.

$$T_{S1}^{min} \leq \overline{T}_{S1}^{t} \leq T_{S1}^{max} \tag{6.59}$$

$$T_{S2}^{min} \leq \overline{T}_{S2}^{t} \leq T_{S2}^{max} \tag{6.60}$$

The constraint in equation (6.61) applies to the maximum flow rate of heat from buffer tank S2 to the underfloor heating system.

$$\phi_{V,heat}^{t} < \phi_{V,maxheat}^{t} \tag{6.61}$$

7.6.3 Pseudo code for temperature control algorithm

The house temperature is kept within range by evaluating the indoor temperature for every 15 minutes. Whenever the indoor temperature drops below the temperature setpoint, heat is supplied to the underfloor heating system. The tank temperatures are controlled in a similar fashion. The control logic prevents short cycling by inspecting the on/off mode for $\hat{P}_{HP}^{t-1}$ and $\hat{P}_{HP}^{t-2}$ If the heat pump has not yet ran for two timeslots (2x15 minutes), the heat pump cannot be turned off.

We present a simplified pseudo code in Table 7.3.

Table 7.3: Temperature control logic

Check temperature set points tank S1 and S2

1. If $\overline{T}_{S1/S2}^{t-1} < T_{S1/S2,HP}^{setpoint}$
2. Calculate Q_{HP1}^{t}, Q_{HP2}^{t}

Compare heat requirement

3. if $Q_{HP1}^{t} \geq Q_{HP2}^{t} : Q_{HP2}^{t} = 0$
4. if $Q_{HP2}^{t} > Q_{HP1}^{t} : Q_{HP1}^{t} = 0$

Check HP capacity range

5. If $Q_{HP1}^{t} / Q_{HP2}^{t} > 6000\text{W} : Q_{HP1}^{t} / Q_{HP2}^{t} = 6000\text{W}$
6. If $Q_{HP1}^{t} / Q_{HP2}^{t} < 1500\text{W} : Q_{HP1}^{t} / Q_{HP2}^{t} = 1500\text{W}$

Check set points of back up heaters

7. If $\overline{T}_{S1/S2}^{t} < T_{S1/S2,coil}^{Setpoint}$
8. Set $P_{S1,coil}^{t} = 1500\text{W}$ and/or $P_{S2,coil}^{t} = 1500\text{W}$

Determine heat pump and back-up power

9. Calculate $\hat{P}_{HP}^{t}$
10. Consider heat pump short cycling $\hat{P}_{HP}^{t-1}$, $\hat{P}_{HP}^{t-2}$

Determine the house temperatures

11. Calculate $\overline{T}_{fl,floor}^{t+1}$, $\overline{T}_{i,air}^{t+1}$, $\overline{T}_{e,enclosure}^{t+1}$ and $\overline{T}_{house}^{t+1}$

Check house temperature set point

12. If $\overline{T}_{house}^{t+1} - 0.5 < \overline{T}_{house}^{Setpoint}$
13. Calculate Q_{heat}^{t+1} and $\phi_{V,heat}^{t+1}$

Check heat transport limit and maximum floor temperature

14. If $\theta_{V,heat}^{t+1} > \theta_{V,maxheat}^{t} : \theta_{V,heat}^{t+1} = \theta_{V,maxheat}^{t}$
15. If $\overline{T}_{fl,floor}^{t} > \overline{T}_{fl,floor}^{max} : \theta_{V,heat}^{t+1} = 0$
16. $Q_{heat}^{t+1} = Q_{heat}^{t+1}(\theta_{V,heat}^{t+1})$

Determine $\overline{T}_{S1}^{t+1}$ and $\overline{T}_{S2}^{t+1}$

7.7 Decision software: Thermal flexibility control

In this section we present the control logic for controlling the thermal flexibility of the heat pumps and electrical coils. . In section 7.7.1, we define the flexibility parameters and constraints. In section 7.7.2, we introduce the flexibility control algorithms. In section 7.7.3, we present the settings for flexibility utilisation and finally in section 7.7.4, we present a pseudo code of the thermal flexibility control algorithm.

7.7.1 Flexibility parameters

For controlling the thermal flexibility, information on the following parameters is required:

1) The direction of the local MG imbalance: The direction of the local MG imbalance is defined as follows: Incase more energy is exported than reported in the E-programme, the direction of the MG imbalance is positive. Conversely, if more energy is imported than reported in the E-programme, the direction of the MG imbalance is negative.

2) Imbalance settlement price components: For controlling the thermal flexibility, information regarding the system imbalance is required. The three settings for utilising thermal flexibility have been listed on the next page. The system imbalance can be evaluated by considering the imbalance settlement prices. The imbalance settlement prices contain two price components: the ''Take-out'' and ''Feed-in'' price. The ''Take-out'' price applies to BRP's with a shortage: an imbalance with a negative direction. During settlement, the BRP pays TenneT the imbalance settlement price based on the ''Take-out'' price. If the ''take-out'' price is negative, TenneT pays the BRP. The ''Feed-in'' price applies to BRP's with a surplus: an imbalance with a positive direction. During settlement, Tennet pays a BRP the imbalance settlement price, based on the ''Feed-in'' price. If the ''feed-in'' price is negative, the BRP pays TenneT.

Microgrid imbalance

The microgrid imbalance is given by equation (6.62)

$$\hat{P}^{t}_{\text{imbalance,R}} = \hat{P}^{h}_{\text{Eprogramme,F}} + \hat{P}^{t}_{\text{Discharge,F}} + P^{t}_{\text{PV,R}} - \hat{P}^{t}_{\text{load,R}} - \hat{P}^{t}_{\text{Charge,F}} \text{ with } h = \left\lfloor \tfrac{t}{4} \right\rfloor \tag{6.62}$$

$$\hat{P}^{h}_{\text{Eprogramme,F}} = \hat{P}^{h}_{\text{Import,F}} - \hat{P}^{h}_{\text{Export,F}} \text{ for every } h \tag{6.63}$$

With, $\hat{P}^{h}_{\text{Eprogramme,F}}$ the scheduled energy imports and exports, $P^{t}_{\text{PV,R}}$ the real time PV production, $\hat{P}^{t}_{\text{load,R}}$ the real time electricity consumption, $\hat{P}^{t}_{\text{Charge,F}}$ the scheduled battery charging and $\hat{P}^{t}_{\text{Discharge,F}}$ the scheduled battery discharging. Note that the load $\hat{P}^{t}_{\text{load,R}}$ is a summation of three parameters given by equation (6.64)

$$\hat{P}^{t}_{\text{load,R}} = P^{t}_{\text{Electricity}} + \hat{P}^{t}_{\text{HP}} + \hat{P}^{t}_{\text{S1,coil}} + \hat{P}^{t}_{\text{S2,coil}} \text{ for every } t \tag{6.64}$$

With $P^{t}_{\text{Electricity}}$ the electricity by appliances and other devices. $\hat{P}^{t}_{\text{HP}}$ the adjustable electricity consumption of the heat pump and $\hat{P}^{t}_{\text{S1,coil}}, \hat{P}^{t}_{\text{S2,coil}}$ the adjustable electricity consumption of the electrical coils.

Net imbalance revenue

The net imbalance revenue are calculated using the microgrid imbalance $P^{t}_{imbalance,R}$ and the imbalance settlement prices components $p^{t}_{feed-in}$, $p^{t}_{take-in}$. Whether an imbalance is penalised or remunerated depends on the direction of the microgrid imbalance and the sign of the price components. The yearly imbalance cost, $\mathbb{C}^{year}_{imbalance}$ are calculated using equation (6.65), the yearly imbalance remuneration's, $\mathbb{R}^{year}_{imbalance}$ are calculated using equation (6.66).

$$\mathbb{C}^{year}_{imbalance} = \sum_{day=1:365} \left[\sum_{t=1:96} \underbrace{P^{t}_{imbalance,R} \cdot \tfrac{1}{4}\delta q \cdot p^{t}_{feed-in}}_{P^{t}_{imbalance,R}>0 \text{ and } p^{t}_{feed-in}<0} + \underbrace{P^{t}_{imbalance,R} \cdot \tfrac{1}{4}\delta q \cdot p^{t}_{take-in}}_{P^{t}_{imbalance,R}<0 \text{ and } p^{t}_{take-in}>0} \right] \tag{6.65}$$

$$\mathbb{R}^{year}_{imbalance} = \sum_{day=1:365} \left[\sum_{t=1:96} \underbrace{P^{t}_{imbalance,R} \cdot \tfrac{1}{4}\delta q \cdot p^{t}_{feed-in}}_{P^{t}_{imbalance,R}>0 \text{ and } p^{t}_{feed-in}>0} + \underbrace{P^{t}_{imbalance,R} \cdot \tfrac{1}{4}\delta q \cdot p^{t}_{take-in}}_{P^{t}_{imbalance,R}<0 \text{ and } p^{t}_{take-in}<0} \right] \tag{6.66}$$

The net imbalance revenue is calculated using equation (6.67).

$$\mathbb{R}^{year}_{net,imbalance} = \mathbb{R}^{year}_{imbalance} - \mathbb{C}^{year}_{imbalance} \tag{6.67}$$

7.7.2 Flexibility control

Heat pump control

Additional set points for controlling the thermal flexibility of the heat pumps are required. To that end we define three additional parameters:

- The minimum HP flexibility set point for tank S1. $T^{flex,setpoint}_{S1,HP,min}$
- The minimum HP flexibility set point for tank S2. $T^{flex,setpoint}_{S2,HP}$
- The maximum flexibility set point for tank S2 $T^{flex,setpoint}_{S2,max} = \bar{T}^{t}_{S1} - \Delta T_{S1-S2}$

The rules for controlling the heat pump flexibility are given by equation (6.68).

$$\text{if} \begin{cases} \bar{T}^{t}_{S1} \geq T^{flex,setpoint}_{S1,HP,min} & \text{then } Q^{t}_{HP1} \text{ may be reduced} \\ \bar{T}^{t}_{S1} \leq T^{max}_{HP} & \text{then } Q^{t}_{HP1} \text{ may be increased} \\ \bar{T}^{t}_{S2} \geq T^{flex,setpoint}_{S2,HP,min} & \text{then } Q^{t}_{HP2} \text{ may be reduced} \\ \bar{T}^{t}_{S2} \leq \bar{T}^{t}_{S1} - \Delta T_{S1-S2} & \text{then } Q^{t}_{HP2} \text{ may be increased} \end{cases} \tag{6.68}$$

Electrical coil control

For controlling the thermal flexibility of the electrical coils, we use the same set points as for the temperature control: $T^{setpoint}_{S1,coil}$, $T^{setpoint}_{S2,coil}$. Given these set points, the rules for controlling the thermal flexibility of the electrical coils are given by equation (6.69).

$$\text{if} \begin{cases} \bar{T}^{t}_{S1} \geq T^{setpoint}_{S1,coil} & \text{then } P^{t}_{S1,coil} \text{ may be reduced} \\ \bar{T}^{t}_{S1} < T^{max}_{S1} & \text{then } P^{t}_{S1,coil} \text{ may be increased} \\ \bar{T}^{t}_{S2} \geq T^{setpoint}_{S2,coil} & \text{then } P^{t}_{S2,coil} \text{ may be reduced} \\ \bar{T}^{t}_{S1} < \bar{T}^{t}_{S1} - \Delta T_{S1-S2} & \text{then } P^{t}_{S2,coil} \text{ may be increased} \end{cases} \tag{6.69}$$

Interconnection capacity constraint

In any case, the total peak demand should not exceed the interconnection capacity when performing passive balancing. This condition is given by equation (6.70).

$$\text{for any } t: P_{inter} < P_{inter}^{max} \tag{6.70}$$

With P_{inter} the active power that is transported over the interconnection line and P_{inter}^{max} the maximum interconnection capacity. To evaluate P_{inter} we use equation (6.71).

$$P_{inter}^{t} = \text{Abs}(\hat{P}_{export,F}^{h} - \hat{P}_{import,F}^{h} + \hat{P}_{imbalance,R}^{t}) \tag{6.71}$$

7.7.3 Settings for utilisation of thermal flexibility

Four flexibility settings have been defined in chapter 4. The four settings are as follows:

0. **No peak shaving or passive balancing**
1. **Peak shaving only**: Thermal flexibility is utilised for peak shaving in case the average power demand exceeds the interconnection capacity. No passive balancing is applied.
2. **Passive balancing in one direction:** Thermal flexibility is utilised to reduce local imbalances that yield imbalance cost. Thereby, the imbalance settlement prices serve as reference. Local imbalances that yield revenue are maintained.
3. **Passive balancing in two directions:** Here, thermal flexibility is utilised to reduce local imbalances that yield imbalance cost. Unlike setting 2, thermal flexibility is also utilised to increase local imbalances, yielding more revenue.
4. **Reduce all imbalances:** For this setting, all imbalances are reduced, regardless of the imbalance settlement prices.

7.7.4 Pseudo code for thermal flexibility

A pseudo code for utilising thermal flexibility is presented in Table 7.4. Here, the control steps and criteria are listed from (1-13). For settings 2 and 3, the following criteria are evaluated.

- Setting 2: Only criteria (2) and (3).
- Setting 3: Criteria (2) and (3) and criteria (4) and (5).

Table 7.4: Thermal flexibility control logic

For every t

Calculate $\hat{P}^{t}_{imbalance}$

Check imbalance and price.

1. $\text{Cost if } \hat{P}^{t}_{imbalance} > 0 \text{ and } \text{Feed}-\text{in}^{t} < 0$
2. $\text{Cost if } \hat{P}^{t}_{imbalance} < 0 \text{ and } \text{Take}-\text{out}^{t} > 0$
3. $\text{Revenue if } \hat{P}^{t}_{imbalance} > 0 \text{ and } \text{Feed}-\text{in}^{t} > 0$
4. $\text{Revenue if } \hat{P}^{t}_{imbalance} < 0 \text{ and } \text{Take}-\text{out}^{t} < 0$

Dissolve/increase imbalance using heat pump

5. Consider peak shaving constraint
6. Consider temperature set points
7. Consider HP capacity and capacity range
8. Consider heat pump short cycling $\hat{P}^{t-1}_{HP}$, $\hat{P}^{t-2}_{HP}$
9. Reduce or increase $\hat{P}^{t}_{HP}$

Dissolve/increase imbalance using backup coils

10. Consider peak shaving constraint
11. Consider temperature set points
12. Consider backup heater capacity
13. Reduce or increase $\hat{P}^{t}_{S1back-up}, \hat{P}^{t}_{S2back-up}$

Recalculate Imbalance based on new $\hat{P}^{t}_{HP}, \hat{P}^{t}_{backup}$

Calculate imbalance cost & profit

Chapter 8

PV and load forecasts

In this chapter, we present the methods for producing forecasts on various energy flows. In section 8.1, we define several requirements for each forecasts. In section 8.2, we present the method for producing forecasts on thermal based electricity demand profiles. Subsequently, in section 8.3, we present the method for producing forecasts on non-thermal based electricity demand profiles. Finally, in section 8.4, we present a method to produce forecasts on solar irradiance, PV production and solar thermal production.

8.1 Forecast methodology

As discussed in chapter 4, imbalances result from prediction errors about future energy flows, in the day-ahead portfolio optimization phase. These imbalances are managed in real time in the passive balancing and peak shaving phase.

8.1.1 Characteristics and requirements

In the day-ahead market, energy is scheduled in hourly blocks for all 24 hours of the next day. In the imbalance market, imbalances are settled per PTU (15 minutes). Hence, each forecast should have a time horizon of 24 hours, with a 15 minute resolution. In addition, we demand that the forecasts should have a similar degree of accuracy, as would be encountered in practise. Lastly, it is required that data from forecasted time series are representative for the area of Schoonschip, Amsterdam.

8.1.2 Thermal and non-thermal related electricity consumption

The electricity load consists of two components: The *thermal based electricity consumption* and the *non-thermal based electricity consumption*. The former relates to the electricity consumption by the heat pumps and back up heaters. The latter is related to all other electrical devices, such as household related applications. Note that the energy consumption by the heat pumps and back up heaters is calculated using the thermal model. Different forecasts tools are used to produce forecasts on all energy flows. The method for producing forecasts on *non-thermal based electricity consumption* is treated in section 8.3.1, the method for producing forecasts on *thermal based electricity consumption* is discussed in section 8.3.2. The method for producing forecasts on PV production, solar thermal production and solar irradiance is treated separately in section 8.4.

8.1.3 Day-ahead forecast error

A measure for estimating the error between a forecast and its actual value is the coefficient of variance. The coefficient of variance (CV) describes the ratio of the prediction error standard deviation to the signal mean. The CV estimates the difference between two time series, X^{t} and its forecast $\tilde{\mathrm{X}}^{\mathrm{t}}$ for $\mathrm{t} = \{1,..\mathrm{T}\}$ as follows:

$$\mathrm{CV}(\mathrm{x},\tilde{\mathrm{x}}) = 100\frac{\sqrt{\frac{1}{\mathrm{T}}(\mathrm{x}^{\mathrm{t}} - (\tilde{\mathrm{x}}^{\mathrm{t}}))^2}}{\frac{1}{\mathrm{T}}\sum_{\mathrm{t}=1}^{\mathrm{T}}\mathrm{x}^{\mathrm{t}}}\% \tag{8.1}$$

8.2 Forecasts: Non-thermal based electricity consumption

8.2.1 Approach

In [123], three methods for producing day ahead energy demand forecasts have been evaluated. The following methods have been examined: *Autoregressive Integrated Moving Average (ARIMA)*, exponential smoothing state space and feed-forward neural networks. In addition, a persistence forecast based on extrapolations of historic data, served as reference. Given the various methods and levels of aggregation, the MAPE varies between 61-119% and 23-49%, for respectively 1 and 6 households. The authors conclude that: *''without further refinement of advanced methods such as ARIMA and neural networks, the persistence forecasts are hard to beat in most situations''*. This finding is supported by [124]. Here, the accuracy of two forecasting tool has been examined for various levels of aggregation. The study found that the advanced tool (Holt winters) only performs slightly better in terms of accuracy, than the simple tool based on historic averages. Given an aggregated load profile of 46 households, the forecasting accuracy is approximately 10% (MAPE), when using the simple method [124].

8.2.2 Conclusions

Based on [2] and [3], we conclude that extrapolations of historic data yields good results in terms of accuracy. Hence, forecasts on non-thermal based electricity consumption profiles can be calculated as follows: The total energy consumption for every PTU of the day is based on a historical average of identical PTUs and similar days of the week. As input, the aggregated non-thermal based electricity consumption profile of the Schoonschip community is used. Given this method it follows that the highest accuracy is obtained for an average of 5 days, as seen in Table 8.1.

Table 8.1: Forecast error for non- thermal based electricity demand

Number of days for average	CV [%]
[no]	[T=31000]
2	33,2
3	17,6
4	17,4
5	17,3
6	17,4

8.3 Forecasts: Thermal-based electricity consumption

8.3.1 Thermal based electricity demand

The thermal based electricity consumption is dependent on 5 exogenous parameters: air temperature, water temperature, water duct temperature, solar irradiance (also used by the thermal model for producing forecasts on the solar thermal production) and DHW demand. As discussed in chapter 4, we have assumed a forecast to be perfect on water ducts temperatures and DHW demand. Hence, we require a method to produce forecasted profiles on water temperatures, air temperatures and solar irradiance.

8.3.2 Forecasting water temperatures

The temperature of water only changes gradually. This the result of the large thermal capacity of the water. Therefore, the water temperature for some day is approximately equal to the temperature of the previous day. As seen in Table 8.2, the forecast accuracy is extremely high when extrapolating historic data. Thus, we conclude that water temperatures for the next day can be predicted using the temperatures of the current day. The source of the time series data on water temperatures, in the surroundings of Schoonschip, is presented in chapter 5.

8.3.3 Forecasting air temperatures

For estimating future air temperatures, historic averages do not result in accurate predictions. As seen in table 6.2, the CV for any historic average is approximately 30%. Clearly, another method is required. Therefore, we turn our attention to weather forecasts by third parties. According to [125], weather forecast technology by the European centre for Medium Range Weather Forecasts (ECMWF) has advanced spectacularly over the past decade. As stated in the latest report by ECMWF, [126]: *''Averaging over the European and North African region, we find daily maximum/minimum temperatures in summer/winter all to be too low by 0.5^{o} K, except for the summer daily minimum which is too high by 0.5^{o} K; these biases have been consistent in operations for the last five years."* Now, the Royal Netherlands Meteorological Institute (KNMI) uses ECMWF results to produce forecasts on local conditions throughout the Netherlands. To that end, the KNMI uses an additional system: the ensemble prediction system (EPS). This system has a resolution of 18 km and produces forecasts for every hour of the day. According to [125], the maximum prediction error, with a 90% confidence index, is approximately 0.5^{o} C for the next day.

8.3.4 Conclusion on air temperature forecasts

We conclude that air temperature forecasts by the EPS system of KNMI are significantly accurate and could be used to produce forecasts for Schoonschip. As no time series on air temperature forecasts are available, the forecast error needs to be modelled. To that end, we produce forecasts by multiplying the air temperature data series (from IWEC, see chapter 5) with a white Gaussian noise, having zero mean and 0.5 variance. Given the small error and 15 minute resolution, it is reasonable to have an uncorrelated noise series. This assumption can be justified by the fact that the local air temperature is continuously influenced by local conditions such as the solar irradiance and local convective schemes.

8.3.5 Matlab implementation of white Gaussian noise

The Gaussian noise error is implemented in Matlab using the ''*awgn*'' function. The signal-to-noise ratio is set to 6 dB. This yields a noise variance of approximately 0.5^{o} C. Given this noise, the coefficient of variance (CV) is equal to approximately 5%.

Table 8.2: Forecast error for air and water temperatures, based on historic averages

	Number of days used for average	CV [%]
		T=31000
Water Temperature forecast	1	0,8
Air temperature forecast	1	30,4
	2	30,6
	3	31,8

8.4 Forecasts: Solar irradiance

8.4.1 Forecast tools

In Schoonschip, two systems will be used to produce forecasts on the PV production. PVCast [127], developed by Fraunhofer, and Icarus [128], developed by Alliander. Unfortunately, no representative time series data is available. Thus, an alternative is required. To that end, we adopt two datasets from Belgium TSO, ELIA [129]. The two datasets by ELIA, contain day-ahead forecasts and realisations on PV production, having a resolution of 15 minutes. The profiles are based on an aggregated PV fleet with a total peak capacity of 48MW. The fleet is located in the area of Brussels. Datasets are available for multiple years. The year of 2016 was selected. It follows that the coefficient of variance (CV) for T=31040 equals 40%.

8.4.2 Producing forecasts: Relative error

The profiles by ELIA cannot be used directly to produce forecasts on the conditions for Schoonschip. Instead, we consider the relative error per quarterly timeslot t, between the forecasted values and realisations in the ELIA datasets. The relative error is used as reference for producing forecasts on the PV production, solar thermal production and solar irradiance. To that end, the relative error for every quarterly timestep *t*, is multiplied with the actual value (for the same t) of solar irradiance, PV production and solar thermal production. The sources and methods for producing the real time data series on PV production, solar thermal production and solar irradiance is treated in chapter 5.2.

Chapter 9

Experiments and results

In this chapter, we analyse the value of flexibility that can be generated with the community microgrid of Schoonschip. We perform experiments and analysis on day-ahead portfolio optimizations with respect to day-ahead market prices (RQ1), Time Of use optimizations with respect to a dual electricity tariff (RQ3) and passive balancing/peak shaving with respect to imbalance settlement prices (RQ2). In addition, we have quantified the percentage of solar-self consumption, along with several other non-financial performance indicators. Finally, we also validate the thermodynamic simulation models.

In section 9.1, present the experimental set-up and describe the models, simulation model and experiments. In section 9.2, we present the results and analysis of the day-ahead portfolio optimization. Subsequently, in section 9.3, we present the results and analysis on Time of Use optimizations with respect to a dual electricity tariff by an energy retailer. Thereby, we provide a comparison between the cost and benefits of day-ahead market participation and a traditional energy retail contract. Next, in section 9.4, we present the cost and benefits associated with passive balancing and peak shaving. In section 9.5, we present a sensitivity analysis to identify appropriate variable settings for buffer tank temperature control and minimum tank capacity. In section 9.6, we present a validation of the thermal simulation model. Finally, in section 9.7, we present a summary of the results.

9.1 Experimental set-up

9.1.1 System models

Several models and decision software has been devised to quantify the value of flexibility. In addition, data has been gathered as input for the simulation model.

- In chapter 5, we have presented the construction of datasets and outlined the characteristics of the Schoonschip community microgrid.
- In chapter 6 and 7, we have presented a battery model and various thermal models for simulating the heat demand and heat supply of the Schoonschip community microgrid.
- In chapter 6, 7 and 8, we have also presented decision software. In chapter 6, we have presented decision software for performing day-ahead portfolio optimizations. In chapter 7 we have presented decision software for temperature and flexibility control. And, in chapter 8, we have defined forecasts on various energy flows that serve as input for the decision software.

The exchange of information between the simulation models (green) and decision software (yellow) is shown schematically in Figure 9.1. The input data and input variables (grey) are supplied to the decision software. The output of the forecast tools is fed directly to the day-ahead optimization and indirectly via the thermal models. The day-ahead optimization is used for portfolio optimizations using the battery model. The output of the thermal models and day-ahead optimizations serve as input to the flexibility control unit. The flexibility control unit is used for real time passive balancing and peak shaving process. Output data (red) is gathered from the day-ahead optimization, the thermal models, the temperature control and flexibility control. For each component, the chapter number is designated in red.

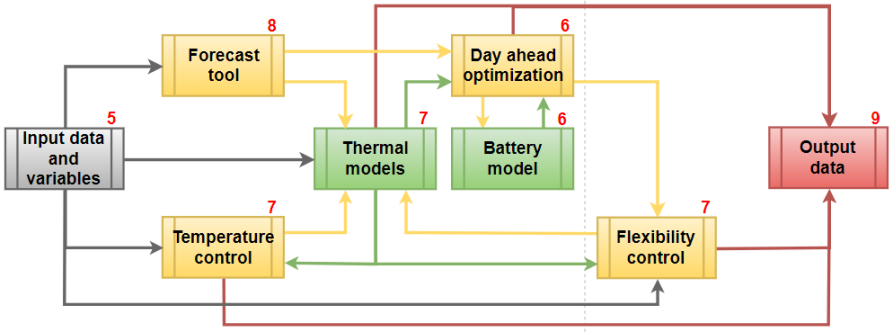

Figure 9.1: Input and output data, input variables, decision software and simulation models

9.1.2 Simulation model

Software environment

For performing experiments, the models are implemented in Matlab R2016a.

The day-ahead portfolio optimization problem is implemented in Matlab using the heuristic solver *''intlinprog''.* The solutions are validated using an exact approach. To that end, the Matlab solver *''linprog''* is used. The optimization algorithm is set to dual-simplex. As the linprog problem solver for linear programming problems does not include heuristics, the mixed integer linear programming solver intlinprog is used instead. To be able to use 'intlinprog', one integer decision variable is included. Obviously, this decision variable is not part of the objective function and does not influence the results.

Parameterisation

The mathematical models have been parametrised based on the characteristics of the Schoonschip community microgrid and its distributed energy resources. These include the battery systems, heat pumps, buffer tanks, solar panels, thermal collectors and electrical coils. The characteristics of the resources are presented in chapter 5.

Sensitivity analysis is used to identify suitable temperature set points. The sensitivity analysis yields suitable set-points, by evaluating for which values the minimum buffer tank temperatures are not violated. The operational constraints and design parameters are presented in chapter 7, section 7.5. In addition, we perform a sensitivity analyses on the buffer tank capacity, in which we quantify violation of minimum tank temperatures. The sensitivity analyses is presented in full in section 9.5.

Simulation model experiments

To answer the research questions, we conduct 365 consecutive day experiments, which accumulate into one year. As input to the experiments, we use the data collections as presented in chapter 5. The intermediate results of each experiment serve as input for the next experiment. For initialising the first experiment, the battery state of charge is set to zero. The average temperatures in buffer tank S1 and S2 are set to respectively 60^{o} C and 46^{o}C. The average house temperature is set to 20^{o}C.

Simulation model validation

The performance of the simulation model is validated using the EPC report of Schoonschip lot 5 and estimates by an energy retailer on electricity consumption and production by the Schoonschip community microgrid. The simulation model validation is presented in section 9.6.

9.2 Results RQ1: Day-ahead portfolio optimizations

In this section we present the experiments and results of the day-ahead portfolio optimizations with respect to day-ahead market prices. In section 9.2.1, we present the input variables, in section 9.2.2 we present the output/measurements variables. Next we the describe the experiments that have been performed in section 9.2.3. Finally, in section 9.2.4, we present the experiments and results.

9.2.1 Input variables

The day-ahead portfolio optimization is influenced by altering the following input variables:

- The cyclic battery degradation price: p_{Bat}^{deg}
- The import fine: p_{fine}
- The interconnection capacity: P_{inter}^{max}
- The day ahead market prices: p_{DA}^{h}
- The effective battery capacity: E_{SOC}^{max}

9.2.2 Output/measurement variables

The control over the independent variables affects the outcome of the day-ahead portfolio optimization. This effect is measured using the following output variables. The formulas for calculating these variables are given in appendix B11.1.

- The net electricity cost per year: $\mathbb{C}_{net,electricity}^{year}$
- The number of full equivalent battery cycles per year: $N_{bat-cycles}^{year}$
- The forecasted percentage of solar self-consumption per year: SSC_{F}^{year}

The net electricity cost is based on the marginal day-ahead market prices only and does not include taxes or other price components.

One full equivalent cycle is defined as the equivalent of discharging a full battery to its minimum state of charge. For example: two discharge activities, each at 50% depth of discharge, are considered one full equivalent cycle.

We use subscript *'F'* to indicate that the solar self-consumption percentage is based on forecasted values. Here, we must note that this percentage is not an actual value, but merely an indicator. Since the schedules on battery operations and energy imports/exports from the day-ahead optimizations are based on imperfect forecasts, the realised percentage of solar self-consumption is likely to be different. In section 9.4, we use the forecasted percentage to quantify the difference between the actual percentage and forecasted percentage.

9.2.3 Five experiments

The following experiments have been carried out with respect to day-ahead portfolio optimizations.

1. Comparing the accuracy of an exact and heuristic solver.
2. The outcome for different import fines.
3. The outcome when adjusting the value that is assigned to the export of energy.
4. The outcome for different day-ahead market prices.

The first experiment is used to compare the results of the heuristic solver with that of the exact solver. In the other experiments, we identify to what extent the solar-self consumption can be optimise. In addition, we evaluate the trade-off between minimising electricity cost and maximising for solar self-consumption. Finally, we quantify the effect of different years with different day-ahead market prices.

9.2.4 Results: Day-ahead portfolio optimizations

The effect of using a heuristic or exact solver

We investigate the use of an exact and heuristic solver for finding feasible solutions to the day-ahead portfolio optimization problems. For evaluation, the cyclic battery degradation price, p_{Bat}^{deg} is set to 0 €/kWh. The interconnection capacity P_{inter}^{max} is set to 136 kW. The import fine p_{fine} is set to 0.05€/kWh. The day-ahead market prices, p_{DA}^{h} of 2015 are used. The results are presented in Table 9.1.

Table 9.1: Heuristic versus exact solver

Input and output variables		Heuristics	Exact (Dual-simplex)
SSC [%/y]	SSC_F^{year}	28.9	28.9
Net cost [€/y]	$\mathbb{C}_{net,electricity}^{year}$	€ 4.142	€ 4.144
Computational time for 365 experiments [s]	-	20	285

Via inspection of the net cost and solar self-consumption percentage in Table 9.1, it is found that both solvers yield (almost) identical results. However, the computational burden differs significantly.

Main observations

- Given almost identical results, together with the tenfold faster computational time of the heuristic solvers, we conclude that the heuristic solver is sufficiently accurate.
- Further analysis on the portfolio optimization problem is carried out using the heuristic solver.

The effect of varying the import fine on self-consumption, net electricity cost and battery cycles

The effect of imposing various import fines, p_{fine} is examined. For evaluation, the cyclic battery degradation price, p_{Bat}^{deg} is set to 0 €/kWh. The interconnection capacity, P_{inter}^{max} is set to 136 kW. The day-ahead market prices, p_{DA}^{h} of 2015 are used. The results are presented in Table 9.2. To evaluate the achieve solar self-consumption, we introduce two benchmarks. The expressions are presented in appendix B11.1.

- The maximum direct and indirect solar self-consumption percentage per year: SSC_{max}^{year}
- The gross solar self-consumption percentage per year: SSC_{gross}^{year}

The *maximum direct and indirect solar self-consumption percentage* quantifies how much solar energy can be used for direct and indirect solar self-consumption, using the Schoonschip battery systems. The *gross solar self-consumption percentage* quantifies which portion of the annual electricity demand could be covered by the annual PV production in Schoonschip.

Table 9.2: The effect of varying the import fine

Import fine [€/kWh]	SSC Gross [%/y]	SSC Maximum [%/y]	SSC Forecast [%/y]	Net cost [€/y]	Full equivalent cycles [no/y]	Simultaneous Imports/exports [no/y]
p_{fine}	SSC_{Gross}^{year}	SSC_{Max}^{year}	SSC_{F}^{year}	$\mathbb{C}_{net,electricity}^{year}$	$N_{bat-cycles}^{year}$	$N_{import/export}^{year}$
0	42.9	36	-	-	-	5275
0.0001			13.9	-€ 190	1550	0
0.01			14.8	€ 500	1140	0
0.03			22.2	€ 3.450	670	0
0.04			27.2	€ 4.000	620	0
0.05			28.9	€ 4.150	607	0
1.0			29.3	€ 5.550	267	0
100.0			29.3	€ 5.900	244	0

Via inspection of Table 9.2, it is found that the import fine significantly affects the outcome of the day-ahead portfolio optimization. It is also found the import fine should be non-zero to prevent simultaneous scheduling of energy imports and exports by the optimization algorithm.

Via inspection of Table 9.2, it is found that import fines of more than 0.05€/kWh result in a maximisation of the forecasted solar self-consumption and minimum full equivalent cycles. However, a larger import fine also results in a higher net electricity cost. The differences between a fine of 1€/kWh and 100€/kWh, suggest that there exists a trade-off between limiting the number of full equivalent cycles and limiting the net electricity cost. Finally, we observe that the forecasted solar self-consumption (29.3%) is not truly maximised (36%). Further analysis is carried out to explain this phenomenon.

Via inspection of Table 9.2, it is found that, given a small import fine, the batteries are primarily used to trade energy in the day-ahead market. In fact, the battery is rarely used to enable solar self-consumption, when assigning a fine of 0.0001€/kWh. This is indicated by the difference between the forecasted percentage of direct solar self-consumption (12.6%) and the total forecasted solar self- consumption percentage (13.9%). When compared to an import fine of 100€/kWh, an import fine of 0.0001€/kWh yields significantly less electricity cost at the expense of significantly more full equivalent cycles.

Main observations

- Day-ahead portfolio optimizations that are geared towards a minimization of net electricity cost results in substantial battery cycling.
- Given the current optimization approach, the forecasted solar self-consumption cannot be maximised.

The effect of excluding exports benefits on the forecasted solar self-consumption and net cost

The previous analysis reveals that the forecasted solar self-consumption is not fully maximised. This implies that the export of energy is not fully minimised. Given the objective function and the goal to minimise cost, we note that the export of energy contributes to a reduction of the cost. Thus, to decrease the value of exporting energy, less weight should be assigned to the benefits of exporting energy, given by $p^{h}_{DA} \cdot \hat{P}^{h}_{export}$. To that end, we propose to implement a factor alpha, α in the objective function. The factor alpha can be seen as an instrument to adjust the value that is assigned to the export of energy, for example to account for taxation losses.

The new objective function is presented in equation (9.1)

$$\min_{h\in\{0,..,23\}} = \sum_{h=0}^{23}\left[(p^{h}_{DA} + p_{fine}) \cdot \hat{P}^{h}_{import} - \alpha \cdot p^{h}_{DA} \cdot \hat{P}^{h}_{export} + \sum_{t=4h}^{4h+3}\left[p^{deg}_{Bat} \cdot \hat{P}^{t}_{discharge} + p_{slack} \cdot \hat{P}^{t}_{slack}\right]\right] \quad (9.1)$$

For evaluation, the day-ahead market prices, p^{h}_{DA} of 2015 are used. The cyclic battery degradation price, p^{deg}_{Bat} is set to 0 €/kWh. The import fine, p_{fine} is set to 0.0€/kWh. The interconnection capacity, P^{max}_{inter} is set to 136kW.. The factor alpha α ,is varied between 1 and 0. The results are presented in Table 9.3

Table 9.3: The effect of assigning less value to the export of energy

Alpha	SSC maximum [%/y]	SSC Forecast [%/y]	Net Cost [€/y]	Full equivalent cycles [no/y]
α	SSC^{year}_{Max}	SSC^{year}_{F}	$\mathbb{C}^{year}_{net,electricity}$	$N^{year}_{bat-cycles}$
1	36	29.3	€ 5.550	267
0.75		29.3	€ 5.550	267
0.25		29.3	€ 5.550	267
0		35.9	€ 5.900	255

Via inspection of Table 9.3, it is found that the forecasted percentage of solar self-consumption can only be maximised for alpha is zero. Effectively, this means that the benefits of exporting energy are excluded from the objective function. As a result, less energy is exported to the grid by discharging the battery, which yields a higher forecasted percentage of solar self-consumption.

Via inspection of Table 9.3, it follows that the minimisation of electricity cost is always favoured over self-consumption. This is indicated by the observation that an alpha of 0.75 or 0.25 does not yield a higher forecasted percentage of solar self-consumption. Thus, for any alpha larger than zero, the export of energy is considered (by the optimization algorithm) a means to reduce the overall cost. From this analysis, it follows that a different optimization approach is needed to establish a trade-off between achieving cost reductions and maximising the forecasted percentage of solar self-consumption. For example by including a strike price for energy exports.

Main Observations

- The forecasted percentage of solar self-consumption can only be maximised if the benefits of exporting energy are excluded from the objective function.
- A different optimization approach is needed to impose a trade-off between the maximisation of the forecasted solar self-consumption and reduction of net electricity cost.

The effect of varying the day-ahead market prices on the net cost

The effect of day-ahead market prices for different years is evaluated. To that end, the day-ahead market prices of 2015 and 2016 are used. The battery degradation cost is set to 0 €/kWh. The import fine is set to 1€/kWh and 0.01€/kWh. Alpha α is set to 1. The interconnection is set to 136kW. The results are shown in Table 9.4.

Table 9.4: The effect of varying the day-ahead market prices

Day-ahead market prices [year]	Import fine [€/kWh]	Net Cost [€/y]	SSC [%/y]	Full equivalent cycles [no/y]
p_{DA}^{h}	p_{fine}	$C_{net,electricity}^{year}$	SSC_{F}^{year}	$N_{bat-cycles}^{year}$
2015	1	€ 5.550	29.3	267
2016	1	€ 4.200	29.4	278
2015	0.01	€ 500	14.8	1440
2016	0.01	-€ 450	15	1080

Via inspection of Table 9.4, it is found that the net electricity cost between 2015 and 2016 vary by more than €1200,-. In addition, we note that the number of full equivalent cycles is approximately equal for both 2015 and 2016. However, in case the optimization is primarily geared towards cost reductions (small import fine), the number of full equivalent cycles is substantially larger for 2015 than for 2016.

Main Observations

- The experiments suggest that the number of full equivalent battery cycles per year can vary substantially when optimizing for a minimisation of net electricity cost.
- Based on our simulation model, and depending on the day-ahead market prices, the net electricity cost can vary by at least 30% per year.

9.3 Results RQ3: Time of use optimizations

9.3.1 Input variables

For performing Time of use (ToU) optimizations with respect to a dual electricity tariff, we assign the following values, depending on the time of the day:

- 23:00-07:00: 0.0318€/kWh Prices for both import and export
- 07:00-23:00: 0.0435€/kWh Prices for both import and export

9.3.2 Results: Traditional energy retail contract

The ToU optimizations is executed using the day-ahead portfolio optimization formulation. To that end, the day-ahead market prices have been replaced with the dual electricity tariff. For the optimisation process, the import fine is set to 1€/kWh and alpha, α is set to 0. The results are presented in Table 9.5 and Table 9.6. For comparison, we also present the cost and benefits associated with day-ahead market prices of 2015 and 2016. In addition, we evaluate the net electricity cost when only optimizing for solar-self consumption. To that end, we adopt the strategy for maximising the solar self-consumption as discussed in chapter 6.2. Finally, we also evaluate the net electricity when excluding batteries all together.

Table 9.5: Time of use optimizations v.s. day-ahead portfolio optimization

		Dual tariff	Day-ahead prices 2015 /2016
'Alpha' [-]	α	0	0
Net cost [€/y]	$\mathbb{C}^{year}_{net,electricity}$	€ 5.200	€ 5.900 / € 4.600
SSC [%/y]	SSC_F^{year}	35.8	35.9
Full equivalent cycles [no/y]	$N^{year}_{bat-cycles}$	237	255 / 262

Table 9.6: Net electricity cost for dual tariff with different optimization goals

	Net cost [€/y]
ToU optimization for self-consumption and minimal net cost	€ 5.200
Optimization for self-consumption only	€7.100
No optimization for self-consumption (no batteries)	€8.750

Based on
Table 9.5, we observe that the net cost of a traditional energy contract may be 11% higher (2016) or 11% lower (2015), when compared to day-ahead portfolio optimizations with respect to day-ahead market prices . Thus, it is found that the traditional energy retail contract may be financially more attractive, because the net electricity cost are lower when compared to day-ahead market participation in 2015. In addition, the number of full equivalent cycles is smaller for a traditional retail contract.

By inspection of Table 9.6, it is clear that Time Of Use (ToU) optimizations with respect to dual electricity tariffs can reduce net electricity cost by €1.900,- . When optimizing with respect to day-ahead market prices, there is a possibility to reduce net cost by €1.200,- for 2015 and €2.500 for 2016.

Main Observations

- Depending on the day-ahead market prices, the net electricity cost associated with direct market access may be higher than the net electricity cost associated with a dual electricity tariff by an energy retailer.
- Given a dual electricity tariff, significant cost reductions can already be realised by performing Time Of use optimizations for solar self-consumption and minimization of net electricity cost.

9.4 Results RQ2: Passive balancing and peak shaving

In this section we present the results of passive balancing and peak shaving. In section 9.4.1 we present the input variables. In section 9.4.2 we touch upon the various flexibility settings that have been defined in chapter 4.3. Next, in section 9.4.3. we define the output variables and subsequently we describe the experiments that have been performed. Finally in section 9.5.4 we present our experiments and results.

9.4.1 Input variables

Temperature control variables

The temperature set points for controlling the temperature in the buffer tanks are derived from the sensitivity analysis in section 9.5.

- $T_{S1,HP}^{setpoint}$, $T_{S2,HP}^{setpoint}$ 65° and 46° Celsius
- $T_{S1,coil}^{setpoint}$, $T_{S2,coil}^{setpoint}$ 60° and 34° Celsius

Flexibility control variables

For controlling the thermal flexibility, the minimum flexibility set points of the heat pump and electrical coils are set as listed below. Note that the heat pump flexibility set points are lower than the HP set points for temperature control of the buffer tanks. This is done to free up more thermal flexibility.

- $T_{S1,HP,min}^{flex,setpoint}$, $T_{S1,coil,min}^{flex,setpoint}$: 63° and 60° Celsius
- $T_{S2,HP,min}^{flex,setpoint}$, $T_{S2,coil,min}^{flex,setpoint}$ 34° and 34° Celsius

Furthermore, we also define maximum flexibility set points. For tank S1, the maximum temperatures are governed by the maximum supply temperature of the heat pump and the maximum temperature of the buffer tank, respectively. For tank S2, the temperature of tank S2 should not exceed that of tank S1. The maximum set point applies to both the heat pump and electrical coil.

- $T_{S1,HP,max}^{flex,setpoint}$, $T_{S1,coil,max}^{flex,setpoint}$: 65° and 75° Celsius
- $T_{S2,HP/coil,max}^{flex,setpoint}$: $\bar{T}_{S1}^{t} - \Delta T_{S1-S2}$
- ΔT_{S1-S2} : 12° Celsius

9.4.2 Flexibility settings

To quantify to what extent thermal flexibility can be utilised for peak shaving and passive balancing, we have defined four settings in chapter 4. the settings are presented in Table 9.7.

Table 9.7: Settings for passive balancing and peak shaving

Setting number	Setting specification	Devices
0	No action	-
1A	Peak shaving	HP
1B		HP and coils
2A	Decrease imbalance cost	HP
2B		HP and coils
3A*	Decrease imbalance cost Increase imbalance revenue	HP
3B		HP and coils
4A	Decrease all imbalances	HP
4B		HP and coils

For each setting, we differentiate between the use of a heat pump only (settings A) and in combination with the electrical coils (settings B). One exception to this, is setting 3A. For this setting, the electrical coils and heat pumps are used to decrease imbalance cost, whereas only the heat pumps are used to increase the revenue.

Note that the process of passive balancing helps avoid cost, by reducing imbalances that yield imbalance cost, and increase revenue by increasing imbalances that yield imbalance revenue. Peak shaving, on the other hand, is used to avoid violation of the interconnection capacity of the microgrid.

9.4.3 Output/measurement variables

The control over the input variables and settings affects the outcome of the passive balancing and peak shaving. This effect is measured using the following dependent variables:

- The net imbalance revenue: $\mathbb{R}^{year}_{net,imbalance}$
- The realised percentage of solar self-consumption: SSC^{year}_{R}
- The realised thermal based electricity consumption: $E^{year}_{HP+coils,R}$

In addition we identify to what extent:

- The interconnection capacity is violated as a result of passive balancing and peak shaving.
- The minimum buffer tank temperatures are violated as a result of passive balancing and peak shaving.

9.4.4 Experiments

For each experiment, the result of the day-ahead portfolio optimisation is used as input for passive balancing and peak shaving. The result of the portfolio optimisations consist of the scheduled energy imports, energy exports, and charge and discharge events. The microgrid imbalance is calculated using this schedule and the real time energy consumption and PV production. For each experiment, we use the settlement prices and day-ahead market prices of either 2015 or 2016. Thus, no experiment uses prices from both 2015 and 2016.

9.4.5 Results: Passive balancing and peak shaving

The effect of different settings and prices on the net imbalance revenue

We evaluate the effect of different settings and settlement prices on the net imbalance revenue. For evaluation, the input variables for day-ahead portfolio optimizations are set as follows: alpha α is set to 0 and the battery degradation costs are set to 0 €/kWh. For passive balancing and peak shaving, the input variables, as presented in section 9.4.1, are used. The results are presented in Figure 9.2, Table 9.8 and Table 9.9. The results for setting 1A and 1B have been excluded from the tables, because these are similar to setting 0. Setting 4A and 4B have also been excluded from the tables, because it is already clear from Figure 9.2 that these settings yield less net imbalance revenue.

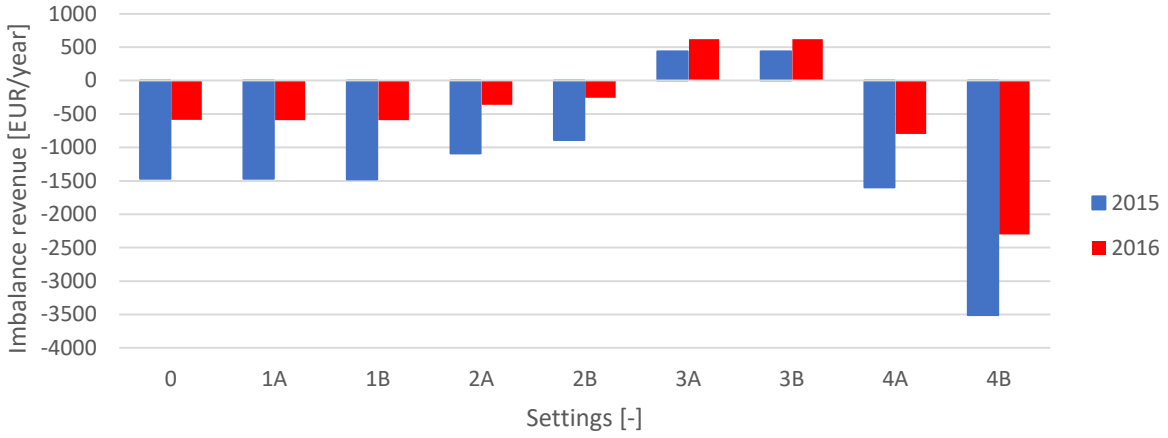

Figure 9.2: Net imbalance cost for different settings and years

Table 9.8: The imbalance cost and revenue for 2015 and different settings

Setting	Imbalance cost		Imbalance revenue		Net Imbalance revenue
	$\mathbb{C}^{year}_{imbalance}$		$\mathbb{R}^{year}_{imbalance}$		$\mathbb{R}^{year}_{net,imbalance}$
	Negative imbalances	Positive imbalances	Negative imbalances	Positive imbalances	
0	€ 2.840	€ 287	€ 322	€ 1.340	-€ 1.470
2A	€ 2.750	€ 101	€ 446	€ 1.320	-€ 1.090
2B	€ 2.790	€ 32	€ 591	€ 1.340	-€ 891
3A	€ 2.550	€ 40	€ 1.450	€ 1.580	€ 440
3B	€ 2.550	€ 40	€ 1.450	€ 1.580	€ 440

Table 9.9: The imbalance cost and revenue for 2016 and different settings

Setting	Imbalance cost		Imbalance revenue		Net Imbalance revenue
	$\mathbb{C}^{year}_{imbalance}$		$\mathbb{R}^{year}_{imbalance}$		$\mathbb{R}^{year}_{net,imbalance}$
	Negative imbalances	Positive imbalances	Negative imbalances	Positive imbalances	
0	€ 1.940	€ 79	€ 184	€ 1.250	-€ 585
2A	€ 1.870	€ 9	€ 287	€ 1.230	-€ 362
2B	€ 1.850	€ 1	€ 353	€ 1.240	-€ 258
3A	€ 1.670	€ 1	€ 840	€ 1.450	€ 619
3B	€ 1.670	€ 1	€ 840	€ 1.450	€ 619

Via inspection of Figure 9.2, it is found that the net imbalance revenue, $\mathbb{R}^{\text{year}}_{\text{net,imbalance}}$ can be improved using settings 2 and 3. As seen in Table 9.8 and Table 9.9, the net imbalance revenue is less negative compared to setting 0. In fact, for setting 3, the net imbalance revenue is even positive. Also, it is found that setting 3B does not improve the net imbalance revenue with respect to setting 3A. This indicates that no thermal flexibility is available for additional passive balancing. Finally, it is found that setting 4A results in even more net imbalance cost than setting 0. Hence, it is financially not attractive to offset all microgrid imbalances.

Thus, in terms of financial benefits, setting 3A and 3B yields the highest net imbalance revenue. By inspection of Table 9.8 and Table 9.9, the improvements between setting 0 and 3A can be attributed to the following changes:

1. Compared to setting 0, setting 3A results in respectively 350% (2015) and 356% (2016) more revenue from negative imbalances that yield imbalance revenue.
2. Compared to setting 0, setting 3A results in respectively 16% (2015) and 18% (2016) more revenue from positive imbalances that yield imbalance revenue.
3. Compared to setting 0, setting 3A results in respectively 14% (2015) and 16% (2016) less cost from negative imbalance that yield imbalance cost.
4. Compared to setting 0, setting 3A results in significantly less cost for 2015 and 2016 as a result of positive imbalances that yield imbalance cost.

The comparison between setting 0 and 3A reveals that most imbalance revenue is generated by increasing negative imbalances that yield imbalance revenue. This is achieved by increasing the heat pump electricity consumption, which causes the negative microgrid imbalance to increase. From this finding it follows that more flexibility is available to increase the thermal based electricity consumption than there is flexibility available to decrease consumption. In part, this is caused by the minimum runtime of the heat pump. Upon activation, the minimum runtime insures that the heat pump cannot be switched off for 30 minutes, to prevent short cycling.

Main Observations

- The simulation model results suggest that passive balancing can be used to generate net imbalance revenue.
- The net imbalance revenue can best be optimised by decreasing imbalance cost and increasing imbalance revenue (setting 3), because this yields the most net imbalance revenue.

The effect of different settings on actual solar self-consumption and thermal electricity consumption

We evaluate the effect of different years and settings on the actual solar-self consumption and thermal based electricity consumption. For evaluation, the input variables for day-ahead portfolio optimizations are set as follows: alpha α is set to 0 and the battery degradation costs are set to 0 €/kWh. For passive balancing and peak shaving, the input variables, as presented in section 9.4.1, are used. The results are presented in Table 9.10.

Table 9.10: Solar self-consumption and thermal based electricity consumption

Setting	Thermal based electricity consumption [MWh/year]		Actual solar self-consumption [%/y]	
	$E^{year}_{HP+coils,R}$		SSC^{year}_{R}	
	2015	2016	2015	2016
0	115	115	25.5	25.7
1B	115	115	25.5	25.6
2B	120	118	25.2	25.1
3A	120	119	24.2	24.5
3B	120	119	24.2	24.5

By inspection of Table 9.10, it is found that the percentage of solar self-consumption decreases with respect to setting 0, when performing passive balancing (settings 2 and 3). It is also found that the thermal based electricity consumption increases with respect to setting 0, as a result of passive balancing and peak shaving (settings 1, 2 and 3).

Main Observations

- The thermal based electricity consumption increases as a result of passive balancing and peak shaving (setting 1,2 and 3), when compared to setting 0
- The percentage of solar self-consumption decreases as a result of passive balancing (setting 2 and 3), when compared to setting 0.

Comparing the actual percentage of solar self-consumption with the forecasted solar self-consumption

It follows from Table 9.10 (and section 9.2), that the actual percentage of solar-self consumption (24.5%) is circa 11% smaller than the forecasted percentage of solar self-consumption (35.9%). The overall reduction is caused by the faulty forecasts on which the day-ahead portfolio optimization is based.

Main Observations

- Based on our simulation model, the actual percentage of solar-self consumption is significantly lower than was predicted in the day-ahead portfolio optimization phase.

The effect of different settings and prices on the violation of the interconnection capacity

Next, we evaluate violation of the interconnection capacity using two variables:

- Number of times that the interconnection capacity is violated per year: $N^{year}_{inter,error}$
- Mean violation error, based on all incidents: $\mu^{year}_{Inter,error}$

To evaluate how much active power is transported over the interconnection line, equation (9.2) is used

$$P^{t}_{inter} = Abs(\hat{P}^{h}_{export,F} - \hat{P}^{h}_{import,F} + \hat{P}^{t}_{imbalance,R}) \quad (9.2)$$

With, P^{t}_{inter} the active power that is transported over the interconnection line, $\hat{P}^{h}_{export,F}$ the scheduled energy exports, $\hat{P}^{h}_{import,F}$ the scheduled energy imports and $\hat{P}^{t}_{imbalance,R}$ the real time imbalance. Given the result of equation (9.2), we check whether the interconnection capacity is violated using equation (9.3).

$$\text{if } \left\{P^{t}_{inter} > 136kW\right\} \text{ then } \begin{matrix} P^{t}_{inter,error} = P^{t}_{inter} - P^{max}_{inter} \\ N^{year}_{inter,error} = N^{year}_{inter,error} + 1 \end{matrix} \quad (9.3)$$

With $P^{t}_{int,error}$ the rate at which the interconnection is violated, P^{max}_{inter} the maximum interconnection capacity and $N^{year}_{int,error}$, the number of times that the interconnection capacity is violated per year. Finally, the mean violation error is given by (9.4).

$$\mu^{year}_{inter,error} = \frac{\sum_{day=1:365}\left[\sum_{t=1:96} P^{t}_{inter,error}\right]}{N^{year}_{inter,error}} \quad (9.4)$$

For evaluation, the input variables for day-ahead portfolio optimizations are set as follows: alpha α is set to 0 and the battery degradation costs are set to 0 €/kWh. For passive balancing and peak shaving, the input variables, as presented in section 9.4.1, are used. The results of setting 0, 1A, 1B, and 3A are presented in Figure 9.3 and Figure 9.4.

Only settings 1A and 1B have been included, because for these settings peak shaving is applied. Setting 3A has been added, because this settings yields the highest net imbalance revenue. Setting 0 is added as reference.

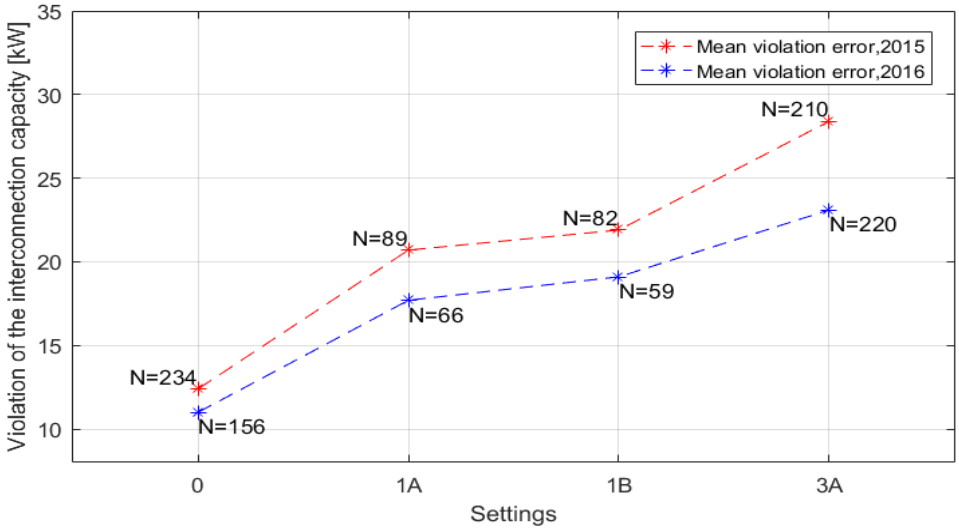

Figure 9.3: Violation of the interconnection capacity for different settings

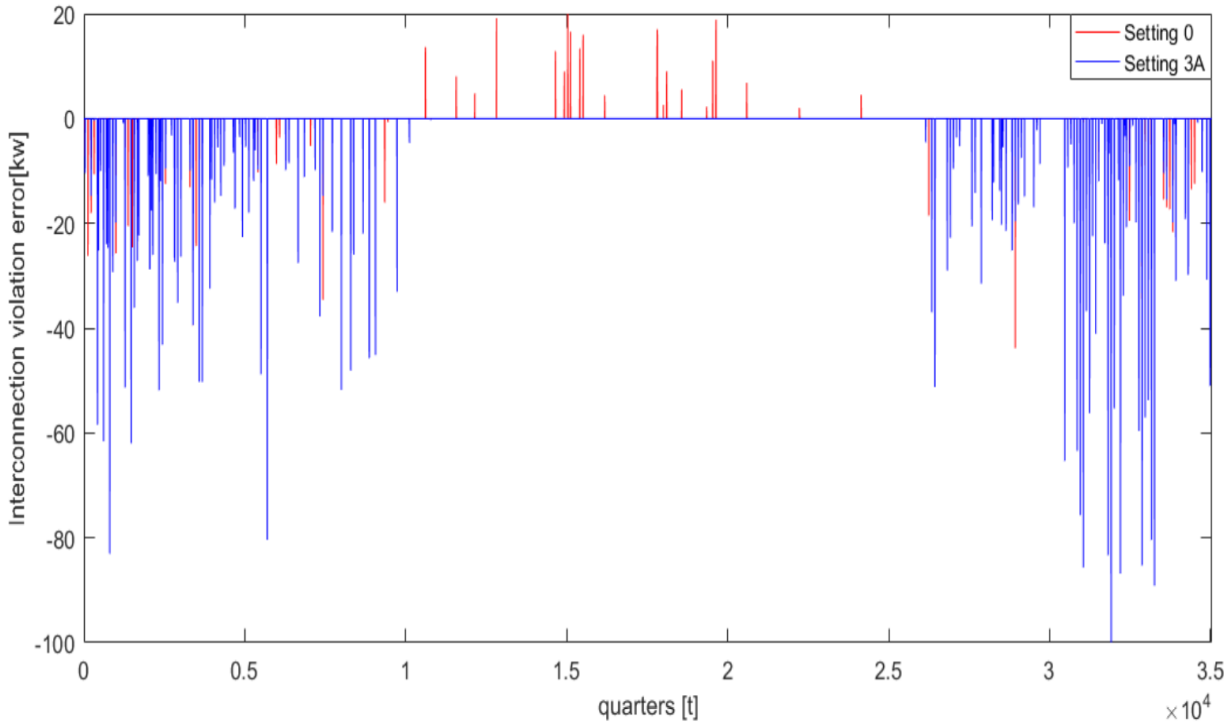

Figure 9.4: Violation of the interconnection capacity for prices of 2015 and settings 0 and 3A

Via inspection of Figure 9.3, it is found that peak shaving using thermal flexibility is not effective, because the mean violation error increases, despite the fact that the number of violations decreases. By inspection of Figure 9.3, it also follows that passive balancing (setting 3A) results in a higher mean violation error. The number of violations decreases slightly for 2015, but increases significantly for 2016. Thus, in general passive balancing causes more problems with the violation of the interconnection capacity than compared to setting 0.

Via inspection of Figure 9.4, it is found that violation of the interconnection occurs throughout the year for setting 0. However, it is also clear that during the heating season, only negative imbalances cause violation of the interconnection capacity. The opposite holds for the cooling season.

Compared to setting 0, setting 3A only results in violation of the interconnection capacity as a result of negative imbalances during the heating season. Especially during winter, the thermal flexibility is lower, because of the higher heat demand. Thus, to prevent violation of the interconnection capacity, the temperature and/or flexibility set points should be altered. Hence, more experiments are needed to identify suitable set points for temperature and flexibility control.

Main Observation

- Thermal flexibility is not a good source for peak shaving. Although the use of thermal flexibility can reduce the number of interconnection violations, the mean interconnection violation increases nonetheless.
- Passive balancing and peak shaving causes an increased violation of the interconnection capacity, compared to setting 0.
- With passive balancing (setting 3A), the interconnection is only violated as a result of negative imbalances during the heating season.
- More experiments are needed to establish suitable temperature and flexibility set points.

The effect of various settings on the violation of minimum buffer tank temperatures

Next, we analyse violation of the minimum tank temperatures. The violation of the minimum tank temperatures is measured using the following four variables. The formulas for calculating these variables are presented in appendix B11.2.

- Mean temperature error per year, based on all cases where TS1<55^{o} C $\mu^{year}_{S1,error,R}$
- Mean temperature error per year, based on all cases where TS2<30^{o} C $\mu^{year}_{S2,error,R}$
- Number of times per year that the minimum temperature is violated of tank S1: $N^{year}_{S1,error,R}$
- Number of times per year that the minimum temperature is violated of tank S1: $N^{year}_{S2,error,R}$

For evaluation, the input variables for day-ahead portfolio optimizations are set as follows: alpha α is set to 0 and the battery degradation costs are set to 0 €/kWh. For passive balancing and peak shaving, the input variables and settings, as presented in section 9.4.1, are used.

We present the results in Figure 9.5. Settings 1A and 1B have been excluded, because it is found (in previous experiments) that peak shaving is not effective for these settings. Setting 4A and 4B are excluded because it is found (in previous experiments) that these settings result in even less net imbalance revenue compared to setting 0.

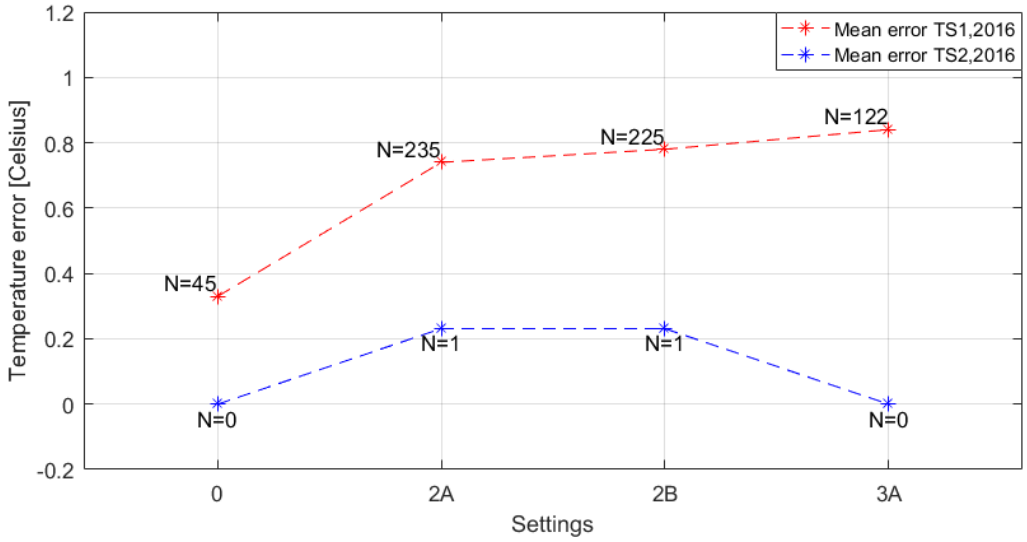

Figure 9.5: Mean temperature violation and number of incidents for different settings

Analysis on different settings and minimum temperature errors

By inspection of Figure 9.5, it is found that any setting (2-3) results in more violations and a higher mean temperature error for tank S1. However, the minimum temperature of tank S2 is hardly violated. This indicates that the HP flexibility setpoint for tank S2 can indeed be reduced from 46^{o}C to 34^{o}C. The increased violation of the minimum tank temperature of S1 can be attributed to the utilisation of thermal flexibility and to some extent to the lower HP flexibility setpoint of tank S1 (63^{o} C instead of 65^{o} C). From this analysis, it follows that more experiments are needed to identify suitable set points for temperature and flexibility control.

Main Observation

- When compared to setting 0, all settings result in more frequent and more intense violation of the minimum temperature of buffer tank S1.
- More experiments are needed to identify suitable temperature and flexibility set points.

9.5 Sensitivity analysis

In this section, we perform a sensitivity analysis to identify for which temperature set points the heat pump should start to supply heat to tank S1 and S2, thereby preventing the minimum temperatures of tank S1 and S2 from being violated. In addition, we vary the buffer tank capacity to find the minimum required tank capacity. Information on the minimum tank temperatures is presented in section 7.6.

9.5.1 Assumptions and variables

For simplicity, we assume that the electrical coil set points are as follows: For tank S1, the coil set point, $T_{S1,coil}^{setpoint}$ is set to 60° C. For tank S2, the coil set point, $T_{S2,coil}^{setpoint}$ is set to 34° C The violation of the minimum tank temperatures is measured using the following dependent variables. The formula's for calculating these variables are presented in appendix B11.2.

- Mean temperature error per year, based on all cases where TS1<55° C $\mu_{S1,error,R}^{year}$
- Mean temperature error per year, based on all cases where TS2<30° C $\mu_{S2,error,R}^{year}$
- Number of times per year that the minimum temperature is violated of tank S1: $N_{S1,error,R}^{year}$
- Number of times per year that the minimum temperature is violated of tank S1: $N_{S2,error,R}^{year}$

9.5.2 Sensitivity analysis on temperature supply set points and buffer tank capacities

The effect of varying the HP set point for tank S1

For sensitivity analysis, the HP temperature setpoint for tank S1, $T_{S1,HP}^{setpoint}$ is varied between 60° to 65° C. A higher setpoint is not possible, because the maximum supply temperature of the heat pump is 65°C. Because the sensitivity analysis shows that a temperature of 60°C already results in many violations, no other temperature set points have been included. The HP temperature setpoint tank for tank S1, $T_{S1,HP}^{setpoint}$ is set to 65° C. The capacities of tank S1 and S2 are set to 300 litres. The results, based on market prices of 2015 are shown in Figure 9.6

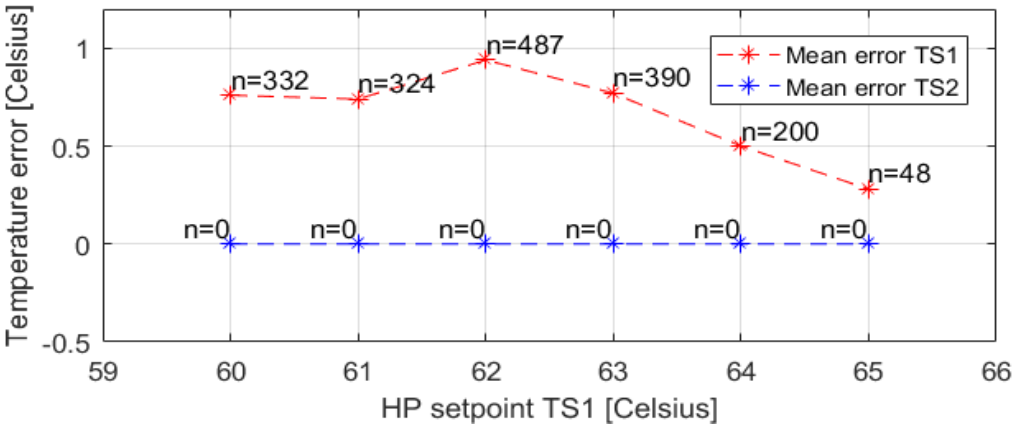

Figure 9.6: Violation of the minimum tank temperatures for different HP set points of tank S1

By inspection of Figure 9.6, it is found that the HP setpoint for tank S1 should be at least 65° C. Given this setpoint, the minimum tank temperatures is still violated, with $N_{S1,error}^{year} = 48$ and $\mu_{S1,error}^{year} = 0.3^{o}C$.

As also seen in Figure 9.6, it is found that compared to a setpoint of 61° C, a set point of 62° yields more frequent and more intense violation of the minimum temperature of tank S1. This effect can be attributed to the design of the temperature control logic. For each timestep t, the temperature control logic evaluates the buffer tank temperature and determines the temperature offset with respect to the HP setpoint of each tank. Heat is then supplied (by the heat pump) to the tank with the highest offset. Apparently, the effect of this logic is that the supply of heat to tank S2 is favoured more frequently at an HP setpoint of 62°C. Similar behaviour is observed when varying the HP setpoint for tank S2, as will be shown in the next experiment.

The effect of varying the HP setpoint for tank S2

For sensitivity analysis, the HP temperature setpoint for tank S2, $T^{setpoint}_{S2,HP}$ is varied between 30° to 50° Celsius. This range is selected, because the minimum required buffer tank temperature is 30°. The upper limit is chosen, because for this temperature no violations are observed. The HP temperature setpoint tank for tank S1, $T^{setpoint}_{S1,HP}$ is set to 65° C. The capacities of tank S1 and S2 are set to 300 litres. The results are presented in Figure 9.7

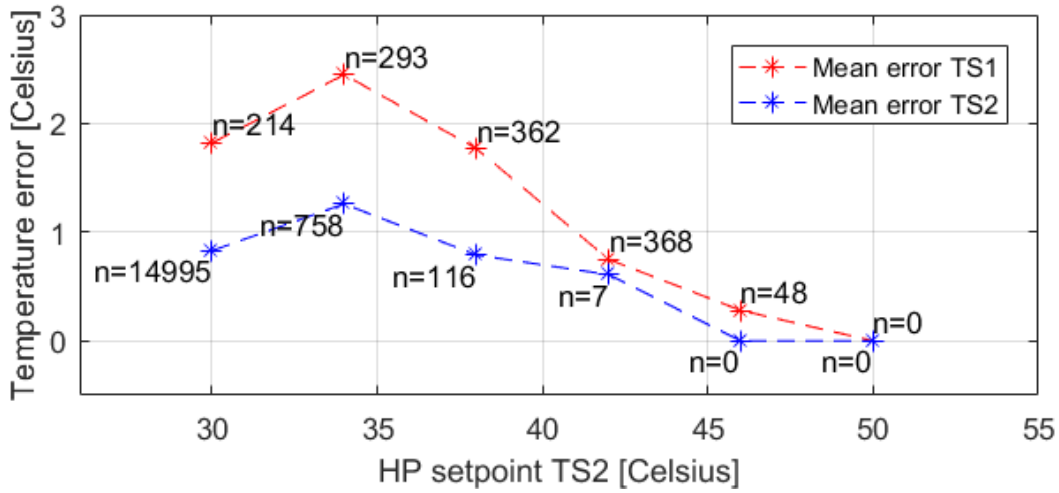

Figure 9.7: Violation of the minimum tank temperatures for different HP set points of tank S2

By inspection of Figure 9.7, it is found that the HP setpoint for tank S2 should be at least 46° C and preferably even higher to prevent violation of the minimum temperatures, at the expense of a higher electricity consumption. An increase in the number and intensity of violation is observed for a set point of 34° C. Again, this unexpected increase can be attributed to the design of the temperature control logic.

The effect of varying the buffer tank capacities

For sensitivity analysis, the capacity of tank S1 and S2 is varied between 100 and 350 litres. The HP temperature setpoint for tank S1, $T^{setpoint}_{S1,HP}$ is set to 65° C. The HP temperature setpoint tank for tank S2, $T^{setpoint}_{S2,HP}$ is set to 46° C. The results are presented in Figure 9.8.

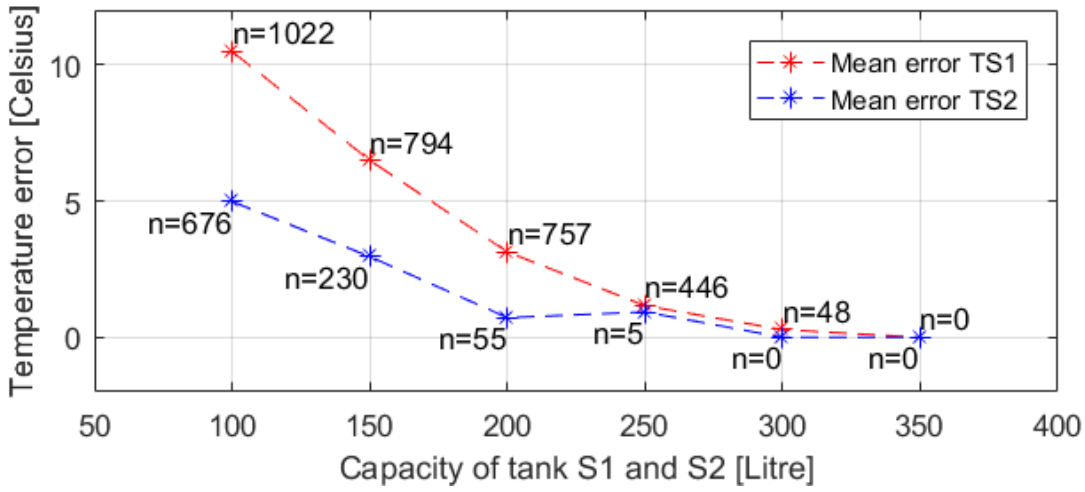

Figure 9.8: Violation of the minimum tank temperatures for cumulative tank capacities

By inspection of Figure 9.8., it is found that a cumulative tank capacity of at least 600 litres is required. Maintaining the temperature of tank S1 is especially challenging for smaller capacities.

9.5.3 Analysis on temperature set points and tank capacities

Based on the sensitivity analysis, the temperature set points and tank capacity should (at least) be as follows:

- $V_{S1} + V_{S2}$ 600 litres
- $T^{setpoint}_{S1,HP}$, $T^{setpoint}_{S2,HP}$ 65° and 46° Celsius
- $T^{setpoint}_{S1,coil}$ $T^{setpoint}_{S2,coil}$ 60° and 30° Celsius

Given the temperature set points as listed here above, the average temperatures of tank S1 and S2 are as shown in Figure 9.9.

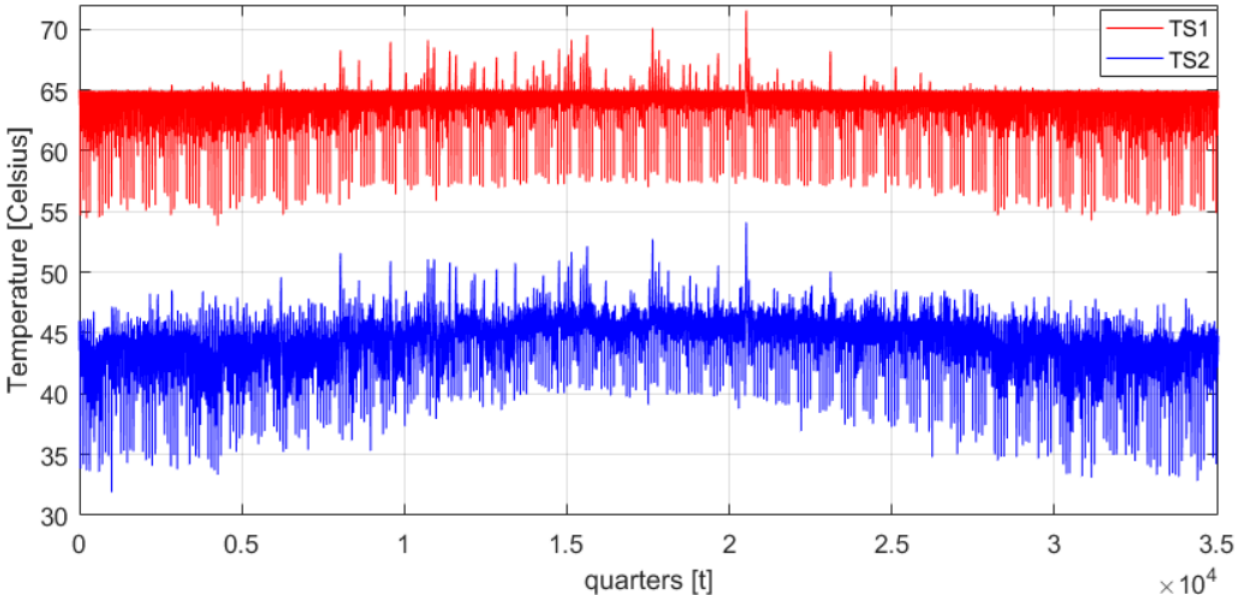

Figure 9.9: Average temperatures of tank S1 and tank S2.

From inspection of Figure 9.9, it is found that the temperature of S2 remains below that of S1. In addition, we observe that the temperature errors only occur during the winter season. The errors only last for 15 minutes and the average temperature of tank S1 is frequently raised beyond 60° Celsius. Given these settings, the risk for legionella growth is small. Thus, we conclude that the boundary conditions are met.

Main Observation

- Based on our simulation model, the set points for which the heat pump should start to supply heat to buffer tank S1 and S2 are respectively 65°C and 46°C.
- Based on our simulation model, the minimum required capacity of the buffer tank is 600L.

9.6 Validation of simulation model

In this section we present a validation of the simulation model. In section 9.6.1, we present various outputs of the simulation model. IN section 9.5.2, we analyse these outputs. For validation we us information from the EPC report [82] of Schoonschip lot 5. In addition, we use estimates by an energy retailer on the electricity production and consumption within the Schoonschip community [130].

9.6.1 Validation: outputs of the simulation models

We obtain an indoor temperature profile and heat demand curve using the heat demand models and temperature control logic, as presented in chapter 7. The average house temperatures, $\overline{T}^{t}_{house}$ and the outside air temperatures are presented in Figure 9.10. The heat supplied to the underfloor heating system, per timeslot t, Q^{t}_{heat} is presented in Figure 9.11. The thermal based electricity consumption by the heat pump and electrical coils is presented in
Table 9.11. In
Table 9.12 we present results on the total annual electricity consumption and PV electricity production.

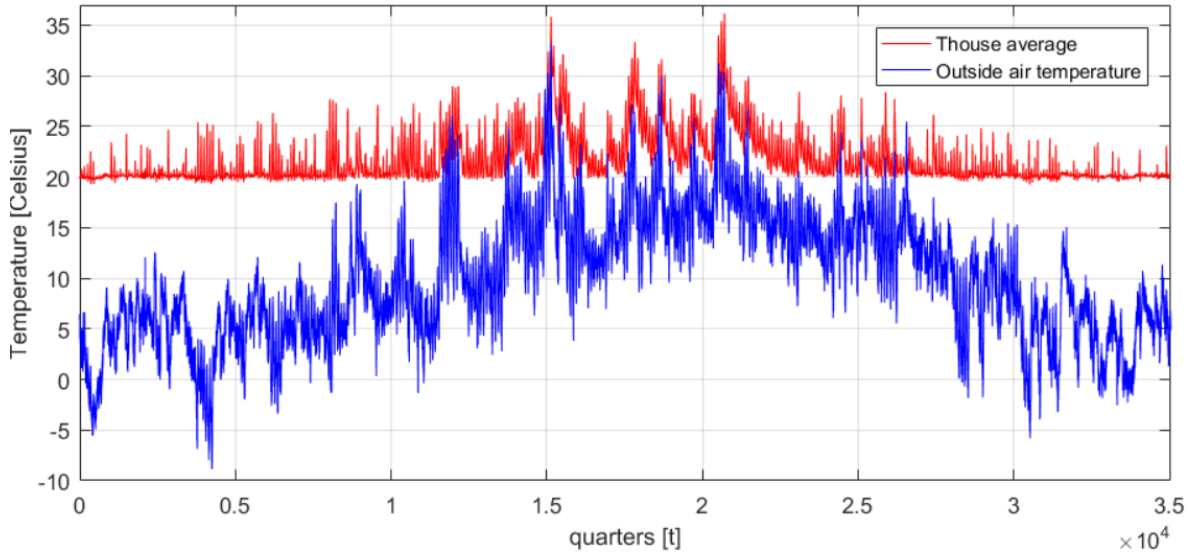

Figure 9.10: Average indoor and outdoor air temperatures

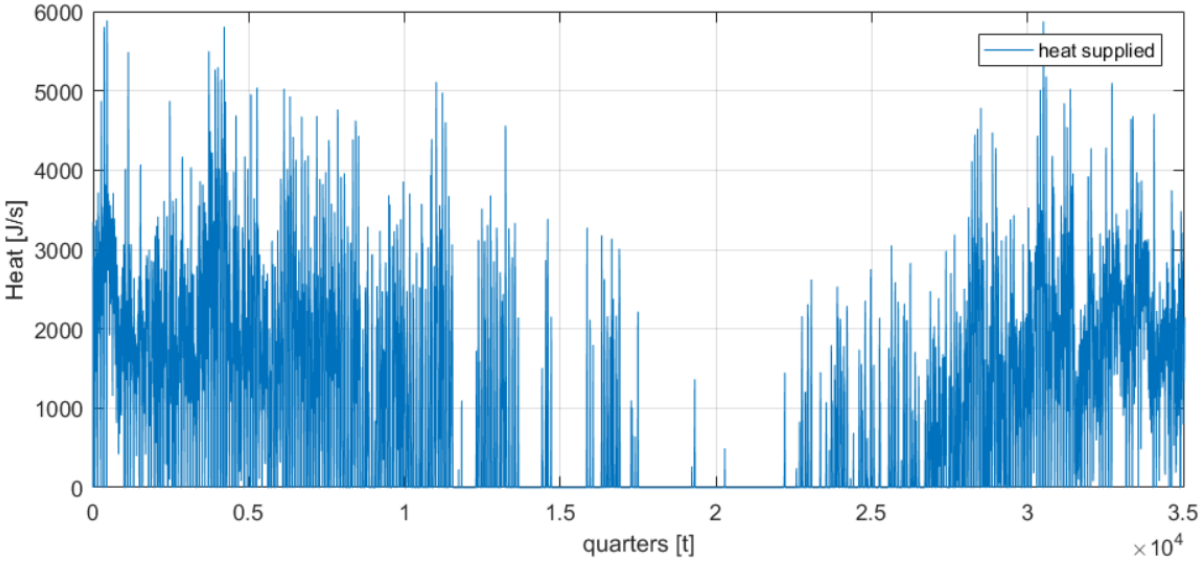

Figure 9.11: Heat supplied to underfloor heating system.

Table 9.11: Heat and electricity demand for Schoonschip lot 5			
Type	Symbol	Model [MWh]	EPC [MWh]
Domestic hot water (DHW) demand	Q_{DHW}^{year}	6	3.5
Heat demand	Q_{heat}^{year}	8.3	9.4
Heat pump electricity consumption	E_{HP}^{year}	3.5	5.8
Electrical coils electricity consumption	E_{coils}^{year}	0.40	0.45

Table 9.12: Community electricity production and consumption			
Type	Symbol	Model [MWh]	Retailer estimates [MWh]
Thermal based electricity consumption	$E_{HP+coils}^{year}$	117	-
Non-thermal based electricity consumption	$E_{electricity}^{year}$	158	-
Total electricity consumption	E_{load}^{year}	275	260
PV production	E_{PV}^{year}	125	137

9.6.2 Validation: analysis

By inspection of Figure 9.10, it is found that the temperature control logic is able to maintain the temperature setpoint of 20^{o}C during the heating season (September to April). However, during the cooling season (May to August) the maximum temperature (24^{o}C) is often violated. This is primarily the result of incoming solar heat gains and because of the fact that no active cooling has been implemented in the current model. In future research, the correctness and accuracy of the dynamic thermal house model should be validated using empirical measurements of the actual house or with a sophisticated thermal dynamic model of the house.

By inspection of
Table 9.11, it is found that the heat demand and resulting thermal based electricity consumption are too low, with respect to the EPC results. Various causes can be distinguished: Firstly, the heat demand is too low, because in our model we only account for the heat demand of the living quarters, located on the upper level of lot 5. The heat demand of the sleeping quarters (located at the lower level), has not been included. Secondly, we have not accounted for residents occupancy and various other time dependent heat demand patterns. Thus, the thermal models require several improvements and refinements. Finally, active cooling during the heating season should be included.

By inspection of
Table 9.11, it is found that the DHW demand is too high with respect to the EPC results. The differences are likely a result of two causes: Firstly, the DHW consumption profiles are based on the DHW demand of 5 residents. However, since Schoonschip accommodates 100 people divided over 30 lots, we expect only 3 or 4 residents per lot. Thus, the number of residents should be lowered in the simulation model. Secondly, the annual DHW profile is based on only one week of simulated data. Thus, the DHW consumption is likely to vary more over the course of a year.

By looking at Table 9.12, it is found that the electricity production and consumption are in the same order of magnitude, as the estimates by the energy retailer. Compared to the estimates by the retailer, the estimated PV production seems too low. However, the simulated PV production profile is based on a fairly accurate simulation, taking into account various aspects. Thus, the PV production simulation does not require major alterations.

9.7 Results summary

In this chapter, we have analysed the value of flexibility that can be generated with the community microgrid of Schoonschip. The value of flexibility has been quantified with respect to day-ahead portfolio optimizations and passive balancing. In addition, we have quantified the percentage of solar-self consumption, along with several other non-financial performance indicators. For comparison, we have also analysed the cost and benefits associated with Time Of use (ToU) optimizations with respect to dual electricity tariff from a traditional energy retailer.

9.7.1 Day-ahead portfolio optimizations and Time of Use optimizations

It is found that day-ahead optimizations can yield substantial cost reductions, in comparison to a case where only the forecasted percentage of solar self-consumption is optimized. The simulation model suggest that the forecasted percentage of solar self-consumption can be maximized, whilst also generating value with battery flexibility. However, the forecasted percentage of solar self-consumption can only be maximized when excluding export benefits from the optimization problem. When maximizing the forecasted solar self-consumption, the simulation model results suggest that day-ahead optimizations yield a net electricity cost reduction of €1.500,- for a dual electricity tariff, €1.200,- for day-ahead market prices of 2015 and €2.500,- for day-ahead market prices of 2016. Here, it must be noted that the net electricity costs only reflect the base energy tariff and do not include cost items like taxes and connection cost. Based on the simulation model, it is found the net electricity cost can be reduced to zero, at the expense of substantially more battery cycles and a significantly lower percentage of (forecasted) solar-self consumption.

9.7.2 Passive balancing and peak shaving

Based on the simulation model results, it is found that without passive balancing, the net imbalance revenue is strongly negative. However, the simulation model suggest that it is possible to generate net imbalance revenue by performing passive balancing. Based on the simulation model results, the maximum net imbalance revenue amounts to €450,- for 2015 and €610,- for 2016. Based on the simulation model, the maximum avoided imbalance cost amount to circa €1500,- for 2015 and circa €600,- for 2016. The simulation model suggests that the thermal based electricity consumption increases slightly as a result of passive balancing, when compared to the situation without passive balancing. The percentage of solar self-consumption decreases slightly, when compared to setting 0. In addition, the simulation model results suggests that the percentage of solar self-consumption is circa 11% lower than was forecasted in the day-ahead portfolio optimization, because no real time optimisation for solar self-consumption has been included.

Based on the simulation model, it is found that any flexibility setting (1 to 4) results in an increased violation of the minimum temperature of tank S1, when compared to setting 0. Therefore, more experiments are needed to identify suitable set points for temperature and flexibility control. Based on the simulation model, it is also found that any setting (0 to 4), results in (frequent) violation of the interconnection capacity. The simulation model suggests that passive balancing results in an increased violation of the interconnection capacity, compared to setting 0. It also follows from the simulation model that violation of the interconnection capacity cannot be avoided using peak shaving (setting 1A and 1B). Again, it follows that more experiments are needed to identify suitable set points for temperature and flexibility control.

9.7.3 Simulation model validation

The thermal models perform sufficiently adequate to approximate the electricity consumption and PV production within Schoonschip. However, the correctness and accuracy of the dynamic thermal house model should still be validated using empirical measurements or an advanced high order model of the house. In addition, the thermal models and DHW profile require various improvements and refinements.

Chapter 10

Conclusions and further research

10.1 Conclusions

The need to decarbonise our economy has led to the uptake of renewable energy resources, a gradual decentralisation of our energy production and a push for electrification of transportation and heating. On a local level, we see an the uptake of distributed energy resources (DER) such as solar PV, heat pumps and batteries. The uptake of DER creates opportunities for maximising the consumption of locally produced energy, local energy exchange and local energy storage. However, the uptake of DER also brings about increased electricity consumption and production, generating more stress on the distribution grid. To utilise the potential of DER, while managing their impact, local energy management (LEM) solutions are required, for which the (community) microgrid can be considered a promising concept. In parallel, the integration of wind and solar energy production is challenging for maintaining grid stability, given the volatile nature of these resources. The provision of flexibility services is considered a solution for enabling integration of the volatile energy production. Were [2] defines flexibility services as: "*a power adjustment sustained at a given moment for a given duration from a specific location within the network.''* The utilisation of flexibility services can be considered inherent to local energy management solutions. Thus, the question is whether provision of flexibility services for managing grid stability can be combined with local energy management via a microgrid. Therefore, the following research question is investigated in this thesis: *''How can a community microgrid provide flexibility services to the current Dutch energy sector, while maximizing solar self-consumption, and what is the value of these services?''.*

For this research, we have considered a collaborative energy community, inspired by the Schoonschip project in Amsterdam north. The community contains 30 floating houseboats, equipped with PV panels, batteries, modulating heat pumps, thermal collectors, buffer tanks, underfloor heating systems and electrical boilers. The resources are integrated via a microgrid that is centrally controlled by an energy management system. The microgrid is connected to the distribution grid via an interconnection of 136kW. The community itself is registered as large-scale consumer (''grootverbruiker'').

Identifying research opportunities and suitable flexibility services

To answer the main research question, it was first necessary to identify which flexibility services can be provided by a community microgrid. To that end, a literature and market survey have been carried out. The literature survey revealed that little attention has been devoted to the optimisation of self-consumption in microgrid scheduling problems. Also, to the best of our knowledge, little research has been done on the provision of flexibility services by a community microgrid. The market survey suggests that the provision of flexibility services is possible to a limited extent, given the current Dutch market design. It is found that community microgrids may provide flexibility services in two ways. The first option is to apply peak shaving and time of use (ToU) optimizations with respect to dual or dynamic electricity tariffs offered by an energy retailer. Although these flexibility services may offer financial benefits to the consumers, it does not address the problem of volatility within the wider grid. A second option is to acquire direct access to the Dutch spot market. To facilitate this, the community microgrid assets could be controlled by a third party that has access to the wholesale market via a balancing responsible party (BRP). Flexibility services may then be used for the sale and purchase of energy in the day-ahead market, peak shaving and passive balancing. The latter enables the microgrid resources to be used for balancing the electricity grid in order to temper the volatile energy production of renewable sources. We define passive balancing as: *"The process whereby a BRP reduces or increases its portfolio imbalance by altering the energy consumption and/or energy production, based on a real time system imbalance signal broadcasted by TenneT".*

Simulation model and decision software

To fully answer the main research question, we have created a comprehensive simulation model and optimization/decision software. This included: 1) The creation of a day-ahead scheduling strategy, that optimises the utilisation of battery flexibility. 2) The creation of day-ahead forecasts on the energy production and consumption within the community microgrid. 3) The development of various thermal dynamic models to quantify the thermal flexibility of the heat pump and electrical boiler. 4)The development of decision software for temperature control over the indoor house- and buffer tank temperatures. 5) And finally, the formulation of a thermal flexibility control strategy for performing passive balancing and peak shaving with respect to imbalance settlement prices and local portfolio/microgrid imbalances.

The day-ahead scheduling strategy has been formulated as a linear programming problem. The objective function can be modified to establish a trade-off between the minimisation of net-electricity cost and maximisation of forecasted solar-self consumption. The thermal dynamic model of the house has been based on a reduced order white-box model. The 3e order white-box model forms a mathematical representation of the physical heat transport phenomena between the house enclosure (first order), the internal air (second order), the underfloor heating system (third order) and the outside environment. A validated model of a stratified buffer tank has been derived from literature. The heat pump model is based on a linear regression derived from literature. The linear regression describes the heat pump coefficient of performance as a function of the (given) inlet and (required) outlet temperatures. The temperature control is a simple thermostat that utilises measured temperatures and temperature set points. Finally, the thermal flexibility control logic consists of a decision tree that is used to perform passive balancing (and peak shaving). The decision tree takes into account the direction of the local imbalance and the sign of the imbalance settlement price components.

Experiments

For our experiment studies, we have assumed that the Schoonschip community can appoint an aggregator with wholesale market access via the license of a (third party) balancing responsible party (BRP). Also, we have assumed that the portfolio of the aggregator/BRP only contains the microgrid. Thus, the portfolio imbalances are the result of the discrepancies between the day-ahead schedule and the actual power production and consumption with the microgrid. Furthermore, we have assumed perfect forecast on day-ahead market prices. Finally, we have assumed perfect forecast, with a 15 minute horizon, on imbalance settlement prices and energy flows within the microgrid.

Thus far, two experimental studies have been conducted to identify trends and tendencies. As a first set of experiments, we have evaluated to what extent: the forecasted percentage of solar self-consumption can be maximised, while minimising the electricity cost with respect to historic day-ahead market prices and dual electricity tariffs. The result of these experiments have been used to answer research question 1 and 3 (RQ1 and RQ3). The output of the first experiments is also used as input for the second set of experiments. In the second experiments, we have evaluated the potential and value of passive balancing and peak shaving with respect to historic imbalance settlement prices and portfolio imbalances. The results of these experiments have been used to answer research question 2 (RQ2).

Initial conclusions

Based on the simulation results, we conclude the following: The forecasted percentage of solar-self consumption can only be maximised under certain settings. Given these settings and compared to the value of ToU optimizations, there is potential to create additional value by performing day-ahead portfolio optimizations. However, the benefits of day-ahead portfolio optimizations vary per year and can be positive (+11%) or negative (-11%) when compared to ToU optimizations. Nonetheless, it is possible to increase the value of day-ahead portfolio optimizations well beyond the value of ToU optimizations. However, this can only be accomplished at the expense of considerably more full-equivalent battery cycles (+300%) and a substantially lower forecasted percentage of solar-self consumption (-60%).

Furthermore, it is found that passive balancing can help prevent imbalance costs and generate imbalance revenues. The latter indicates that the community microgrid can contribute to grid stability and can help mitigate volatility issues. However, given the current decision software and settings, the actual solar self-consumption is not maximised. In addition, the minimum buffer tank temperatures and interconnection capacity are frequently violated as a result of passive balancing. Thus, it is yet unclear whether (sufficient) value can be generated by performing day-ahead portfolio optimizations and passive balancing.

Sensitivity analysis is needed to determine whether passive balancing can be applied without violation of system constraints, while still generating (sufficient) value. In addition, the trade-off between generating value and maximising the solar self-consumption should be investigated more thoroughly. Also, the simulation model should be validated and requires further refinements. In general, this thesis has resulted in a simulation model that can easily be improved for studies into microgrids and flexibility services.

10.2 Further research

In this chapter we present the limitations of our simulation models and methodology. Based on the limitations, we also identify potential research opportunities.

Methodological limitations and suggestions for further research

I. The (optimal) allocation of flexibility resource should be investigated in more detail. Currently, battery flexibility is used to perform day-ahead optimisations, while the heat pumps and electrical coils are used for managing real-time microgrid imbalances. Instead of using the battery flexibility only during the day-ahead optimisation process, the battery charge and discharge schedule could be scheduled on the day itself. Furthermore, the heat pump is not necessarily the best source of flexibility for real time balancing, given compressor limitations. Thus, instead the heat pumps could be included in the day-ahead optimization problem.
II. The real time optimisation of solar-self consumption could also be included in the (optimal) allocation of flexibility resources.
III. The assumption of perfect forecast on imbalance settlement prices should be revised. The prediction of imbalance settlement prices is challenging, given the highly volatile nature of the imbalance market. Therefore, the implementation of imperfect forecasts will affect the effectivity of passive balancing in terms of the imbalance cost reductions and potential revenue.
IV. The same holds for the assumption of perfect forecast on day-ahead market prices. However, the day-ahead market is not very volatile. Therefore, we expect that imperfect forecasts will only result in minor changes to the net electricity cost for day-ahead market participation. However, to confirm this, further (desk) research is required.
V. The net electricity cost associated with ToU optimizations could be investigated. Currently, the evaluation of net electricity cost relies on imperfect forecasts. Therefore, the actual net electricity cost will be different when executing the schedule from the day-ahead ToU optimization. This difference could be quantified in further research.
VI. The use of a deterministic approach in solving day-ahead optimizations should be revised. Given that the day-ahead forecasts on energy flows and prices are imperfect, it is noteworthy to investigate the use of other approaches such as stochastic or robust optimizations. This line of research is incentivised by the finding that the interconnection capacity is frequently exceeded.
VII. Another option in regards to the violation of the interconnection capacity would be to investigate the effect of scheduling smaller power imports and exports in the day-ahead optimization. This is because, by lowering the power, the imbalances are less likely to cause a violation of the interconnection capacity.

Limitations of simulation models and suggestions for further research

I. The physical representation of the microgrid has been greatly simplified. Only the active power flow limitations of the microgrid interconnection have been accounted for. Hence, other network conditions and physical constraints should be accounted for in further modelling efforts. More detailed suggestions are presented in chapter 2, section 2.4.1.
II. The simulation of thermal-based electricity demand of the entire community has been simplified. The simulation model can be improved by considering multiple houses having different heat- and Domestic Hot Water (DHW) consumption patterns.
III. The house model has been simplified by neglecting the heat demand of the sleeping quarters that are located on the lower level of the house. In further modelling efforts, this should be accounted for.

IV. The house model does not account for residents' occupancy or other heat demand patterns that vary as function of time. Hence, these could be accounted for in further modelling efforts.

V. The solar collector model should be improved. A more detailed model is required that can more accurately simulate the heat and temperature output of a solar collector.

VI. The heat pump model should be refined. Currently, the heat pump performance is a function of the inlet and outlet temperature. However, the heat pump performance should be expressed as a function of the inlet temperature, outlet temperature and compressor frequency. This yields a better representation of the (maximum) heat production and associated electricity production

VII. In addition, the heat pump model should account for the limited acceleration/deceleration rate of the heat pump compressor.

Chapter 11

Appendix A

11.1 House model: heat losses and heat gains

In this appendix, we present the formula's for calculating the individual heat gains and heat losses between the external air and various thermal capacities (floor, internal air and house enclosure). A schematic representation of all terms is given in Figure 11.1.

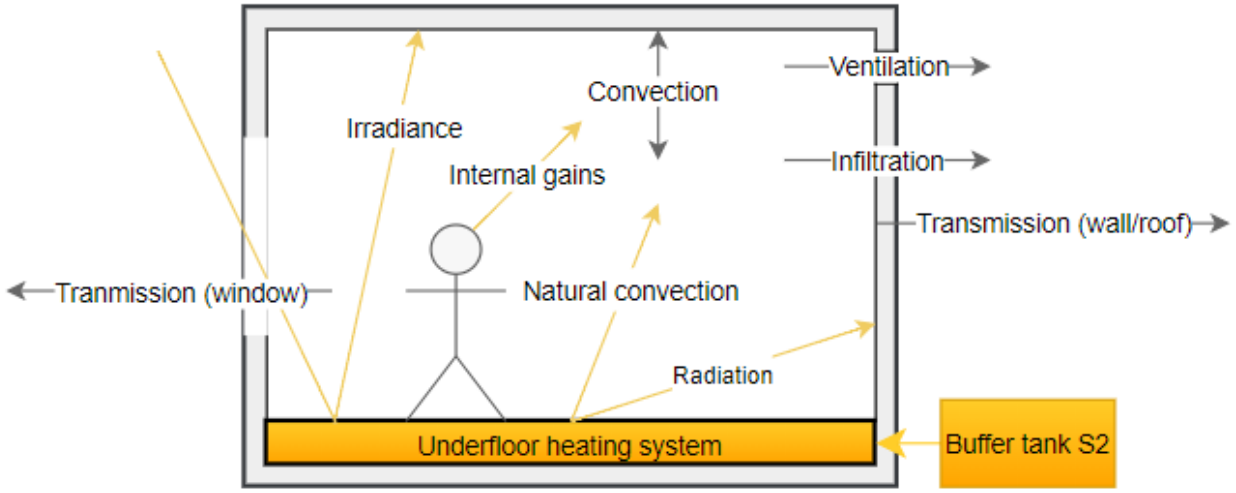

Figure 11.1: Heat transfer within the house and to the environment.

11.1.1 Formulas by [103] and [104]

Transmission losses, based on [103]

The transmission of heat from the house to the external air occurs via the walls, roof and windows. The heat transfer from the enclosure to the external air is given by equation (11.1) The heat transfer via the windows from the internal air to the external air is given by equation (11.2).

$$Q^{t}_{e-o,Transmission} = \sum_{Orientations} U_{enclosure,orientation} \cdot A_{enclosure,orientation} \cdot (\bar{T}^{t}_{e,enclosure} - T^{t}_{o,air}) \quad (11.1)$$

$$Q^{t}_{i-o,Transmission} = \sum_{Orientation} U_{window,orientation} \cdot A_{window,orientation} \cdot (\bar{T}^{t}_{i,air} - T^{t}_{o,air}) \quad (11.2)$$

With $U_{window,orientation}$ the overall heat transfer coefficient of windows for some orientation, $A_{enclosure,orientation}$ the surface area of the walls and roof for some orientation, $U_{enclosure,orientation}$ the overall heat transfer coefficient of the roof and walls for some orientation, $A_{window,orientation}$ the window area for some orientation. $\bar{T}^{t}_{i,air}$ the temperature of the air in the house and $\bar{T}^{t}_{e,enclosure}$,the temperature of the enclosure, $T^{t}_{o,air}$ the temperature of the outside air.

Ventilation and infiltration losses, based on [103]

The ventilation losses are given by equation (11.3). The and infiltration losses are given by equation (11.4). Here, the heat recovery factor f_{rec} represents the heat that is recovered from the outgoing ventilation stream. Such systems are referred to as balanced ventilation. In case of unbalanced ventilation, no heat is recovered, with $f_{rec} = 0$. The permeability of the building envelope is a function of the infiltration rate.

$$Q^t_{i-o,ventilation} = c_{p,air} \cdot \rho \cdot (1 - f_{rec}) \cdot \varphi_{ventilation} \cdot (\overline{T}^t_{i,air} - T^t_{o,air}) \quad (11.3)$$

$$Q^t_{i-o,infiltration} = c_{p,air} \cdot \rho \cdot \varphi_{infiltration} \cdot (\overline{T}^t_{i,air} - T^t_{o,air}) \quad (11.4)$$

With $c_{p,air}$ the specific heat of air, ρ the density of air, f_{rec} the ventilation recovery factor, $\varphi_{ventilation}$ the ventilation rate in [m3/s] and $\varphi_{infiltration}$ the rate of infiltration in [m3/s].

Internal heat production, based on [116]

The appliances and people also contribute to the heat gains within a building. According to [116], this contribution can be estimated using equation (11.5).

$$Q_{internal} = q_{ig} \cdot A_{floor} \quad (11.5)$$

With q_{ig} the average internal heat production per square meter.

Solar heat gains to the internal air and house enclosure

A part of the incoming solar radiation through windows is absorbed by the internal air. This heat contribution is given by equation (11.6). The other solar irradiance is absorbed by the enclosure. This contribution is given by equation (11.7).

$$Q^t_{i,irradiance} = C_f \cdot Q^t_{irradiance} \quad (11.6)$$

$$Q^t_{e,irradiance} = \alpha_{abs} \cdot (1 - C_f) \cdot Q^t_{irradiance} \quad (11.7)$$

With $Q^t_{i,irradiance}$ the solar heat gains to air, $Q^t_{e,irradiance}$ the solar heat gains to the enclosure, C_f the fraction of solar irradiance that is absorbed by the air and α_{abs} the absorption factor by white walls.

Radiation gains through windows, based on [103]

The radiation gains through all windows, can be calculated using equation (11.8).

$$Q^t_{irradiance} = f_{vervuiling} \cdot f_{beschaduwing} \cdot \sum_{orientation} A_{window,orientation} \cdot ZTA_{window,orientation} \cdot G^t_{Window,orientation} \quad (11.8)$$

$Q^t_{irradiance}$ the received irradiance through radiation, $f_{vervuiling}$ a correction factor to account for pollution. Based on [82], the pollution reduction factor is set to 0.95. $f_{Beschaduwing}$, a factor to account for shading during the heating season. Based on [103], the shading factor of each window is set to 0.8. With $A_{window,orientation}$, the surface area of the window for each orientation, ZTA, the ''Zontoetredingfactor'' at 90° inclination and $G^t_{Window,orientation}$ the incident irradiance on a window with some orientation.

11.1.2 Solar irradiance on windows, based on [104]

We describe the method for calculating the incident irradiance on a window with certain orientation $G^t_{Window,orientation}$. We adopt the formula's for calculating the solar irradiance on a solar module, as presented in [104]. The total irradiance received by a window $G^t_{Window,orientation}$ is then given by (11.9)

$$G^t_{Window,orientation} = G^t_{Window,dir} + G^t_{Window,dif} + G^t_{Window,ground} \quad (11.9)$$

Here, $G^t_{Window,dir}$ is the contribution of direct normal irradiance, $G^t_{Window,dif}$ the contribution of diffuse irradiance and $G^t_{Window,ground}$ the contribution of reflected irradiance from the surrounding ground.

Direct normal irradiance, based on [104]

The direct solar irradiance $G^t_{Window,dir}$ is dependent on the direct solar irradiance I^t_{dir}, solar azimuth, A^t_S and solar altitude a^t_S. In addition, the direct irradiance also depends on the azimuth angle (A_{Window}) and altitude a_{Window} of the windows. The window altitude (a_{Window}) is calculated using equation (11.10) . With θ_{Window} the inclination angle, where the inclination angle is zero for a vertically positioned window.

$$a_W = 90^0 - \theta_{Window} \quad (11.10)$$

Based on [104], the direct normal irradiance $G^t_{WIndow,dir}$ for a window is then given by equation (11.11).

$$G^t_{Window,dir} = I^t_{dir}[\cos(a_{Window})\cos(a^t_S)\cos(A_{Window} - A^t_S) + \sin(a_{Window})\sin(a^t_S)] \quad (11.11)$$

With I^t_{dir} the direct irradiance. According to [104], equation (11.11) only holds for $a^t_S > 0$ and when the solar azimuth A^t_S, is within +/-90^o of the azimuth angle of the window:

$$A_{Window}, A^t_S \in \left[A^t_S - 90^o, A^t_S + 90^o\right], \text{ else } G^t_{window,dir} = 0 \quad (11.12)$$

Indirect diffuse irradiance, based on [104]

The indirect irradiance $G^t_{Window,dif}$ is proportional to the sky view factor (SVF). The SVF factor resembles the fraction of diffuse radiation I^t_{dif} received by the window. The expression for SVF and indirect diffuse irradiation are given respectively by equation (11.13) and equation(11.14).

$$SVF = \frac{1+\cos(\theta_{Window})}{2} \quad (11.13)$$

$$G^t_{Window,dif} = I^t_{dif} \cdot SVF \quad (11.14)$$

With I^t_{dif} the indirect irradiance and θ_{Window} the window angle of inclination.

Reflective irradiance, based on [104]

The reflective irradiance $G^t_{Window,ref}$ can be calculated using equation (11.15) and equation (11.16).

$$G^t_{Window,ref} = GHI \cdot \alpha \cdot (1 - SVF) \quad (11.15)$$

$$GHI = G^t_{window,dir} \cdot \cos(a_s) + G^t_{window,dir} \quad (11.16)$$

With α the albedo coefficient, i.e. the reflection of the surrounding water. GHI the global horizontal irradiance and $G^{t}_{Window,dir}$ the direct normal horizontal radiation.

Heat transfer between internal air and house enclosure

The transport of heat between the protected air volume to the enclosure is dependent on the temperature of each. The heat transfer is governed by a convective heat transfer coefficient, the average temperature of the enclosure $\overline{T}^{t}_{e,enclosure}$, the average temperature of the internal air $\overline{T}^{t}_{i,air}$ and the internal area of the house enclosure (walls and ceiling). Hence, the heat transport per second, between both heat capacitances, may then be given by equation (11.17)

$$Q^{t}_{i-e,convection} = \overline{h}^{t}_{C,i-e} \cdot A_{enclosure} \cdot \left(\overline{T}^{t}_{i,air} - \overline{T}^{t}_{e,enclosure} \right) \qquad (11.17)$$

With $\overline{h}^{t}_{air-house}$ the temperature dependent heat transfer coefficient between the protected air volume and house, $A_{enclosure}$ the surface area of the house, $\overline{T}^{t}_{i,air}$, the average internal air temperature and $\overline{T}^{t}_{e,enclosure}$ the average temperature of the house enclosure.

11.2 Heat pump model: Survey on heat pumps

In this section, a literature study on ground source heat pumps is conducted. Special emphasis was placed on characterising the overall system performance of ground source heat pumps. In section 11.4.1, the general operation principle of two types of ground source heat pumps is presented. In section 11.4.2, the steady state performance of heat pumps is discussed. In section 11.4.3, the seasonal performance is reviewed. In section 11.4.4 the effects of dynamically operating ground source heat pumps are identified. In section 11.4.5, the effects and recommendations on short cycling heat pumps are reviewed. Finally, in section 11.4.6, we present our conclusions based on the literature survey.

11.2.1 Characterising ground source heat pumps

Vapour compression heat pumps

Vapour compression heat pumps use mechanical work to transfer heat from a colder environment to a hotter location. This process has been depicted in Figure 11.2. In this study, a ground heat source or GSHP for short, is considered. A GSHP uses heat from the surrounding earth. Various types of ground source configurations can be distinguished. In our study, a horizontally configured, closed loop heat source is considered. In closed cycle heat sources, the GSHP is connect to a series of tubes that are buried under ground. Using a coolant, circulating within the tubes, heat is transferred from the soil to the coolant. Now, the GSHP system itself contains four main components: Two heat exchangers (2 and 4), a compressor (1) and a expansion valve (3). One heat exchanger, called evaporator (4), is used to extract heat from the coolant to the heat pump system. Using a special fluid, called the refrigerant, energy is carried within the heat pump. In the next step, the refrigerant is compressed (1), raising the pressure of the refrigerant. As a result of the work performed on the refrigerant, it's temperature increases. Using a second heat exchanger, the condenser (2), heat is transferred from the hot refrigerant to the heat carrier of the house: water or air. The hot/warm water/air can then be used for heating and DHW purposes. Finally, the refrigerant passes a pressure valve (3), which returns the refrigerant back to below ambient temperatures as a liquid.

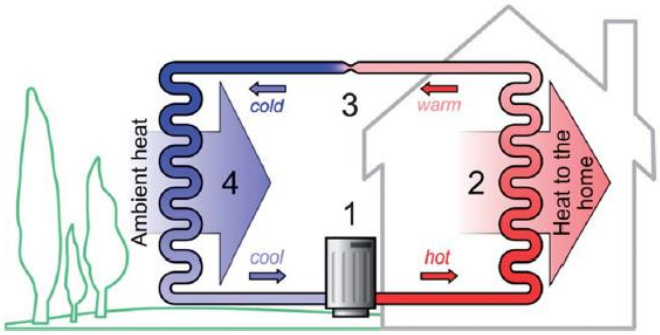

Figure 11.2: Heat pump with vapour compression cycle, adopted from [110]

Heat pump types

The design of heat pumps has changed over the past decades. According to [110], ''*the most basic heat pumps featured a fixed-speed reciprocating compressor that could only operate at full power and so must regularly switch on and off in order to maintain a given internal temperature.*'' In a study on heat pump control strategies from 2008, see [131], it is stated that the on/off control strategy is still widely used. But, as stated in [132], ''*researchers have recently focused on capacity control, primarily by means of variable speed compressors*.'' According to [133], variable speed drive motors (VSD) are commonly used to control the compressor capacity. To that end, inverter based switching circuits are implemented to control the electricity fed to the VSD. According to [131], static expansion valves, as found in on/off based heat pumps, have been replaced by electronic expansion valves. This to operate over a wider range of flow rates, as governed by the temperature and energy output of the heat pump.

On/off versus *variable capacity* based heat pumps.

In response to the development of variable speed compressors, scientists have conducted various experiments to compare the on/off based heat pumps with variable speed heat pumps. In a study from 2007, it was found that, on average, the condenser temperature of on/off based heat pumps is higher, then it is for variable speed types [134],. Consequently, the energy performance of on/off heat pumps is lower compared to variable speed heat pumps. This finding is supported by the work in [135].

In [135], the scholars investigated the performance of both heat pumps, as a function of the dimensioning of the on/off based heat pump. For comparison, the dimensioning of the on/off based heat pump was varied with respect to the ability to cover some percentage of the building peak demand. For evaluation, they compared the annual energy performance and overall system cost of both models. As a result, they found that the variable speed heat pump performs better in terms of seasonal performance. Importantly, this is the case when the on/off heat pump is dimensioned to cover 55% of the buildings peak demand. The decline in annual performance is the result of intensified use of the back-up heaters, having a lower efficiency than the heat pump. However, both types perform equal in terms of energy performance, when the on/off system is oversized. This occurs when the on/off heat pump can cover more than 65% of the buildings peak demand. However, as shown by [135] the economic cost of oversizing the on/off based heat pump do not outweigh the benefits. Hence, we can conclude that the variable speed heat pump performs better in terms of cost and annual energy performance than the on/off based heat pump. Next we will further investigate how to characterise the steady state performance of variable capacity heat pumps.

11.2.2 Steady state GSHP performance

The mechanical work performed by the compressor raises the temperature of the refrigerant at the condenser side. According to [110], it is this process that consumes the most electricity. Commonly, the coefficient of performance (COP) is used to quantify the heat production versus the electricity consumption by the compressor. The COP can then be denoted as in equation (11.18)

$$\mathrm{COP}_{\mathrm{HP}} = \frac{\mathrm{Q}_{\mathrm{heat}}}{\mathrm{E}_{\mathrm{compressor}}} \tag{11.18}$$

With $\mathrm{COP}_{\mathrm{HP}}$ the coefficient of performance of the heat pump, $\mathrm{Q}_{\mathrm{heat}}$ the heat output by the heat pump and $\mathrm{E}_{\mathrm{compressor}}$ the energy fed to the heat pump compressor. The COP as a function of the compressor frequency is depicted in Figure 11.3. A higher compressor frequency results in a higher heat output, but a lower coefficient of performance, as relatively more electricity is required.

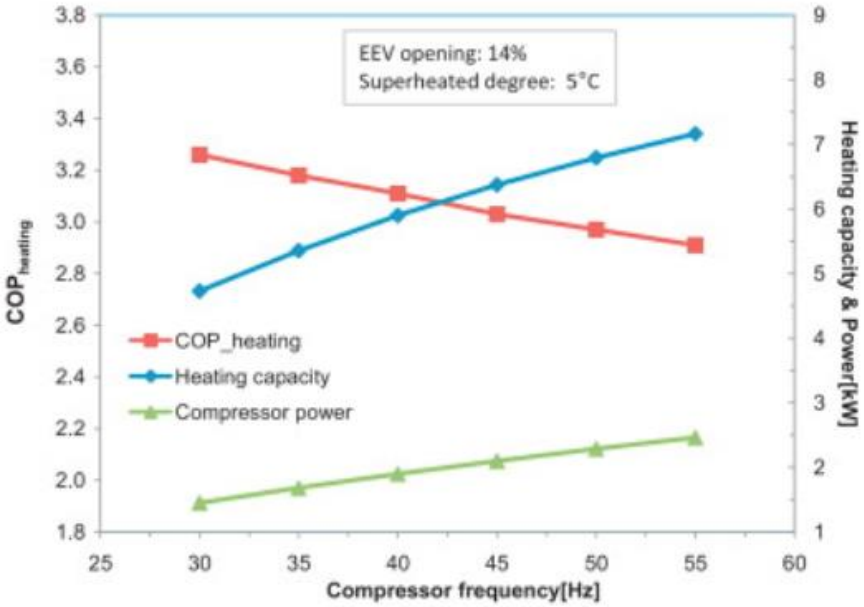

Figure 11.3: The COP as a function of the compressor frequency, adopted from [18] .

Circulation pump losses

Next to the energy consumption of the compressor, two secondary system components also consume considerable amounts of energy as a function of the heat pump capacity. In ground source heat pump systems, two pumps are installed for circulating fluids. One pump circulates brine water along the evaporator and external ground loop. The other pump circulates water along the condenser to provide DHW and heat to the building. We refer to these secondary systems as the external and internal circuit. Now, it follows from several studies, [131]–[133], [136] that the power consumption of these pumps has a significant impact on the energy consumption by the entire heat pump system.

The system COP

To account for the circulation pump losses, equation (11.18) should also include power consumption by the internal and external circuit pumps. Thereby, the coefficient is a measure of the heat pump system performance and can be denoted as in equation (11.19).

$$COP_{system} = \frac{Q_{heat}}{E_{compressor} + E_{parasitic} + E_{pump,external} + E_{pump,internal}} \tag{11.19}$$

Where COP_{system} is the system COP, $E_{pump,external}$ the power consumption by the external pump, $E_{pump,internal}$ the power consumption by the internal pump and $E_{parasitic}$ the parasitic losses due to the consumption of the electronic devices of the heat pump (such as the electronic expansion valves and control system.

The impact of circulation pumps on system COP

Different studies [131], [132], [13], [137] recognise the importance of the *system coefficient of performance*. In [131], two strategies were tested. One strategy was to maximise the heating capacity, whilst the other was to maximise the system COP. According to [131], the latter results in a 12% increase of the system COP and a 5% heating capacity reduction, compared to the capacity maximisation strategy. As seen in [137], the system COP is greatly influenced by the load ratio. THe load ratio was defined as the heat produced by the heat pump versus the heat required by the building. Some of the results by [137] are presented in Figure 11.4. Clearly, a temperature dependent system COP can be distinquished. Also, the system COP is significantly lower at a small load ratio / minimum heat output.

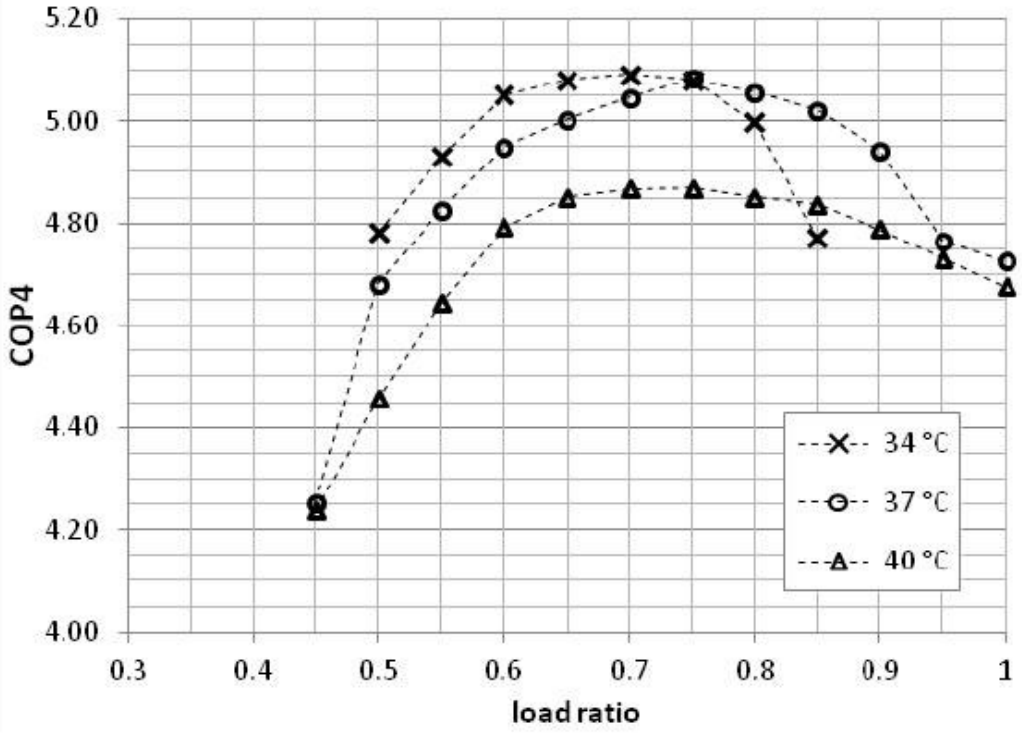

Figure 11.4: System COP for different load ratios and supply temperatures, adopted from [16].

Steady state and seasonal performance

As mentioned by [110], the COP represents a steady state value. The COP is an important characteristic of the heat pump. However, it is widely recognised [131]–[133], [136], [138], that other system losses should also be included when assessing the annual performance of a heat pump. Often, scholars refer to these losses as cycling losses. Cyclic losses can be divided into two categories: standby losses and start-up losses.

Standby losses

As stated in [138], ''*standby losses are mainly caused by the consumption of the electronics , the consumption of the electronic valves and the consumption of the crankcase heater.* '' In [131], the authors refer to standby losses as being the off-cycle pump power consumption and power consumption by the heat pump control systems. Finally, in [110], it is stated that air source heat pumps encounter losses as a result of defrosting the system, when the outdoor temperature is below zero. As the supply temperature of ground sources is often above zero, no defrost losses are encountered for ground source heat pumps.
Important to mention is that the standby losses refer to the losses incurred by the system, when the heat pump is not operating!

Start-up losses

The other cycling losses are related to start-up losses. According to [138], the start-up losses can be attributed to:

- *''The electrical energy losses inherent in the electrical start-up process*.''
    - As stated in [131], *this may be related to the thermal mass of the compressor, other heat pump components and secondary system components.*
- *''The energy necessary to compress the refrigerant from the low pressure side to the high pressure side''*
- *''The energy required to reach operation temperatures''*

11.2.3 Seasonal GSHP performance

Early work on heat pump operation has focussed on heat pumps that continuously switch between zero and full capacity. Now, the process of cycling results in cycling losses. Thereby, cycling is referred to as repeatedly switching on and off the heat pump. By accounting for the cyclic losses, the steady state COP can be adjusted in order to calculate the annual energy performance. Thereby, the seasonal energy performance is an average of all adjusted steady state coefficients. To express the impact of cycling losses, scholars refer to the part load ratio (PLR). According to [132], the partial load ratio can be calculated as in equation (11.20), where t_{on} and t_{off} are the duration of the on and off cycles.

$$PLR = \frac{t_{on}}{t_{on} + t_{off}} = \frac{Q_{building}}{Q_{HP}} \qquad (11.20)$$

Alternatively, as also seen equation (11.20), the PLR may also be expressed as the ratio of the thermal load of the building and heat pump capacity. As stated in [132] ''*the PLR is a parameter that stands for the thermal demand of the building, defined as: the relation between the instantaneous thermal load of the building* $Q_{Building}$ *and the heat pump capacity* Q_{HP}*.* For on/off heat pumps, heat is delivered during each ''on'' period, for as long as the temperature within the building is below a certain temperature setpoint. As this period is dependent on the characteristic of the building, the PLR is a characteristic of the time required to heat the building to comfortable levels. Therefore, the PLR can also be expressed as the ratio of the building instantaneous thermal load and the heat pump heat pump capacity.

Part load is not part capacity

It is important to realise that the PLR is not some percentage of the maximum thermal capacity at which the heat pump operates. Instead, part load or PLR refers to the heat pump cycling mode, resulting in some number of cycles, over the course of a year. This nuance can best be understood by considering a statement from the researchers that originally proposed the PLR in [139]:''*Full load performance is defined as that resulting from continuous operation of the unit, whereas part load performance occurs for cyclic operation.''*

COP at part load

To account for the cycling losses, the steady state COP should be adjusted. According to [131], the part load performance of a heat pump, denoted as $\mathrm{COP}_{\mathrm{PL}}$, is dependent on the *''the cycling rate (PLR)'' and a ''time constant of the heat pump system, which is the response of the system at start-up''.*

As also stated by [131], '*the authors in* [139]*, combined the time constant and cycling rate into a degradation coefficient* $\mathrm{C_D}$ *, which was used to develop a part load correlation.''* Based on this correlation, the authors in [139] have derived an expression that is known as the part load factor (PLF). The PLF is the ratio of the part load performance $\mathrm{COP}_{\mathrm{PL}}$ and the steady state heat pump performance $\mathrm{COP}_{\mathrm{HP}}$. The PLF is given by equation (11.21)

$$\mathrm{PLF} = \frac{\mathrm{COP}_{\mathrm{PL}}}{\mathrm{COP}_{\mathrm{HP}}} = 1 - \mathrm{C_D}(1 - \mathrm{PLR}) \tag{11.21}$$

Here, $\mathrm{C_D}$ is the degradation coefficient. According to [140], equation (11.21) is a US standard. Also, according to [140], the norm is different for ground source heat pumps.

As stated by [138], the PLF for GSHP's, as prescribed by EN14825 standards, was obtained empirically in the work of Anglesio et al. It is given by equation (11.22).

$$\mathrm{PLF} = \frac{\mathrm{PLR}}{\mathrm{C_C} \cdot \mathrm{PLR} + (1 - \mathrm{C_C})} \tag{11.22}$$

With PLR, the load ratio and $\mathrm{C_C}$, a degradation coefficient. Now, using (11.21) or (11.22) the part load performance, related to cycling losses, can be calculated using equation (11.23).

$$\mathrm{COP}_{\mathrm{PL}} = \mathrm{PLF} \cdot \mathrm{COP}_{\mathrm{HP}} \tag{11.23}$$

Impact of cycling losses on annual performance

Using (11.23), one can account for cyclic losses by calculating the PLF. This figure is particularly helpful when calculating the annual energy performance of a ground source heat pump. Thereby, one must realise that this method simply lowers the steady state COP, to account for losses incurred during the off and start up period. Hence, the partial load COP is not an accurate representation of the steady state COP during some time interval! In addition, the PLF does not include the losses related to the circulation pumps. Also, the PLF and PLR have been developed to characterise on/off based heat pumps. Therefore, the PLR/PLF are not necessarily useful when describing variable capacity based heat pumps! Nonetheless, also variable capacity heat pumps may be turned off. To that end, we must further analyse the factors that impact the cyclic losses.

Factors that impact cyclic losses

As shown in [140] and argued by [138], start-up losses can be neglected in some cases. This is true, in case the thermal mass of water in the external circuits is sufficiently large. However, as found by [140], the UNI/EN14825 standard, see equation(11.22), does not perform well for low thermal inertia conditions. According to [140], this is because the start-up losses have been disregarded by the standard. The error that follows from this, can be observed in Figure 11.5. Here, the PLF is a function of the PLR. To account for this error, the authors in [140] have proposed a new method for calculating the PLF. Their ''new method'' is based on the work of [138], in which an expression for the PLF was obtained analytically.

In addition, the effect of stand-by losses on annual average performance may also be disregarded if the ON period is sufficiently large . As stated by [138], ''*the influence of stand-by losses depends on the ratio between the OFF period and the ON period and this ratio increases asymptotically at low thermal loads. That is the reason for the observed fast degradation at low load ratios''* Hence, in case the heat pump can almost run continuously, the effect of stand-by losses diminishes. This asymptotical relation between the PLF and PLR can be observed graphically in figure D5.5 as well.

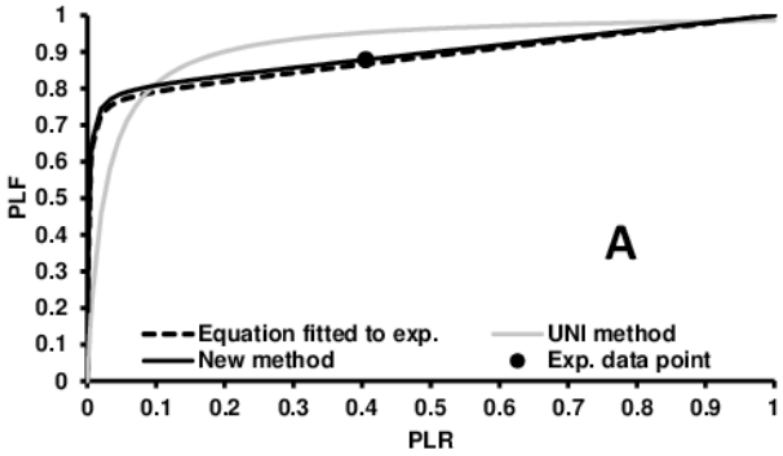

Figure 11.5: PLF/PLR graph, adopted from [23]

Conclusive remarks on cyclic losses

Having quantified the factors that impact the PLF, it must still be stressed, that the PLF is primarily used to characterise the seasonal behaviour of on/off based heat pumps. Nonetheless, we now fully understand the limitations of equation (11.22). According to [140], the UNI/EN14825 standard, as seen in (11.22) achieves good agreement for systems with a water volume of 1000 L. Hence, when modelling heat pump systems, one can only neglect cyclic losses if the thermal inertia of the secondary system is sufficiently large. Given all these considerations, on/off based heat pump can quite accurately be characterised. However, the question remains how one should model the dynamic behaviour of variable speed/capacity heat pumps. In the next section, we will derive some considerations and assumptions as to how to do this, based on the work in [12], [137], [19] and [21].

11.2.4 D6.4 Characterising dynamic GSHP performance

To investigate the dynamic behaviour of variable capacity heat pumps, we differentiate between three scenario's:

1. The transient response at start-up and the effects on output capacity and electrical power consumption
2. The transient response, when running the heat pump in steady state
3. The transient/step response, when adjusting the electrical power input to have the GSHP run at a different output capacity.

Transient response 1 and 2

According to [140], the GSHP system reponse at start-up, in terms of the output of heat and input of electric power is consistent for any thermal inertia (in the secondary circuits) and any load duty (PLR) condition. As stated in [140], ''*the thermal capacity reaches its maximum only after 42-60 s from the onset of start-up, while the electrical power consumption reaches its full value in less than 20 s''.* This effect can be observed in figure 5.6. Here, orange represents the system COP, whereas green represents the electrical power consumption. Clearly, it takes some time before the COP reaches its maximum value, whereas the electrical power consumption is relatively constant. Another phenomena that can be observed is the declining COP and the increasing power consumption. As described by [138], this effect can be explained by considering the changing water inlet temperature at the condensor. As stated in [138], ''*…an increase of the water inlet temperature at the condenser leads to an increase in the pressure ratio and consequently an increase of the compressor consumption and a reduction in the heating capacity''*

Hence, as the inlet temperature of the water at the condensor increases, as a result of heating the water in the secondary circuit, the temperature difference between the evaporator and condensor must increase, to maintain a similar heat output. To that end, the pressure must be increased, which increases the compressor power consumption. However, as the heat output does not remain constant, the COP decreases and so does the heat output.

Quasi steady state

This behaviour is known as the quasi steady state. Given the characteristic response of operating a GSP in quasi steady state, the authors in [138], conclude: ''*The dynamic performance of the HP is almost quasi-steady, i.e., the HP can be considered as working at each instant under steady conditions at the instantaneous values of the inlet water temperatures to the evaporator and condenser.*''

The quasi steady response characteristic of a ground source heat pump is shown in Figure 11.6

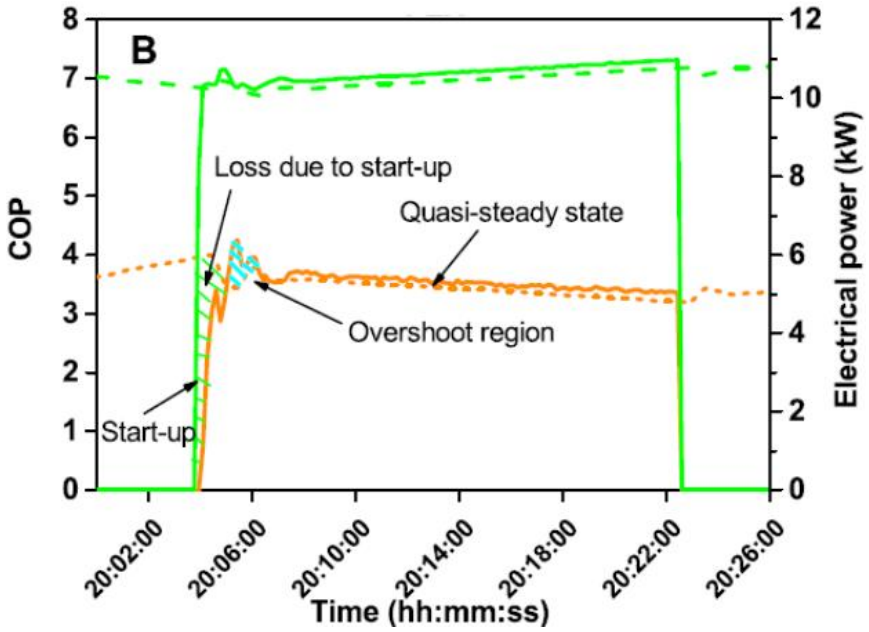

Figure 11.6: GSHP system response at start-up, adopted from [20].

Transient response 3

In [12], the authors analyse the operation of a variable capacity based GSHP, by performing interval analysis with an one hour resolution. Thereto, the heat pump COP is determined for each interval, given some steady state COP and PLF value. To that end, they have used system COP figures based on steady state experiments. Hence, one can estimate the output capacity and electrical consumption by simply taking some fixed characteristics. However, in a non scientific newsletter, published by the european heat pump association (EHPA), constrains for operating variable capacity GSHP's become clear. As seen in Figure 11.7, the heat pump output capacity cannot be adjusted instantly. An explananation follows.

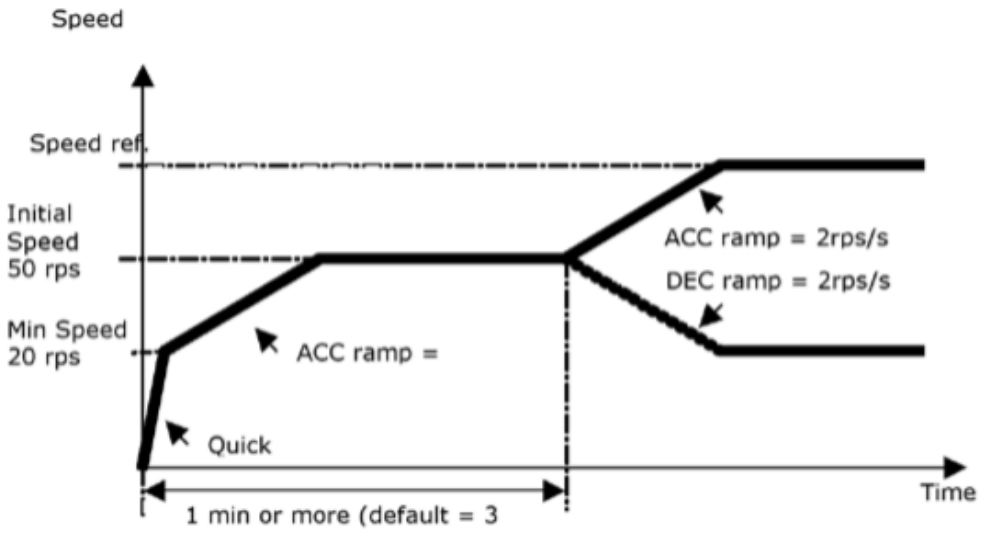

Figure 11.7: Acceleration and deceleration ramps for HP compressor, adopted from [22]

Ramp rates and heat pump control

The system under consideration in [141], is a GHSP with an inverter driven Brushless direct current compressor. Now, as discussed in [141], the HP control system controls the electricity fed to the compressor, electronic expansion valves and secondary circuit pumps.

As stated in [141], ''*the control systems contain all the firmware with the default values provided by the manufacturer for managing the acceleration and deceleration ramps."* To ensure safe operation, the compressor must be protected during start-up. To that end, the ramp rates must be respected, as well as the pressure range over which the heat pump may operate. This can be observed in figure 5.8. At start up, the acceleration ramp takes approximately 1 to 3 minutes. After this period, the HP reaches its nomial power. Hence, contineous operation of variable capacity heat pumps, is constrainted by the acceleration and deceleration ramp rates.

Importantly, according to [133], the pressure difference is not dependent on the flow rate/compressor speed, but on the temperature difference between condenser and evaporator. And as stated by [133]: ''*It is the temperature-related difference between condensor and evaporator that decides the torque on the compressor motor."* Hence, the pressure range is governed by the maximum allowable temperature difference. The heat output is governed by the angular speed of the compressor and pumps.The angular speed and torque together govern the electrical power input to the compressor.

11.2.5 Heat pump short cycling

The ability to ramp up, down or turn off a GSHP, increases its value to serve as flexible load and reduce imbalances. However, short cycling may have disadvantageous effects on heat pump performance and lifetime. Short cycling occurs when heat pump control settings results in run times of less than 10 minutes.

A study on heat pump cycling, see [142], revealed that a minimum run time of circa 6 minutes is required to avoid poor performance (in terms of COP). In addition, the researchers in [142] found that there appears to be an optimum performance (in terms of COP) at around 10 to 15 minutes for ground source heat pumps (GHSP).

In contrast to [142], a study on HP cycling and HP lifetime suggests that extending the runtime can increase the lifetime of the compressor and associated electrical components. The authors in [143] state: ''*we recommend designers and installers to aim for a maximum of 3 or 4 complete 'on/run/off' cycles per hour*.'' The authors in [143] argue that these recommendations may not hold when considering variable speed, inverter driven compressors. This may be interesting as the GSHP systems in Schoonschip are based on variable speed, inverter driven compressors. The authors in [143] stated: ''*Whilst there may still be thermal inefficiencies at start-up, there are no impacts from high start -up currents, and the motor and compressor do not suffer the same electrical and mechanical shocks on starting."*

NIBE ground source heat pump: NIBE FC1255-6PC

To better understand the limitations of the HP systems that will be implemented in Schoonschip (Nibe F1255-6PC), we turn our attention to the manufacturer:

According to Mr. Peter Schipperen, employee at NIBE NL, see interview [144], the F1255-6PC has built-in safety requirements that limits heat pump cycling to a minimum of 20 minutes. Moreover, the HP decreases its output power when approaching the temperature set point, in order to avoid shut down after 20 minutes. According to Mr. Schipperen, it is not a problem to adjust the power output of the heat pump during operation. However, the power output can only be adjusted every minute and the ramp rate is restricted to 20 Hz/minute over a range of 17-120Hz. Finally the interview with Mr. Schipperen revealed that the 6 KW Heat pump system can be operated at a maximum of 8 kW.

In light of the recommendations by [143]. And given the built in safety requirements by Nibe, we can conclude that a minimum runtime of 20 minutes should be considered. We will take this limitation in consideration when designing the flexibility control logic.

11.2.6 Conclusions from literature survey

Two types of heat pumps can be distinguished. Single capacity, on/off based heat pumps and variable capacity heat pumps. The latter use variable speed, inverter powered compressors, electronic pressure valves and inverter driven circulating pumps to adjust the output capacity. Given low energy building, the variable capacity based heat pump outperforms the on/off based heat pump. Both in terms of cost and efficiency.

The steady state performance of the HP system only is expressed in terms of the COP. In variable speed compressors, the energy consumption by circulation pumps is significant. Therefore, the energy consumption by both circulation pumps should be included in the COP. Thereby, the COP is a function of the temperature lift and output capacity.

For calculating the seasonal performance, one uses the partial load ratio (PLR) and part load factor (PLR) to characterise the cyclic losses. The cyclic losses can be attributed to electric losses during standby mode and start-up. Hence, the PLF is a discount factor. It can be used by discounting the impact of cyclic losses with respect to the COP.

The dynamic response of a GSHP can be approximated with the quasi steady state response. The COP only changes as a function of the varying inlet temperature at the condenser. The electricity consumption over time can be assumed constant. The heat output decreases slightly over time.

Short cycling should be avoided to increase the GSHP lifetime and increase system performance. A minimum cycle time of 20 minutes should be taken into account.

11.3 Heat pump model: Heat pump performance characteristics

11.3.1 Comparison of NIBE characteristics and correlation by [110]

In this section, we compare the correlation by [110] with the performance characteristics on the NIBE F1255-6PC heat pump. These characteristics are based on the NEN-EN norm.

NEN-EN norm

The standard rating conditions for evaluating GSHP performance, are given by the norm: NEN-EN 14511 [145]. According to [145], the system COP should be determined at steady state, for the entire HP system. These rating conditions are shown in Table 11.1. For these conditions, the system COP is the ratio of the heat output and total electricity input. The total electricity consumption includes all primary and secondary systems: the compressor, pumps, control system etc.

Table 11.1: NEN-EN 14511 standards for measuring the COP, adopted from [145]

Type of HP	**Evaporator**		**Condenser**
	Type of source	**Temperature [^oC]**	**Temperature [^oC]**
Air source: Air-water	Outside air	7	35 or 45
	Waste heat	20	
Ground source: Water-Water	Water (open)	10	35 or 45
	Brine (closed)	0	

NIBE F1255-6PC performance

The performance characteristics of the NIBE system at nominal power, are shown in Table 11.2. Unfortunately, NIBE does not provide information on the system COP at an output temperature of 60^o Celsius. Therefore, we use a different measure. Instead, the *efficiency factor* for producing domestic hot water, is adopted from the EPC report in [82]. This factor is based upon the conditions as specified by the Dutch norm: NEN7120. It is, however, unclear at which frequency, supply and output temperatures these figures have been derived. Nonetheless, we will use this figure as a rough estimate of the system COP at a supply temperature of 60^o Celsius .

The efficiency factor by [82], are as follows:

- Production efficiency heating: – heat pump - 5,800
- Production efficiency DHW: – heat pump - 2,200
- Production efficiency – back up heaters - 1,0

Comparison between characteristics and correlation

In this section, the NIBE characteristics are compared with the correlation by [110]. To compare the correlation with NIBE specifications, we vary T^t_{out} given a fixed supply temperature T^t_{supply} of 0^o or 10^o Celsius. The results are shown in Table 11.3 and Figure 11.8.

Table 11.2: NIBE GSHP system COP, according to EN 14511 standard. Adopted from [84]

Supply/output Temperatures [C]	COP system [-]	Heat [kW]	Frequency of compressor [hz]
0/35	4.72	3.15	50
0/45	3.61	2.87	50
10/35	6.49	4.30	50
10/45	4.79	3.98	50

Table 11.3: Results of correlation by [110].

Supply/output Temperatures [C]	COP system [-]
0/35	4.4
0/45	3.5
10/35	5.5
10/45	4.4

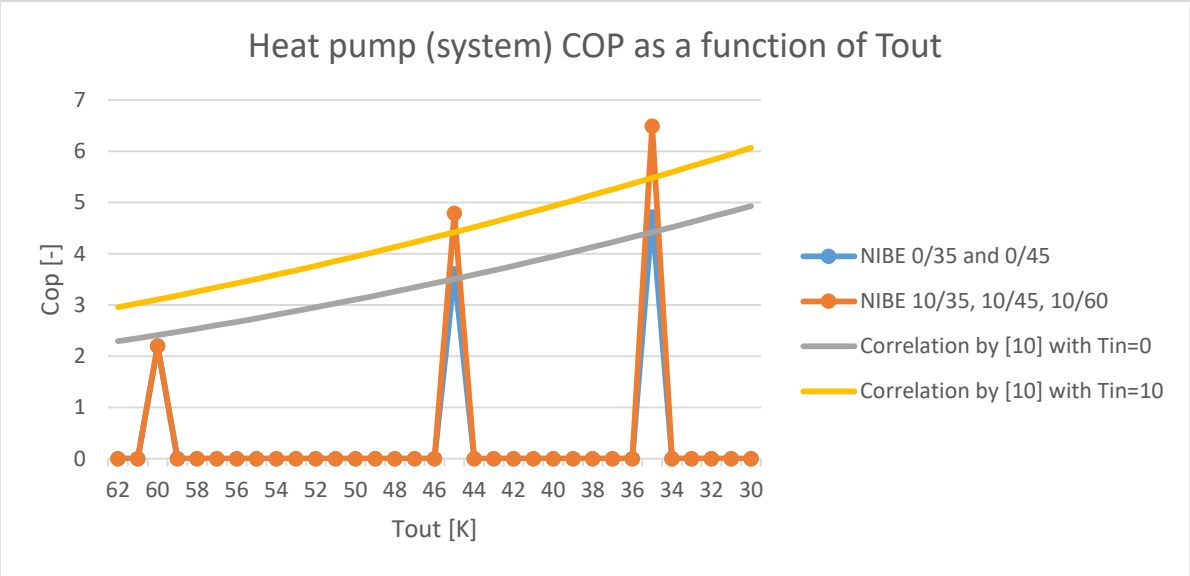

Figure 11.8: The system COP, for fixed inlet temperature and varying outlet temperature.

Appendix B

11.4 Results: input and output variables

Absolute maximum mean solar self-consumption percentage per year

The expression for calculating the absolute maximum mean percentage of solar self-consumption per year, $SSC_{abs\_max}^{year}$ is given by (11.24).

$$SSC_{abs\_max}^{year} = \frac{1}{365} \cdot \sum_{day=1:365} \left(\frac{E_{PV}^{day}}{E_{load}^{day}} \right) \cdot 100\% \tag{11.24}$$

With $E_{PV,F}^{day}$ the total PV electricity production per day, given by equation (11.33) and $E_{load,F}^{day}$ the total electricity consumption per day, given by equation (11.32).

Maximum mean solar self-consumption percentage per year

The expression for calculating the maximum mean percentage of solar self-consumption per year, SSC_{max}^{year}, is given by (11.25).

$$SSC_{max}^{year} = \frac{1}{365} \cdot \sum_{day=1:365} \left(\frac{E_{PV}^{day} - E_{Max,export}^{day}}{E_{load}^{day}} \right) \cdot 100\% \tag{11.25}$$

With $E_{Max,export}^{day}$ the maximum amount of energy exports per day. This value is obtained using a base case scenario, as discussed in chapter 6, section 6.2.1.

Mean solar self-consumption percentage per year

The mean solar self-consumption percentage quantifies the percentage of solar self-consumption for the day-ahead optimization problem. To determine this percentage, information from the base case scenario is used. In addition, a utilisation factor η_{ISSC}^{year} is proposed for evaluating the percentage of indirect solar self-consumption. The expression for calculating the mean percentage of solar self-consumption per year, SSC^{year} is given by equation (11.26).

$$SSC^{year} = SSC_{Max,direct}^{year} + \eta_{ISSC}^{year} \cdot SSC_{Max,indirect}^{year} \tag{11.26}$$

With, $SSC_{Max,direct,F}^{year}$ the maximum mean percentage of direct solar self-consumption per year and $SSC_{Max,indirect,F}^{year}$, the maximum mean percentage of indirect solar self-consumption per year. These values are obtained from the base case scenario, as discussed in chapter 6, section 6.2.1. The utilisation factor for indirect solar self-consumption, η_{ISSC}^{year} is given by equation (11.27).

$$\eta_{SSC}^{year} = \frac{1}{365} \cdot \sum_{day=1:365} \frac{E_{Max,export}^{day}}{E_{Export}^{day}} \tag{11.27}$$

With, E_{Export}^{day} the total amount of energy that is exported per day and, $E_{Max\_Export}^{day}$ the maximum amount of energy exports per day. The latter is obtained from the base case scenario. For more information, consult section 6.2.1.

Number of equivalent full battery cycles

The expression for calculating the number of full equivalent battery cycles per year is given by (11.28).

$$N^{year}_{cycles,bat} = \frac{1}{E^{max}_{SOC}} \cdot \sum_{day=1:365} \left[\sum_{t=1:96} \hat{P}^{t}_{discharge} \cdot \tfrac{1}{4} \delta q \right] \tag{11.28}$$

With E^{max}_{SOC}, the effective battery capacity and $\hat{P}^{t}_{discharge}$ the rate at which energy is discharged from the battery, for some time interval t.

Cost and benefits of importing or exporting energy

The expression for calculating the annual cost of importing energy from the main grid is given by equation (11.29). The expression for calculating the annual benefits of exporting energy to the main grid is given by equation (11.30).

$$\mathbb{C}^{year}_{import} = \sum_{day=1:365} \left[\sum_{h=1:24} \left(\hat{P}^{h}_{import} \cdot p^{h}_{DA} \right) \right] \tag{11.29}$$

$$\mathbb{R}^{year}_{export} = \sum_{day=1:365} \left[\sum_{h=1:24} \left(\hat{P}^{h}_{export,F} \cdot p^{h}_{DA} \right) \right] \tag{11.30}$$

With $\hat{P}^{h}_{import}$ and $\hat{P}^{h}_{export}$ the rate at which energy is imported or exported for some hour h and. p^{h}_{DA} .the day-ahead market prices for that same hour h.

Net electricity cost

The expression for calculating the net electricity cost per year is given by equation (11.31).

$$\mathbb{C}^{year}_{net,electricity} = -\mathbb{C}^{year}_{import} + \mathbb{R}^{year}_{export} \tag{11.31}$$

Total daily electricity consumption and production

The total forecasted electricity consumption is given by equation (11.32). The total forecasted PV electricity production is given by equation (11.33). The total amount of scheduled energy exports per day is given by equation (11.34) The total amount of scheduled energy imports per day is given by equation (11.35). The expression for calculating the annual electricity consumption by the heat pump, is given by (11.36)

$$E^{day}_{load} = \sum_{t=1:96} (P^{t}_{Electricity} + \hat{P}^{t}_{HP} + \hat{P}^{t}_{S1,coil} + \hat{P}^{t}_{S1,coil}) \cdot \tfrac{1}{4} \delta q \tag{11.32}$$

$$E^{day}_{PV} = \sum_{t=1:96} P^{t}_{PV} \cdot \tfrac{1}{4} \delta q \tag{11.33}$$

$$E^{day}_{export} = \sum_{h=1:24} \hat{P}^{h}_{export} \cdot \tfrac{1}{4} \delta q \tag{11.34}$$

$$E^{day}_{import} = \sum_{h=1:24} \hat{P}^{h}_{import} \cdot \tfrac{1}{4} \delta q \tag{11.35}$$

$$E^{year}_{HP+coils} = \sum_{day=1:365} \left[\sum_{t=1:96} (\hat{P}^{t}_{HP} + \hat{P}^{t}_{S1,coil} + \hat{P}^{t}_{S2,coil}) \cdot \tfrac{1}{4} \cdot \delta q \right] \tag{11.36}$$

With, $P^{t}_{Electricity,F}$ the non-thermal based electricity consumption, $\hat{P}^{t}_{HP}$ the thermal based electricity consumption by the heat pumps, $\hat{P}^{t}_{S1,coil}$, $\hat{P}^{t}_{S2,coil}$ the thermal based electricity consumption by the electrical coils, P^{t}_{PV} the PV electricity production, $\hat{P}^{t}_{export}$ and $\hat{P}^{t}_{import}$ the power that is exported/imported per hour.

Tank temperature violations

The expression with which we assess the violation of the minimum temperature of tank S1, $T^{t}_{S1,error}$ and the number of incidents $N^{year}_{S1,error}$ is given by equation (11.37). A similar equation is used for tank S2.

$$\text{if } \left\{ T^{t}_{S1} < 55^{o}C \right\} \text{ then } \begin{matrix} N^{year}_{S1,error} = N^{year}_{S1,error} + 1 \\ T^{t}_{S1,error} = 55 - T^{t}_{S1} \end{matrix} \tag{11.37}$$

The expression for calculating the annual mean temperature error is given by equation (11.38).

$$\mu^{year}_{S1,error} = \frac{\sum_{day=1:365} \left[\sum_{t=1:96} T^{t}_{S1,error} \right]}{N^{year}_{S1,error}} \tag{11.38}$$

Appendix C

11.5 Matlab simulation model description

In this section, we describe the different parts, parameters and inputs of the simulation model. First we describe the general outline of the simulation model. Subsequently, we present each part in more detail.

11.5.1 General outline of simulation model software

The simulation model has been in implemented in Matlab in four separate M-files. The information exchange between the M-files is shown schematically in Figure 11.9. Note that the thermal models are implemented twice. Once the thermal models are solely used for calculating the thermal based electricity demand, based on forecasted energy flows. In the second application, the thermal models are used to quantify the thermal based electricity consumption and availability of thermal flexibility.

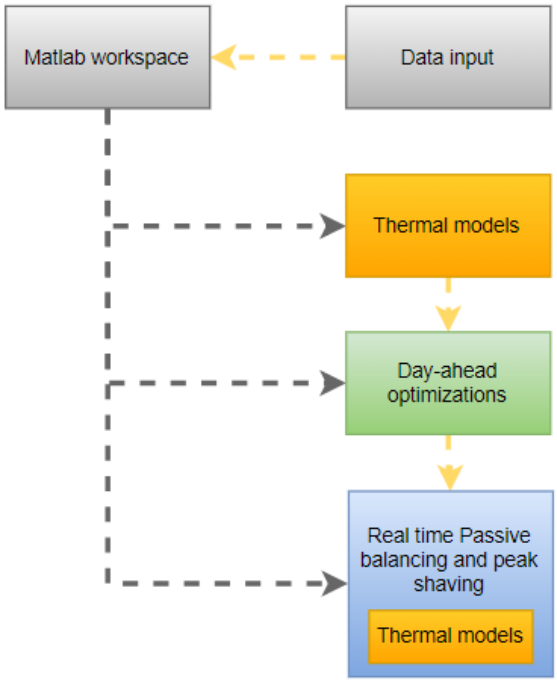

Figure 11.9: Schematic overview of simulation model in four M-files

11.5.2 Data input

Shown in Figure 11.10 is the M-file that contains various parts for importing and pre-processing the data from excel files. Also shown are the required data collections and parameters that can be altered by the user. The pre-processed data is stored in the Matlab workspace.

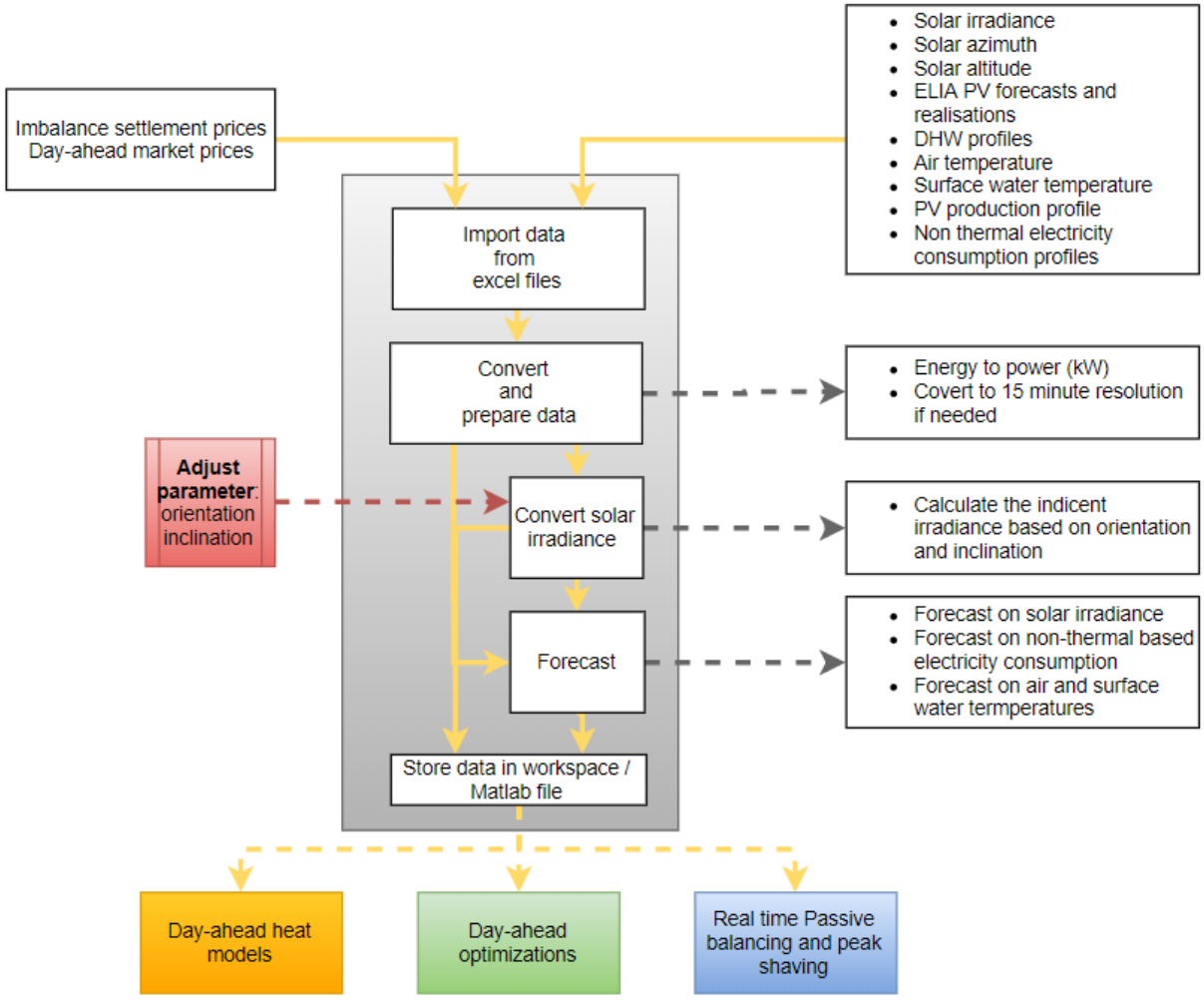

Figure 11.10: Schematic overview of M-file for data import and data pre-processing

11.5.3 Heat models

Shown in Figure 11.11 is a schematic representation of the M-file that contains the mathematical formulations of the thermal models. Also shown are the required data collections and parameters that can be altered by the user to perform experiments. The output of the M-file is stored in the Matlab workspace. Note that mostly forecasted data collections are used from the workspace. The output of this M-file is used as input for the day-ahead optimizations.

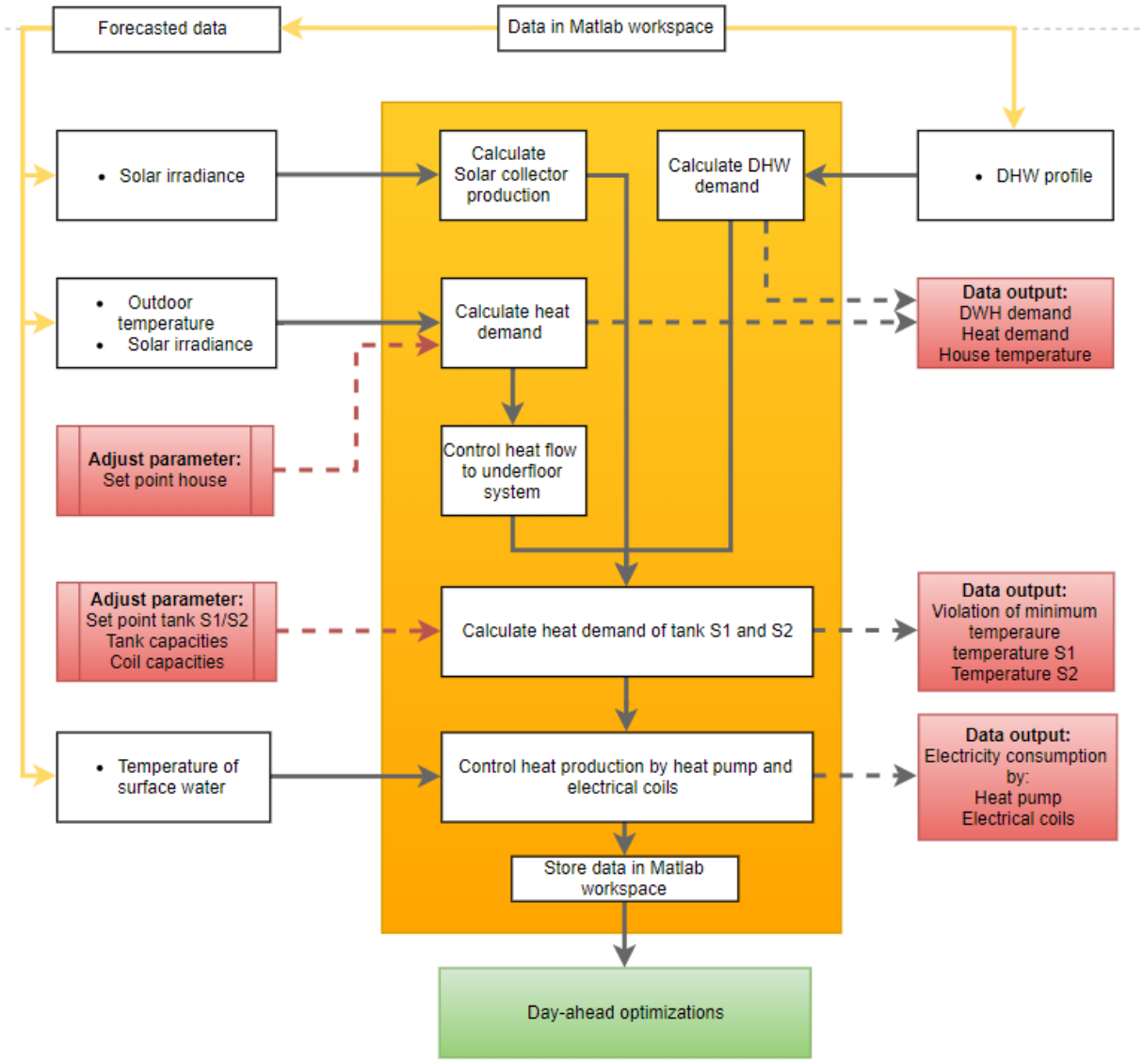

Figure 11.11: Schematic overview of M-file with the thermal models

Day-ahead optimizations

Shown in Figure 11.12 is a schematic overview of the M-file that contains the linear programming optimization. Also shown are the required data collections and parameters that can be altered by the user to perform experiments. In addition, the user can differentiate between the use of day-ahead market prices or dual electricity prices. Also, the user can choose the use an exact or heuristic solver. The output of the M-file is stored in the Matlab workspace.

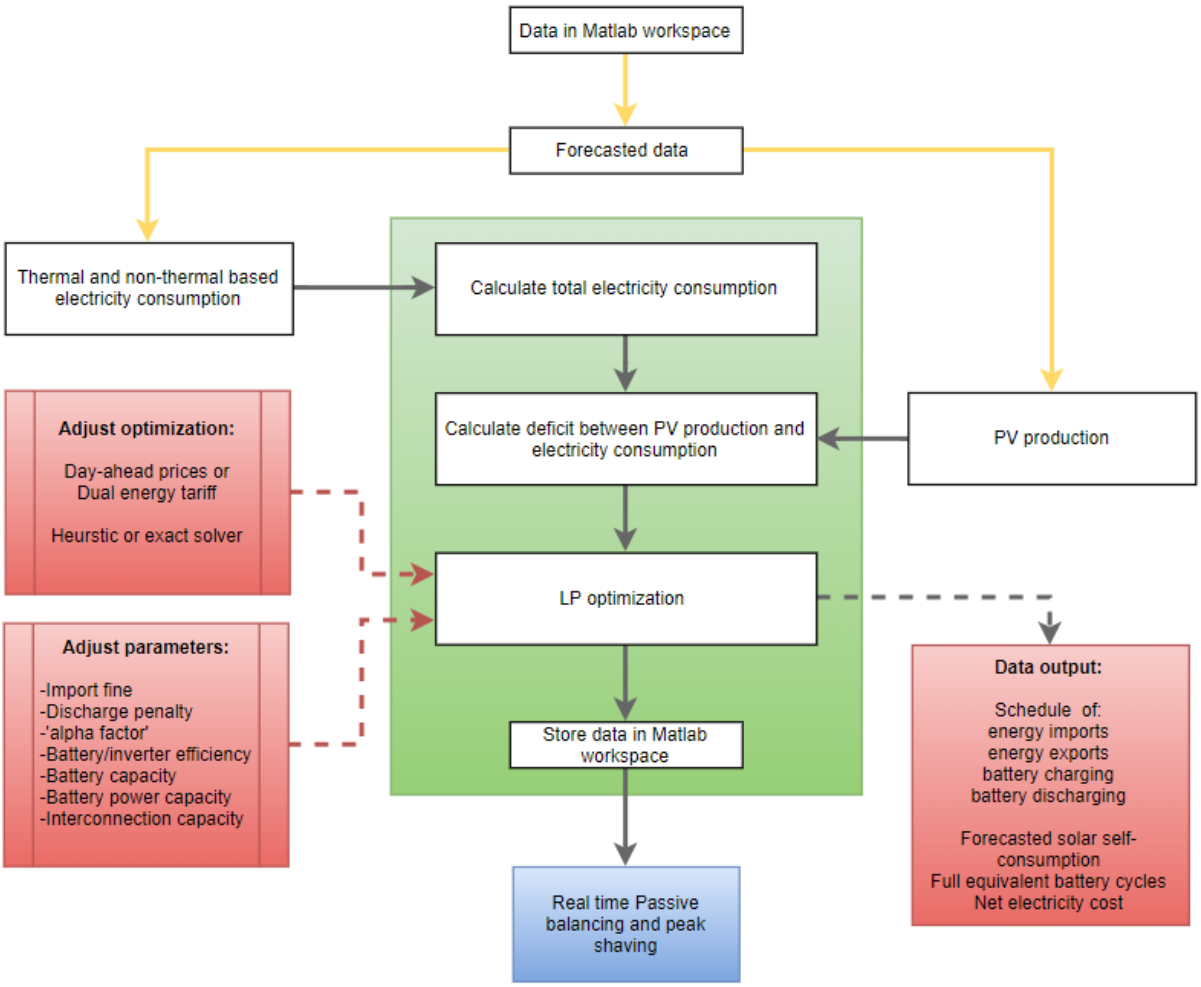

Figure 11.12: Schematic overview of M-file for day-ahead optimizations

Passive balancing and peak shaving

Shown in Figure 11.13 is a schematic overview of the M-file that contains the formulation of the passive balancing and peak shaving models and decision software. Also shown are the required data collections and parameters that can be altered by the user to perform experiments. The output of the M-file is stored in the Matlab workspace. Note that this M-file also contains the thermal models as presented in figure Figure 11.11.

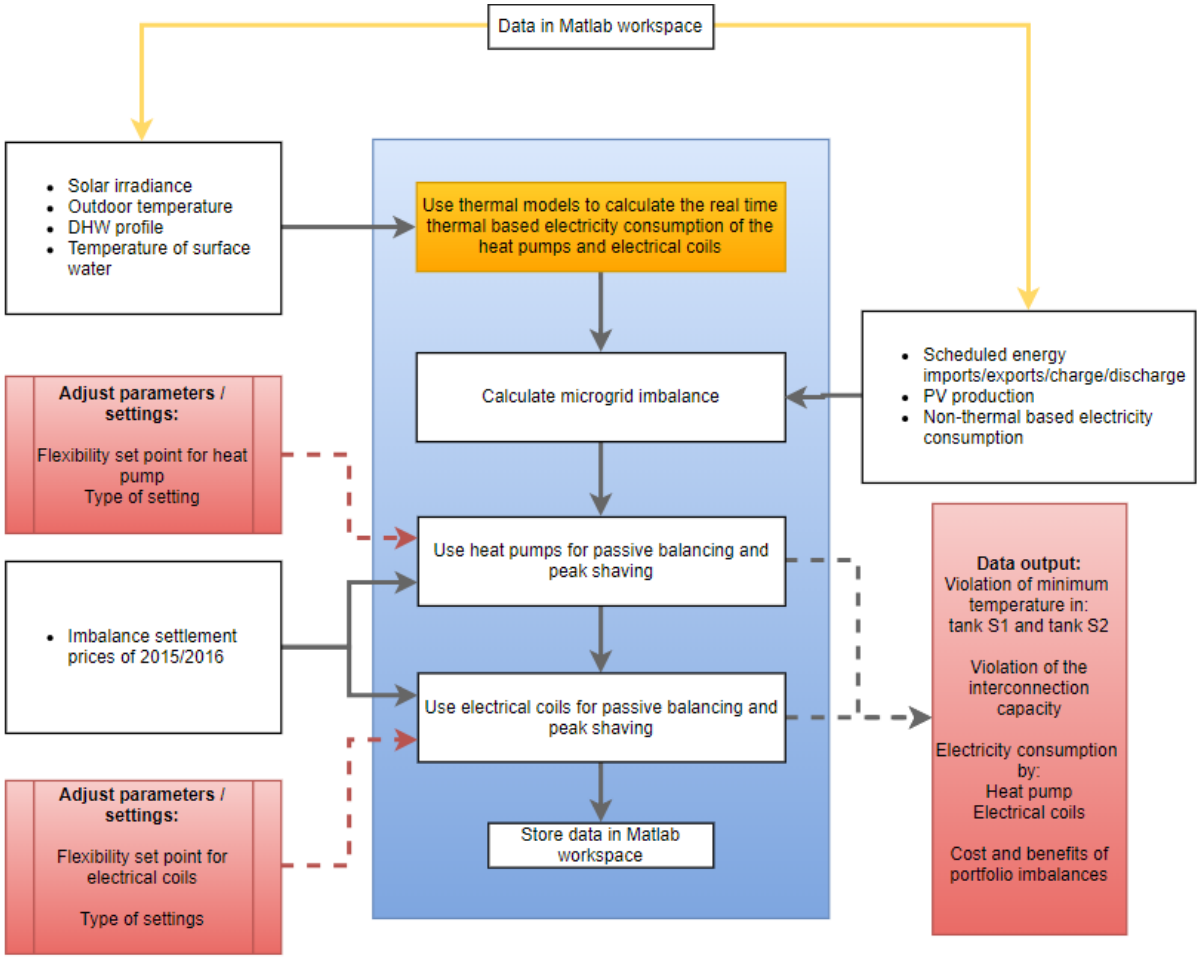

Figure 11.13: Schematic overview of M-file for passive balancing and peak shaving

List of abbreviations

Table 11.4: List of abbreviations	
BRP	*Balancing responsible party*
CF	*Convection factor*
COP	*Coefficient of performance of heat pump*
COP_{GSHP}	*Coefficient of performance of ground source heat pump*
DER	*Distributed energy resources*
DG	*Distributed generation*
DR	*Demand response*
DMS	*Demand side management*
DSO	*Distribution system operator*
EAN	*Identification number for grid connection*
EMS	*Energy management system*
EPEX spot	*Dutch electricity wholesale market*
HP	*Heat pump*
LEM	*Local energy management*
MG	*Microgrid*
MAS	*Multi-agent system*
PTU	*Programme time unit (15 minutes)*
SES	*Smart energy system*
RES	*Renewable energy resource*
TSO	*Transmission system operator*
VPP	*Virtual power plant*
ZTA	*Zonnetoetredingsfactor*

List of symbols

Table 11.5: List of symbols I

Endogenous variables

• Power	$\hat{P}$	[W]
• Energy	$\mathbb{E}$	[J]
• Cost	$\mathbb{C}$	[€]

Exogenous variables / parameters

• Power	P	[W]
• Energy	E	[J]
• Price	p	[€/J]

Subscripts

• e	House enclosure	[-]
• fl	floor heating system	[-]
• i	Internal air temperature	[-]
• o	Outside air temperature	[-]

Superscript

• t	15 minute timeslot
• h	1 hour timeslot
• day	1 day timeslot
• year	1 year timeslot

Time notation

• δq	One hour time interval	[s]

Table 11.6: List of symbols II

Variables	Meaning	Unit
α_{abs}	Solar radiation absorption coefficient of white walls	[-]
$A_{enclosure,orientation}$	Surface area of walls/roof for some orientation	[m2]
A_{floor}	Area of heated floor	[m2]
A_{S1}	Surface area of buffer tank S1	[m2]
A_{S2}	Surface area of buffer tank S2	[m2]
$A_{window,orientation}$	Surface area of windows for some orientation	[m2]
C_f	The fraction of absorbed solar radiation by internal air	[-]
$c_{enclosure}$	Specific heat capacity of house	[J/K·m3]
$c_{p,air}$	Specific heat capacity air	[J/K·m3]
$c_{p,concrete}$	Specific heat capacity concrete	[J/K·m3]
COP^{t}_{GSHP}	Coefficient of performance of heat pump	[-]
C_{S1}, C_{S2}	Heat capacity of buffer tank S1 and S2	[J/K]
$\mathbb{C}^{t}_{Bat}$	Cyclic battery degradation cost for one quarter	[€]
$\mathbb{C}^{Day}_{netto}$	Cost of energy and battery cycling for some day	[€]
$E^{Day,max}_{Export}$	Total maximum export for some day	[J]
$E^{Day,max}_{Import}$	Total maximum import for some day	[J]
E^{max}_{SOC}	Maximum battery state of charge (SOC)	[J]
E^{t}_{SOC}	Battery state of charge	[J]
$f_{Beschaduwing}$	Factor to account for shading of windows	[-]
f_{rec}	Heat recovery factor for ventilation	[-]
$f_{vervuiling}$	Correction factor for pollution incoming solar radiance	[-]
$G^{t}_{Window,dif}$	Diffuse solar irradiance on a window	[J/m2]
$G^{t}_{Window,dir}$	Direct normal solar irradiance on window	[J/m2]
$G^{t}_{Window,ground}$	Reflected solar irradiance on window	[J/m2]
$G^{t}_{Window,orientation}$	The total solar irradiance on a vertical window	[J/m2]
$\bar{h}^{t}_{C,i-e}$	Convective heat transfer coefficient, air to enclosure	[J/m2K]
$\bar{h}^{t}_{C,fl-i}$	Convective heat transfer coefficient, floor to air	[J/m2K]
$h_{enclosure}$	Height of the house	[m]
$\bar{h}^{t}_{R,fl-e}$	Radiative heat transfer coefficient, floor to enclosure	[J/m2K]

$h_{S1/S2}$	Heat transfer coefficient of insulation S1 and S2	[J/m·K]
$l_{enclosure}$	thickness of the house	[m]
P^t_{load}	Electricity consumption	[W]
P^t_{PV}	Solar electricity production	[W]
p^{deg}_{Bat}	Virtual cyclic battery degradation cost	[€/J]
p^h_{DA}	Day-ahead market prices	[€/J]
p_{fine}	Penalty for importing energy	[€/J]
p_{slack}	Virtual cost of relaxing constraints with slack variable	[€/J]
$\hat{P}^t_{charge}$	Charge rate (decision variable)	[W]
$\hat{P}^t_{discharge}$	Discharge rate (decision variable)	[W]
$\hat{P}^h_{export}$	Grid export (decision variable)	[W]
$\hat{P}^t_{HP}$	Electricity fed to heat pump	[W]
$\hat{P}^t_{imbalance,R}$	Real time microgrid imbalance	[W]
P^{max}_{inter}	Maximum interconnection capacity	[W]
$\hat{P}^h_{import}$	Grid import (decision variable)	[W]
$\hat{P}^t_{slack}$	Slack variable (decision variable)	[W]
$\hat{P}^t_{S1,coil}$	Electricity fed heating coil in buffer tank S1	[W]
$\hat{P}^t_{S2,coil}$	Electricity fed heating coil in buffer tank S2	[W]
q_{ig}	The internal heat production	[W/m2]
$Q^t_{C,fl-i}$	Convective heat transfer from floor to internal	[J/s]
Q^t_{DHW}	DHW heat demand	[J/s]
Q^t_{DHW1}	DHW heat extracted from buffer tank S1	[J/s]
Q^t_{DHW2}	DHW heat extracted from buffer tank S2	[J/s]
$Q^t_{i-e,convection}$	Convective heat loss from internal air to enclosure	[J/s]
$Q^t_{i-o,Infiltration}$	Infiltration losses from internal air to outside air	[J/s]
$Q^t_{i-o,Ventilation}$	Heat losses through ventilation	[J/s]
$Q^t_{i-o,trans}$	Transmission losses via window from air to outside air	[J/s]
$Q_{i,Internal}$	Heat gains from people/appliances	[J/s]
$Q^t_{i,Irradiance}$	Solar radiation heat gains to internal air	[J/s]
$Q^t_{e,Irradiance}$	Solar radiation heat gains to enclosure	[J/s]
Q^t_{heat}	Heat from Buffer S2 to floor	[J/s]
Q^t_{HP}	Heat supplied to buffer tanks	[J/s]

Q^t_{HP1} / Q^t_{HP2}	Heat supplied to buffer tank S1/S2	[J/s]
$Q^t_{R,fl-e}$	Radiative heat transfer from floor to enclosure	[J/s]
Q^t_{SC1}	Solar collector heat supplied to buffer tank S1	[J/s]
Q^t_{SC2}	Solar collector heat supplied to buffer tank S2	[J/s]
Q^t_{S1loss}	Heat losses by buffer tank S1	[J/s]
Q^t_{S2loss}	Heat losses by buffer tank S2	[J/s]
$\overline{T}^t_{b,enclosure}$	Average house enclosure temperature	[K]
$\overline{T}^t_{fl,floor}$	Average floor temperature	[K]
$\overline{T}^t_{house}$	Average indoor temperature of the house	[K]
$\overline{T}^t_{i,air}$	Average internal air temperature	[K]
$\overline{T}^t_{S1}$	Average temperature of buffer tank S1	[K]
$\overline{T}^t_{S2}$	Average temperature of buffer tank S2	[K]
$T^{min}_{S1,}, T^{min}_{S2}, T^{max}_{S1,}, T^{max}_{S2}$	Minimum and maximum temperature of buffer tanks	[K]
$T^{setpoint}_{S1,HP}, T^{setpoint}_{S2,HP}$	Setpoint temperature for supplying heat by HP	[K]
$T^{setpoint}_{S1,coil}, T^{setpoint}_{S2,coil}$	Setpoint temperature for supplying heat by coils	[K]
$\overline{T}^{max}_{floor}$	Maximum floor temperature	[K]
$\overline{T}^{setpoint}_{house}$	Setpoint temperature of the house	[K]
T^t_{out}	Outlet temperature of heat pump	[K]
T^t_{supply}	Supply temperature of heat exchanger	[K]
$\overline{T}^t_{waterworks}$	Average water duct temperature	[K]
ΔT^t	Temperature lift by heat pump	[K]
$U_{enclosure,orientation}$	Overall heat transfer coefficient for walls and roof	[W/m3K]
$U_{window,orientation}$	Overall heat transfer coefficient for windows	[W/m3K]
V_{air}	Volume of air within protected volume	[m3]
V_{S2} / V_{S1}	Volume of buffer tank S1/S2	[m3]
ZTA	Coefficient on solar irradiance received by window	[-]
$\varphi_{ventilation}$	The rate of ventilation	[m3/s]
$\varphi_{infiltration}$	The rate of infiltration	[m3/s]
$\phi^t_{V,heat}$	Volume flow rate of water from S2 to floor	[m3/s]
$\phi^t_{V,maxheat}$	Maximum volume flow rate of water from S2 to floor	[m3/s]
η_{DHW}	DHW distribution efficiency	[-]
η_{Bat}	Charge/Discharge efficiency battery/inverter	[-]

Bibliography

[1] CBS, “share-of-renewable-energy,” 2018. [Online]. Available: https://www.cbs.nl/en-gb/news/2017/22/share-of-renewable-energy-at-5-9-in-2016. [Accessed: 05-Mar-2018].

[2] TNO, “FLEXIBILITEIT ÉN ZEKERHEID ESSENTIEEL IN TOEKOMSTBESTENDIG ENERGIESYSTEEM,” 2015. [Online]. Available: https://www.tno.nl/nl/aandachtsgebieden/energie/roadmaps/sustainable-energy/smart-energy-system-solutions/flexibiliteit-en-zekerheid-essentieel-in-toekomstbestendig-energiesysteem/. [Accessed: 05-Mar-2018].

[3] ECN, “FLEXibility of the power system in the NETherlands.” [Online]. Available: https://www.ecn.nl/nl/nieuws/item/zes-keer-meer-vraag-naar-flexibiliteit-in-2050-rol-voor-opslag-kleiner-dan-gedacht/. [Accessed: 05-Mar-2018].

[4] F. Braam, R. Hollinger, F. Braam, R. Hollinger, C. Lübeck, S. Müller, and B. Wille-haussmann, “Grid-Oriented Operation of Photovoltaic- Battery Systems Grid-Oriented Operation of Photovoltaic-Battery Systems,” no. January 2013, 2015.

[5] Solasave, “Can we store energy generated from our solar panels?” [Online]. Available: https://www.solasave.co.uk/blog/2015-06/60/can-we-store-energy-generated-from-our-solar-panels.html. [Accessed: 05-Mar-2018].

[6] CBS, “Toename elektrische auto’s zet door,” *2-17*. [Online]. Available: https://www.cbs.nl/nl-nl/nieuws/2017/21/toename-elektrische-auto-s-zet-door. [Accessed: 05-Mar-2018].

[7] CBS, “Warmtepompen; aantallen, thermisch vermogen en energiestromen.” [Online]. Available: http://statline.cbs.nl/StatWeb/publication/?VW=T&DM=SLNL&PA=82380NED&LA=NL. [Accessed: 05-Mar-2018].

[8] D. Pudjianto, P. Djapic, M. Aunedi, C. K. Gan, G. Strbac, S. Huang, and D. Infield, “Smart control for minimizing distribution network reinforcement cost due to electrification,” *Energy Policy*, vol. 52, pp. 76–84, 2013.

[9] L. J. de Vries, A. F. Correljé, and H. P.A. Knops, “Electricity: Market design and policy choices,” 2010.

[10] E. Vastgoed, “Dossier: Salderen zonnepanelen,” *2014*. [Online]. Available: http://www.energievastgoed.nl/dossiers/dossier-salderen-zonnepanelen/. [Accessed: 26-Feb-2018].

[11] E. van der Hoofd, “Demandresponse en balancering,” 2015.

[12] X. Fang, S. Misra, G. Xue, and D. Yang, “Smart Grid — The New and Improved Power Grid: A Survey,” *IEEE Commun. Surv. Tutorials*, vol. 14, no. 4, pp. 944–980, 2012.

[13] M. Soshinskaya, W. H. J. Crijns-Graus, J. M. Guerrero, and J. C. Vasquez, “Microgrids: Experiences, barriers and success factors,” *Renew. Sustain. Energy Rev.*, vol. 40, pp. 659–672, 2014.

[14] B. P. Koirala, E. Koliou, J. Friege, R. A. Hakvoort, and P. M. Herder, “Energetic communities for community energy: A review of key issues and trends shaping integrated community energy systems,” *Renew. Sustain. Energy Rev.*, vol. 56, pp. 722–744, 2016.

[15] C. Eid, P. Codani, Y. Perez, J. Reneses, and R. Hakvoort, “Managing electric flexibility from Distributed Energy Resources: A review of incentives for market design,” *Renew. Sustain. Energy Rev.*, vol. 64, pp. 237–247, 2016.

[16] S. Community, “Schoonschip,” 2018. [Online]. Available: http://schoonschipamsterdam.org/. [Accessed: 01-Apr-2018].

[17] J. Hoppmann, J. Volland, T. S. Schmidt, and V. H. Hoffmann, “The economic viability of battery storage for residential solar photovoltaic systems - A review and a simulation model,” *Renew. Sustain. Energy Rev.*, vol. 39, pp. 1101–1118, 2014.

[18] D. Pudjianto, D. Pudjianto, C. Ramsay, C. Ramsay, G. Strbac, and G. Strbac, “Virtual power plant and system integration of distributed energy resources,” *Renew. Power Gener. IET*, vol. 1, no. 1, pp. 10–16, 2007.

[19] C. Eid, P. Codani, Y. Chen, Y. Perez, and R. Hakvoort, “Aggregation of demand side flexibility in a smart grid: A review for European market design,” *Int. Conf. Eur. Energy Mark. EEM*, vol. 2015–Augus, no. April, 2015.

[20] C. Eid, E. Koliou, M. Valles, J. Reneses, and R. Hakvoort, “Time-based pricing and electricity demand response: Existing barriers and next steps,” *Util. Policy*, vol. 40, pp. 15–25, 2016.

[21] M. Alizadeh, X. Li, Z. Wang, A. Scaglione, and R. Melton, “Demand-side management in the smart grid: Information processing for the power switch,” *IEEE Signal Process. Mag.*, vol. 29, no. 5, pp. 55–67, 2012.

[22] R. Deng, Z. Yang, M. Y. Chow, and J. Chen, “A survey on demand response in smart grids: Mathematical models and approaches,” *IEEE Trans. Ind. Informatics*, vol. 11, no. 3, pp. 570–582, 2015.

[23] F. N. Claessen and H. La Poutré, “Towards a European smart energy system,” *EIT ICT Labs*, 2014.

[24] Eurelectric, “Flexibility and aggregation - requirements for their interaction in the market,” *Ieee Trans. Power Syst.*, vol. 30, no. January, p. 13, 2015.

[25] USEF Foundation, *USEF: The Framework Explained*. 2015.

[26] C. Eid, L. A. Bollinger, B. Koirala, D. Scholten, E. Facchinetti, J. Lilliestam, and R. Hakvoort, “Market integration of local energy systems: Is local energy management compatible with European regulation for retail competition?,” *Energy*, vol. 114, pp. 913–922, 2016.

[27] L. Bosc?n and R. Poudineh, *Business Models for Power System Flexibility: New Actors, New Roles, New Rules*. Elsevier Inc., 2016.

[28] K. Kok, Z. Derzsi, J. Gordijn, M. Hommelberg, C. Warmer, R. Kamphuis, and H. Akkermans, “Agent-based electricity balancing with distributed energy resources, a multiperspective case study,” *Proc. Annu. Hawaii Int. Conf. Syst. Sci.*, no. March, 2008.

[29] C. Hügel, “Interview with Mr. Eric Woittiez, program manager of the Koplopers project.” 2017.

[30] D. T. Ton and M. A. Smith, “The U.S. Department of Energy’s Microgrid Initiative,” *Electr. J.*, vol. 25, no. 8, pp. 84–94, 2012.

[31] P. Asmus, “Microgrids, Virtual Power Plants and Our Distributed Energy Future,” *Electr. J.*, vol. 23, no. 10, pp. 72–82, 2010.

[32] C. Marnay, *Microgrids: Finally Finding their Place*. Elsevier Inc., 2016.

[33] S. M. Nosratabadi, R. A. Hooshmand, and E. Gholipour, “A comprehensive review on microgrid and virtual power plant concepts employed for distributed energy resources scheduling in power systems,” *Renew. Sustain. Energy Rev.*, vol. 67, pp. 341–363, 2017.

[34] A. Bagherian and S. M. Moghaddas Tafreshi, “A developed energy management system for a microgrid in the competitive electricity market,” *2009 IEEE Bucharest PowerTech Innov. Ideas Towar. Electr. Grid Futur.*, pp. 1–6, 2009.

[35] C. Chen, S. Duan, T. Cai, B. Liu, and G. Hu, “Smart energy management system for optimal microgrid economic operation,” *IET Renew. Power Gener.*, vol. 5, no. 3, p. 258, 2011.

[36] X. Kong, L. Bai, Q. Hu, F. Li, and C. Wang, “Day-ahead optimal scheduling method for grid-connected microgrid based on energy storage control strategy,” *J. Mod. Power Syst. Clean Energy*, vol. 4, no. 4, pp. 648–658, 2016.

[37] A. G. Tsikalakis and N. D. Hatziargyriou, “Centralized control for optimizing microgrids operation,” *IEEE Trans. Energy Convers.*, vol. 23, no. 1, pp. 241–248, 2008.

[38] T. Logenthiran, D. Srinivasan, A. M. Khambadkone, and H. N. Aung, “Multiagent system for real-time operation of a microgrid in real-time digital simulator,” *IEEE Trans. Smart Grid*, vol. 3, no. 2, pp. 925–933, 2012.

[39] S. Kahrobaee, R. A. Rajabzadeh, L. K. Soh, and S. Asgarpoor, “A multiagent modeling and investigation of smart homes with power generation, storage, and trading features,” *IEEE Trans. Smart Grid*, vol. 4, no. 2, pp. 659–668, 2013.

[40] L. Shi, Y. Luo, and G. Y. Tu, “Bidding strategy of microgrid with consideration of uncertainty for participating in power market,” *Int. J. Electr. Power Energy Syst.*, vol. 59, pp. 1–13, 2014.

[41] G. Ferruzzi, G. Cervone, L. Delle Monache, G. Graditi, and F. Jacobone, “Optimal bidding in a Day-Ahead energy market for Micro Grid under uncertainty in renewable energy production,” *Energy*, vol. 106, pp. 194–202, 2016.

[42] D. T. Nguyen and L. B. Le, “Optimal bidding strategy for microgrids considering renewable energy and building thermal dynamics,” *IEEE Trans. Smart Grid*, vol. 5, no. 4, pp. 1608–1620, 2014.

[43] X. Ayón and J. Usaola, “An optimal scheduling for aggregators in smart grids,” *Int. Conf. Eur. Energy Mark. EEM*, vol. 2015–Augus, 2015.

[44] I. Electricity and S. Markets, “Aggregators’ Optimal Bidding Strategy in Sequential Day-Ahead and Intraday Electricity Spot Markets,” 2017.

[45] H. Shayeghi and B. Sobhani, “Integrated offering strategy for profit enhancement of distributed resources and demand response in microgrids considering system uncertainties,” *Energy Convers. Manag.*, vol. 87, pp. 765–777, 2014.

[46] S. Ø. Ottesen, A. Tomasgard, and S. E. Fleten, “Prosumer bidding and scheduling in electricity markets,” *Energy*, vol. 94, pp. 828–843, 2016.

[47] S. W. Kim, J. Kim, Y. G. Jin, and Y. T. Yoon, “Optimal bidding strategy for renewable microgrid with active network management,” *Energies*, vol. 9, no. 1, pp. 1–15, 2016.

[48] R. Baetens and D. Saelens, “Multi-criteria grid impact evaluation of heat pump and photovoltaic based zero-energy dwellings,” *BS2013, 13th Conf. Int. Build. Perform. Simul. Assoc.*, no. August, pp. 3529–3536, 2013.

[49] R. Baetens, R. De Coninck, J. Van Roy, B. Verbruggen, J. Driesen, L. Helsen, and D. Saelens, “Assessing electrical bottlenecks at feeder level for residential net zero-energy buildings by integrated system simulation,” *Appl. Energy*, vol. 96, pp. 74–83, 2012.

[50] B. Palmintier, J. Giraldez, P. Gotseff, A. Nagarajan, T. Harris, B. Bugbee, M. Baggu, B. Palmintier, J. Giraldez, P. Gotseff, A. Nagarajan, T. Harris, B. Bugbee, M. Baggu, J. Gantz, and E. Boardman, “Feeder Voltage Regulation with High-Penetration PV Using Advanced Inverters and a Distribution Management System A Duke Energy Case Study,” *Nrel/Tp-5D00-65551*, 2016.

[51] TenneT TSO B.V., “TenneT is op zoek naar pilot participanten die FCR willen leveren, maar op dit moment niet in staat zijn om te voldoen aan de product specificaties uiteengezet door TenneT,” 2016. [Online]. Available: https://www.tennet.eu/nl/nieuws/nieuws/tennet-is-op-zoek-naar-pilot-participanten-die-fcr-willen-leveren-maar-op-dit-moment-niet-in-staat/. [Accessed: 16-Nov-2016].

[52] ACM, “Codewijziging meerdere leveranciers op een aansluiting,” 2017. [Online]. Available: https://www.acm.nl/nl/publicaties/publicatie/17003/Codewijziging-meerdere-leveranciers-op-een-aansluiting. [Accessed: 16-Nov-2017].

[53] Jules Energy, “Jules Energy: Revolutionary solutions for energy suppliers,” 2017. [Online]. Available: http://julesenergy.com/. [Accessed: 16-Nov-2017].

[54] ETPA, “ENERGY TRADING PLATFORM AMSTERDAM,” 2017. [Online]. Available: https://www.etpa.nl/. [Accessed: 16-Nov-2017].

[55] Liander, “Liander zoekt marktpartijen voor flexibiliteitsmarkt in energie,” 2016. [Online]. Available: https://www.liander.nl/nieuws/2016/11/04/liander-zoekt-marktpartijen-voor-flexibiliteitsmarkt-energie. [Accessed: 16-Nov-2017].

[56] E.X.E, “E.X.E. Driving your energy concept,” 2017. [Online]. Available: https://exe.energy/nl/. [Accessed: 16-Nov-2017].

[57] E.D.mij, “E.D.mij,” 2017. [Online]. Available: http://edmij.nl/. [Accessed: 16-Nov-2017].

[58] C. Hügel, “Interview with a senior enforcement official at ACM.” 2017.

[59] C. Hügel, “Interview with Mr. Matthijs van Rijn, former project manager at Alliander.” 2017.

[60] C. Hügel, “Interview with Mr. Guy Rutten, former consultant at Sia partners.” 2017.

[61] C. Hügel, “Interview with Mr. Heine prins, board member and co-founder of E.D.mij.” 2017.

[62] J. Bozuwa, M. Bravard, B. Kyengo, K. Luxenberg, and L. Sawyer, “Interview with Mr. George Trienekens, business developer at E.X.E.” Utrecht University, 2017.

[63] J. Bozuwa, M. Bravard, B. Kyengo, K. Luxenberg, and L. Sawyer, “Interview with Mrs. Gerda de Jong, electricity market developer at TenneT.” Utrecht University, 2017.

[64] J. Bozuwa, M. Bravard, B. Kyengo, K. Luxenberg, and L. Sawyer, “Interview with Mr. Phillippe Vassilopoulos, head of product design at EPEX SPOT.” Utrecht University, 2017.

[65] I. Lampropoulos, “A SYSTEM PERSPECTIVE TO THE DEPLOYMENT OF FLEXIBILITY THROUGH AGGREGATOR COMPANIES,” no. December, pp. 297–304, 2016.

[66] Bloemisterij, “Nieuw handelsplatform voor elektriciteit: ETPA,” *maart 2016*, 2016. [Online]. Available: https://www.hortipoint.nl/vakbladvoordebloemisterij/nieuw-handelsplatform-voor-elektriciteit-e-t-p-a. [Accessed: 18-Apr-2017].

[67] ETPA, “Veel gestelde vragen,” 2017.

[68] TenneT TSO B.V., “TenneT bereidt elektriciteitssysteem voor op toename duurzame energie,” *01-08-16*, 2016. [Online]. Available: https://www.tennet.eu/nl/nieuws/nieuws/tennet-bereidt-elektriciteitssysteem-voor-op-toename-duurzame-energie-1/. [Accessed: 21-Jun-2017].

[69] Tennet, “Market review 2016,” vol. 8, no. 3, pp. 285–288, 2016.

[70] M. Van Hout, P. Koutstaal, O. Ozdemir, A. Seebregts, M. van Hout, P. Koutstaal, O. Ozdemir, and A. Seebregts, “Quantifying flexibility markets,” *Ecn-E--14-039*, no. December, p. 52, 2014.

[71] SEDC, “Mapping Demand Response in Europe Today,” *SEDC. Smart Energy Demand Coalit.*, no. April, p. 92, 2014.

[72] E. SPOT, “Day-Ahead Auction,” *2017*. [Online]. Available: https://www.apxgroup.com/trading-clearing/day-ahead-auction/.

[73] A. Van Der Welle, M. V. E. Zaken, P. Koutstaal, and T. Van Dril, “Notitie Ontwerp van elektriciteitsmarkten – benodigde aanpassingen voor een flexibeler energiesysteem op korte termijn Executive summary,” 2016.

[74] P. Fcr, G. The, E. R. Group, and C. Europe, “DRAFT,” 2015.

[75] D. Fcr, “FAQ Primaire Reserve (FCR),” 2017.

[76] Tennet, “Implementation Guide,” pp. 1–38, 2012.

[77] TenneT TSO B.V., “Manual Bidding of Regulating and Reserve Power (RRP),” vol. 2, no. May, pp. 1–9, 2012.

[78] S. Hers, F. Rooijers, M. Afman, H. Croezen, and S. Cherif, “Markt en Flexibiliteit,” *Publ. 16.3E90.35*, p. 37, 2016.

[79] S. Weckx, R. D'Hulst, and J. Driesen, "Primary and Secondary Frequency Support by a Multi-Agent Demand Control System," *IEEE Trans. Power Syst.*, vol. 30, no. 3, pp. 1394–1404, 2015.

[80] Frontier Economics, "Scenarios for the Dutch electricity supply system," no. September, 2015.

[81] Wikipedia, "Thermal mass," *2017*. [Online]. Available: https://en.wikipedia.org/wiki/Thermal_mass. [Accessed: 17-Dec-2017].

[82] MTB architecten, "EPC report," 2016.

[83] Solarclarity, "LG Chem RESU10," *2018*. [Online]. Available: https://solarclarity.nl/project/lg-chem-resu10/. [Accessed: 18-Apr-2018].

[84] NIBE, "GElijkwaardigheidsverklaring NIBE FC1255-6PC," *2017*, 2017. [Online]. Available: https://www.nibenl.eu/producten/waterwater-warmtepompen/nibe-f1155-pc/#downloads. [Accessed: 21-Dec-2017].

[85] E. R. Group, "Day-ahead prices," *2017*. [Online]. Available: https://www.entsoe.eu/data/Pages/default.aspx. [Accessed: 12-Dec-2017].

[86] TenneT TSO B.V., "Verrekenprijzen," *2017*. [Online]. Available: http://www.tennet.org/bedrijfsvoering/Systeemgegevens_afhandeling/verrekenprijzen/index.aspx. [Accessed: 12-Dec-2017].

[87] AHSREA, "IWEC weather data Amsterdam," 2000. [Online]. Available: https://energyplus.net/weather-location/europe_wmo_region_6/NLD//NLD_Amsterdam.062400_IWEC.

[88] Waterbase, "Water temperatures." [Online]. Available: http://live.waterbase.nl/waterbase_locaties.cfm?whichform=1&wbwns1=44%7CTemperatuur+in+oC+in+oppervlaktewater&wbthemas=&search=. [Accessed: 12-Dec-2017].

[89] Liander, "Zonnedael slimme meter dataset." [Online]. Available: https://www.liander.nl/over-liander/innovatie/open-data/data. [Accessed: 03-Apr-2017].

[90] I. Richardson, M. Thomson, D. Infield, and C. Clifford, "Domestic electricity use: A high-resolution energy demand model," *Energy Build.*, vol. 42, no. 10, pp. 1878–1887, 2010.

[91] ASHRAE, "https://www.ashrae.org/," 2018. [Online]. Available: https://www.ashrae.org/. [Accessed: 18-Apr-2018].

[92] DesignBuilder Software Ltd, "Designbuilder," *2018*, 2018. [Online]. Available: https://www.designbuilder.co.uk/. [Accessed: 18-Apr-2018].

[93] DesignBuilder, "Simulation Hourly Weather Data," 2015. [Online]. Available: http://www.designbuilder-v2.co.uk/helpv2/Content/Hourly_Weather_Data.htm.

[94] S. Dubey, J. N. Sarvaiya, and B. Seshadri, "Temperature dependent photovoltaic (PV) efficiency and its effect on PV production in the world - A review," *Energy Procedia*, vol. 33, pp. 311–321, 2013.

[95] L. Lundström, "Weather data for building simulation - New actual weather files for North Europe combining observed weather and modeled solar radiation," 2012.

[96] W. G. J. H. M. van Sark, "Opbrengst van zonnestroomsystemen in Nederland," no. CIER-E2014-1, 2014.

[97] CBS, "Hernieuwbare energie in Nederland 2014," *Rep. number 60115201401 C-89*, pp. 1–106, 2014.

[98] E. M. and M. Thomson, "CREST demand model." [Online]. Available: http://www.lboro.ac.uk/research/crest/demand-model/. [Accessed: 12-Dec-2016].

[99] Milieucentraal, “Drinkwater consumptie,” *2017*. [Online]. Available: https://www.milieucentraal.nl/in-en-om-het-huis/gezonde-leefomgeving/gezond-in-en-om-huis/drinkwater/. [Accessed: 12-Dec-2017].

[100] A. Barr, B. Deguilhem, S. Grolleau, M. Gerard, F. Suard, and D. Riu, “A review on lithium-ion battery ageing mechanisms and estimations for automotive applications,” *J. Power Sources*, vol. 241, pp. 680–689, 2013.

[101] M. D. Hopkins, A. Pahwa, and T. Easton, “Intelligent dispatch for distributed renewable resources,” *IEEE Trans. Smart Grid*, vol. 3, no. 2, pp. 1047–1054, 2012.

[102] M. Kaisers and A. van der Veen, “Computing the value of flexibility in electricity retail , ahead and balancing markets,” *Innov. Smart Grid Technol. (ISGT Eur. 2016 6th IEEE PES Int. Conf. Exhib.*, 2016.

[103] “FORMULESTRUCTUUR Energieprestatiecertificaat bestaande gebouwen met woonfunctie,” 2017.

[104] Z. M. Smets Arno H. M., Jäger Klaus, Isabella Olindo, Van Swaaij René, *The Physics and Engineering of Photovoltaic Conversion, Technologies and Systems*. Cambridge, England : UIT Cambridge Ltd., 2016., 2016.

[105] M. Akmal and B. Fox, “Modelling and simulation of underfloor heating system supplied from heat pump,” *Int. J. Simul. Syst. Sci. Technol.*, vol. 17, no. 35, p. 28.1-28.9, 2016.

[106] A. F. Mills, *Basic heat & mass transfer*. 1999.

[107] H. van den Akker and R. F. Mudde, *Transport Phenomena - The Art of Balancing*, First edit. Delft: Delft Academic Press / VSSD, 2014.

[108] D. Fischer, T. R. Toral, K. B. Lindberg, B. Wille-Haussmann, and H. Madani, “Investigation of Thermal Storage Operation Strategies with Heat Pumps in German Multi Family Houses,” *Energy Procedia*, vol. 58, no. 0, pp. 137–144, 2014.

[109] D. Fischer, H. Madani, A. Zottl, and S. Braungart, “GreenHP Deliverable 2.1 - Building Integration Concepts,” pp. 1–87, 2014.

[110] I. Staffell, D. Brett, N. Brandon, and A. Hawkes, “A review of domestic heat pumps,” *Energy Environ. Sci.*, vol. 5, no. 11, p. 9291, 2012.

[111] E. McKenna and M. Thomson, “High-resolution stochastic integrated thermal-electrical domestic demand model,” *Appl. Energy*, vol. 165, pp. 445–461, 2016.

[112] G. Reynders, D. Saelens, and T. Nuytten, “Robustness of reduced-order models for prediction and simulation of the thermal behavior of dwellings,” *BS2013, 13th Conf. Int. Build. Perform. Simul. Assoc.*, pp. 660–667, 2013.

[113] P. Bacher and H. Madsen, “Identifying suitable models for the heat dynamics of buildings,” *Energy Build.*, vol. 43, no. 7, pp. 1511–1522, 2011.

[114] E. Nederland, “Energiebewust ontwerpen van nieuwbouwwoningen,” 2015.

[115] E. D. P. Wp, “Literatuurstudie thermisch comfort,” 2015.

[116] A. C. Van der Linden, P. Erdtsieck, I. Kuijpers - van Gaalen, A. Zeegers, and Et all, *Bouwfysica*. Utrecht/Zuthpen: ThiemeMeulenhoff, 2006.

[117] R. Projectnr, C. D. Consult, and C. D. Consult, “Leeswijzer NEN 7120,” no. september, pp. 1–59, 2011.

[118] ISSO Publicatie 51 (2017), “Thermische massa,” 2017. [Online]. Available: http://help.vabi.nl/elements/nl/index.html#!Documents/gebouweisen.algemeen.htm. [Accessed: 17-Dec-2017].

[119] M. Rahimi and A. Sabernaeemi, “Experimental study of radiation and free convection in an enclosure with under-floor heating system,” *Energy Convers. Manag.*, vol. 52, no. 7, pp. 2752–2757, 2011.

[120] “Model voor de berekening van de watertemperatuur in het leidingnet Volgens het Waterleidingbesluit mag de temperatuur van het water in het,” vol. v, pp. 46–49, 2010.

[121] B. Quigley, “Technical Checklist for underfloor heating installation.” [Online]. Available: http://www.nutechrenewables.com/technical-checklist-for-underfloor-heating-installation/. [Accessed: 05-Feb-2018].

[122] U. H. B. Gb, “User manual NIBE F1155PC Ground source heat pump Quick guide.”

[123] A. Veit, C. Goebel, R. Tidke, C. Doblander, and H.-A. Jacobsen, “Household Electricity Demand Forecasting -- Benchmarking State-of-the-Art Methods,” no. April, 2014.

[124] P. Goncalves Da Silva, D. Ilic, and S. Karnouskos, “The Impact of Smart Grid Prosumer Grouping on Forecasting Accuracy and Its Benefits for Local Electricity Market Trading,” *IEEE Trans. Smart Grid*, vol. 5, no. 1, pp. 402–410, 2014.

[125] W. Prediction, “Een stille revolutie in de meteorologie,” no. december, 2015.

[126] R. J. Hogan, M. Ahlgrimm, G. Balsamo, A. Beljaars, A. Bozzo, F. Di, R. M. Forbes, S. Lang, M. Mayer, I. Sandu, F. Vitart, and N. Wedi, “prediction,” no. October, pp. 9–11, 2017.

[127] Fraunhofer, “PV cast,” *2017*. [Online]. Available: https://www.pvcast.de/. [Accessed: 14-Feb-2017].

[128] Icarus, “Icarus,” *2018*. [Online]. Available: https://icarus.energy/. [Accessed: 14-Feb-2018].

[129] ELIA, “PV forecasts,” *2018*. [Online]. Available: http://www.elia.be/nl/grid-data/productie/Solar-power-generation-data/Graph. [Accessed: 27-Feb-2018].

[130] C. Hügel, “Estimated production and consumption by energy retailer.” Greenchoice/Spectral, p. 1, 2018.

[131] D. Finn, F. Murphy, and S. Shannon, “Control Algorithms for System Integration of Heat Pumps : Steady State and Seasonal Analysis,” no. May, pp. 20–22, 2008.

[132] J. Cervera-Vázquez, C. Montagud, and J. M. Corberán, “In situ optimization methodology for the water circulation pumps frequency of ground source heat pump systems: Analysis for multistage heat pump units,” *Energy Build.*, vol. 88, pp. 238–247, 2015.

[133] “Capacity control of heat pumps,” no. October, pp. 28–31, 2012.

[134] F. Karlsson and P. Fahlén, “Capacity-controlled ground source heat pumps in hydronic heating systems,” *Int. J. Refrig.*, vol. 30, no. 2, pp. 221–229, 2007.

[135] H. Madani, J. Claesson, and P. Lundqvist, “Capacity control in ground source heat pump systems part II: Comparative analysis between on/off controlled and variable capacity systems,” *Int. J. Refrig.*, vol. 34, no. 8, pp. 1934–1942, 2011.

[136] D. Del Col, G. Benassi, and M. Azzolin, “Energy Efficiency in a Ground Source Heat Pump With Variable Speed Drives,” *Int. Refrig. Air Cond. Conf.*, pp. 1–10, 2012.

[137] C. Montagud, J. M. Corberán, and Á. Montero, “In situ optimization methodology for the water circulation pumps frequency of ground source heat pump systems,” *Energy Build.*, vol. 68, pp. 42–53, 2014.

[138] J. M. Corber, D. Donadello, I. Martinez-Galvan, and C. Montagud, “Partialization losses of ON/OFF operation of water-to-water refrigeration/heat-pump units,” *Int. J. Refrig.*, vol. 36, no. 8, pp. 2251–2261, 2013.

[139] B. R. Parken W, Kelly G, “Factors affecting the performance of a residential air-to-air heat pump,” *ASHRAE Trans. 83839-849*, 1977.

[140] E. Fuentes and D. Waddicor, “Improved characterization of water-to- water heat pumps part load performance,” no. August, pp. 45–49, 2016.

[141] A. Müller, “European Heat Pump NEWS,” *Eurpean Heat Pump NEWS, ehpa*, no. 1, pp. 13–14, 2011.

[142] R. Curtis and T. Pine, “Effects of cycling on domestic GSHPs Supporting analysis to EA Technology Simulation / Modelling,” no. 7440646, p. 28, 2012.

[143] R. Green, “The Effects of Cycling on Heat Pump Performance,” no. November, p. 53, 2012.

[144] C. Hügel, “Interview with Mr. Peter Schipperen, employee of NIBE NL.” 2017.

[145] Leo Hendriksen, Jan Afink, Tjerk Epema, Harm Schiphouwer, and Hans van Wolferen, “Opwekkingsrendementen lokale technieken onder laboratoriumomstandigheden,” 2010.